A MAJOR REDESIGN OF THE UNIVERSITY OF MANITOBA CYCLOTRON AND A STUDY FOR AXIAL INJECTION OF IONS INTO THE PRINCETON UNIVERSITY AVF CYCLOTRON

BY

MOOHYUN YOON

A thesis
submitted to the Faculty of Graduate Studies
of the
University of Manitoba
in partial fulfillment of the requirements
of the degree of

DOCTOR OF PHILOSOPHY

Department of Physics

Winnipeg, Manitoba
September, 1986

ISBN Ø-315-33918-7

A MAJOR REDESIGN OF THE UNIVERSITY OF MANITOBA CYCLOTRON AND A STUDY FOR AXIAL INJECTION OF IONS INTO THE PRINCETON UNIVERSITY AVF CYCLOTRON

by

MOOHYUN YOON

A thesis submitted to the Faculty of Graduate Studies of
the University of Manitoba in partial fulfillment of the requirements
of the degree of

DOCTOR OF PHILOSOPHY

To the Memory

of

my Mother

Synopsis

Two independent cyclotron improvement projects are treated separately: a major redesign of the University of Manitoba cyclotron and a study for axial injection of ions into the Princeton University AVF cyclotron.

The upgrading program for the University of Manitoba cyclotron included, among other projects, the mapping/shimming of the magnetic field and the design of the new dee-tips. The first step of this major undertaking involved a thorough analysis of the magnetic field mapping data that was previously obtained in 1982. This analysis led to the conclusion that the cyclotron's operation could be enhanced by improving the isochronism and the axial focusing for both H^- and D^- ions. In 1984, such improvements were achieved by significantly modifying the magnetic field through the introduction of the new shims and the optimization of the Invar block temperatures, which trim the field. Simultaneously, a new central region for accelerating the H^- beam was designed on the basis of detailed computer-aided beam orbit dynamics studies. The recent successful and much improved acceleration of H ions in the University of Manitoba cyclotron utilized the designed values and fully confirmed the predictions of these studies.

The improvement program for the Princeton University AVF cyclotron included the design of the axial injection system and of the accompanying central region. The focusing lenses along the axial injection system were carefully chosen in order to prevent any severe depolarization of the polarized ions. All the parameters associated with the focusing lenses were obtained from detailed beam optics investigations. The beam orbit dynamics in the existing central region of the cyclotron was also thoroughly investigated. Subsequently, a design study was carried out for the new central region that would be required in view of the new injection system. The total transmission efficiencies through the axial injection system and the new central region were also calculated for various particles. Finally, the problem of resonant depolarization of polarized ions during acceleration was considered, and shown to be minor.

Acknowledgements

There are many individuals whom I would like to thank for their support, comments, help, encouragement, and love while performing the work described in this thesis.

For providing me with an opportunity to enter into the "world" of particle accelerator physics and thereafter continuously supporting me, I am indebted to my advisor, Professor Saewoong Oh. Through many invaluable discussions and comments during the past four years, I have obtained a great deal of benefit from him.

For their helps during the magnetic field mapping in 1984, I am grateful to all the members of the machine development group at the University of Manitoba Cyclotron Laboratory: Irv Gusdal, Vladimir Derenchuk, John Lancaster, Jim Anderson, and Tony Smith. Their enthusiastic and unyielding efforts toward the development of the mapping devices should be recognized as one of the vital factors that resulted in such a successful and satisfactory acceleration of the H^- beam. John Bruchshaw also spent a lot of time during the design study of the new central region, changing my drawing into the real "drawing". For this, I would like to thank to him.

I was also fortunate to spend a couple of years in Princeton during the process of my second project. Both Professor Frank Calaprice and Professor Arthur McDonald must be thanked for providing me with such a chance and supporting me continuously till the end of the project. Dr. William Moore helped me in various aspects during the study of the central region of the Princeton cyclotron. I wish to thank to him for the long list of assistance he gave me. I also obtained a great deal of benefit from Dr. Richard Kouzes who not only helped me to familiarize myself in using Data General MV10000 computer but also read carefully the original manuscripts of this thesis to suggest a number of improvements. Dr. Yizhak Sharon spent a lot of time reading the first part of this thesis and in improving my English. Therefore I would like to thank to him.

Finally, for their love, encouragement, and support, I wish to express my deepest and warmest gratitude to my parents, without whom I would have never started this work.

Table of Contents

Part II A Study for Axial Injection of Ions into the Princeton University AVF Cyclotron

List of Figures

List of Tables

Introduction

The concept of a cyclotron was visualized by Lawrence in 1930 [LAW30], who then implemented the first prototype model at Berkeley which produced a proton beam of 1 MeV [LAW32]. This successful acceleration of particles stimulated many laboratories in many countries around the world, hence more higher energy cyclotrons were built during the next two decades, culminating with the University of Birmingham cyclotron which could accelerate a proton beam up to about 40 MeV.

However, the classical cyclotron, as it is usually called nowadays, imposed a limitation on the maximum obtainable energy because of two mutually contradictory requirements on the magnetic field ([LIV61], [LIV62]).

Since the ion rotates a hundred turns or more to reach its maximum energy, the motion inside a cyclotron must be stable in both the radial and the axial directions. In the axial direction, the ion has to feel a force toward the median plane and this requires that the magnetic field decrease with radius ([LIV61],[LIV62]). However, if the cyclotron resonance frequency, $\omega = qB/m$, were to be constant, the magnetic field B would have to increase with radius in order to compensate for the relativistic increase in mass m with velocity.

Though attempts were made to solve this problem, eventually the best solution was devised by Thomas, which led to the appearance of the relativistic cyclotron. In his paper published in 1938 [THO38], Thomas formulated the additional focusing term by employing the idea of an azimuthally varying magnetic field (AVF). The focusing term due to the AVF component turned out to be independent of the requirement on isochronism. Therefore isochronism can be retained by increasing

the average magnetic field with radius, while the axial focusing force can be obtained from the AVF component of the magnetic field. The cyclotron based on this principle is called an AVF cyclotron.

Later, Kerst also discovered that further axial focusing could be obtained when spirally shaped magnet sectors were employed. This idea was suggested by the principle of edge focusing in the theory of beam optics [LAW77]. The term due to the spiral focusing was again found to be independent of the requirement on isochronism, and therefore a spiral-ridge cyclotron emerged.

The advent of the idea of the relativistic cyclotron gave an impetus to build new cyclotrons in many laboratories around the world since the 1950's. Both the University of Manitoba cyclotron and the Princeton University cyclotron (whose upgrading studies form the two main constituents of this thesis) were built in the early and in the late 1960s, respectively. From then till the present time, they have been continuously devoted to fundamental subatomic physics investigations.

In the two decades that have passed since these two cyclotrons were built, there has been a significant advance in cyclotron technology, progress that was in part due to the appearance of solid-state electronic devices and the emergence of powerful computers. The solid-state based instrumentation made it possible to carry out precise mapping and analysis of the cyclotron magnetic field. The powerful new generation of computers enabled one to calculate the RF electric field distribution inside a cyclotron and then to trace particles' trajectories, from the ion source to the extraction radius, under the influence of this calculated electric field and the measured magnetic field. The accuracy of these calculations is much better than what could be obtained at the birth of these first-generation AVF cyclotrons.

In a separate development, nuclear physics experiments became more and more sophisticated during the same time span, resulting in needs for beams of higher intensity and better quality. In response to this demand, together with the availability of enormously more advanced cyclotron technology of the 1980's, many laboratories around the world began to embark upon ambitious upgrading programs for their cyclotrons.

The University of Manitoba Cyclotron Laboratory was no exception. In fact, members of the machine development group at this laboratory started investigating the possibility of such an upgrading as early as 1976, when they carried out exploratory magnetic field mappings. Later, in 1982, more elaborate field mappings [DER83], based on computer-aided technology were performed with much higher precision. The result was quite encouraging; it convinced us that a substantial improvement in beam quality would be achievable by upgrading the cyclotron. This finally led to a decision to initiate an extensive and intensive improvement program for the cyclotron, a project which was started in 1984. The author's contribution to the project dates from 1982 when he analyzed the 1982 field mapping data. During the next two years, the author was engaged in design studies for a new central region of the cyclotron (based on the 1982 field mapping data). The 1984 upgrading program included, among other projects, a series of field mappings and shimmings in which some 80 field maps were taken as successively better magnetic shims were installed. The result was better than expected; an H^- beam was subsequently accelerated and extracted without having to retune the cyclotron parameters from design values. The author's contribution to this project was to analyze the measured data and then to suggest the improved shape and position of the magnetic

shims for the next mapping. After completion of this mapping program, the author then refined the design study for the central region based on the new magnetic field data.

The Princeton University AVF Cyclotron Laboratory also turned its attention to the type of improvements described earlier. This cyclotron is noted for its single-turn extraction capability. It can accelerate high charge-state light heavy ions as well as protons and deuterons. In the past, such ions were provided by an internal PIG (Penning Ionization Gauge) [BEN69] source. Naturally, however, the research needs increasingly required higher beam intensity and energy as well as better beam quality. The development in the 1970s of an ECR (Electron Cyclotron Resonance) source [GEL79] started to have a major effect on cyclotrons. This source cannot be installed inside the cyclotron. However, its capability for producing high quality, intense beams of high-charge state light heavy ions made it far more profitable to externally inject the beam from the ECR source into the cyclotron than to rely on the internal PIG source.

Another area of interest is the study of spin-dependent nuclear interactions, an area which requires polarized beams. Such beams with reasonable intensity can only be obtained by the external injection of polarized ions into the cyclotron. Thus, the Princeton University AVF Cyclotron Laboratory decided to initiate a feasibility study for converting the cyclotron to external injection of ions. The central question was whether the single-turn extraction capability could still be retained at the same time as achieving an excellent overall beam transmission efficiency through the cyclotron. An accurate assessment of these points necessitated an extensive computer-based design study of the central region based on the beam orbit dynamics

investigations inside the cyclotron, an investigation which the author has performed since July 1984.

This thesis consists of two independent parts under the following headings: (1) A major redesign of the University of Manitoba cyclotron, and (2) A study for axial injection of ions into the Princeton University AVF cyclotron.

The first part discusses the magnetic field mapping and the design study of the new central region of the University of Manitoba cyclotron as integral parts of the major upgrading projects. At the beginning, a brief historical background of the University of Manitoba cyclotron is presented. Then the motivation for and the importance of, the cyclotron improvement program are presented in some detail. A considerable amount of space is allocated to describe the methods and the results of the new magnetic field mappings and the shimming program performed in 1984. The need for a new central region and the design study of it, as well as the beam orbit dynamics for H^- ions are then delineated. This part concludes with a presentation of the markedly improved performance of the cyclotron after the upgrade. Possible future improvements are also suggested.

The second part of this thesis deals with the improvement program of the Princeton University cyclotron. This consists of a design study of the axial injection system and of the new central region. It starts with an introduction to the Princeton University cyclotron. A detailed design study of the axial injection system then follows. Finally, design studies for the new central region, based on the beam orbit dynamics investigations, are presented. A brief consideration associated with the depolarization problem of polarized ions during acceleration in the cyclotron central region is also given.

Part I

A Major Redesign

of

the University of Manitoba Cyclotron

Chapter 1

Historical Background

The University of Manitoba cyclotron is a four-sector, spiral-ridge, variable energy machine, which was designed to accelerate an H^- beam whose energy can range from 20 to 50 MeV [STA62]. The unique feature of this cyclotron is the method that is employed in it for trimming the magnetic field. Here, unlike other machines, the field is trimmed by individually controlling the permeability of 64 blocks of Invar alloy ([PIC40], [BUR65], [BUR66]). These blocks are placed, eight at a time, sandwiched between each hill piece and the corresponding pole piece (8 blocks/hill piece $\times$ 2 hill pieces/hill $\times$ 4 hills). The radial profile of the magnetic field can be shaped by adjusting the temperatures of the Invar blocks which are arranged underneath each hill piece successively in eight radial positions, along the radius of the cyclotron.

In 1975, the original internal source was replaced by an external source ([MCI75], [BAT76], [AND79]). At that time, an 11 keV H^- beam from a duoplasmatron source was axially injected. That axial injection system consisted of a set of electrostatic quadrupole triplets, a beam buncher and an electrostatic mirror, *etc.*.

The mirror bent the axially injected beam by 90° to launch the beam into an accelerating orbit. The beam then made about 1200 turns in the central region before its energy reached 50 MeV. The central region consisted of two 45° dees diametrically placed and operated in the fundamental harmonic mode. The dee voltage and its oscillating frequency were 28.5 kV (peak to ground) and 28.48 MHz, respectively. In order to overcome the multipactoring problem the dees were biased

to -1.2 kV.

The extraction of a beam was achieved simply by stripping the two electrons in the H^- ions by a thin aluminum foil, a process which reverses the curvature of the orbit. With this method, the extraction efficiency was close to 100%. The extraction energy could be altered by changing the radial position (and, to an extent, also the azimuthal position) of a foil inside the cyclotron by means of a remote-controlled foil probe. Therefore, no re-trimming of the cyclotron magnetic field was necessary, regardless of the energy of the H^- beam.

In 1976, D^- ions were also accelerated and extracted [GUS76]. To do so, however, large changes in the cyclotron parameters were required. The acceleration of the D^- ions in the fundamental harmonic mode resulted in low beam current and poor beam quality; this, in turn, was the reason that experiments with D^- ions were seldom performed.

The successful conversion of the University of Manitoba cyclotron to an external injection scheme extended the capability of the cyclotron. In fact, polarized D^- ions of up to 19 MeV have been obtained since 1980. The acceleration of polarized H^- ions, however, turned out to involve serious problems owing to the resonant depolarization in the intrinsic fundamental mode [DEJ81]. Nevertheless, the cyclotron had provided, continuously and successfully, useful beams for nuclear physics experiments until recent years.

However, as time passed, the experiments became more and more sophisticated, requiring beams of increasingly higher quality and versatility, and hence the need to upgrade the cyclotron performance to meet the above demand became acute.

By a happy coincidence, the emergence of powerful computers and of advanced solid-state electronics devices, had already led many facilities around the world – including the University of Manitoba Cyclotron Laboratory – to launch upgrading projects involving their cyclotrons.

An inherent problem with the University of Manitoba cyclotron before the upgrade was that nearly 1200 turns were required for particles to reach the outermost radius. This is in contrast to other cyclotrons, in which the number of turns is only of the order of 300. The amount of precision required for the parameters of this cyclotron to achieve the desired improvement is, therefore, much greater than the precision that is required in other cyclotrons.

To contain the phase excursion to within $\pm 10°$, for instance, would require a magnetic field stability of the order of 10^{-4}, with a similar requirement for the isochronism. Such stabilities were totally out of reach at the time of the original of this cyclotron (*i.e.*, in the early 1960's). To complicate the situation further, the Invar blocks had a temperature time constant that ranged between 10 minutes (for a 5°C change) and 10 hours (for a 200°C change), making it essentially impossible to tune the magnetic field empirically. When all of the above difficulties were taken into consideration, it was not surprising that many problems (such as those that are enumerated in chapter 4) occurred regularly whenever the University of Manitoba cyclotron was operated.

In order to solve those problems, and to improve cyclotron performance, an exploratory mapping of the H^- field was carried out in 1976 [UMC77], using a Hall probe. Although the precision of this mapping was limited to 0.2%, the result clearly indicated that the axial focusing completely disappeared at about 42 MeV (48 cm

in radius). Furthermore, the isochronism was far from satisfactory. A mapping of the D^- field also revealed that this field was even worse, as was expected.

The 1976 mapping program underscored the need for a better field mapping device as well as for a reliable program for mapping analysis. However, the realization of this goal had to be deferred until 1982 when we finally constructed a superior flip-coil based field mapping system and acquired a new computer. Before 1982, the on-line computer was a PDP-15 machine with 32 K of random access memory (RAM). This computer was far too slow and its memory size was too small, thus making it impossible to carry out any on-line analysis of data. It was therefore impossible to perform the mapping and shimming cycle within any reasonable time frame.

This situation changed in 1982, when the laboratory purchased a VAX-11/750 on-line computer with a 1 Mb of RAM and with a 56 Mb disc storage. These computer parameters were later increased to 2.75 Mb of RAM and approximately 450 Mb of disc space, *i.e.*, to capacities that were large enough to perform computer-automated field mappings and on-line analyses of the data. This progress, together with the use of more advanced electronics, made it possible to carry out a field mapping program in 1982 at a much faster rate and with considerably improved precision ($\sim$0.04%). The results revealed two more dips in axial focusing. Chapter 2 of this dissertation starts with the presentation of the results of the 1982 field mapping.

Based on the field maps that were obtained in 1982, the author started a design study for two new central regions for the cyclotron, one for the H^- ions and the other for D^- ions. Simultaneously, the cyclotron development group at the University

of Manitoba started redesigning the dees and liners, modified the method of RF coupling and tuning, and upgraded the final-stage RF amplifiers [UZA85]. The dee was widened from 45° to about 60°. These modifications, along with the increase in dee voltage to 40 kV, boosted the energy gain per turn to 80 keV for the H^- ions, and to 138 keV for the D^- ions. Thus, the total number of turns, formerly approximately 1200, now became only 625 for the H^- beam at 50 MeV, and 196 for the D^- beam at 27 MeV. An enhancement by an order of magnitude was also achieved in the cooling of the dees, the dee stems and dee liners, an advance which served to reduce significant fluctuations in the beam that had been associated with the thermal expansion of these parts of the cyclotron [UZA85].

The 1982 mapping also confirmed the impossibility of producing an isochronous D^- field beyond 45 cm radius if we continued to utilize the existing oscillation frequency of the electric field of 14.24 MHz (*i.e.*, one half of the frequency for the H^- ions). This led us to attempt, in the new field mapping program that was initiated in 1984, to increase the oscillation frequency to 30.4 MHz; the magnetic field becomes flatter at higher excitation owing to different magnetic saturation effects in the iron of the pole-tips at different radii.

The 1984 field mapping program [UMC84], which forms the main theme of the next chapter, marked the culmination of a number of years of preparatory works by the members of the cyclotron development group at the University of Manitoba. The mapping device and its electronics were further improved. The calibration of the flipping coils was made much more precise, and subsequently the accuracy of the data was improved to 0.01%, an accuracy which was sufficient to provide a detailed picture of the magnetic field.

The first part of this thesis describes the author's work in the upgrading project, involving the analyses of the field mapping data and the shimming, and the design studies for a new central region for the H^- ion acceleration. The results of the magnetic field measurement and shimming, for both H^- and D^- ions, are described in great detail in chapter 2.

In chapter 3, design studies of new dee-tips for the acceleration of H^- ions and investigations of the beam orbit dynamics are presented. After explaining the necessity for having the new central region, and introducing some features of this new region, the method that was utilized to obtain the electric potential distribution inside the cyclotron is briefly described. A detailed account of the beam orbit dynamics studies then follows.

Finally, chapter 4 is devoted to the discussion of the results of the upgrading projects, especially in comparison with the situations that prevailed before the upgrade. Possible future improvements of the University of Manitoba cyclotron are also suggested.

Chapter 2

The Magnetic Field Mapping

2.1 Introduction

An exploratory magnetic field mapping of the H^- field in the University of Manitoba (hereafter U of M) cyclotron was carried out in 1976, when the cyclotron was converted to the axial injection of ions. The field measurements were taken by a single Hall probe which was mounted on a rotating arm. A gear mechanism advanced the probe along this arm in steps of 2.54 cm (1″), to cover 22 radial points for each angle, and then the arm was rotated by 2°, azimuthally. Using this approach, it took 11 hours to complete the whole (360°) mapping. Unfortunately, however, neither the mapping system, nor the cyclotron remained stable during such a long period. With this method, there was also an unavoidable error in the positioning of the Hall probe, an error that was estimated to be at least 0.25 mm per each radial position. This uncertainty induces an error of up to 0.1% (~2 mT) in the determination of the magnetic field at each point. In addition, the mapping had to be carried out in a vacuum because the temperature of the Invar had to be set as high as 240°C for some of the blocks. Therefore, the Hall probe must have experienced a large temperature fluctuation as it was moved across the Invar blocks. Although some cooling was provided, the temperature sensitivity of the Hall probe cast serious doubts upon the precision of this mapping.

The results of the mapping revealed the total disappearance of the axial focusing at about r=48 cm. The cause of this phenomenon was subsequently attributed to a large magnetic shim that had been placed in the leading edge (beam entrance side)

of the valley starting at this radius. The purpose of this shim was to boost the magnetic field for the H^- ions, from this radius outward, since otherwise the field would have been too weak to accelerate any H^- ions beyond this point. However, this shim, while improving the isochronism, also introduced a rapid increase in the magnetic field and a momentary disappearance of the spiralling of hills at about this radius. It is well-known that both of these effects reduce the axial focusing and, in fact, the axial focusing was completely lost and the effect became defocusing.

2.2 Analysis of the 1982 mappings

2.2.1 The 1982 mapping apparatus

The field mapping program carried out in 1982 [BRU83] concentrated on correcting the problem, that occurred at about r=48 cm, by placing a magnetic shim on the trailing edge (beam exit side) of the valley. In the 1982 mapping, the Hall probe was replaced by 52 flipping coils, mounted on a rotating arm whose length was 70 cm. The coils were accurately embedded on the arm to within 0.05 mm. They were then mounted on a rotating shaft with a counterbalance attachment to keep the shaft horizontal. A precision laser optical shaft-encoder was attached to read the azimuthal position of the arm to within 0.02°. With this arrangement, it was possible to measure the field every 1.27 cm (0.5″) radially and every 2° azimuthally. Each flip coil had its own current amplifier and integration circuit, these electronic components being located outside the cyclotron vault. The measurement was taken first at a given azimuthal angle. The integration circuit then integrated the current and retained this information for about 30 seconds, until the circuit re-established the temperature equilibrium. A precision electronic voltmeter read

successively all the 52 data (from the 52 coils). Then all the circuits were reset and the arm was rotated by 180° to take another reading. The final data was taken to be the corrected average of these two readings. The arm was subsequently advanced by 2° in azimuth and the whole process was repeated for the new angular setting. Most of the mappings were performed over only one sector (90°) of the cyclotron. A time period of 1.5 hours was required to complete one such mapping. Measurements were carried out at night, when the electric main voltage fluctuation was at a minimum. In order to reduce the heating of the flip coils, the arm was rendered vacuum-tight and the inside of the probe was cooled by air. Over 70 field maps were taken. The precision of the measurement was estimated to be 0.04%.

The time allocated for this mapping program was only three weeks, but the mappings did lead to a good estimation for the size and the location of the replacement shim that was needed to improve the axial focusing which occurred at about r=48 cm.

2.2.2 The magnetic fields for the H^- and D^- ions in 1982

Figs. 2.1, 2.2 and 2.3 show some of the results of the 1982 field mappings. These figures provide the H^- particle's revolution frequency (ν) as well as the axial (ν_z) and radial (ν_r) focusing frequencies. All these frequencies, the three most important characteristics of the cyclotron magnetic field, are plotted as a function of the radius of the H^- beam.

Ideally ν should be a constant all along the radius. However, fig. 2.1 indicates that it fluctuates considerably beyond r=10 cm. A particularly conspicuous fluctuation is seen to occur at a radius of approximately 10 cm. This is caused by a

Figs. 2.1, 2.2, 2.3 Results of the magnetic field mapping that was carried out in 1982. For each plot, the horizontal axis denotes the radius of H^- ion in centimeters, and the vertical axis represents the H^- ion's revolution frequency (fig. 2.1), axial focusing frequency (fig. 2.2) and radial focusing frequency (fig. 2.3) in figs. 2.1, 2.2, and 2.3, respectively.

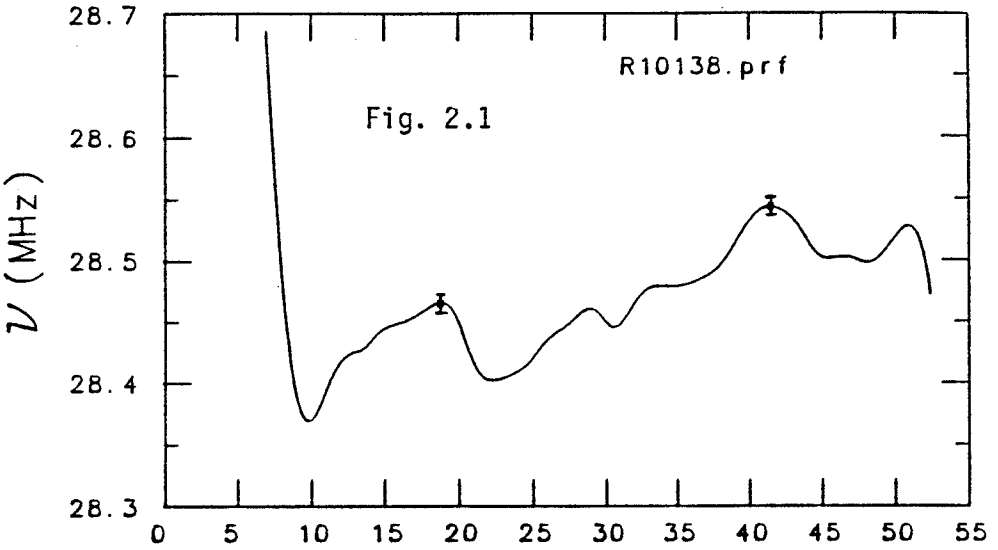
R10138.prf
Fig. 2.1
28.7
28.6
28.5
28.4
28.3
ν (MHz)
0
5
10
15
20
25
30
35
40
45
50
55

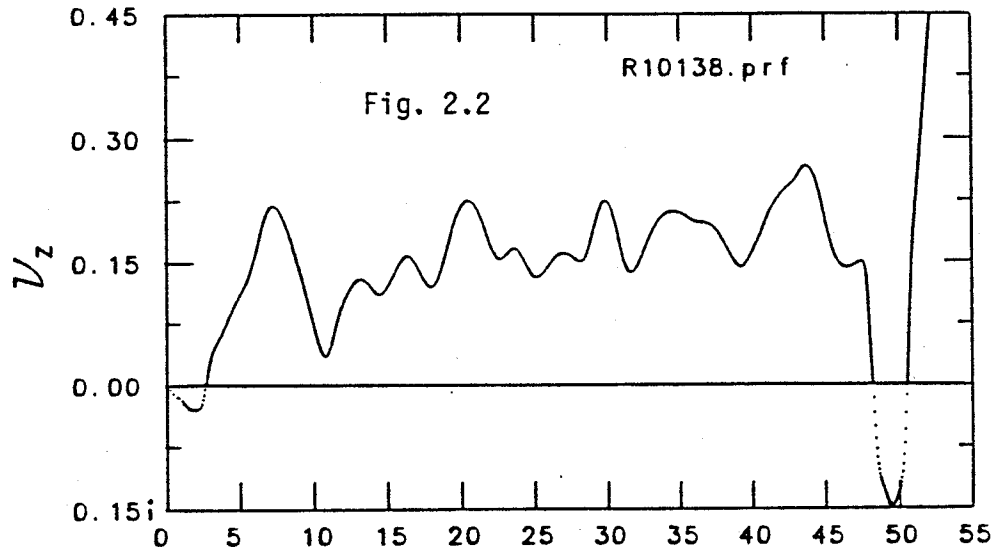
R10138.prf
Fig. 2.2
0.45
0.30
0.15
0.00
0.15i
ν_z
0
5
10
15
20
25
30
35
40
45
50
55

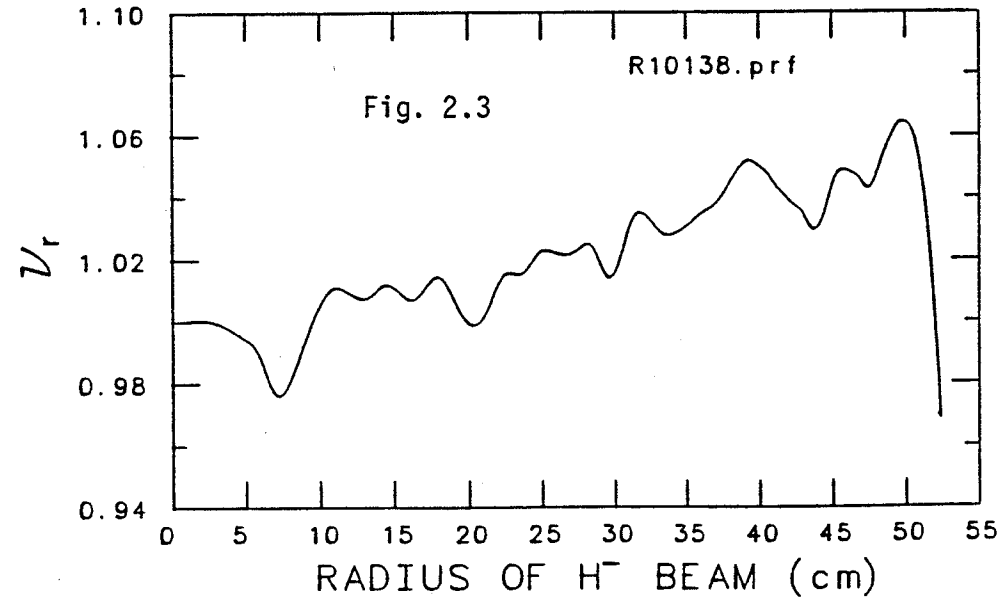
R10138.prf
Fig. 2.3
1.10
1.06
1.02
0.98
0.94
ν_r
0
5
10
15
20
25
30
35
40
45
50
55
RADIUS OF H⁻ BEAM (cm)

premature termination of the central bump magnetic field. Such a bump pulls the flux from the surrounding area, and therefore tends to leave a shadow just outside the bump. A peak in ν_z between r=3 and 10 cm (fig. 2.2) is due to the steep negative slope of the bump field. In this region, there is no flutter field component. Therefore, the axial focusing can be expressed by the simple relation which holds for a classical cyclotron,

$$\nu_z(r) = \sqrt{k} = \sqrt{-\frac{r}{B}\frac{dB}{dr}} \quad . \tag{2.2.1}$$

Here k is the field index and $B(r)$, in tesla, is the magnetic field at r, in meters. Let us now apply this formula to the field parameters at a radius of 7 cm (the point where the field gradient is the largest) in fig. 2.1. The measured values at r=7 cm are: dB = 0.03 T, B= 1.87 T, r= 0.07 m, and dr= 0.02 m. Therefore, we obtain there, ν_z = 0.24, a value which agrees well with fig. 2.2. We see from fig. 2.1 that the slope of ν (thus, B) is zero at r=10 cm. We therefore expect ν_z to be zero at this radius. The fact that this ν_z is non-zero but has a small positive value implies that some AVF component is already present there.

The drop in ν_r at r=7 cm (see fig. 2.3) can be understood in a similar way. The expression for ν_r in a classical cyclotron is

$$\begin{aligned} \nu_r(r) &= \sqrt{(1-k)} \\ &= 0.972 \qquad when \qquad r = 7\ cm. \end{aligned} \tag{2.2.2}$$

This value agrees well with the one that is obtained from fig. 2.3. This dip is the third most serious imperfection of this cyclotron that had to be corrected. The other two major imperfections will be discussed later in this section.

Departure from isochronism results in a phase oscillation of the particles during acceleration. Let us now utilize the following notation: we define ϕ to be the phase of a particle with respect to the RF voltage, N the turn number, ω_{RF} the angular oscillation frequency of the electric field, $\omega(E)$ the particle's revolution frequency at the energy E, h the integral harmonic ratio. We also let E_1 denote the maximum energy gain per turn [which is a function of the charge number, the total number of dees, the dee voltage, the harmonic mode, and the dee angle; see eq. (3.1.3)]. One can then formulate the expressions for the phase change per turn and for the energy gain per turn as,

$$\frac{d\phi(E)}{dN} = 2\pi\left(\frac{\omega_{RF}}{\omega(E)} - h\right) \qquad and \qquad \frac{dE}{dN} = E_1 \cos\phi(E) \quad . \tag{2.2.3}$$

From these equations, it is straightforward to derive a formula for the phase oscillation as a function of energy. The result is given by

$$\sin\phi(E) = \sin\phi_0 + \frac{2\pi h}{E_1}\int_{E_i}^{E_f}\left(\frac{\omega_{RF}}{h\omega(E)} - 1\right)dE \quad , \tag{2.2.4}$$

where ϕ_0 and E_i, respectively, are the RF phase and the beam energy at the center of the first gap (between the mirror and the dee-tips in the case of the U of M cyclotron).

We now apply the above equation to fig. 2.1 and substitute the following values: ϕ_0=+7°, h=1, ω_{RF}=2π × 28.48 MHz, E_i=26 keV, E_f=50 MeV and E_1 ranging from 47 keV to 98 keV, depending on the turn number. The result that we obtain is shown in fig. 2.4. From this figure, we notice a very large phase oscillation (of +82°) at 17.5 MeV (r=31.7 cm). The figure indicates that when the particle reaches

30.3 MeV (r=41 cm), the phase already becomes $-90°$. Therefore, with the field configuration that leads to fig. 2.4, it is no longer possible to accelerate an H^- particle with an energy that is higher than 30.3 MeV. Moreover, these large phase excursions cause the beam to take as much as 1050 turns to reach 30 MeV, and the turn separation in this energy region is, in fact, almost unrecognizable. It is therefore expected that there will be a large number of turns among the particles extracted from the cyclotron. This kind of spread may lead to a deterioration in beam quality (*e.g.*, a large energy spread or a large center spread, *etc.*).

In general, fluctuations in any of the above three cyclotron parameters (*i.e.*, ν, ν_z, and ν_r) should be carefully studied. They can indicate the existence of serious problems, particularly if the fluctuations take place in a non-adiabatic manner. An example is the steep rise in ν starting at around r=48 cm in fig. 2.1. The peak in ν is not so conspicuous, but the corresponding dip in ν_z is really noticeable. Therefore, a detailed analysis of this problem will be given in connection with our discussion of ν_z.

However, this rise in ν means that there can be a corresponding reduction in the axial focusing, unless a remedial feature is included in the design (such as a rapid increase in the spiral angle at this radius). It will be seen later that this problem is actually even worse than the above discussion suggests.

Another noticeable feature of fig. 2.1 is a broad dip in ν at around r=22 cm (8.3 MeV). It is in this region that the particle's phase excursion starts rising rapidly, to reach its positive extremum (*i.e.*, trailing behind the RF) at r=31.7 cm (17.56 MeV). A corresponding dip in ν_r at around this radius (r=22 cm) is evident in fig. 2.3. This decrease in ν_z is more serious than the diminution of ν; therefore this

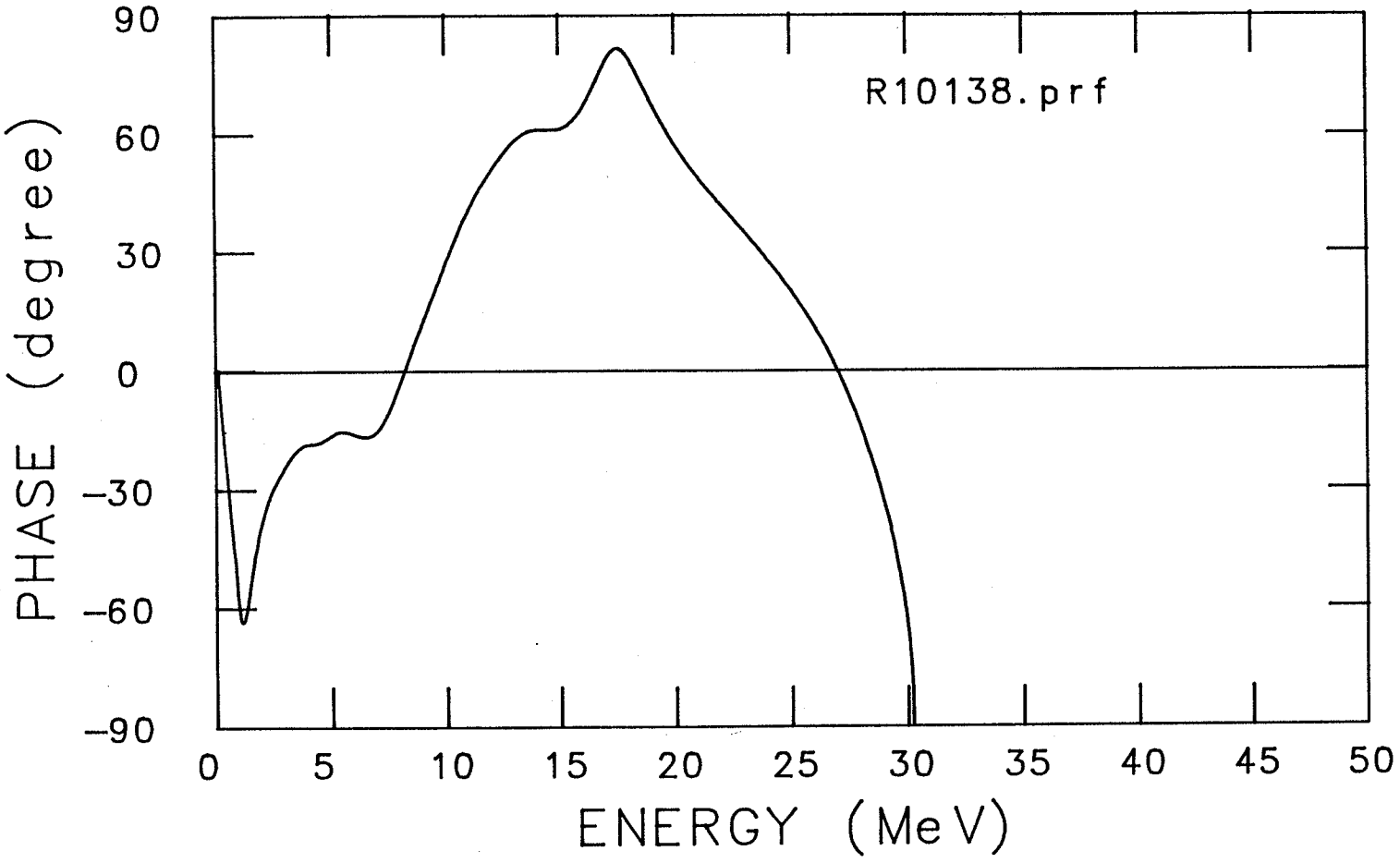

Fig. 2.4 The phase excursion of the H^- particle as a function of the energy for typical 30 MeV field that was measured in 1982.

problem will be considered later, when we discuss ν_r.

The highest energy that a given cyclotron can achieve is always of great interest. Figs. 2.1 and 2.4 indicate that the maximum energy that an ion could reach, with magnetic field configuration that leads to these figures, is about 30 MeV, a value which is in agreement with our experiences before 1984. In order to obtain beams of higher energy, the pre-1984 field used to require a small readjustment. The optimum field at the U of M cyclotron thus used to be energy-dependent. However, because of the large axial defocusing near r=48 cm, before the upgrade, the machine was not quite suitable at that time to produce energies much above 42 MeV.

The precision of the 1982 field mapping was, as mentioned earlier, 0.04%. This translated to 0.011 MHz in uncertainty in ν, an error which is large from the phase-excursion point of view.

Let us now turn our attention to the axial motion, fig. 2.2. We already considered the peak at around r=7 cm and the dip at r=48 cm. Here, we will now consider the latter problem in more detail. The dip is seen to fall to zero at r= 48 cm and then for larger radii, ν_z acquires an imaginary value, indicating that the axial motion experiences a defocusing force. The axial displacement, z, when ν_z varies adiabatically, is given by [LIV61];

$$z = \frac{const}{\sqrt{\nu_z B_0}} e^{\pm i \int \nu_z \omega dt} \quad , \tag{2.2.5}$$

where B_0 ($=\omega M/q$) is the average magnetic field, and ω is the cyclotron angular frequency. This expression indicates that the motion in the z direction grows exponentially when ν_z is imaginary with a rate of growth ($\Delta z/\Delta r$) that is proportional

to $\pm i\nu_z$, where $i = \sqrt{-1}$. Therefore, most of the ions are expected to be lost in passing through this region, either by hitting dee structures or through a serious downgrading of its quality. Fig. 2.2 shows that there is a large defocusing between r=48 and 51 cm. The extent of the defocusing can be shown to be larger than the positive gradient of ν at this region [see fig. 2.1, and eq. (2.2.1)]. It is therefore reasonable to suspect that the spiral angle might also be reduced suddenly. This effect was eventually found to be due to the presence of a large magnetic shim placed in the leading edge of each valley at this radius and further outward. The sudden rise in ν_r, starting at r=48 cm in fig. 2.3, results from the effect of this shim. This is the most serious imperfection of the U of M cyclotron that had to be corrected.

We will now consider the radial focusing, ν_r. For an AVF cyclotron, ν_r is always close to 1, resulting in strong focusing. Therefore, apart from resonances, there is not much cause for worry about radial focusing in such machines. The main contribution to the radial focusing comes from the zeroeth-harmonic component of the cyclotron magnetic field; this component is actually just the average magnetic field at a given radius. The contribution to ν_r from this term is 1 in the non-relativistic case. For an AVF cyclotron, ν_r is kept sufficiently above 1 to avoid not only the $\nu_r = 1$ resonance crossing with the first-harmonic (imperfection) field component, but also any near approach to the region of resonance with this first-harmonic component. These resonances, particularly the former, could present very serious problem. If present, they have to be carefully studied. The first-harmonic component tends to shift the center of the beam orbit along a line that is perpendicular to the direction of the harmonic field. This shift is initially a cumulative one. Eventually, the precessional motion of the beam center prevents

the shift from undergoing further increases. The number of turns at which the excursion of the center stops growing in the vicinity of this resonance is given approximately by

$$nshift = \frac{1}{\pi(\nu_r - 1)} \quad . \tag{2.2.6}$$

If we let dr denote the shift per turn caused by the first-harmonic component in the region near ν_r=1, then the maximum excursion of the beam orbit center (δr) is expressed by

$$\delta r = \frac{dr}{\pi(\nu_r - 1)} \quad . \tag{2.2.7}$$

When a resonance is crossed, δr is approximately twice as large. Since the value of ν_r stays close to unity throughout the acceleration, the shift of the beam center tends to accumulate. Therefore, an initially well centered beam might develop into a seriously off-centered beam after passing through the region of the first-harmonic field.

The seriousness of the effect of this component on the orbit center can be demonstrated by the following example. Let us suppose that a first-harmonic component of 0.2 mT is present at r= 26 cm in the U of M cyclotron. Then, from figs. 2.1 and 2.3, $B = 2\pi(m/e)\nu$ = 1.9 T, ν_r = 1.004. And, dr will be of the order of 0.1 mm. Therefore, we then have $nshift$= $1/\pi(1.004 - 1) \approx$ 80 turns, and δr= 0.1 mm/$\pi(1.004 - 1) \approx$ 8 mm. This is an unacceptably large excursion of the beam orbit center.

Such resonances are seen in fig. 2.3 to occur at three radii, with r being approximately 10, 20 and 52 cm, respectively. The resonance at r=10 cm arises from the

disappearance of the central bump field, as was discussed earlier. The H^- particle, however, remains in resonance there for only two turns, and hence this effect by itself may not be too serious.

The second resonance, at r= 20 cm, is seen to arise from a steep negative gradient in ν at this radius (r=20 cm) [see fig. 2.1 and eq. (2.2.2)]. Fig. 2.2 shows that there is a corresponding rise in ν_z [see eq. (2.2.1)]. The particle spends over 20 turns in the resonance crossing at around this radius. As was discussed earlier, the related dip in ν is also rather undesirable. This problem is the second most serious imperfection that had to be corrected in the U of M cyclotron.

A third resonance occurs at a radius of approximately 52.3 cm. This happens beyond the 48 cm radius (*i.e.*, in a region where most of the beam is lost due to the lack of axial focusing). This problem is therefore of little practical interest.

The coupling resonance between the radial and axial motion can cause a serious problem if uncorrected. This type of resonance is expressed by

$$m\nu_z + n\nu_r = l \quad , \tag{2.2.8}$$

where l, m, n are all integers. Again, only the lowest-order resonances are of importance. For l=0, figs. 2.2 and 2.3 indicate that $2\nu_z = \nu_r$ is the only resonance that could have significance. It occurs at a radius of about 52.5 cm. For $l \neq 0$, we have couplings of the axial, the radial and the l^{th}-harmonic imperfection fields. This resonance is seen to occur at r= 11 cm, where the condition $\nu_r - \nu_z = 1$ is almost satisfied. The seriousness of this problem depends also upon the strength of the first-harmonic component of the field, a value that is, at the most, several gauss.

Since the first-harmonic component of the field was not measured, this resonance was not investigated.

In general, it is highly desirable to keep ν_z between 0.1 and 0.5. Otherwise, a dangerous $\nu_r = 2\nu_z$ coupling (or Walkinshaw) resonance may result. In crossing the Walkinshaw resonance, the transverse energy of a beam can be transferred to the longitudinal one [COU58], or *vice versa*, resulting in a large axial oscillation. This effect will be treated in more detail in a later section of this chapter.

The 1982 data also included a series of mappings of the D^- field. Arguments similar to those that were presented above revealed that the field for D^- ions also had large deviations from isochronism—deviations which actually appeared to be more serious than the deviations from isochronism for the H^- ions. The axial focusing was found to suffer badly, and by the time the beam reached a radius where the particle could be extracted, the beam had already deteriorated in the axial direction and suffered from a large phase excursion. The phase excursion is seen to accumulate all along the radius. These two combined effects, thus, could explain why the maximum obtainable energy for D^- beam was 19 MeV instead of achieving the design goal of 22.5 MeV.

It is now clear that the magnetic field in the U of M cyclotron had serious imperfections before 1984. These problems could be corrected only by reoptimizing the cyclotron field through a series of field mapping and shimming programs. None of the above-mentioned imperfections could be corrected by simply readjusting the temperatures of Invar blocks. We therefore decided to carry out an ambitious major upgrading program that began in November 1983. The field mapping and shimming program was the first step of this project.

In the remainder of this chapter we will consider the methods and the analyses of this new field mapping. The experimental procedures will be outlined here only to the extent necessary for the reader to understand the basic principles that are involved. Instead, our emphasis will be placed on presenting the theoretical methods used in the data analyses and on describing the results of the field mappings in 1984.

2.3 The 1984 mapping apparatus

The method of the 1984 field measurement was basically the same as the one that was utilized in 1982, *i.e.*, the "flipping coil method" [BRU83]. The apparatus which was originally used in the 1982 mapping program was upgraded for this purpose. It consisted of an assembly of 52 coils equally spaced along the radius of the cyclotron, apart 1.27 cm (0.5″). With this instrument we scanned in the median plane of the cyclotron at one azimuthal angle, and then successively moved the assembly through two azimuthal degree (2°) intervals until a whole sector (90°) was covered. The coils were recalibrated, prior to the 1984 mapping, to a better precision than in 1982. The currents induced in coils, when the coils were flipped, flowed to chopper-stablized integrators in a temperature-stabilized environment. A digital voltmeter measured individual integrated voltages through the multiplexer. All the data and control signals passed through interfaces on a LSI-11/23 microcomputer. Once a mapping had been started, this computer controlled all the measuring events and recorded the field measurements at uniform intervals of azimuth and time. All the mappings were carried out in a vacuum. The resulting raw field values were transferred to the VAX-11/750 computer to be stored in the disk. Before starting the next mapping, this stored data was analyzed thoroughly (by the method that will be described in the next section), making it possible to utilize these results in preparing for the

next mapping.

2.4 Data analysis and results

The raw field mapping data from the LSI-11/23 computer were transformed into a form that could be utilized for the final analysis. During this procedure, any bad data were rejected and such data were replaced by those obtained by interpolating between the adjacent field values. After that, the fields were Fourier-analyzed to sort out the intrinsic harmonic components (multiples of the magnetic field periodicity). These intrinsic harmonic components are the field components to be used for the final analysis. The resulting magnetic field in the median plane (z=0) of the cyclotron can then be expanded as

$$B_z(r,\theta) = B_0(r) + \sum_{n=1}^{\infty}(H_{nN}(r)\cos nN\theta + G_{nN}(r)\sin nN\theta) \quad , \qquad (2.4.1)$$

where $B_0(r)$ is the average field (averaged over all θ) at radius r, and N is the number of magnet sectors (which is 4 for the U of M cyclotron). Here, $H_{nN}(r)$ and $G_{nN}(r)$, represent the amplitudes of the n^{th} multiples of the N^{th} harmonic component of the magnetic field.

Once the magnetic field in the median plane is known, the field off the median plane can be calculated by using expansion method. The results can then be expressed as

$$\begin{aligned} B_z(z) &\approx B_z(0) \\ B_r(z) &\approx z\left(\frac{\partial B_r}{\partial z}\right)_{z=0} = z\left(\frac{\partial B_z}{\partial r}\right)_{z=0} \\ B_\theta(z) &\approx z\left(\frac{\partial B_\theta}{\partial z}\right)_{z=0} = \frac{z}{r}\left(\frac{\partial B_z}{\partial \theta}\right)_{z=0} \quad , \end{aligned} \qquad (2.4.2)$$

where we used $\nabla \times \vec{B} = 0$.

The main analysis was carried out by using the program MAPANL which was developed at the U of M Cyclotron Laboratory. The basic algorithm of MAPANL was introduced in the work of Gordon and Welton ([GOR59], [WEL59]) who developed methods to find the equilibrium orbit and to calculate ν, ν_r, ν_z, *etc.* as functions of the energy. The *mks* system of units is used in MAPANL, in contradistinction to the original program of Gordon and Welton's, which employed the "cyclotron" system of units.

With the particle energy as an input, the program integrates the equations of motion over one magnetic field periodicity (90°) using the azimuthal angle (θ) as the independent variable. Since the equlibrium orbit, by definition, is smoothly closed on itself, the initial values of r and p_r are the same as the final values of these variables along the equiliblium orbit. The determination of an equilibrium orbit then reduces to the determination of the initial values of r and p_r, as is detailed below.

First, the radial equations of motion are integrated numerically, to obtain r and p_r through a process of successive iteration, and to determine the transfer matrix over one periodicity. Once r and p_r have been found, then subsequently all the equations including the axial equations, are integrated. Then the knowledge of transfer matrices for the radial and the axial motions enables us to calculate ν_r and ν_z by using the following two relations [LIV61]:

$$\nu_r = \frac{1}{\theta_0}\cos^{-1}\left(\frac{J_{11}+J_{22}}{2}\right), \qquad \nu_z = \frac{1}{\theta_0}\cos^{-1}\left(\frac{K_{11}+K_{22}}{2}\right) \quad . \tag{2.4.3}$$

Here, θ_0 is 2π divided by the number of sectors and J_{ij}, K_{ij} are the corresponding elements of the radial and axial transfer matrices, respectively. From the above

equations, it is apparent that the motion stays bounded if the absolute value of the trace of each of the transfer matrices is less than two.

The revolution frequency, ν can be easily evaluated after all the integrations over one periodicity have been carried out with respect to the independent variable θ. This is because the time t is also integrated as a function of θ. See references ([GOR59], [WEL59]) for the explicit forms of the equations of motion and for more details about the computing procedures.

By repeating the above proceduress for different input energies, one can obtain curves of ν, ν_z and ν_r, all as functions of r. These three values were then investigated to obtain improved shapes and locations for shims to be placed inside the cyclotron in order to enhance its operation. On the basis of these three curves, we can also choose a better set of temperature settings for the Invar blocks for the succeeding mapping. The shims, after being machined, were placed in the indicated position inside the cyclotron. We then closed the cyclotron for pumping, reset the temperature of the Invar blocks and waited for the temperature to reach equilibrium. The cycle time of this successive process was typically of the order of one day. During a three month period in 1984, we were able to complete over 80 mappings. Our primary objective was to correct the three imperfections, to improve isochronism, and to enhance ν_z all the way down to a radius as small as 2 cm (the radius for the second turn of the particle's orbit). We aimed to achieve these goals, for both the H^- and D^- ions, throughout the entire length of the cyclotron.

2.4.1 The magnetic field for the H^- ion

The results of the field mappings for an H^- ion are depicted in figs. 2.5, 2.6,

and 2.7. They indicate that the three serious defects of the field, mentioned earlier, have now all disappeared. The improvement in isochronism can be clearly seen by comparing fig. 2.5 with fig. 2.1. The width of the fluctuations in ν, for instance, is 190 kHz in fig. 2.1 whereas it is only 60 kHz in fig. 2.5. The axial focusing frequency, ν_z, has also improved significantly, as can be seen by comparing fig. 2.6 with fig. 2.2. All of these improvements were achieved by readjusting the Invar centigrade temperatures (T_1=110, T_2=180, T_3=215, T_4=130, T_5=215, T_6=160, T_7=80, T_8=35° C), by choosing the main magnet current to be 2830 A, and by placing three set of shims in the valley. The first set of shims, a very large one, extends from the 40 cm radius to the outer edge of pole-tips, and is placed on the trailing edge of the valley. The second set of shims is medium size, and is centered around the 20 cm radius. The third set is a small one, and is located at a radius of approximately 8 cm. This last set of shims was introduced in order to reduce the slope of ν in this region and to extend the central bump field further out, while at the same time improving the behaviors of ν_z in this region.

The degree of improvement can also be seen from fig. 2.8. This graph shows the beam phase excursion as a function of energy, obtained by using eq. (2.2.4). The solid curve represents the case for which the beam can reach 50 MeV by going through the least number of turns. In this calculation, we have neglected a small (less than 5%) difference in dee voltage between the injection and the extraction radii. The parameters that were substituted into eq. (2.2.4) had the following values: $\phi_0 = +45°$, $h = 1$, $\omega_{RF} = 2\pi \times 28.3709$ MHz, E_i= 32 keV, E_f= 50 MeV, and E_1 ranging from 80 keV to 160 keV, depending on the turn number. From fig. 2.8 we see that the phase excursion has improved significantly. Except for the

Figs. 2.5, 2.6, 2.7 Results of the magnetic field mapping that was carried out in 1984. For each plot, the horizontal axis denotes the radius of H^- ion in centimeters, and the vertical axis represents the H^- ion's revolution frequency (fig. 2.5), axial focusing frequency (fig. 2.6) and radial focusing frequency (fig. 2.7) in figs. 2.5, 2.6 and 2.7, respectively.

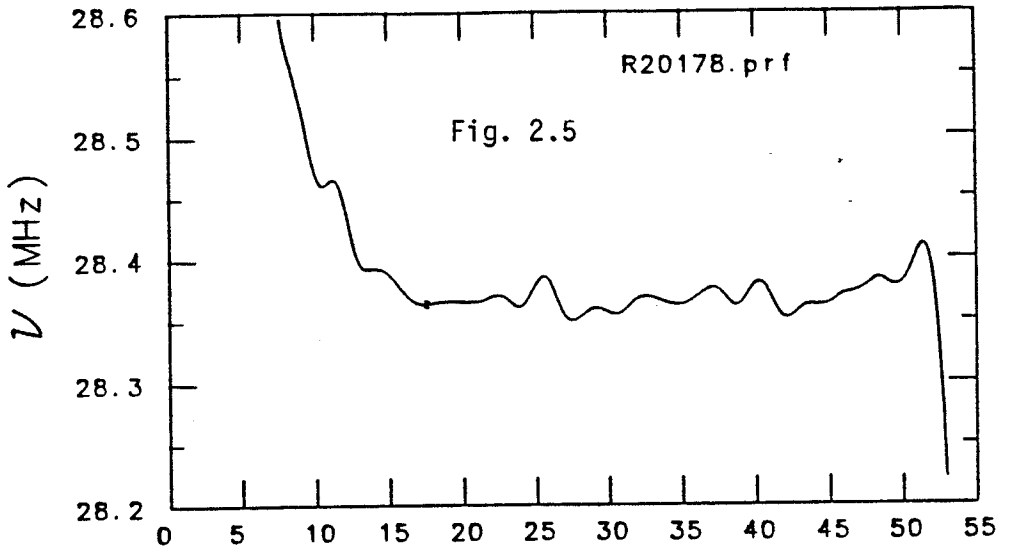
R20178.prf
Fig. 2.5
ν (MHz)
28.6
28.5
28.4
28.3
28.2
0 5 10 15 20 25 30 35 40 45 50 55

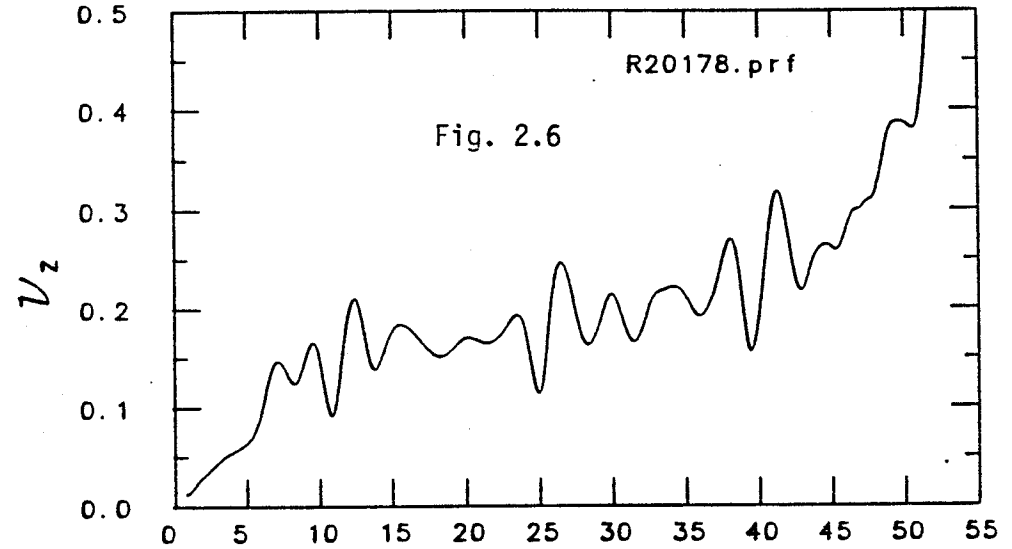
R20178.prf
Fig. 2.6
ν_z
0.5
0.4
0.3
0.2
0.1
0.0
0 5 10 15 20 25 30 35 40 45 50 55

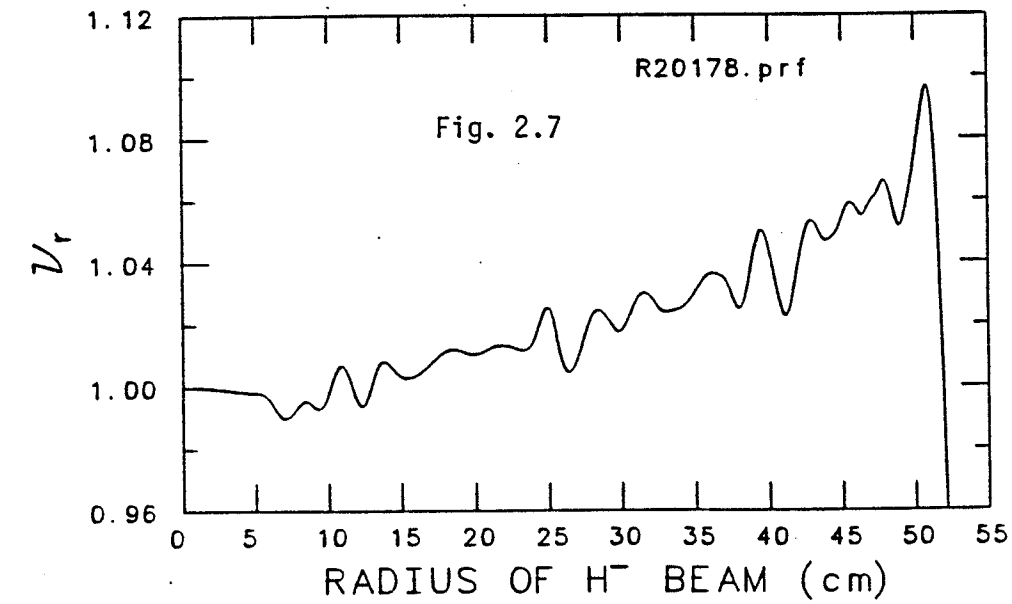
R20178.prf
Fig. 2.7
ν_r
1.12
1.08
1.04
1.00
0.96
0 5 10 15 20 25 30 35 40 45 50 55
RADIUS OF H⁻ BEAM (cm)

central region (where there is a bump field), the phase excursion is contained within the range from $-17°$ to $+14.5°$. The precision of the field mapping was estimated to be 0.01%. Since this corresponds to an uncertainty in the phase excursion of $\pm 12°$ (when the total number of turns of orbit is assumed to be 630, which is close to what is observed after the upgrade), further improvements in the phase excursion much beyond this range cannot be expected.

The radial dependence of the isochronism upon four sets (out of the eight sets) of radial gradient Invar blocks was also investigated. The measurements for the remaining four sets were not carried out because the allocated time for the mapping program had expired. Fig. 2.9 shows the change in isochronism, with radius, when the temperature of each Invar block set was raised by 10°C. The change in isochronism ranges between 3 and 70 kHz, which represents a shift of one part in 10^4 in the frequency ratio, $\Delta\nu/\nu$. It is estimated that each flip coil can measure a difference in the field of 0.03 mT ($\Delta\nu/\nu \approx 10^{-5}$). The overall precision of a mapping is determined mainly by the calibration errors of two adjacent flip coils, whereas the change in the field value at a specific point (caused by the temperature variation) is measured by one and the same flip coil, thus making the attainable precision higher for the latter measurement. The dotted curve in fig. 2.8 represents the phase excursion after the isochronism was computer-optimized among the four sets of Invar blocks mentioned above ($\Delta T_6 = -10°$ C, $\Delta T_7 = +10°$ C). This curve suggests that the phase excursion may be further reduced to $\pm 10°$.

An improvement in axial focusing can also be seen clearly from fig. 2.6. The disappearances of the axial focusing at radii of 10 and 48 cm (see fig. 2.2) have obviously been corrected. Furthermore, ν_z is now seen to increase smoothly throughout

Fig. 2.8 The phase excursion (solid curve) of the H^- particle as a function of the energy for upgraded field in 1984. The dotted curve represents the predicted phase excursion after carrying out a computer-optimization of the temperature of Invar blocks (see fig. 2.9). In order to obtain the dotted curve, the temperatures of the number 6 and the number 7 Invar blocks were decreased and increased by 10°C, respectively. Comparing this figure with fig. 2.4, a marked improvement in isochronism for the new field can be seen clearly.

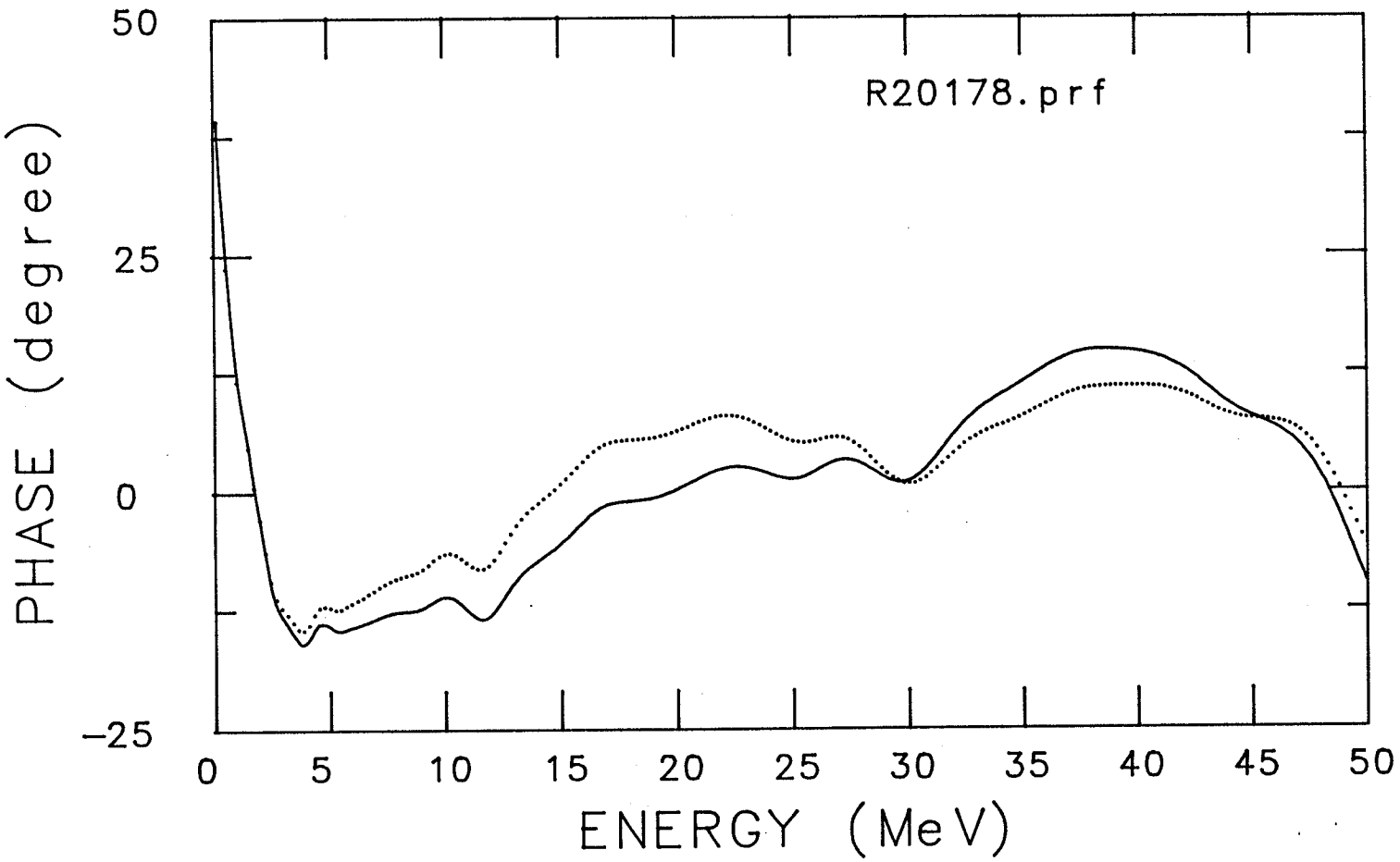
R20178.prf
PHASE (degree)
50
25
0
−25
0
5
10
15
20
25
30
35
40
45
50
ENERGY (MeV)

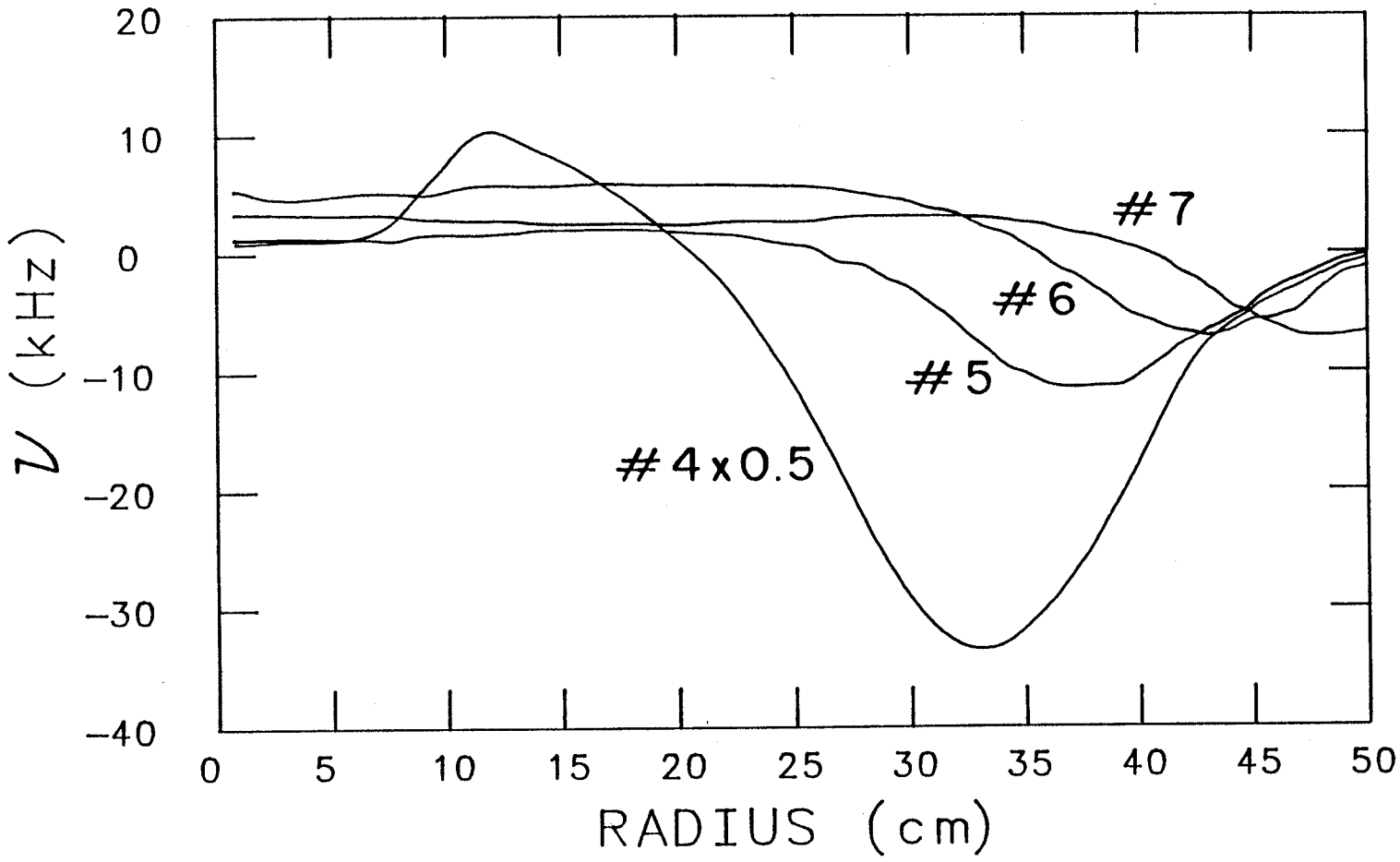

Fig. 2.9 The data for the change in revolution frequency (or magnetic field) for varying the temperature of each Invar (4,5,6,7) by +10°C.

the entire region.

The radial focusing has also improved significantly. When fig. 2.7 is compared with fig. 2.3, one immediately notices the disappearance of the two big dips. On the basis of this result, it is expected that both the transmission efficiency and the stability of a beam will have been improved.

2.4.2 The Magnetic field for the D^- ion

Significant improvements in the isochronism and the axial focusing have also been achieved for the magnetic field for the D^- ions. This can be seen from figs. 2.10, 2.11 and 2.12. It is seen there that $\delta\nu$ between 13 and 40 cm is within 30 kHz (60 kHz with the second-harmonic mode of acceleration). This improvement, for the D^- ion, was achieved without any change in the shims that were placed to upgrade the H^- field. Only the temperatures of the Invar blocks had to be readjusted (T_1=40, T_2=50, T_3=154, T_4=95, T_5=230, T_6=105, T_7=180, T_8=230° C), and the main magnet current was chosen to be 3350 A. A dip in ν in the outer region still appears. However, we believe that this dip can be reduced by readjusting the temperature of the sixth and the seventh Invar blocks. This was indirectly verified when we substituted the corresponding H^- field data into the region corresponding to the number six and seven Invar blocks. The result is displayed in fig. 2.13. The dip is seen to be largely removed, so that the maximum D^- ion energy attainable with this configuration extends to 26 MeV.

The radial contour maps of the new magnetic field in the median plane of the cyclotron for the H^- and the D^- ions are depicted in figs. 2.14 and 2.15, respectively.

Figs. 2.10, 2.11, 2.12 Results of the magnetic field mapping that was carried out in 1984. For each plot, the horizontal axis denotes the radius of D^- ion in centimeters and the vertical axis represents the D^- ion's revolution frequency (fig. 2.10), axial focusing frequency (fig. 2.11) and radial focusing frequency (fig. 2.12) in figs. 2.10, 2.11, and 2.12, respectively.

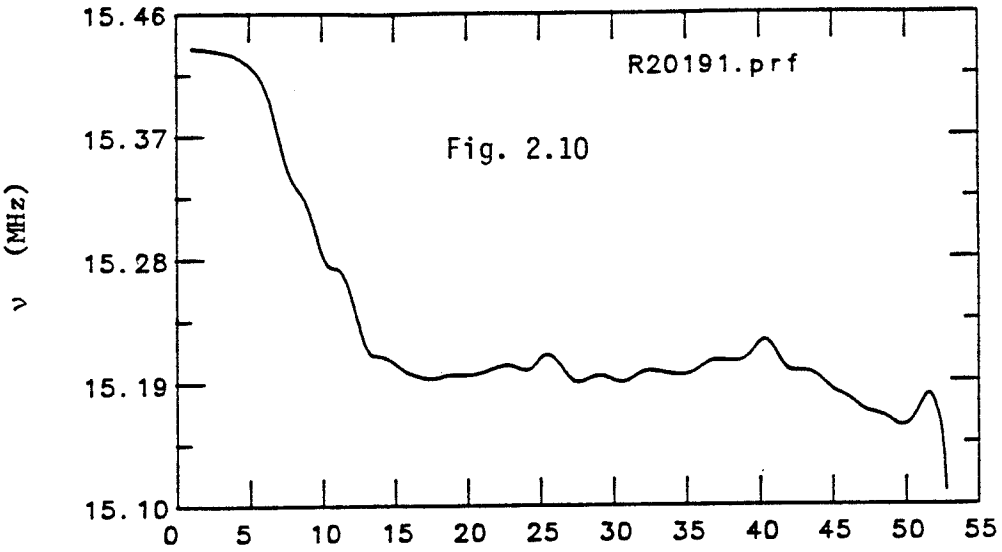
R20191.prf
Fig. 2.10
ν (MHz)
15.46
15.37
15.28
15.19
15.10
0 5 10 15 20 25 30 35 40 45 50 55

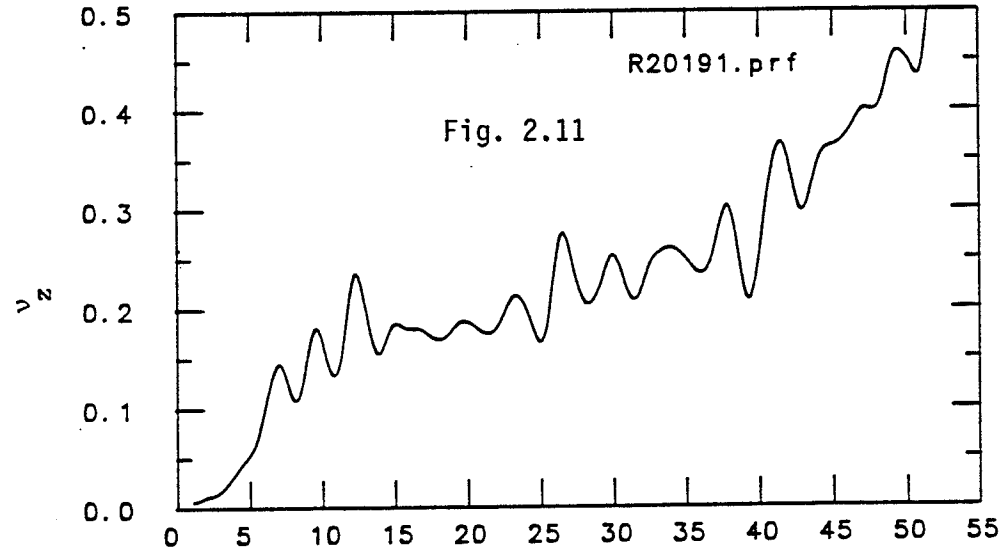
R20191.prf
Fig. 2.11
ν_z
0.5
0.4
0.3
0.2
0.1
0.0
0 5 10 15 20 25 30 35 40 45 50 55

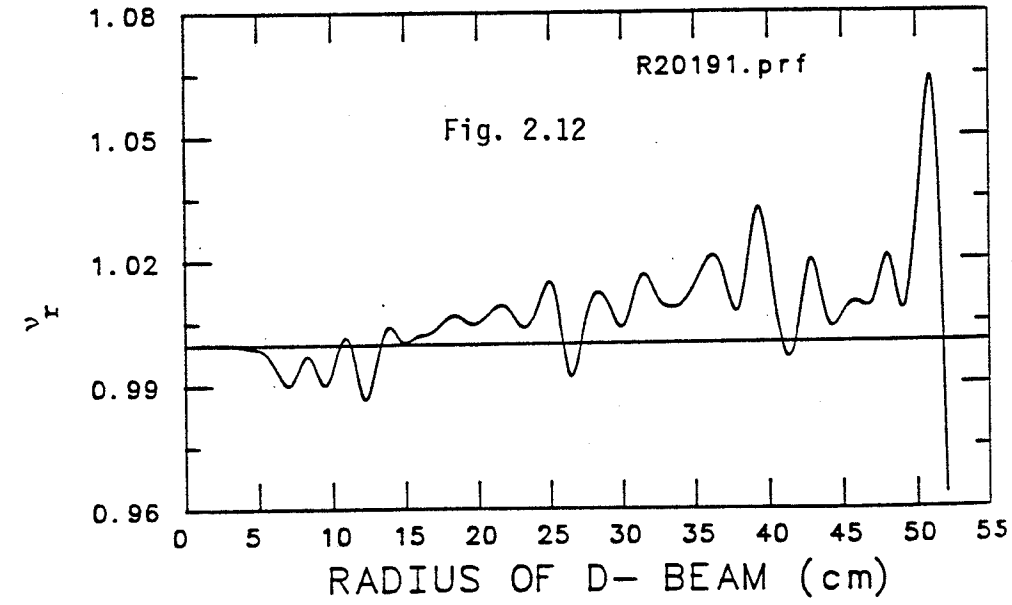
R20191.prf
Fig. 2.12
ν_r
1.08
1.05
1.02
0.99
0.96
0 5 10 15 20 25 30 35 40 45 50 55
RADIUS OF D− BEAM (cm)

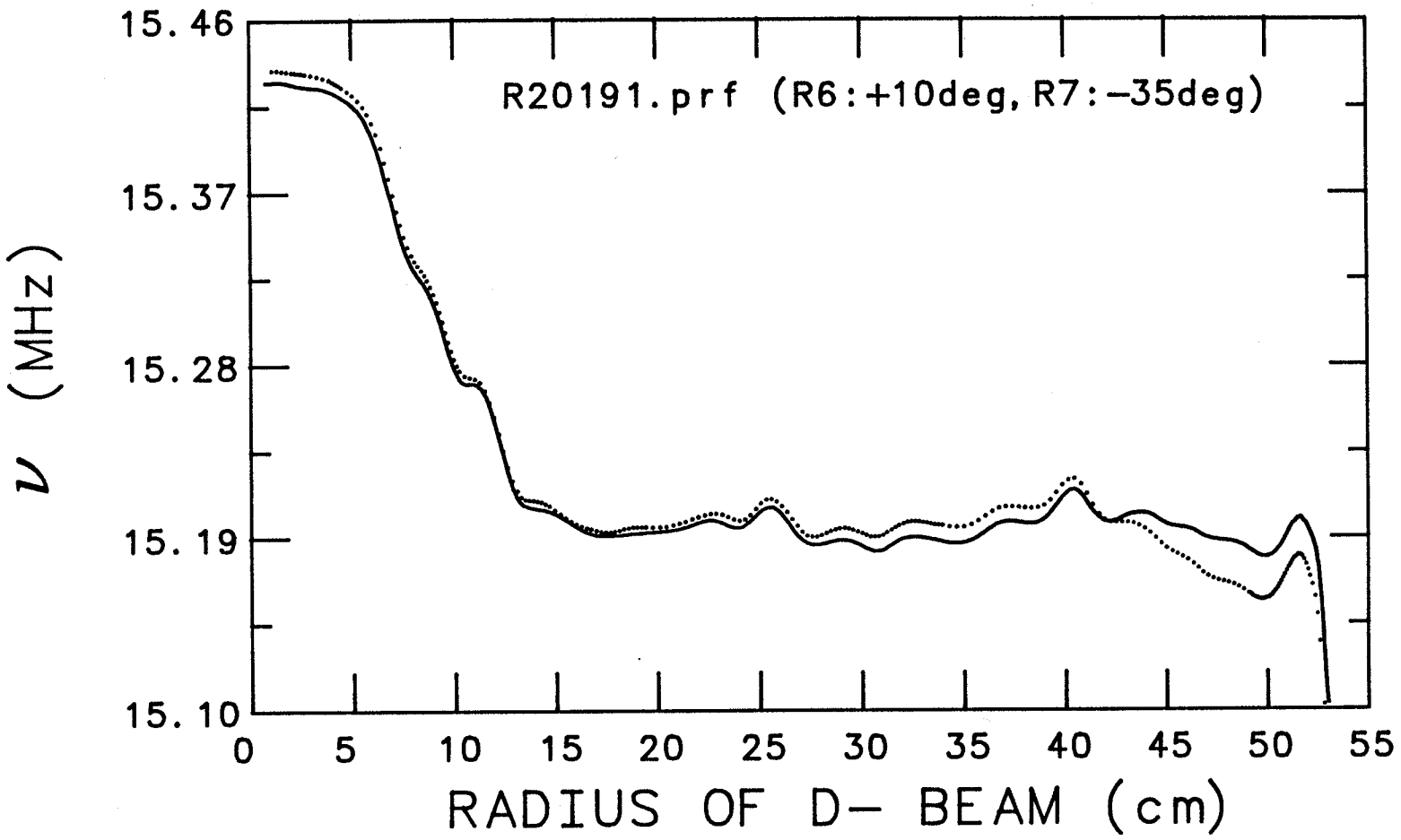

Fig. 2.13 The modified and improved revolution frequency (solid curve) of the D^- ion in the 1984 field. The dotted curve represents the revolution frequency without modification. In obtaining the solid curve, the temperatures of the number 6 and 7 Invars were changed by the amount shown in the figure.

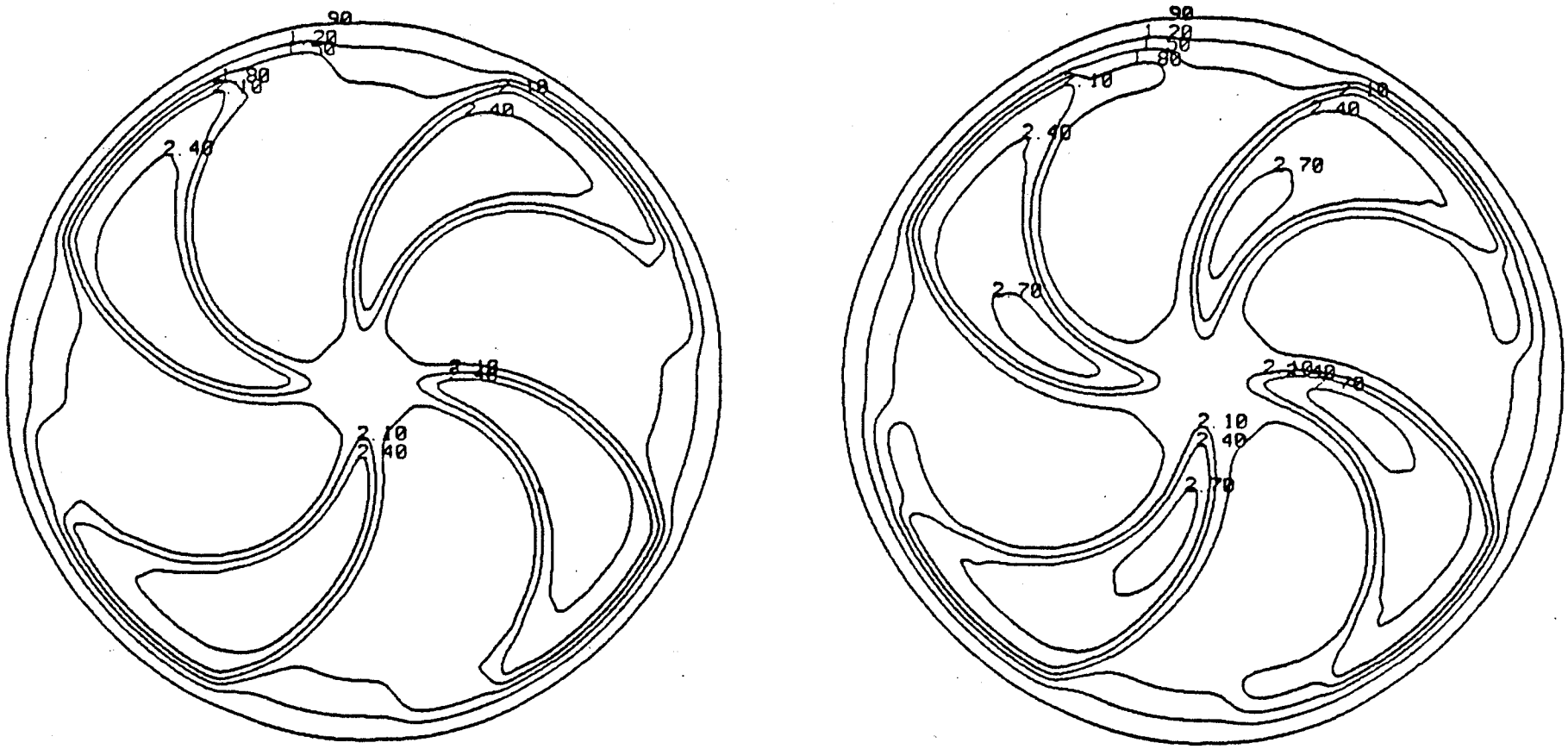

Figs. 2.14, 2.15 The radial contour map of the H^- field (fig. 2.14) and of the D^- field (fig. 2.15) of the University of Manitoba cyclotron. In obtaining the figures, four-fold symmetry of the magnetic field was assumed.

2.4.3 Summary of resonances in the University of Manitoba cylotron

As was discussed earlier, the crossings of the integer resonance is not a problem in the U of M cyclotron.

It was shown ([COU58], [HOP66]) that sum resonances [m and n having the same sign in eq. (2.2.8)] may lead to instabilities. This is because energy is transferred from the rotational to the betatronic motion. On the other hand, difference resonances, when m and n have opposite signs, we have a sharing of energy between the motions in the r and z directions, and in this case, the increase of the amplitude is limited. In any case, the system is stable even at resonance whenever

$$|m| + |n| > 5. \tag{2.4.6}$$

See [COU58] for more detail. If the above equation is applied to the U of M cyclotron, which has a four-sector structure, we see that the possible resonances which may lead to serious instabilities include the following equations:

$$\begin{aligned} \nu_r + 2\nu_z &= 1 \\ \nu_r - 2\nu_z &= -1 \\ 2\nu_r - \nu_z &= -1 \\ \nu_r &= \nu_z \\ \nu_r + \nu_z &= 2 \\ \nu_z &= \frac{\nu_r}{2}. \end{aligned} \tag{2.4.7}$$

The crossings of these resonances for the H^- and the D^- ions are plotted in fig. 2.16. This figure shows that, in the U of M cyclotron, the resonance crossings for

both types of ions occur beyond the maximum extraction energy. An exception is the Walkinshaw resonance ($\nu_r = 2\nu_z$), for the H^- beam, that is encountered at 49.6 MeV. As was discussed earlier, as the ions pass this resonance, the radial oscillation energy is transferred to the axial oscillation energy, or *vice versa*. In our case, the energies of these two modes are not expected to differ significantly as long as the oscillation amplitudes are small (less than 2 mm for the radial and less than 3 mm for the axial). Therefore, no further studies have been carried out concerning the effects of the crossings of such a resonance.

In an effort to expedite the program, the mapping was cut short and covered only one sector of the field. As a result, the investigation of imperfection-induced resonances was not carried out.

Fig. 2.16 The coupling resonance crossings for the H^- and D^- ions in the University of Manitoba cyclotron. Each dotted line represents:
1: $\nu_r - 2\nu_z = -1$
2: $\nu_r + 2\nu_z = 1$
3: $\nu_r = \nu_z$
4: $\nu_r = 2\nu_z$
5: $2\nu_r - \nu_z = -1$
6: $\nu_r + \nu_z = 2$
It is seen that most of the resonance crossings occur beyond the maximum extractable energies that are represented by the filled circles. The Walkinshaw resonance (*i.e.*, $\nu_r = 2\nu_z$) crossing for the H^- ions at 49.6 MeV is not considered as a problem because of the smallness in the oscillation amplitude at around this region.

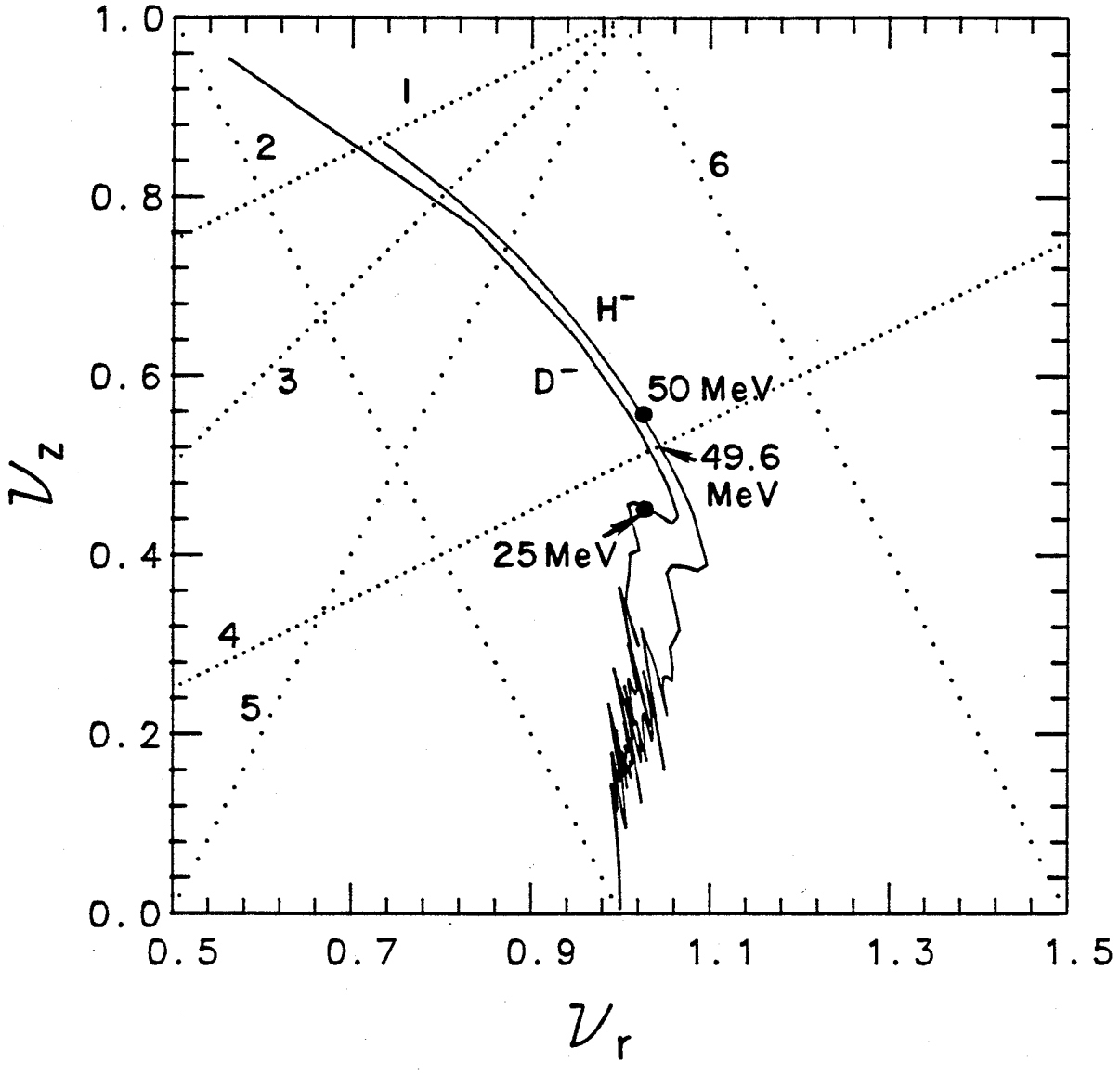
1.0
0.8
0.6
0.4
0.2
0.0
0.5
0.7
0.9
1.1
1.3
1.5
ν_z
ν_r
1
2
3
4
5
6
H⁻
D⁻
50 MeV
49.6 MeV
25 MeV

Chapter 3

The New Central Region and the H^- Beam Orbit Dynamics

3.1 Introduction

In the beginning of this thesis we noted that the idea of an azimuthally varying field (AVF) led to the emergence of a sector-focused cyclotron, for which the axial focusing term from this AVF component was found to be independent of the requirement of isochronism. To be more specific, we will now look into the first-order expression for the axial focusing frequency for a sector-focused cyclotron. It is given by [SYM56]

$$(\nu_z)^2 = k + F(1 + 2\tan^2\alpha) \qquad , \tag{3.1.1}$$

where k is a field index defined by $-(r/B)(dB/dr)$ and α describes the spiral angle of the magnetic field [LIV61]. The flutter function, F, is actually a measure of the azimuthally varying part of the magnetic field, and is defined by

$$\begin{aligned} F &= \frac{\langle B^2\rangle - \langle B\rangle^2}{\langle B\rangle^2}, \qquad where \qquad \langle\cdots\rangle = \frac{1}{2\pi}\int_0^{2\pi}\cdots d\theta \\ B &= B(r,\theta,z=0) = \langle B\rangle + \sum_{n=1}^{\infty} B_{nN}(r)\cos nN(\theta - \delta(r)), \end{aligned} \tag{3.1.2}$$

where N is the total number of identical sectors (which is 4 for the U of M cyclotron). Eq. (3.1.1) indicates that the second term, the term that is related to the axial focusing due to an AVF does not depend upon the first term (which is required to be negative to satisfy the isochronous condition). Therefore, if the value of the second term is much greater than that of the first term, then ν_z^2 becomes positive, a condition which is enough to provide a sufficient focusing force in the axial direction.

In general, however, the flutter field in a sector-focused cyclotron begins only at a certain distance from the center of the cyclotron. Such is the case in the U of M cyclotron, as can be seen from fig. 3.1, where the amplitudes of the first five intrinsic harmonic field components [$B_{n\times 4}(r)$ in eq. (3.1.2)] are plotted as a function of the distance from the center of the machine. From the profiles of the harmonic components, we see that they are small near the center of the cyclotron. We therefore have, at small radii,

$$B \approx \langle B \rangle, \qquad F \approx 0, \qquad \nu_z^2 = k < 0 \qquad . \tag{3.1.3}$$

The beam would then experience an exponential growth in the z (axial) direction, as is indicated by eq. (2.2.5). This has disastrous consequences because the vacuum chamber or the dee is of fixed height in any cyclotron.

To solve this problem, Richardson [RIC65] suggested that a magnetic cone (*i.e.*, "field bump") be inserted at the center of a machine. By so doing, the magnetic field away from the center decreases and approaches the isochronous field value, causing k to be greater than zero and ν_z^2 to be positive. Therefore axial focusing can be achieved. In the U of M cyclotron, this approach is utilized and through the use of a pair of center plugs a bell-shaped field bump of approximately 250 gauss at peak has been achieved. Subsequently the effect of this field extends up to approximately 13 cm ($\sim 5''$) in radius (see fig. 3.2).

However, figs. 2.6 and 2.11 indicate that in the U of M cyclotron, the focusing effect due to the field bump starts to become evident at radii larger than 7 cm. These two figures clearly show that the values of ν_z for radii that are smaller than 7 cm, for both H^- and D^- ions, are still less than 0.1, values which are too small

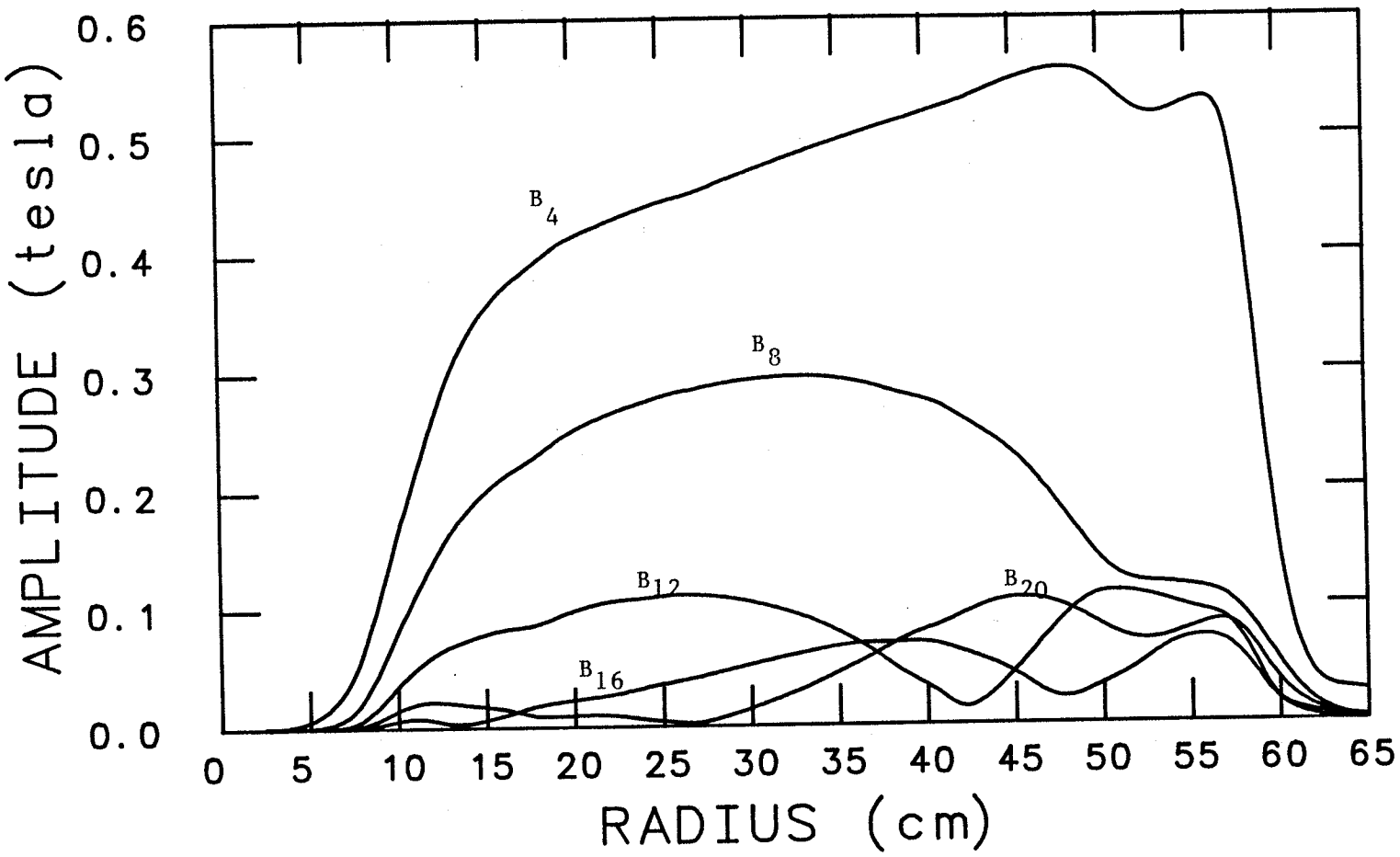

Fig. 3.1 The amplitudes of the first five perfect harmonic components of the H^- field in the University of Manitoba cyclotron. This figure indicates that the effect of these perfect harmonic components becomes appreciable after the radius of about 7 cm.

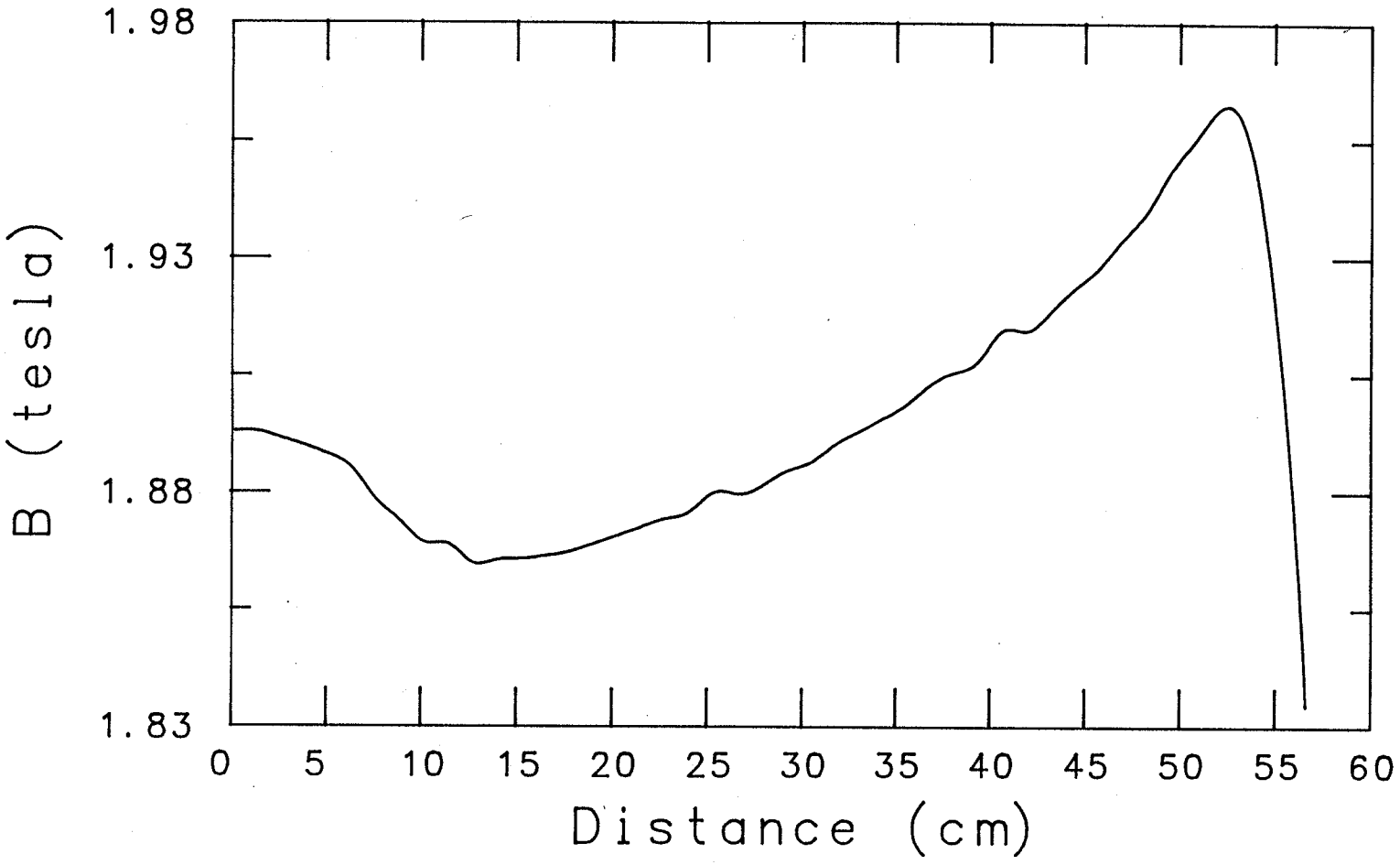

Fig. 3.2 The average magnetic field for the H^- ion of the University of Manitoba cyclotron. It is seen that the effect of the field bump, that is required to improve the axial focusing near the center of the cyclotron, extends up to about 13 cm.

to provide a sufficient focusing force. This lack of focusing can be attributed to the uniformity of the magnetic field in the region near the beam injection point. We note that obtaining an adequate focusing force in this region is very necessary, because the subsequent motion of a beam is greatly dependent upon its motion in the early turns.

As we will see later in this chapter, such a focusing force in the central region can be provided by the electric field. The precise control of the beam's early motion can then be achieved by properly designing the electrodes (dee-tips in the case of the U of M cyclotron), by utilizing the results of the studies of the beam orbit dynamics.

The above considerations, therefore, led to an ultimate decision to carry out a design study of the new dee-tips for the U of M cyclotron. This investigation was initiated in 1982, soon after the analyses of the results of the 1982 field mapping. In view of the problem described above, the goals of that design study were aimed to obtain sufficient axial focusing near the center of the cyclotron, thereby improving the beam quality of both the H^- and D^- ions. Therefore, plans were made for the introduction of two separate dee-tips, one for the H^- ion acceleration and the other for the D^- ion acceleration. This would make it possible for the D^- ions to be accelerated in the second-harmonic mode, and consequently should lead to a significant improvement in beam quality for both the H^- and D^- ions, as is described below.

For a cyclotron with a two-dee structure, the approximate formula for the energy

gain per turn can be written as

$$\Delta E = 4qV_D \sin\frac{N\theta_D}{2}\cos\phi_0 \quad , \tag{3.1.4}$$

where q is the charge number, V_D the dee voltage, N the integral harmonic number, θ_D the dee angle, and ϕ_0 the RF phase in the middle of the dee gap. The integral harmonic number is defined as ω_{rf}/ω_0 where ω_{rf} is the angular oscillation frequency of the electric field and ω_0 is the cyclotron frequency. Assuming that the fields are perfectly isochronous, *i.e.*, $\phi_0 = 0$, if one plots $\Delta E/4qV_D$ as a function of θ_D for N=1 and N=2 respectively, then fig. 3.3 is obtained. It shows that in order to gain maximum energy, the dee angle should be 180° for the N=1 mode while it would have been 90° for the N=2 mode. However, if only one single central region is to be utilized with both N=1 and N=2, then an optimization of the dee angle should be carried out and fig. 3.3 indicates that this angle should be 120°. Having two central regions which are optimized individually for each harmonic mode, therefore, leads to a notable increase in the energy gains for both the H^- and the D^- ions, thereby reducing the total number of turns that are required in order to reach a desired energy. This in turn mitigates any undesirable effects on the motion of the beam that may arise from any imperfections of the magnetic fields. The overall outcome would then be a significant enhancement in beam quality.

The newly designed dee-tips for H^- and D^- ions, as viewed from the top of the cyclotron, are depicted in fig. 3.4, where the trajectories of particles are also given. The difference in their dee angles is apparent.

In the rest of this chapter, we will now present a detailed computer-aided design study of the new central region for the H^- ions. We shall first review briefly the

Fig. 3.3 Plot for the energy gain of the particle per turn vs. the dee angle. This figure shows that for the first-harmonic mode of acceleration, the maximum energy gain can be obtained when the dee angle is 180°. On the other hand, this angle has to be 90° for the maximum energy gain in the second-harmonic mode of acceleration. For double-harmonic mode system, the optimization of the dee angle should be carried out and the figure indicates that it would have to be 120° [see eq.(3.1.4)].

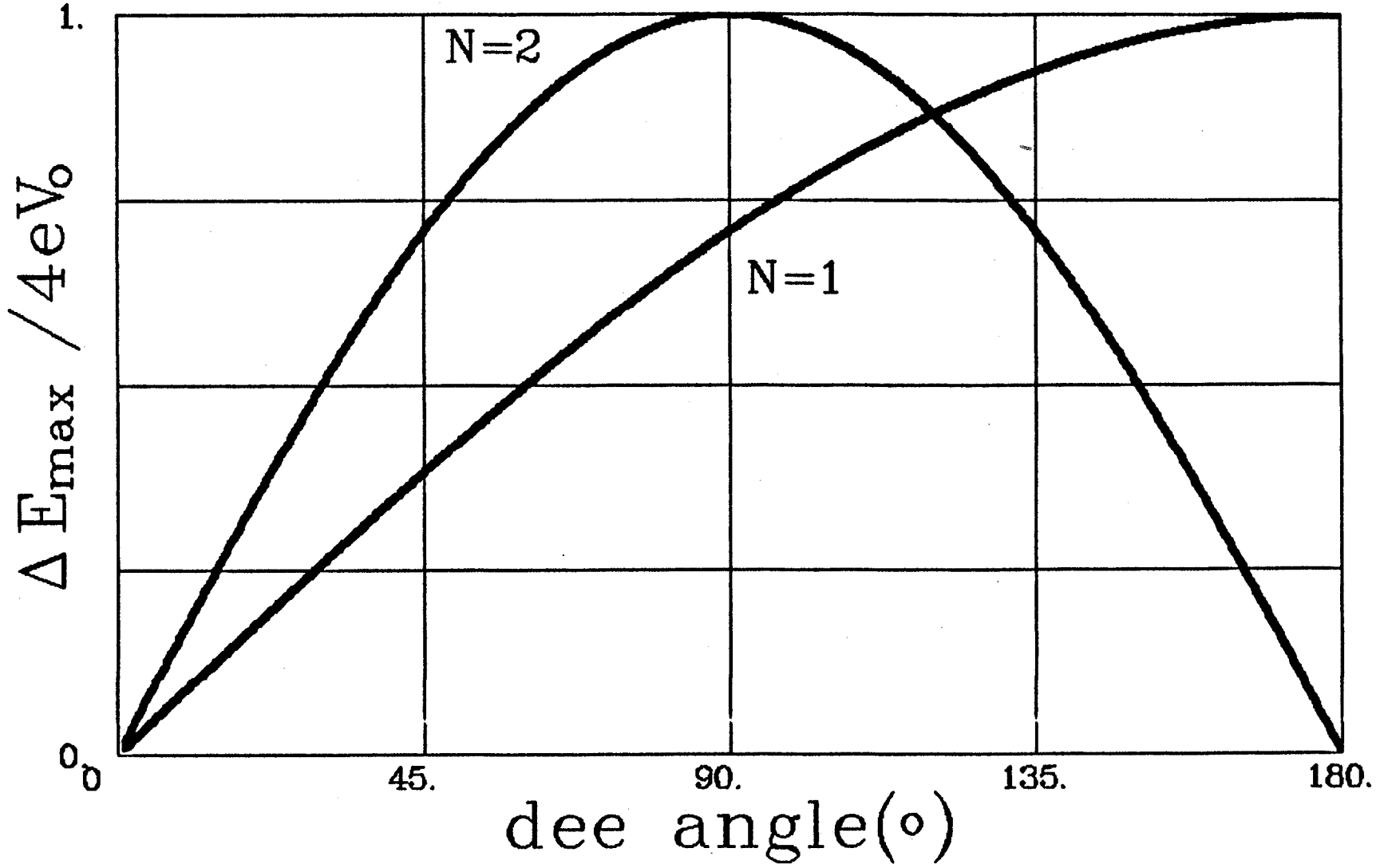
1.
0
0
45.
90.
135.
180.
N=2
N=1
Δ Emax /4eVo
dee angle(°)

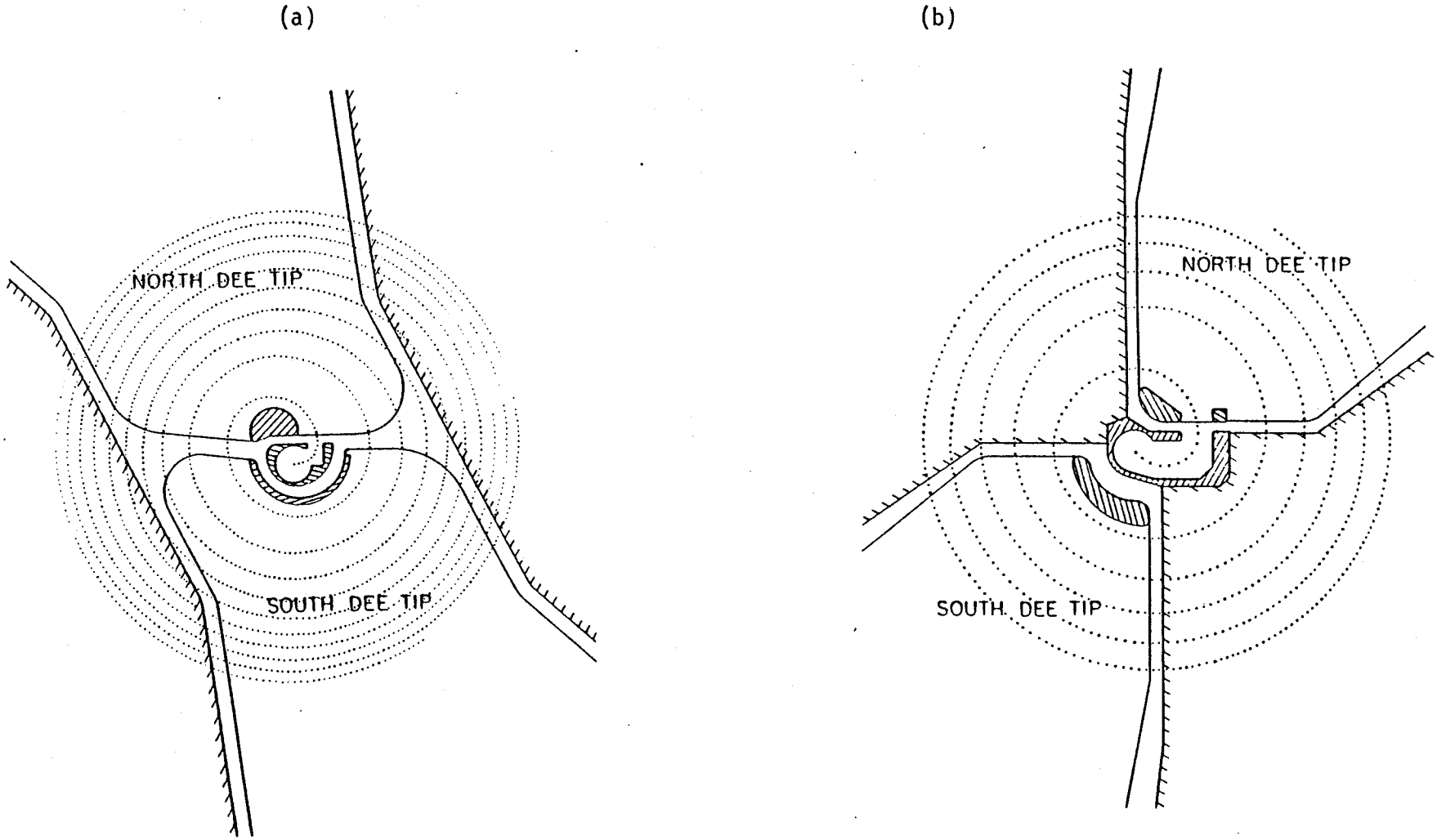

Fig. 3.4 The new central regions of the University of Manitoba cyclotron and the beam trajectories for the first-harmonic (a) and the second-harmonic (b) mode of particle accelerations. In order to yield maximum energy gain per turn of a particle, the dee angle was optimized for each harmonic mode [see eq.(3.1.4) and fig. 3.3].

numerical method that was used to obtain the electric potential distribution in the U of M cyclotron. This approach utilizes the application of a successive over-relaxation method to the new central region of the U of M cyclotron. Subsequently we shall provide descriptions of the new central region and of the beam orbit dynamics studies.

3.2 The calculation of the electric potential

A prior knowledge of both the electric and the magnetic field distributions inside a cyclotron is one of the fundamental requirements for successful investigations of the beam orbit dynamics. For the U of M cyclotron, the magnetic field distribution can be obtained from the measured data, an approach which was described in chapter 2. However, the data for the electric field distribution in this cyclotron was not available. For a simple dee structure ($e.g., \theta_D$=180°), as in the case of the classical cyclotron, the electric field distribution may be obtained in a closed form by utilizing the Schwartz-Cristoffel transformation method [MUR53]. However, the dee structure of the sector-focused cyclotron is, in general, too complicated for analytical calculations of the electric field distribution to be possible. One could also try to obtain this distribution by direct measurements in the median plane of the model electrodes; for example, by using the eletrolytic tank (or trough) method ([REI65], [ZIN69]). Yet, this method also has the following significant drawback, and hence can not be utilized in our design studies of the new central region; more specifically, whenever the change in the geometry is necessary, this method requires an actual re-machining of the model electrode, a very expensive and time-consuming procedure. Furthermore, a significant error may also occur during the measurement process due to the mechanical instability of the apparatus. The accuracy of the

result obtained from this method seems to be no better than 1%.

On the other hand, a numerical solution of the Laplace equation by using the successive over-relaxation (SOR) method enables us to obtain a very accurate static electric potential distribution. When applied to a cyclotron, this method assumes that the real dynamic field is approximated by a "quasi-static" field, a static field with an uniform potential that varies sinusoidally with time. The SOR method has many advantages over other methods of obtaining the electric field distributions, being more accurate (0.1%), inexpensive, and less time-consuming [LOU71]. We therefore employed this method to obtain the electric potential distribution in the central region of the U of M cyclotron. The detailed theory of the SOR method can be found elsewhere ([NEL69a], [NEL69b], [LOU71], [CHE81]). Consequently, in the following pages, only a very brief review of the SOR method is given and instead we shall emphasize its application to the calculation of the electric potential in the U of M cyclotron's central region.

3.2.1 Summary of the successive over-relaxation method

The numerical solution of the Laplace equation can be obtained by approximating this differential equation by the corresponding difference equation. For the actual computation, the region of interest is divided into a number of cubic meshes. The potential at each node is then calculated iteratively, by averaging the potentials at adjacent nodes, until it converges. To make the convergence faster, the successive over-relaxation coefficient α, a numerical factor which usually lies between one and two, is employed. The potential at node (i, j, k) at the n^{th} iteration is then given

by the expression

$$\phi_{ijk}^{n} = \phi_{ijk}^{n-1} + \alpha[\frac{1}{6}(\phi_{i-1}^{n} + \phi_{i+1}^{n-1} + \phi_{j-1}^{n} + \phi_{j+1}^{n-1} + \phi_{k-1}^{n} + \phi_{k+1}^{n-1}) - \phi_{ijk}^{n-1}]. \quad (3.2.1)$$

The optimum value of α depends on the dimensions of the meshes and it is given by [FOR60]

$$\alpha = 2 - 2\pi\sqrt{\frac{1}{3}(\frac{1}{p^2} + \frac{1}{q^2} + \frac{1}{r^2})}, \quad (3.2.2)$$

where (p, q, r) is the dimension of the meshes in the i, j, k directions, respectively.

3.2.2 Computational details

In our design studies of the new central region of the U of M cyclotron, the mesh dimensions and the value of α were taken to be (256,256,15) and 1.5, respectively. We see from eq. (3.2.2) that the optimum theoretical value of α for these mesh dimensions is 1.7573. However, it should be noted that the formal derivation of eq. (3.2.2) was carried out by imposing fixed Dirichlet or Neumann conditions on the boundary planes while all interior points were free to vary [FOR60]. The real situation does not quite correspond to this picture; the potentials in many interior points are also fixed, and therefore the effective mesh dimensions (p, q, r) are smaller than the real dimensions, making the value of α smaller than the one that is predicted by eq. (3.2.2). Since the design investigation of our new central region required studies of many trial geometries in order to find the best geometry, it appears to be somewhat time-consuming to search for the optimized value of α that corresponds to each new geometry. Therefore, in our investigations, no such effort was made to optimize α; instead, the value of α was fixed at α=1.5 throughout the

calculation, greatly simplifying the computations. With this value of α, the total number of iterations that are required to achieve an average fractional change in the potential (per iteration) of 10^{-6} was found to be about 120.

In order to achieve faster computational convergence we initially assign the value of the same potential to each point in the "empty" space of our region (*i.e.*, to each point which is not on the outside boundary or the electrode boundary). This value is taken to be half the sum of the maximum and minimum potential values that are assigned by us to the electrodes in the region. Dirichlet conditions are imposed on the boundary region. In order to carry out the actual SOR calculation, the FORTRAN packages RLX3D were developed at the U of M Cyclotron Laboratory [OH83]. The packages consist of several independent main programs. These include the program for initializing the potential, the main relaxation program, and the program for expanding the region by reducing the mesh size. The more detailed structures of these programs can be found in the reference just quoted above.

The accuracy of the calculation of the electric potential depends upon the mesh size. As was mentioned earlier, the effect of the electric field on the motion of a beam is most important during the first few turns. Therefore, meshes of 0.25 mm were taken to cover this region, which are sufficiently small. As a particle moves toward the outer region, successively bigger and bigger meshes can be utilized. In order to cover the entire acceleration range of the cyclotron, as well as to include all the ground shields, the RLX3D program starts with 4 mm meshes. Then, in sequence, the program carries out the SOR calculation, reduces the mesh size by half and re-calculates the potential, *etc.*, until the calculation with meshes of 0.25 mm is finished. The data that were actually used in the beam dynamics studies

involved meshes which ranged from 2 mm down to 0.25 mm.

3.3 Beam orbit dynamics for the H^- ions

We mentioned earlier that one of our motivations for embarking upon a design study of the new dee-tips was to provide a sufficient axial focusing force in the region of the cyclotron before the effect of magnetic field bump becomes important. The design study, therefore, must also include the beam orbit dynamics investigations, in which the motion of a beam in a specific design geometry is scrutinized to see whether that geometry yields a satisfactory beam. Such studies, in fact, were carried out utilizing a successive approach; first, a trial new geometry was designed. Then the motion of a beam in this particular geometry was carefully studied. Subsequently, the geometry was modified to obtain a beam whose motion was more satisfactory. The detailed procedures and the results of these studies will be described in this section.

Before the advent of powerful modern computers, studies of beam orbits were usually carried out by employing an "impulse approximation". In this approach, it is assumed that the beam moves along circular trajectories in the hill regions and along straight lines in the valleys; when the beam reaches the dee gap a sudden rise in the electric field is applied, thereby increasing the particle's energy and orbit radius. While this method provides reasonably accurate results for a beam of a high energy, this approach turns out to be invalid for a low-energy beam, a failure that is due to the significance of the finite transit-time effect during the particle's crossing of the dee gap.

The numerical integration of the Lorentz equations of motion, on the other

hand, produces results that are much more reliable and accurate. To carry out the numerical integrations a computer program, NUTRACK, was developed as a special version of the numerical orbit tracking program. NUTRACK is relativistically correct, utilizes double-precision and has a capability of tracing three-dimensional particle motions both forward and backward in time. The analyzed magnetic field mapping data (R20178.PRF) and the calculated electric potential data are both read in as inputs for NUTRACK. Then, utilizing additional inputs (such as particle specifications, initial conditions, oscillation frequency of the electric field, dee voltage, *etc.*), the program starts integrating the following equations of motion:

$$\begin{aligned} \frac{d\vec{r}}{dt} &= \frac{\vec{p}}{m\gamma} \\ \frac{d\vec{p}}{dt} &= q(\vec{E}\cos\omega t + \frac{d\vec{r}}{dt} \times \vec{B}) \\ \frac{dW}{dt} &= \vec{F}\cdot\vec{v} = \frac{d\vec{p}}{dt}\cdot\frac{d\vec{r}}{dt} \end{aligned} \qquad (3.3.1)$$

During the integration procedure, both the magnetic field and the electric field at the particle's position are calculated by employing the cubic spline method. A fourth-order Runge-Kutta method is used to carry out the integration. The time is taken as the independent variable and a total of 2000 integration steps are taken per one period of revolution of the particle. The output of the NUTRACK program consists of the instantaneous values of the particle's coordinates, momentum, energy, RF phase, *etc.*. A thorough analysis of these parameters then provides very useful information about the motion of the beam.

The study of beam orbit dynamics consists of (1) a search for optimal injection conditions, (2) investigations of the isochronism, the beam orbit center, the radial and axial motion, and (3) studies of other accelerator parameters such as the dee

voltage, oscillation frequency of the electric field, *etc.*. The injection conditions include the starting RF phase of the reference particle, the injection angle at the mirror center, the injection energy, and the position of the injection point. The optimization of all of these parameters involves a thorough study of both the radial and the axial motions in the central region.

The starting point for the reference particle (beam injection point) was always chosen to be at the center of the mirror (see fig. 3.4). The radial position of the mirror along with beam injection angle was then successively optimized to yield a well-centered beam. Since such optimization procedures are associated with a detailed study of the radial motion, we will discuss these procedures in greater detail later in this chapter.

Once these parameters are fixed, then the determination of the starting RF phase (ϕ_0) follows. Two conditions were imposed in order to determine the ϕ_0: (1) the reference particle had to gain the maximum possible energy after the traversal of the first gap, and (2) the energy spread of a beam had to be as small as possible [*i.e.*, $\int \sin\phi_0(E)dE = 0$]. The second condition, in fact, is also imposed during the determination of the optimal oscillation frequency of the electric field [ω_{RF}; see eq. (2.2.4)]. The starting RF phase of the reference particle was almost completely determined from the consideration of the phase excursion for a 50 MeV beam (see fig. 2.8).

The values that were obtained by this procedure were $\phi_0 = -56°$ and $\nu_{RF} = 2\pi\times$ 28.3709 MHz. The injection energy and the peak dee voltage were taken to be 12 keV and 40 keV, respectively. The total number of turns needed to reach 50 MeV, with these values, was estimated to be 625. We will consider more details

related to these values when we discuss the radial motion.

Once the optimal injection conditions have been found, then the isochronism, the radial motion and the axial motion can all be studied. Such investigations, especially of the radial and the axial motions, can be simplified if we assume that these two motions are decoupled (a first-order theory), an approximation which is permissible owing to the smallness of the particle's oscillation amplitude. Therefore in the following sections, we will treat the two motions separately; the study of the radial motion will be restricted to motion in the median plane of the cyclotron.

3.3.1 The radial motion

A radially stabilized beam is a "well-centered" beam whose center coincides with the center of a machine. Since the motion in the outer region always depends upon the previous history of the beam, once the beam is off-centerd (*i.e.*, when the beam center no longer coincides with the machine center), this off-centering effect becomes cumulative; under these conditions a significant deterioration in the beam quality will occur.

In order to study the radial motion of a beam, it is, therefore, appropriate to start by investigating the instantaneous motion of the orbit center. Let us assume that $\vec{R}$ is the position vector, $\vec{\rho}$ is the radius of curvature and $\vec{r}$ is the radial vector from the center of a cyclotron to the center of curvature as described in fig. 3.5. Then a straightforward vector consideration yields the relationship $\vec{r} = \vec{R} + \vec{\rho}$. Substituting $\vec{P} = q\vec{B} \times \vec{R}$ into the above equation, we then obtain the position of the center in terms of the Cartesian coordinates:

$$X_c = X - \frac{P_y}{qB_z}, \qquad Y_c = Y + \frac{P_x}{qB_z} \quad , \tag{3.3.2}$$

where (X, Y) and (P_x, P_y), respectively, are the position and the momentum of a particle at the time t. Note that both B_r and B_θ are zero because here we confine the motion to the median plane (z=0). The above equations indicate that the x-component of the center depends on the y-component of the momentum of the particle, and that the y-component of the center depends on the x-component of the momentum of the particle.

The instantaneous motion of the center of the reference particle for the H^- beam up to 50 turns was obtained from eq. (3.3.2) and is illustrated in fig. 3.6. The X and Y axes of this figure represent the directions along, and perpendicular to, the dee-gap, respectively. The origin denotes the center of the cyclotron. Each point on the figure indicates the instantaneous orbit center of the H^- beam. A "well-centered" beam is then the one whose reference particle's orbit center (averaged over one complete orbit turn) converges onto the machine center. The figure shows that the overall center of the particle is relatively well-converged onto the origin.

Such a centered beam in the new central region was obtained through a rigorous optimization of the injection conditions and of the radial geometry of the new dee-tips. We mentioned earlier that the injection energy and the dee voltage were taken to be 12 keV and 40 keV, respectively. With these values, the radii of curvature at the injection point and after the first gap traversal become 8.36 mm and 17.4 mm, respectively. It is well-known that in order to achieve a centered orbit, the beam injection axis must be off-centered and its displacement from the center is approximately given by the half of the radius gain after the first gap crossing [*i.e.*, here, $(17.4 - 8.36)/2 = 4.52$ mm]. Though this is a good method for estimating the position of the injection point, the exact determination of this point must resort to

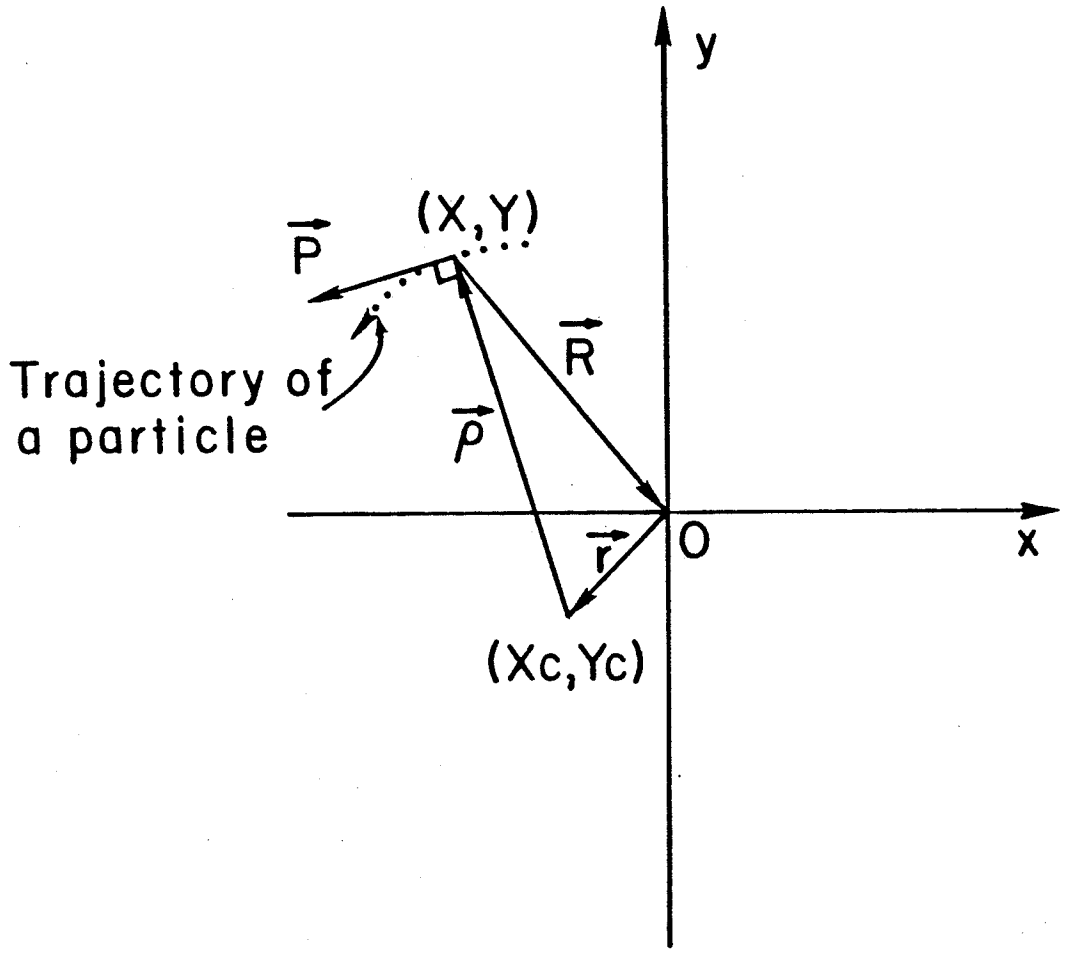

Fig. 3.5 The beam's trajectory and center of curvature in the median plane of the cyclotron. The horizontal and the vertical axes are along and perpendicular to the dee-gap, respectively. In the figure, $\vec{R}$ is a position vector, $\vec{\rho}$ is a radius of curvature, and $\vec{r}$ is a vector from the origin to the center of curvature. This geometrical configuration leads to the following vector relationship; $\vec{r} = \vec{R} + \vec{\rho}$.

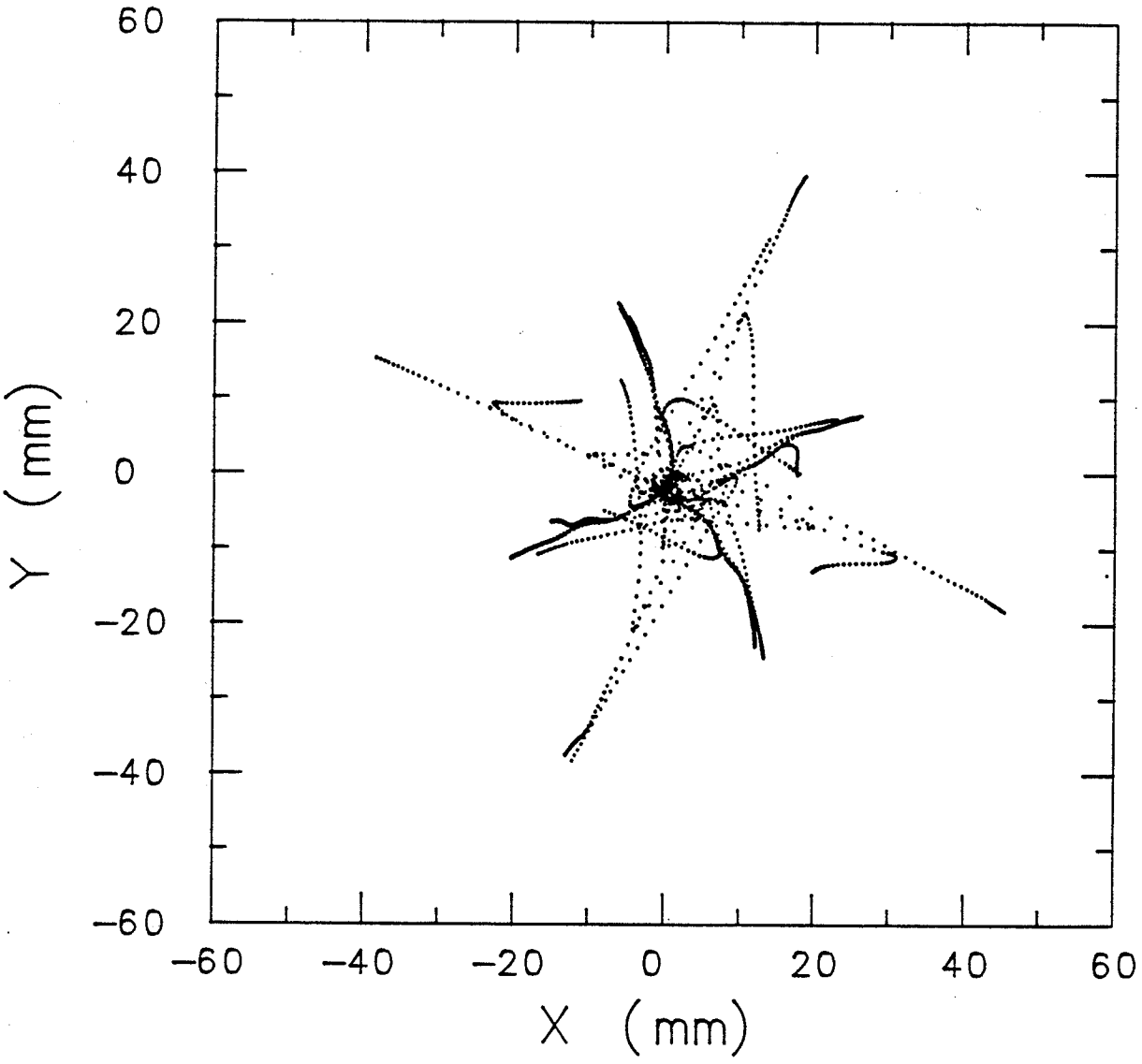

Fig. 3.6 The instantaneous motion of the center of the H^- beam in the newly designed central region of the University of Manitoba cyclotron. The horizontal and vertical axes denote along and perpendicular to the dee-gap, respectively. The origin of the graph represents the center of the cyclotron. This figure shows that the center of gravity is well converged to the origin of the graph.

the detailed numerical orbit tracking study that we are considering here. Eventually, the injection point was found to be displaced by 5.5 mm from the machine center. This, therefore, fixes the radial position of the mirror. Further studies of the motion of the beam center then subsequently determine the injection angle, and it was found to be 177°. Once these have been found, it was then possible to fix the horizontal position of the mirror gap in such a way that the reference particle will pass through the mirror gap at the center of the gap.

The final geometry of the mirror and the central region, viewed from the top, is displayed in fig. 3.7. The shaded region around the center shows the electrostatic mirror whose position was determined from the above considerations.

In fig. 3.8, the trajectories of fifty particles up to ten orbit turns are simultaneously depicted. The initial conditions of these particles at the injection point were chosen from the $r - p_r$ phase space ellipse whose area is 120 mm mrad. The spreads in phase ($\pm 10°$) and energy (± 0.2 keV) were also taken into account in the calculation so that the diagram should closely resemble the real situation.

3.3.2 The axial motion

As was mentioned earlier, a major problem that is associated with the axial motion of a beam in the central region of the cyclotron (especially for the U of M cyclotron) is a lack of axial focusing. In order to confine a beam to the vicinity of the median plane, an adquate axial focusing force is strictly required. Such a focusing force not only prevents a beam from hitting the dee wall (or the vacuum chamber), but also restricts the beam to a first-order region. The latter condition is very important, for otherwise higher-order effects will become dominant, thus inval-

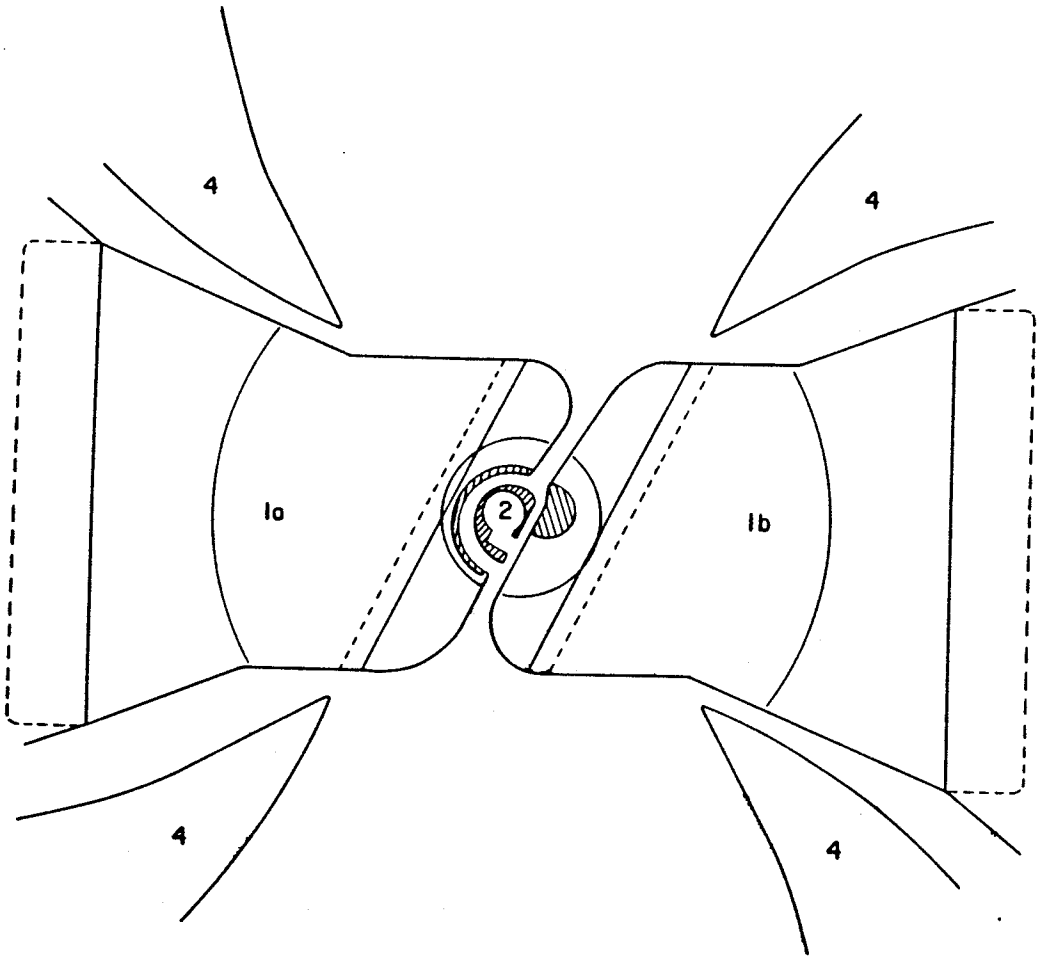

Fig. 3.7 The new N=1 central region of the University of Manitoba cyclotron, as viewed from the top of the cyclotron. 1a: South dee-tip, 1b: North dee-tip, 2: electrostatic mirror assembly, 4: hill.

Fig. 3.8 Fifty H^- particles' radial trajectories up to ten orbit turns. The initial conditions of the particles were arbitrarily distributed; the phase space area was 120 mm mrad, the energy spread was ± 0.2 keV and the RF phase spread was $\pm 10°$.

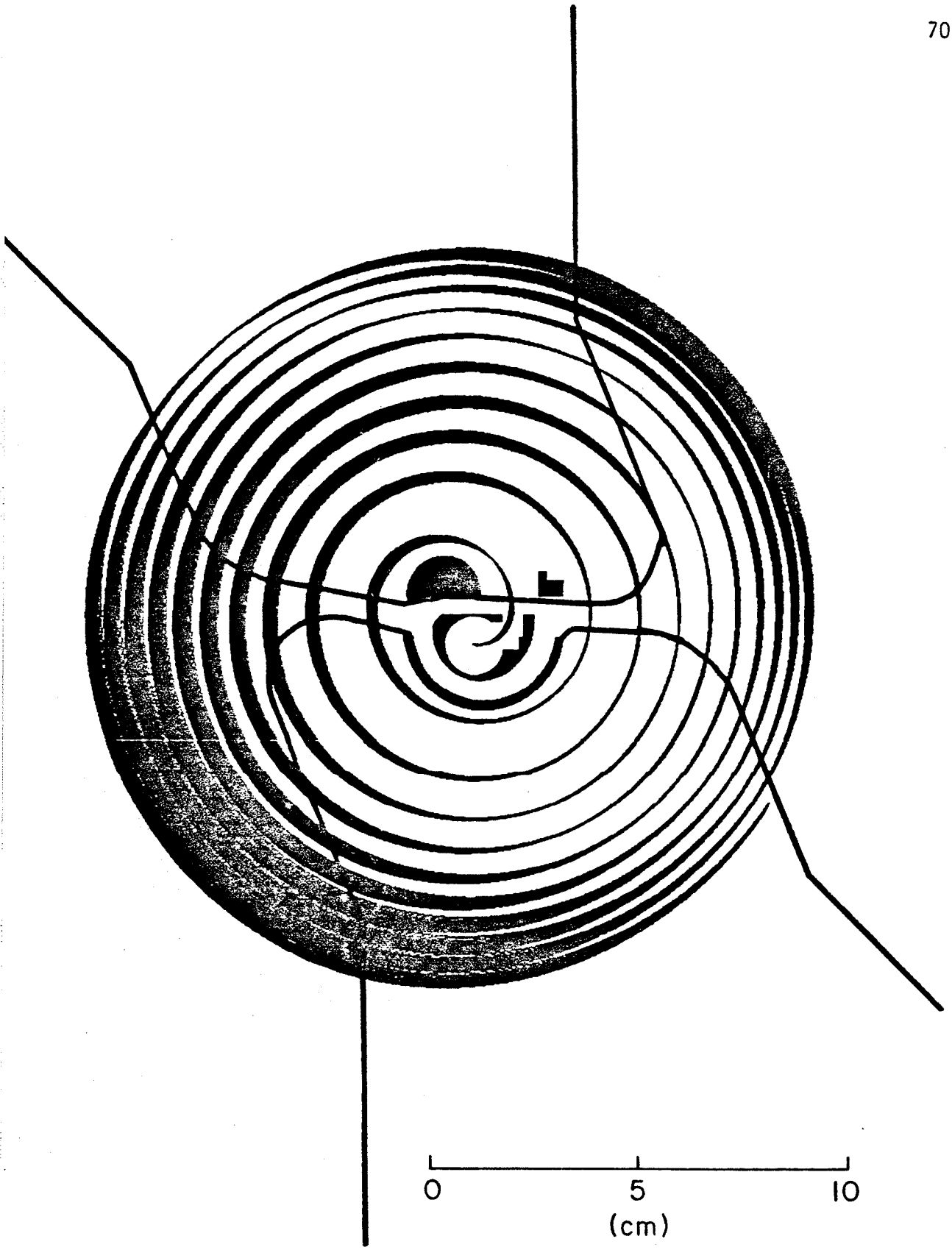
0
5
10
(cm)

idating the assumption of decoupled radial and axial motions. The axial geometry of the new central region of the U of M cyclotron was carefully optimized along these lines. The final geometry is depicted in fig. 3.9 which shows that the internal height of the dee is z=6 mm up to r=2.6 cm, and that the internal dee height then increases linearly with r till r=11 cm, where z is 2.2 cm.

Before we describe the more realistic numerical orbit tracking study of the axial motion of a beam in this geometry, we will first consider a more theoretical approach. The theoretical considerations that are discussed below over-simplify the complicated effects of the electric field on the axial motion of a beam, but do help us thoroughly understand the result of the numerical orbit study that was subsequently carried out.

As early as in 1938, Rose formulated, for the first time, the electric field dependence of the axial motion of a beam [ROS38]. Rose's formula involves two terms, namely a field-variation term and an energy-variation term. The axial focusing due to the energy-variation (or acceleration) of a particle during the dee-gap crossing was found to yield a net focusing force and to depend on the geometry of the electrodes. On the other hand, the field-variation term depends on the RF phase; this term focuses the beam during the first half of the RF phase (while the field is falling) and defocuses the beam during the remaining half (while the field is rising). Rose assumed, in deriving his formula, that the beam entered the dee-gap parallel to the median plane ($dz_0/dx = 0$).

Rose's formula was extended by Cohen who included the effect of a non-zero dz_0/dx [COH53]. Later, Reiser [REI71] further added the effects of a dee-liner. The resulting formula for the electric field dependence of the the axial motion of a beam

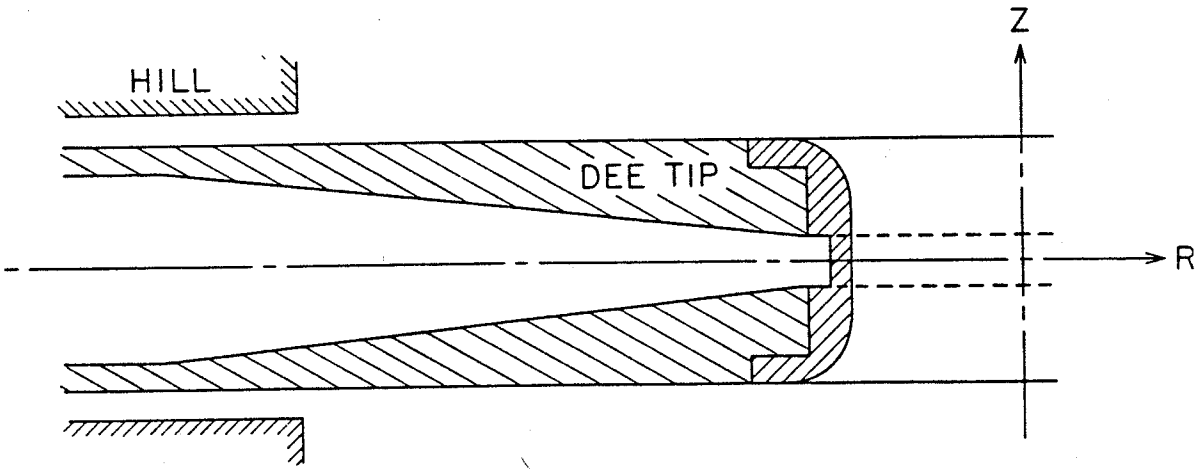

Fig. 3.9 The vertical cross-sectional view of the new N=1 dee-tip of the University of Manitoba cyclotron.

is given by the following equation:

$$\Delta\frac{dz}{dx} = -z_0[\frac{N}{r}(\frac{qV_0}{E_c})\sin\phi_c + \frac{2F(a,b,c)}{\pi b}(\frac{qV_0}{E_c})^2\cos^2\phi_c] - \frac{qV_0}{E_c}\cos\phi_c\frac{dz_0}{dx}, \quad (3.3.3)$$

where the x direction is perpendicular to the dee-gap and N, r, V_0, E_c, ϕ_c are the integral harmonic ratio, the radius, the normal dee voltage, the energy and the RF phase of the particle at the gap center, respectively. Here, $F(a,b,c)$ is a numerical factor which depends on the geometry of the dee (*i.e.*, on the gap width, internal dee height, and dee-to-liner spacing). The first term on the right-hand side in the above formula represents the dynamic nature of the electric field. This term defocuses the beam when the field is rising (for a negative RF phase, the field in the second half of the dee-gap increases by the time the particle reaches this region), and focuses the beam when the field is falling (for a positive RF phase, the field is weaker in the second half of the dee gap). The second term represents the focusing that is entirely due to the energy variation. This term depends on the geometrical factor, F, and always gives a focusing force because of the acceleration (the particle spends less time in the second half of the gap, *i.e.*, in the defocusing region).

In applying the above formula to a cyclotron with a simple dee structure, Reiser assumed the dee structure to be that of a two-dimensional electric lens, an approximation which enabled him to utilize the Schwarz -Christoffel transformation to obtain the electric potential distribution. He then used eq. (3.3.3) to trace the axial trajectories of the particle and then compared these trajectories with the results of the exact numerical integration of the equations of motion. Reiser's results indicated that the approximate analytical theory became valid after two orbit turns. Such, however, is not the case for the U of M cyclotron, where about ten orbit turns

are required for the beam to clear the dee-tips. Therefore, the effect of the transit-time is very significant at least for the first five or six turns. The accurate motion of a beam in this region can only be obtained by using the numerical integration method.

Two particle trajectories off the median plane in the new central region of the U of M cyclotron up to ten turns are displayed in fig. 3.10. These trajectories were obtained by numerical integration of the particle orbits. In fig. 3.10, the horizontal axis denotes the particle's revolution number and the vertical axis represents the displacement from the median plane of the cyclotron. The two particles shown in the figure are the orthogonal rays; they correspond to two linearly independent solutions of the second-order differential equation. These two particles were chosen from the boundary in the beam phase space ellipse, whose area is 120 mm mrad, a value which corresponds to the emittance of the beam from the axial injection system. Fig. 3.10 indicates that the maximum amplitude of the oscillation is about 8 mm, a value that is unacceptably large. For such a large oscillation amplitude, most of the particles will hit the dee wall and will be lost.

The above problem was solved in the early days (*i.e.*, in the 1960's), by introducing an arrangement of grids along the edges of the dee [COX62]. This development, however, resulted in a noticeable reduction in the beam transmission. Such an adverse effect can be avoided when we simply replace the grid by a post. As was discussed in connection with eq. (3.3.3), there is an axially defocusing force in the second half of the dee-gap crossing. If posts are placed on the image side, some of the field lines will end at the posts (the field has no axial component at the post), thereby reducing the defocusing part (see fig. 3.11). By reducing the gap be-

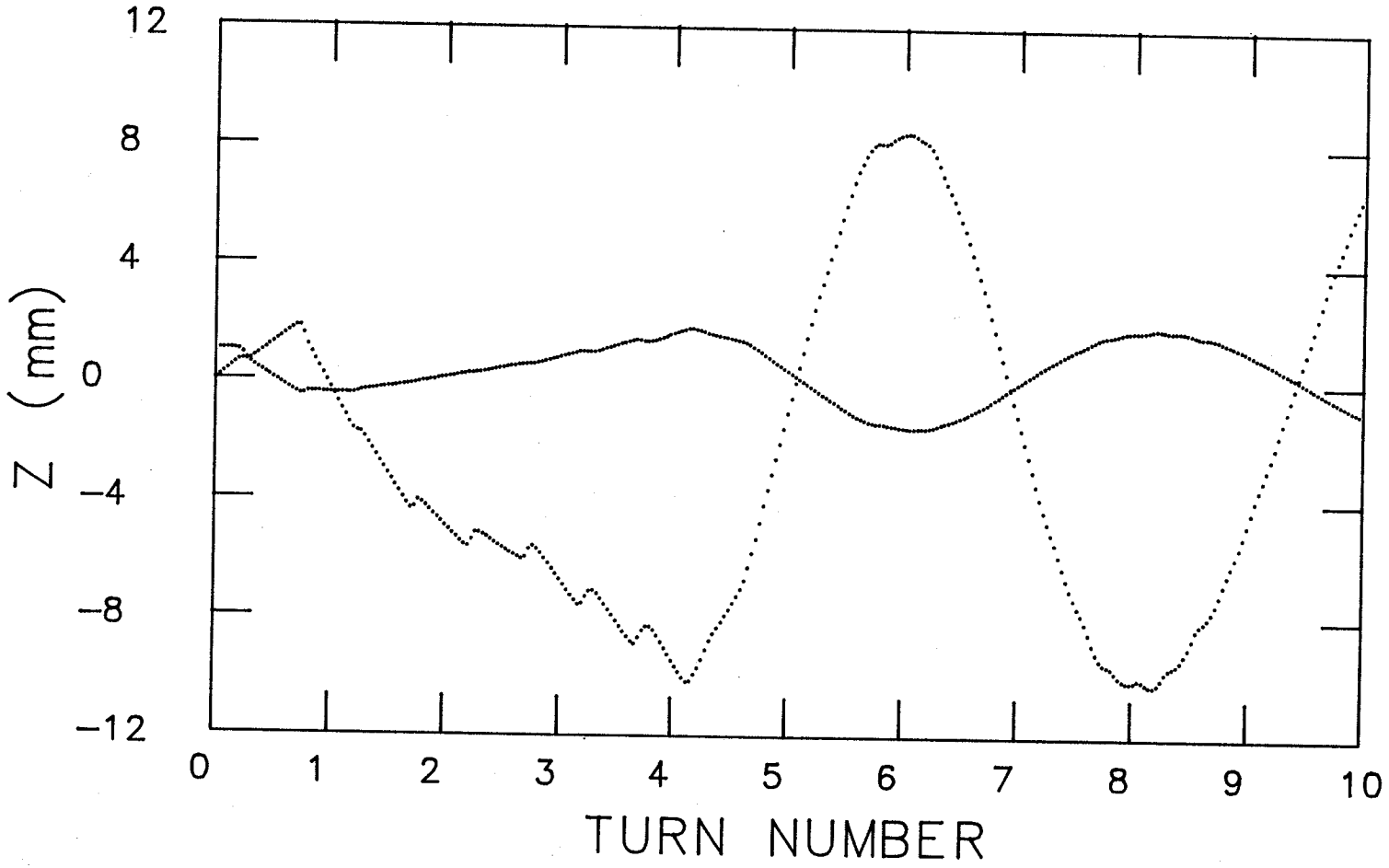

Fig. 3.10 The axial motion of the two orthogonal H^- particles in the new N=1 central region of the University of Manitoba cyclotron. The horizontal and the vertical axes denote the turn number and the displacement from the median plane, respectively. No posts were placed. It is seen that the maximum oscillation amplitude is about 8 mm.

tween the posts, we can reduce the defocusing effect of these second gaps by a large amount. In the U of M cyclotron, therefore, a number of posts were placed along the leading edges of the two dee-tips. Having the posts on the leading sides of the ground shield will further enhance the focusing (see fig. 3.7). Such an arrangement, however, causes a mechanical problem in adjusting the position of the dee-tips. It was, therefore, decided to place the posts along the edges of the dee rather than along the edges of the ground shield; such placements result in much more flexibility and allow the fine-adjustment of the horizontal position of the dee-tips.

The resulting axial motion of the H^- beam up to ten turns is depicted in fig. 3.12. To obtain this figure, a total of fourteen identical posts with 1.5 mm diameter, were placed along the leading edges of the dee-tips (seven for the South dee-tip and seven for the North dee-tip). The posts cover up to five turns of orbit. The positions, the diameter and the number of the posts were carefully determined on the basis of the orbit studies in order to maximize the beam transmission. With the help of fig. 3.8, which provided a realistic picture of the radial trajectories of a number of particles, we can select precisely all the parameters for the posts. It is evident from fig. 3.8 that adjacent orbit turns overlap after the sixth turn, and that the turn spacing between the sixth and the seventh turns is very narrow. Therefore, any arrangement of the post between these two turns would intercept the beam. Fig. 3.12, compared with fig. 3.10, apparently describes the effect of these posts. The two particles' initial conditions are the same as those utilized in fig. 3.10. It is seen that the particles are relatively well confined to the vicinity of the median plane; maximum amplitude is reduced to about 2 mm.

In reality, the particles injected axially can differ in their initial energies, RF

(a)

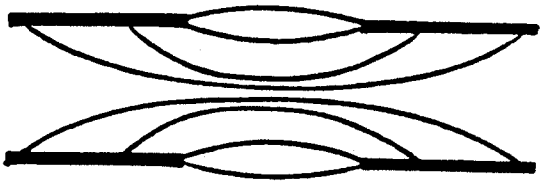

(b)

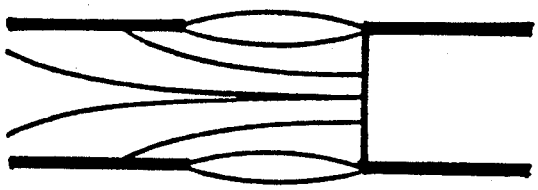

Fig. 3.11 The line of the electric field without (a) and with (b) the post. These figures show that the presence of the post in the downstream side (on the right-hand side removes the defocusing parts of the electric field line.

Fig. 3.12 Two orthogonal particles' axial motion in the new N=1 central region of the University of Manitoba cyclotron. The horizontal and the vertical axes denote the turn number and the displacement from the median plane of the cyclotron, respectively. The posts were in place. It is seen that the maximum amplitude is about 2 mm (see fig. 3.9 for comparison).

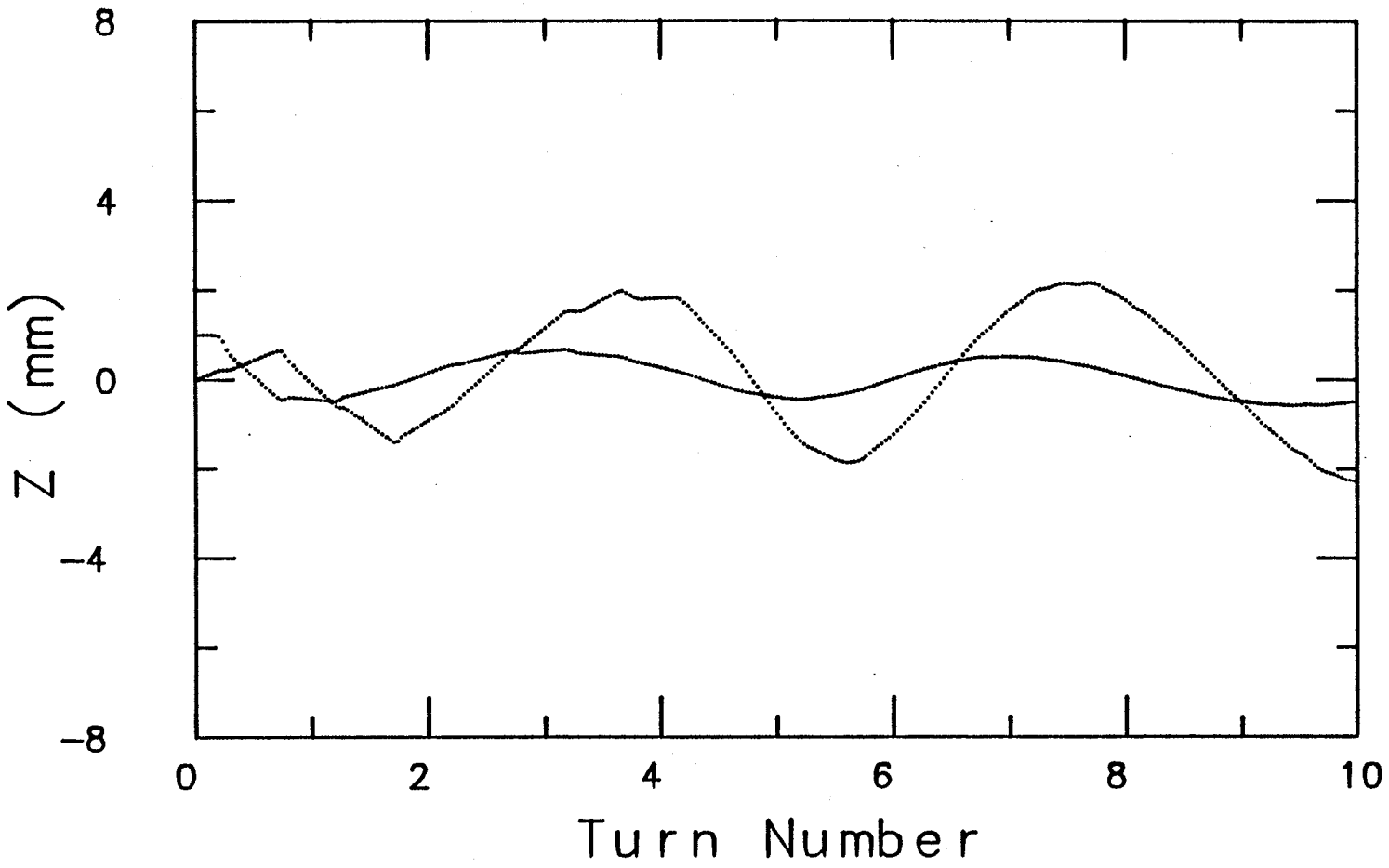
8
4
0
−4
−8
Z (mm)
0
2
4
6
8
10
Turn Number

phases, displacements and divergences with respect to the median plane. All these parameters are centered around those of the reference particle. The central region, which is sensitive to these particle parameter spreads, will not accelerate some particles, and therefore the acceptance of the cyclotron will be reduced. To increase this acceptance, and therefore to maximize the transmission of a beam throughout the central region, it is very desirable to have the central region insensitive to these particle parameter spreads. Fig. 3.13 shows 100 particle trajectories off the median plane. The initial conditions are set for these particles in such a way that their trajectories form an area of 150 mm mrad in $z - p_z$ phase space and that their energies and RF phases are (12±0.2) keV, and (−56±5°), respectively. The figure clearly reveals the insensitivity of the central region to these variations in energies and RF phases; the particle motions are extremely well confined to the median plane of the cyclotron, a valuable achievement.

Once the beam gets beyond ten turns, the effect of the magnetic focusing due to the field bump slowly predominants over the effect of the electric focusing. It is well-known that the amplitude of the axial motion due to the magnetic field is adiabatically damped; this amplitude is inversely proportional to the square root of the mass (*i.e.*, average magnetic field) along the radius, as eq. (2.2.5) indicated. Therefore, the beam will hardly suffer from any loss of axial focusing once the beam clears the dee-tips.

Fig. 3.13 The axial motion of one hundred particles in the new N=1 central region of the University of Manitoba cyclotron. The horizontal and the vertical axes denote the turn number and the displacement from the median plane of the cyclotron, respectively. The Posts were placed. In this figure, all the possible spreads of the initial conditions were included. It is seen that the maximum oscillation amplitude is about 3 mm.

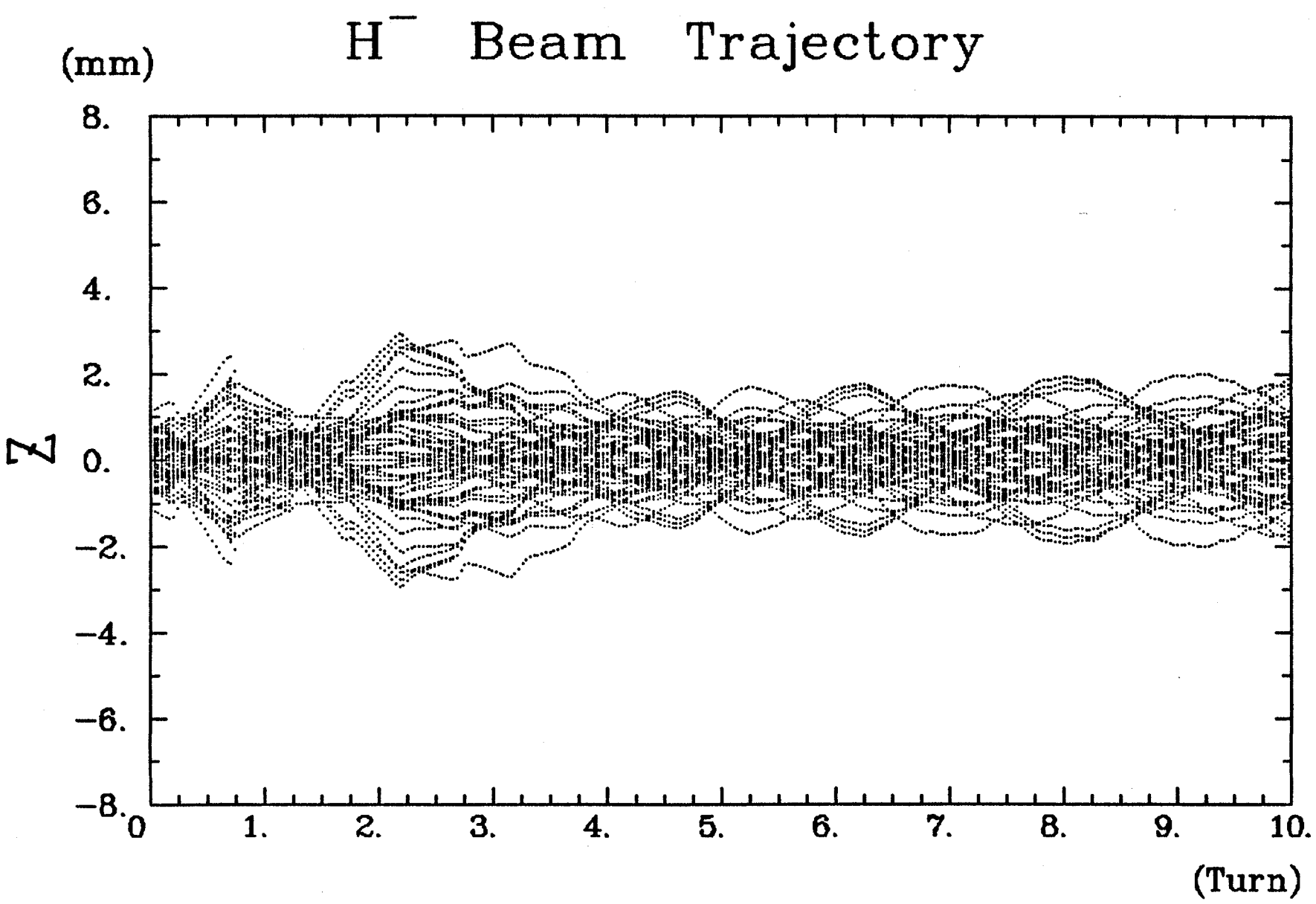
H⁻ Beam Trajectory
(mm)
8.
6.
4.
2.
0.
−2.
−4.
−6.
−8.
Z
0
1.
2.
3.
4.
5.
6.
7.
8.
9.
10.
(Turn)

Chapter 4

Conclusion

In the preceding chapters, we have described in detail a major upgrade of the University of Manitoba cyclotron.

Based on our design study of the new central region and on the beam orbit dynamics investigations, all of which were described in chapter 3, a new pair of dee-tips was installed in August 1984.

In parallel with this work, until the end of 1983, the installation and the calibration of the magnetic field mapping apparatus were carried out by the machine development group. The actual field measurements and the shimming were started in February 1984, and continued for the next three months.

In September 1984, the new dee-tips and their assemblies were placed in the central region of the cyclotron. Thereafter, the RF conditioning and its testing were continued until December 1984.

After we had optimized the magnetic field on the basis of the 1984 field mapping data, the first H^- beam was successfully accelerated in December 1984. For the next five months, the cyclotron accelerated proton beams for research while we continued debugging of the RF system. In May 1985, the cyclotron finally became fully operational. The following several improvements in the cyclotron's operation have been observed since then.

1. The maximum obtainable energy of H^- beam was increased to about 50 MeV when the cyclotron's operation was optimized by using the computer predicted

parameters. Before the upgrading, the cyclotron was not always reliable in producing H^- beam with energies above 42 MeV. Beyond these energies, the cyclotron started rapidly losing beam and, in addition, the beam current exhibited large flucuations. In particular, it was seldom possible to obtain energies above 46 MeV; even when such energies were achieved, they were not reproducible. The extension of the energy range, after the upgrading, confirms the validity of the predictions of our magnetic field mapping and analysis work. Our investigations had predicted that an improved isochronism would lead to an extension of the maximum obtainable energy (see fig. 2.8).

2. The beam quality has also been improved. The observed beam spot size, after extraction, was smaller by a factor of two than the size that was observed before the upgrading. Moreover, though it was not actually measured, the beam transport (after the extraction) to the target location appeared to be much better than before. Prior to the upgrading, the beam reaching the experimental area fluctuated in both intensity and direction. It used to be necessary, before 1984, to retune the cyclotron approximately every ten minutes in order to restore the beam to its original condition. With the new system, we can now quite often leave the cyclotron untouched for a full day without any appreciable drift in the beam current. After 1984, when there have been drifts, these were usually traced to an instability in the ion source or to other effects that were not related to the operation of the cyclotron.

3. The beam transmission efficiency through the cyclotron has increased and has become much more stabilized. At 25 MeV, for instance, the transmission efficiency before the upgrading was approximately 8 to 17%, and it was also

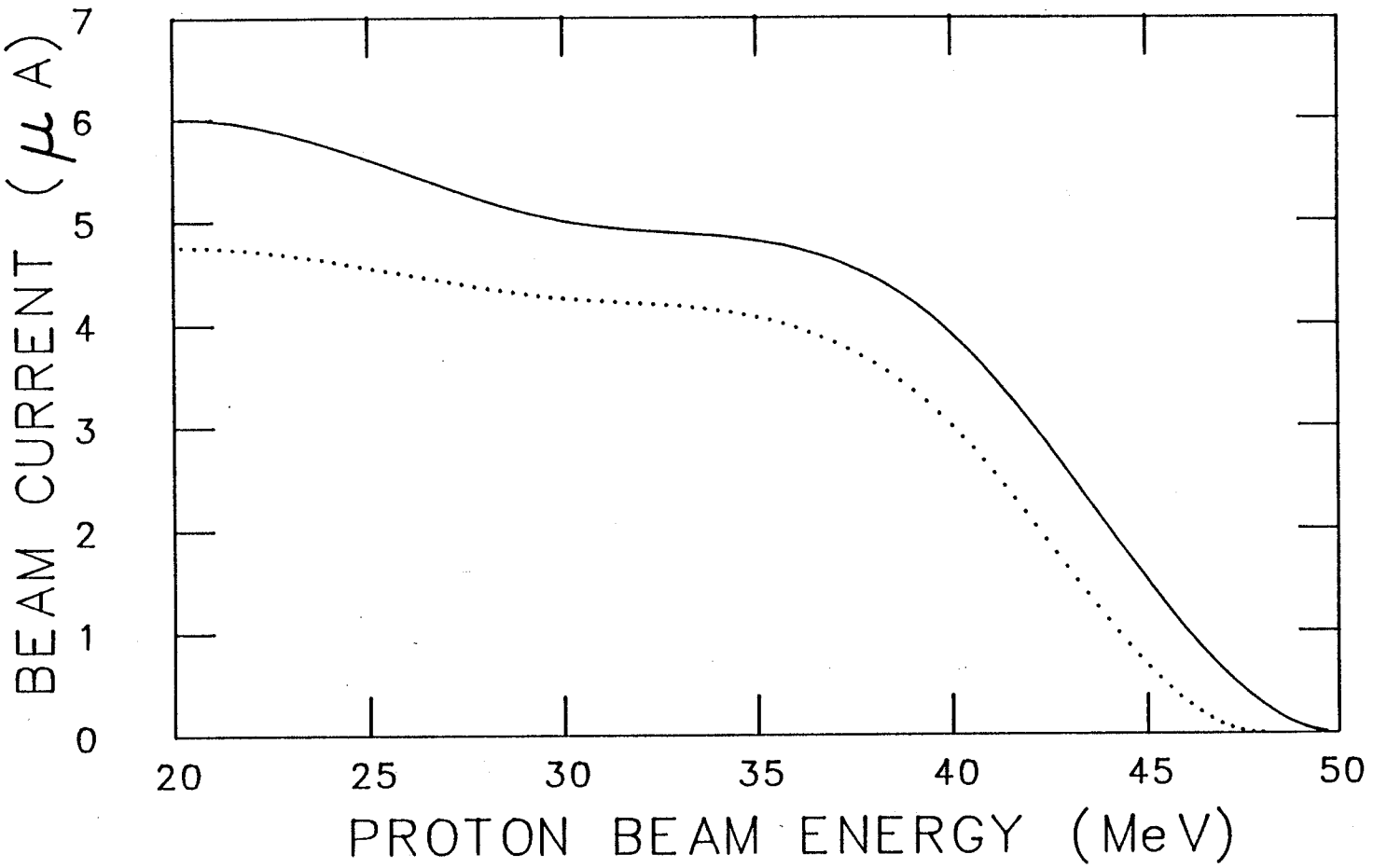

Fig. 4.1 The beam current at the stripping point vs. proton beam energy, before (dotted curve) and after (solid curve) the upgrade of the University of Manitoba cyclotron.

very unstable. However, after the upgrading, the transmission efficiency has always been very close to 20% and also much more stable. Fig. 4.1 shows the average beam current *vs.* energy for the old and the new systems. It is apparent that the new central region of the University of Manitoba cyclotron produces a higher current than before. This increase in the current has been attributed to an improved isochronism, an enhanced axial focusing, and a better RF system. This again confirms the validity of the studies that were described in chapters 2 and 3.

4. The new central region also produced a much more stable beam. For example, the beam intensity of the H^- ions before the upgrading fluctuated by as much as a factor of four within 24 hours. On the other hand, after the upgrading, the beam intensity remained constant to within 20% over a 24 hour period.

All these observed improvements in the cyclotron performance are very consistent with the predictions of the beam orbit dynamics studies described earlier in this dissertation. Since May 1985, the University of Manitoba cyclotron has been operating continuously and satisfactorily to be devoted to experiments.

The studies described in this part were based on the assumption that the axial injection system of the University of Manitoba cyclotron was completely optimized. The new central region was designed in such a way that the emittance of the axial injection system would match with the acceptance of the cyclotron. Therefore, a careful study of the axial injection system, based on the new central region, would result in a further improvement of the beam transmission efficiency as well as in the beam quality.

Such a study of the axial injection system would require a detailed recalculation of the beam optics and the reoptimization of the lenses along the injection system, (such as the matching of the electrostatic quadrupoles, the adjustments of the buncher voltage and its position, *etc.*).

As was mentioned earlier, by having two separate central regions in the upgraded University of Manitoba cyclotron, a significant improvement in the quality of the D^- beam could be expected solely from the increase in the energy gain per turn, thereby reducing the total number of turns required to reach the maximum energy. The reduction in the total number of turns inside the cycloton, before extraction, will lead to a corresponding reduction in the beam phase excursion during the acceleration. Furthermore, the turn-spacing will be much larger than that of the double-harmonic mode (*i.e.*, one central region is operated for both the first and the second harmonic mode of accelerations). Therefore, this may lead to the possibility of quasi single-turn extraction [GOR66]. For this purpose, a system consisting of four remotely controlled radial slits was designed. The single-turn extraction of D^- ions in the University of Manitoba cyclotron will be possible only when the stripping foil is positioned precisely at the desirable point. The calculation of the stripping position requires detailed beam orbit studies using the orbit tracing program (and the equilibrium orbit code).

These studies will further enhance the performance of the cyclotron, thereby providing H^- and D^- beams that will be still more intense and of even better quality.

Part II

A study for
Axial Injection of Ions into
the Princeton University Cyclotron

Chapter 5

Historical Background

The Princeton University cyclotron was completed in 1969. It is a constant orbit, multi-particle, variable energy machine. A close copy of the Michigan State University's old K=50 cyclotron*, it has a three-sector, pseudo spiral-ridge magnetic field configuration. The choice of the cyclotron control setting parameters (*e.g.*, RF, dee voltage, profile coil currents, *etc.*) was such that the saturation in the cyclotron magnetic field is small enough to accelerate a range of ions in a fixed orbit acceleration mode [POL69]. The accelerating system consists of two 134° dees, which can be operated in either push-pull or push-push modes over a frequency range of approximately 14 to 23.5 MHz, allowing for acceleration of particles on almost any harmonic mode. Maximum energies for typical particles are: 48 MeV protons, 29 MeV deuterons, 58 MeV alpha particles, 85 MeV $^{3}He^{++}$ ions, and 75 MeV $^{12}C^{4+}$ ions. A complete listing of the energy ranges for various particles that can be accelerated in the Princeton University cyclotron is given in fig. 5.1.

Extraction of the beam is achieved by means of so called precessional extraction. With this method, a magnetic first-harmonic field which starts near 63 cm (25″) radius (where ν_r crosses 1) shifts the orbits toward an electrostatic deflection channel. The natural turn separation of 1.5 mm (arising from the energy gain per turn) is at the same time enhanced by a factor of three, thereby easing the extraction. A strong electrostatic deflection channel followed by a magnetic channel then completes the extraction. If the neighbouring turns do not overlap on entering the

* K is defined as $E_{max}=Kq^2/A$, where E_{max} is the maximum energy in MeV, q is the charge number (q=1 for proton), A is the mass number(A=1 for a proton)

Fig. 5.1 The energy vs. the orbital frequency diagram for the Princeton University AVF cyclotron for the acceleration of various particles. The gap band in the figure indicates that the frequency is outside the range of the RF tuning.

PRINCETON AVF CYCLOTRON

ENERGY vs. TUNING RANGE

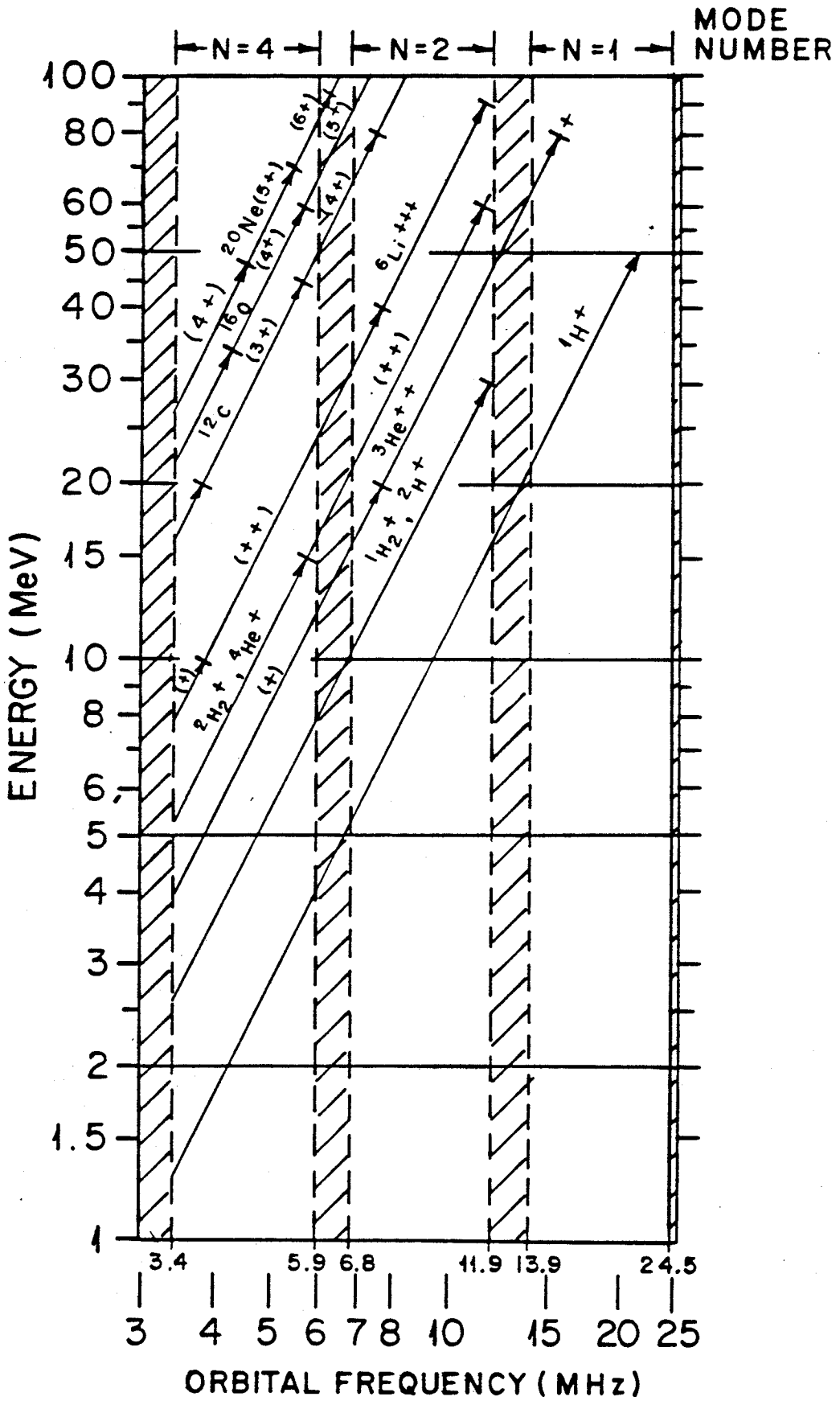

electrostatic deflection channel, then single turn extraction of the beam is achieved, resulting in a beam with an extremely small energy spread.

Lately, production of high charge-state light heavy ions with reasonable beam currents was increasingly requested at this laboratory. The internal PIG source is known to be able to provide satisfactory beams for only low charge-state ions. The recent development of the ECR source paved the way for revolutionizing the design of particle accelerators. It is now established that a cyclotron with axial injection of high charge-state light heavy ions from an ECR source can provide comparable beams to those of the conventional method in which the beam from an injector is stripped to a higher charge-state and then injected into a booster cyclotron. This is well described in references ([GEL79],[WOR85]). The conventional method meant that it was not feasible to upgrade an existing facility for production of higher charge-state ions without a major financial investment associated with the changes in the layout. With an ECR source, the task is simply to convert the cyclotron for axial injection and then obtain a source. The necessary space for axial injection was already provided in the Princeton University cyclotron at the time of construction which makes the task considerably easier.

In parallel with this, interest has been increasing at the Princeton University AVF Cyclotron Laboratory for carrying out experiments using polarized beams. Experimental studies to investigate the spin-dependent nature of the nuclear force require a polarized beam. In the early days, polarized beam had been obtained from double-scattering or triple-scattering of unpolarized beams from cyclotrons [HAE67]. The polarized beams obtained in this way, however, suffered from low intensity. Now, such a polarized beam is best obtained from an external polarized

source, which is then accelerated in the central region of a cyclotron. It is well-estabilished that there is no appreciable depolarization of polarized proton, deuteron and $^3He^{++}$ beams for conventional three-sector AVF cyclotrons. The question is then how to obtain intense beams from the Princeton University cyclotron using axial injection with two alternative options. The first option is with single-turn extraction retained, and the second option is without such provision.

The design study for the two cases has in fact been carried out by the author. The aim is to predict, through detailed studies, the amount of beam obtainable for externally injected ions from an ECR source or a polarized ion source. The heart of such a study is the design of a new central region for the cyclotron in the light of the following considerations.

If the beam is to be axially injected, its optimum injection energy should be non-zero and depend upon desired beam extraction energy, which is different from the internal PIG source where it is near zero. For instance, the injection energy for protons is 15 keV when desired extraction energy is to be 48 MeV. The trajectories for the two cases will, therefore, differ in the central region. The difference, however, rapidly becomes negligible as the beam is accelerated, and, by the time the beam reaches near 20 turns (~4.5 MeV) it is indistinguishable.

Therefore, this study was aimed at designing a central region for which the beam orbit for axial injection smoothly converges into the existing trajectory. The work started with the study of the beam orbit dynamics in the existing central region. Then a new central region was designed and studied in comparison with the former.

Another important part of the study is the beam emittance and the cyclotron

admittance matching. The purpose of this study is, of course, to increase the beam transmission efficiency throughout the central region. An accurate understanding of this problem can be obtained only when the trajectories of a number of particles are traced from the ion source to the extraction radius in the cyclotron. However, carrying this out requires an unrealistically large amount of computing time and memory. Therefore, an alternative method was devised, which actually allowed us to carry out the design study of the new central region independently in parallel with the design study of the axial injection system.

In the remainder of part II of this dissertation, the design studies described above are presented. It starts with a description of the axial injection system in chapter 6. Chapter 7 then presents the beam orbit dynamics studies both in the existing central region and in the new central region for the first-harmonic and the second-harmonic mode of accelerations, respectively. The calculated and the estimated total transmission efficiencies of the various particles in the designed axial injection system and the new central region are shown. The chapter ends with a description of the depolarization study of polarized ions during acceleration in the cyclotron central region. Finally, chapter 8 is devoted to summarizing the study, to presenting the problems in the existing central region, and to making suggestions for possible future improvements of the Princeton University AVF cyclotron.

Chapter 6

The Axial Injection System

6.1 Introduction

If high charge-state heavy ions or polarized ions are to be accelerated in the cyclotron, it is necessary to inject a beam from an external source. This is because the size of a source to produce such ions is much too large to place in the center of the cyclotron.

An external source, when compared with an internal source, is easier to service because of its location outside the cyclotron. It is easier to control the beam properties through the external beam transport system, and it does not impose any restrictions on the size of the source. It can have its own vacuum system, thereby improving the performance of the cyclotron.

The method of external injection can be classified as radial injection or axial injection, depending on the direction of injecting the beam into the cyclotron.

Radial injection schemes can be divided into injecting the beam toward the hill-valley boundary (trochoidal injection), injecting the neutral beam with thermal velocity followed by ionization by an electron beam or arc near the center of the cyclotron (neutral beam injection), and injecting ions followed by stripping it near the center to higher charge states (stripping), *etc.*. Detailed accounts of these injection methods can be found in the references ([CLA71],[CLA72]).

The axial injection of ions into a cyclotron was pioneered by Powell's group ([COX62], [POW65]) at the University of Birmingham in 1962, when the beam

from an RF source was injected into the 12 MeV radial-ridge cyclotron. Later a polarized deuteron source was installed on the injection line. Compared with radial injection, an axial injection system is much more flexible in the sense that a number of focusing elements can be placed along the injection line, enabling one to control the optics of the beam. It also allows one to place a beam buncher near the central region of the cyclotron to increase the RF phase acceptance of a DC beam. The focusing elements usually consist of einzel lenses, solenoidal lenses, electric or magnetic quadrupoles, and so forth. One general peculiarity with the axial injection system is the cyclotron axial magnetic field which acts like a half-solenoidal lens. Therefore in calculating the beam trajectories along the axial injection system, one must take into account the focusing effect due to the axial magnetic field in the yoke.

In view of those advantages of the axial injection scheme mentioned above, it was natural that they lead to the eventual decision to initiate the design study of the axial injection system for the Princeton University (hereafter PU) cyclotron.

This chapter describes a detailed design study of the axial injection system of the PU cyclotron. First of all, various kinds of focusing elements will be considered to single out the most suitable one. Here, the study was focused on the injection of polarized ions in order to exclude the possibility of a significant depolarization during the transportation along the injection system. Detailed descriptions of the elements and the beam optics studies are then presented.

6.2 Choice of the focusing elements

There are many different types of focusing elements that can be considered

and each of them has its own merits and demerits depending on size, simplicity of construction, aberrations, power requirements, space charge neutralization, and depolarization of the polarized ions, *etc.*.

Out of many types, four elements were considered seriously for the axial injection system of the PU cyclotron, namely the einzel lens, the axial magnetic lens (or the solenoidal lens), the magnetic, and the electric quadrupoles.

The three tube einzel lens [KLE71] is the simplest and the smallest in size. It yields the largest phase space acceptance. Its small size makes placement possible anywhere along the injection line where no other types of focusing element can be conveniently placed — a very desirable feature for the PU cyclotron. However, when the beam arrives close to the cyclotron median plane, it feels a strong axial magnetic field of as much as 1.5 T, which acts as a magnetic lens with focal length of about 4 cm. The beam also sees up to several hundred gauss of leakage magnetic field along the axial injection line close to the cyclotron center. To keep the beam diameter small so that the effect of the cyclotron leakage magnetic field on the beam optics is within an acceptable range, it is highly desirable to have a strong focusing element close to the entrance to the cyclotron central region [around 15.24 cm (6″) above the median plane of the cyclotron]. The available space in this region, however, is less than 2.54 cm (1″) in diameter which is just enough for a small einzel lens. However, use of einzel lenses in this leakage field tends to trap a large number of electrons, causing an unacceptable instability in beam properties. It also has large aberration coefficients.

An axial magnetic lens [BAN66] is one with $B=B_0$ inside (of length L) and a diminishing B field outside. This lens provides radial focusing and, for axial injection,

yields the second largest phase space acceptance. The space charge neutralization due to residual gas molecules is probably the least disturbed. It also has relatively small aberration coefficients. Owing to these advantages, an axial injection system based on these lenses was studied in detail. This lens, however, turns out to induce large depolarizations for $^3He^{++}$ and, to a lesser extent, proton beams as will be described later. Repeated use of these elements can severely depolarize the $^3He^{++}$ and, proton beams. The axial magnetic lens also requires more power than other lenses for a given focusing power.

The magnetic quadrupole lens [HAW82] needs nearly a 70% larger aperture than the axial magnetic lens for a given beam since it defocuses the beam in one of the two planes. It has to be used with two or three elements in combination to form a lens in both planes. The space charge neutralization, mentioned above, is relatively free from disturbance and the aberration coefficients are small compared with the electrostatic quadrupole lens which will be considered below. The elements, however, not only focus ions but also perturb the spin of the ions. This deflection causes some depolarization although it is not as serious as the axial magnetic lens. Repeated use of these elements does not aggravate the depolarization problem so long as the drift spaces between them are free from any axial magnetic field. This, however, is not the case for the PU cyclotron, and in fact varying degrees of depolarization (several %) depending on the beam energy are expected. Pole piece windings require space, and therefore for a given space the available aperture for beam tends to be somewhat less than the equivalent electrostatic quadrupoles.

Lenses based on electrostatic quadrupoles [SEP67] provide acceptable focusing properties. Their size is somewhat less than that of an equivalent magnetic quad-

rupole element — an important factor for the design of the axial injection system of the PU cyclotron. The only disadvantage is the disturbance of the space charge neutralization.

Among the four types of focusing elements considered above the einzel lens was ruled out almost outright. The instability in the beam was totally unacceptable. The use of axial magnetic lenses was studied seriously. In fact, an injection system consisting of three such lenses, a pair of deflection magnets, a beam buncher and a 90° bending magnet was possibly the best realizable system for unpolarized beams for the PU cyclotron. The system is described briefly in appendix 6-A. However, a depolarization study based on this system indicated that for polarized $^3He^{++}$ beams and, to a lesser extent, for proton beams there can be a serious depolarization as mentioned earlier.

Tables 6.1 to 6.4 show the survival of polarization as a function of beam radial position and its divergence at the entrance to the cyclotron field. It is seen that up to 48% depolarization is expected for a $^3He^{++}$ beam component which has 60 mradian in divergence. In obtaining these results neither the effect of the cyclotron fringe field nor the effect of the other magnetic lenses were taken into account but only the effect of a single axial magnetic lens (the last stage lens) was considered. It is obvious, however, that the depolarization is serious enough with this one axial magnetic lens. This problem led to the eventual rejection of the system based on axial magnetic lenses. Before this conclusion was reached, however, efforts were made to reduce depolarization to an acceptable level by placing an axial magnetic lens of about 0.6 T at 15.24 cm (6″) above the median plane of the cyclotron. The placement of such a lens would reduce the radial size of the beam by a factor of

Table 6.1 Survival of the beam polarization through a single solenoidal lens as a function of the proton beam's radial position and its divergence at the entrance to the cyclotron magnetic field. This table shows that up to 30% depolarization is expected for a proton beam whose divergence is a 60 mradian.

Proton at V = 15000. eV

Mass= 1.0 Spin= 0.5 Charge= 1. Myu= 2.7928456

Starting condition; R0= 1.59074202 mm

Maximum Divergence = 60.0 m Radian Upright ellipse

% Polarization

as a function of radial position (R in mm) and dR/dz (divergence in m radian)

at the entrance to the cyclotron field

R	dR/dz (m Radian)												
mm	-60mR	-50mR	-40mR	-30mR	-20mR	-10mR	0mR	10mR	20mR	30mR	40mR	50mR	60mR
0.00	70.7	79.3	86.5	92.3	96.5	99.1	100.0	99.1	96.5	92.3	86.5	79.3	70.7
0.16	*	79.5	86.7	92.4	96.6	99.2	100.0	99.1	96.5	92.2	86.3	79.0	*
0.32	*	79.7	86.8	92.6	96.7	99.2	100.0	99.0	96.4	92.0	86.1	78.8	*
0.48	*	79.9	87.0	92.7	96.8	99.3	100.0	99.0	96.3	91.9	86.0	78.6	*
0.64	*	80.1	87.2	92.8	96.9	99.3	100.0	98.9	96.2	91.8	85.8	78.4	*
0.80	*	80.3	87.3	92.9	97.0	99.3	100.0	98.9	96.1	91.6	85.6	78.2	*
0.95	*	*	87.5	93.1	97.1	99.4	100.0	98.8	96.0	91.5	85.4	*	*
1.11	*	*	87.7	93.2	97.1	99.4	100.0	98.8	95.9	91.4	85.3	*	*
1.27	*	*	*	93.3	97.2	99.5	100.0	98.7	95.8	91.2	*	*	*
1.43	*	*	*	*	97.3	99.5	100.0	98.7	95.7	*	*	*	*
1.59	*	*	*	*	*	*	99.9	*	*	*	*	*	*

Table 6.2 Survival of the beam polarization through a single solenoidal lens as a function of the deuteron beam's radial position and its divergence at the entrance to the cyclotron magnetic field. This table shows that approximately 4% depolarization is expected for the vector component of a deuteron beam which has 60 mradian in divergence

Deuteron at V = 15000. eV

Mass= 2.0 Spin= 1.0 Charge= 1. Myu= 0.8574376

Starting condition; R0= 1.59074202 mm

Maximum Divergence = 60.0 m Radian Upright ellipse

% Polarization (Vector component)

as a function of radial position (R in mm) and dR/dz (divergence in m radian)

at the entrance to the cyclotron field

R	dR/dz (m Radian)												
mm	-60mR	-50mR	-40mR	-30mR	-20mR	-10mR	0mR	10mR	20mR	30mR	40mR	50mR	60mR
0.00	95.7	97.0	98.0	98.9	99.5	99.9	100.0	99.9	99.5	98.9	98.0	97.0	95.7
0.16	*	97.0	98.1	98.9	99.5	99.9	100.0	99.9	99.5	98.9	98.0	96.9	*
0.32	*	97.0	98.1	98.9	99.5	99.9	100.0	99.9	99.5	98.9	98.0	96.9	*
0.48	*	97.1	98.1	99.0	99.5	99.9	100.0	99.9	99.5	98.8	98.0	96.9	*
0.64	*	97.1	98.1	99.0	99.6	99.9	100.0	99.8	99.5	98.8	97.9	96.8	*
0.80	*	97.1	98.2	99.0	99.6	99.9	100.0	99.8	99.4	98.8	97.9	96.8	*
0.95	*	*	98.2	99.0	99.6	99.9	100.0	99.8	99.4	98.8	97.9	*	*
1.11	*	*	98.2	99.0	99.6	99.9	100.0	99.8	99.4	98.8	97.9	*	*
1.27	*	*	*	99.0	99.6	99.9	100.0	99.8	99.4	98.7	*	*	*
1.43	*	*	*	*	99.6	99.9	100.0	99.8	99.4	*	*	*	*
1.59	*	*	*	*	*	*	100.0	*	*	*	*	*	*

Table 6.3 Survival of the beam polarization through a single solenoidal lens as a function of the deuteron beam's radial position and its divergence at the entrance to the cyclotron magnetic field. This table shows that approximately 13% depolarization is expected for the tensor component of a deuteron beam which has 60 mradian in divergence.

Deuteron at V = 15000. eV

Mass= 2.0 Spin= 1.0 Charge= 1. Myu= 0.8574376

Starting condition; R0= 1.59074202 mm

Maximum Divergence = 60.0 m Radian Upright ellipse

% Polarization (Tensor component)

as a function of radial position (R in mm) and dR/dz (divergence in m radian)

at the entrance to the cyclotron field

R	dR/dz (m Radian)												
mm	-60mR	-50mR	-40mR	-30mR	-20mR	-10mR	0mR	10mR	20mR	30mR	40mR	50mR	60mR
0.00	87.3	91.0	94.2	96.7	98.5	99.6	100.0	99.6	98.5	96.7	94.2	91.0	87.3
0.16	*	91.1	94.3	96.8	98.6	99.6	100.0	99.6	98.5	96.7	94.1	91.0	*
0.32	*	91.2	94.3	96.8	98.6	99.7	100.0	99.6	98.5	96.6	94.1	90.9	*
0.48	*	91.3	94.4	96.9	98.6	99.7	100.0	99.6	98.4	96.5	94.0	90.8	*
0.64	*	91.4	94.5	96.9	98.7	99.7	100.0	99.5	98.4	96.5	93.9	90.7	*
0.80	*	91.5	94.6	97.0	98.7	99.7	100.0	99.5	98.3	96.4	93.8	90.6	*
0.95	*	*	94.6	97.0	98.7	99.7	100.0	99.5	98.3	96.4	93.8	*	*
1.11	*	*	94.7	97.1	98.8	99.8	100.0	99.5	98.2	96.3	93.7	*	*
1.27	*	*	*	97.1	98.8	99.8	100.0	99.5	98.2	96.2	*	*	*
1.43	*	*	*	*	98.8	99.8	100.0	99.4	98.2	*	*	*	*
1.59	*	*	*	*	*	*	100.0	*	*	*	*	*	*

Table 6.4 Survival of the beam polarization through a single solenoidal lens as a function of the $^3He^{++}$ beam's radial position and its divergence at the entrance to the cyclotron magnetic field. This table shows that approximately 48% depolarization is expected for a $^3He^{++}$ beam which has 60 mradian in divergence.

$^3He^{++}$ at V = 15000. eV

Mass= 3.0 Spin= 0.5 Charge= 2. Myu=-2.1276240

Starting condition; RO= 1.59074202 mm

Maximum Divergence = 60.0 m Radian Upright ellipse

% Polarization

as a function of radial position (R in mm) and dR/dz (divergence in m radian)

at the entrance to the cyclotron field

R	dR/dz (m Radian)												
mm	-60mR	-50mR	-40mR	-30mR	-20mR	-10mR	0mR	10mR	20mR	30mR	40mR	50mR	60mR
0.00	52.7	66.2	77.9	87.3	94.3	98.6	100.0	98.6	94.3	87.3	77.9	66.2	52.7
0.16	*	66.5	78.2	87.6	94.5	98.6	100.0	98.5	94.2	87.1	77.6	65.9	*
0.32	*	66.9	78.4	87.8	94.6	98.7	100.0	98.4	94.0	86.9	77.3	65.5	*
0.48	*	67.2	78.7	88.0	94.7	98.8	100.0	98.3	93.9	86.7	77.0	65.2	*
0.64	*	67.5	79.0	88.2	94.9	98.9	100.0	98.3	93.7	86.5	76.8	64.9	*
0.80	*	67.9	79.3	88.4	95.0	98.9	100.0	98.2	93.5	86.2	76.5	64.5	*
0.95	*	*	79.5	88.6	95.2	99.0	100.0	98.1	93.4	86.0	76.2	*	*
1.11	*	*	79.8	88.8	95.3	99.0	100.0	98.0	93.2	85.8	75.9	*	*
1.27	*	*	*	89.0	95.4	99.1	99.9	97.9	93.1	85.6	*	*	*
1.43	*	*	*	*	95.6	99.2	99.9	97.8	92.9	*	*	*	*
1.59	*	*	*	*	*	*	99.9	*	*	*	*	*	*

three and therefore would reduce the depolarization to a less serious level (several %). Axial magnetic lenses can not be made to fit in the proposed place because of size, and therefore a permanent magnet was considered instead. However, it turns out that a number of such magnets are required so that whenever the extraction energy of the beam is changed the one with the right magnetic field is in place. Such replacements would be time consuming as well as inconvenient. Therefore this scheme has been reluctantly discarded for now. This decision might be reversed if the priority shifted towards heavy ion beams from polarized beams.

The use of magnetic quadrupoles was thought to be superior to electrostatic quadrupoles from the space charge neutralization point of view. For the PU cyclotron, it is expected that the neutralization has a noticeable effect starting at around 100 μA (15 keV proton beam) and becomes very important at around the 500 μA level. The injection of unpolarized proton and deuteron beams falls into this category, and therefore the space charge neutralization is very important. This point has to be weighed against the disadvantages of the magnetic elements which were discussed above. Unpolarized proton and deuteron beams, however, can be obtained from the existing internal source if we accept changing back to it whenever intense beams of these ions are required. It was eventually decided to retain the internal injection scheme for acceleration of intense unpolarized beams comming out of the PIG source while the axial injection system mainly takes care of the polarized ions and the high charge-state light heavy ions.

6.3 The Axial injection system of the Princeton University cyclotron

The designed injection system is schematically shown in figs. 6.1, 6.2 and

Fig. 6.1 The newly designed axial injection system for the Princeton University cyclotron. This figure shows that the axial injection system consists of a 90° bending/switching magnet at 4.63 m above the cyclotron median plane, three electrostatic quadrupole triplets, a beam buncher (combined first and second-harmonic mode), and an electrostatic mirror.

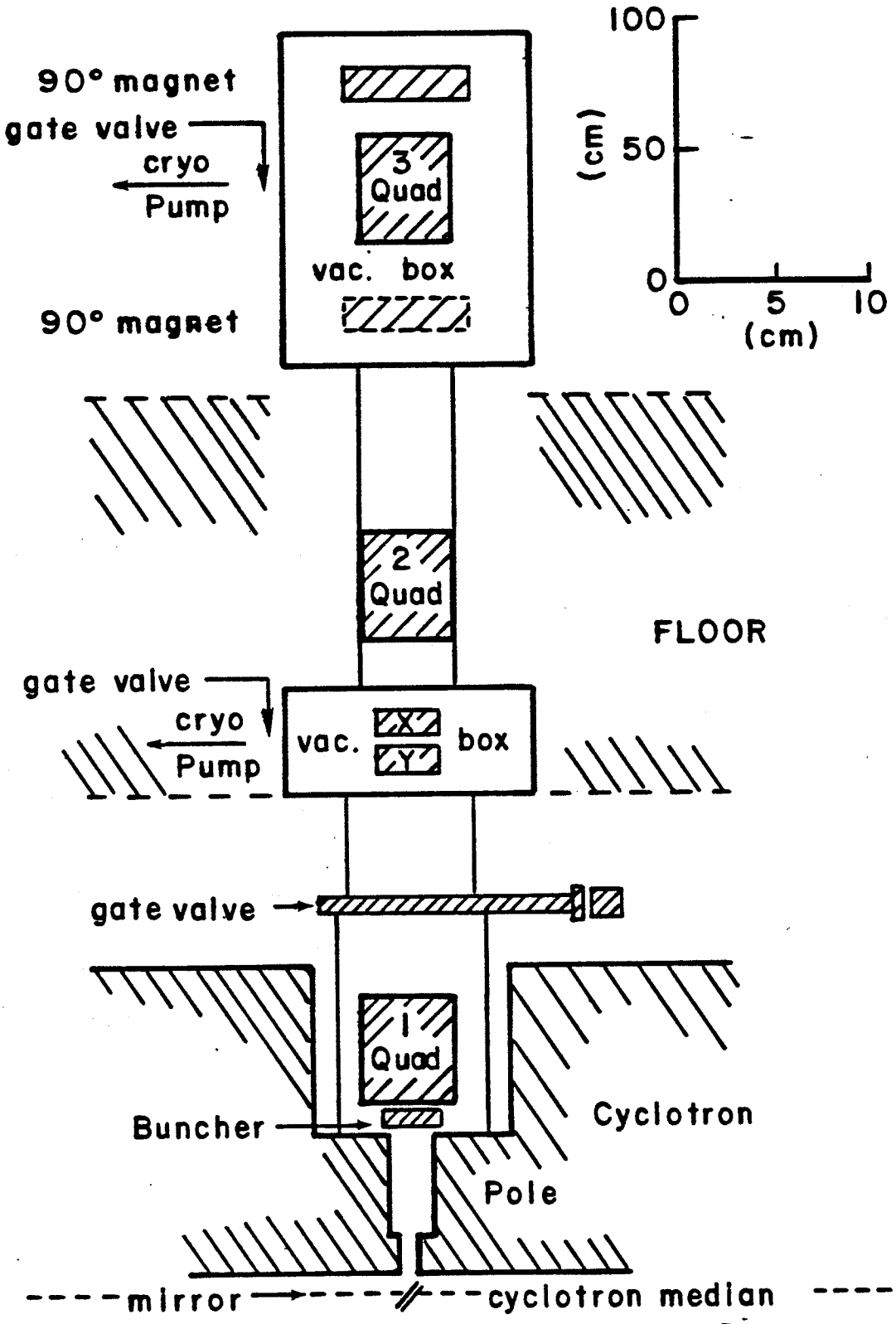
90° magnet
gate valve
cryo
Pump
3
Quad
vac. box
90° magnet
100
(cm) 50
0
0 5 10
(cm)
2
Quad
FLOOR
gate valve
cryo
Pump
vac.
box
gate valve
1
Quad
Buncher
Cyclotron
Pole
mirror
cyclotron median

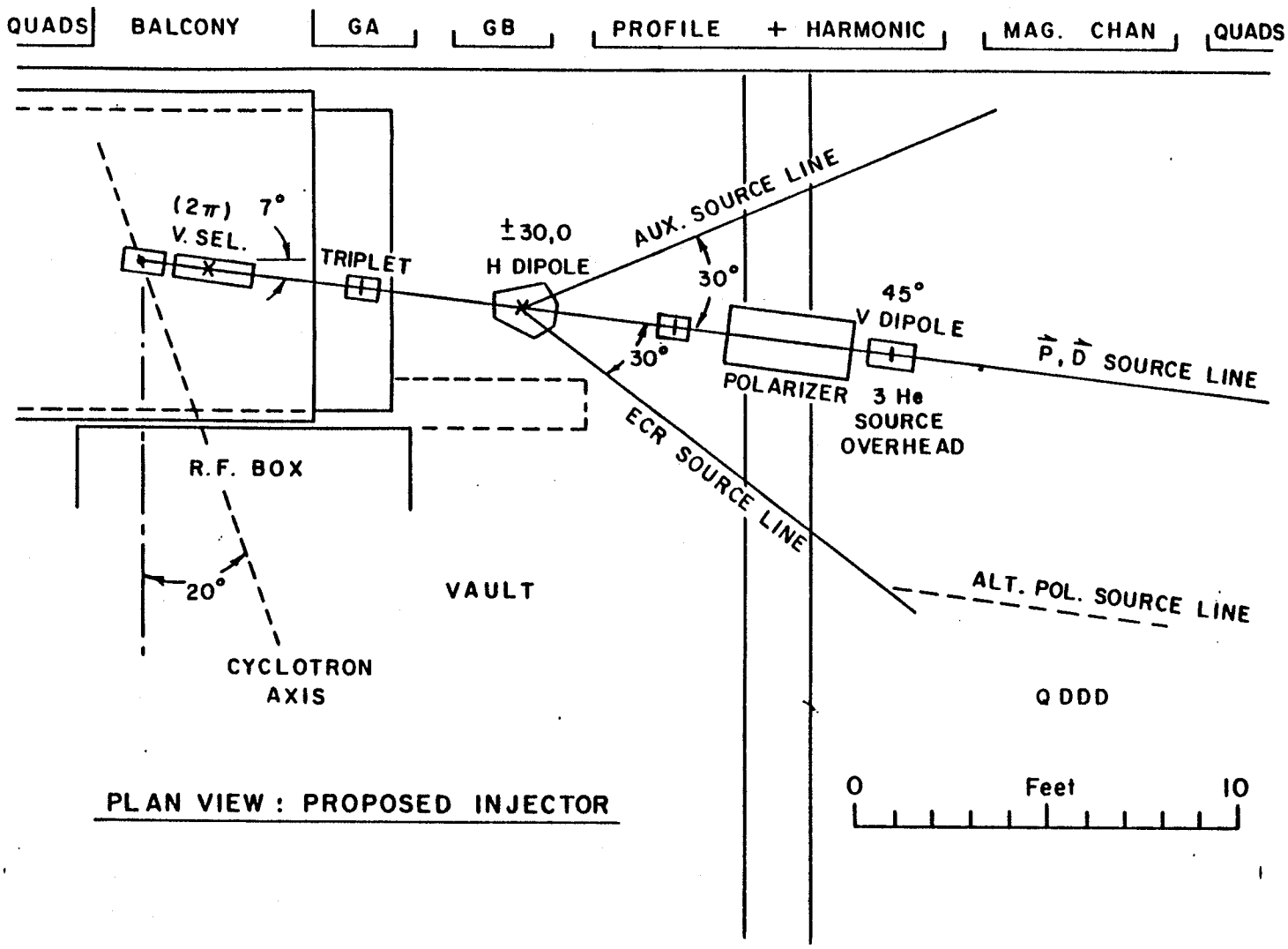

Fig. 6.2 The injector of the Princeton University cyclotron (plan view).

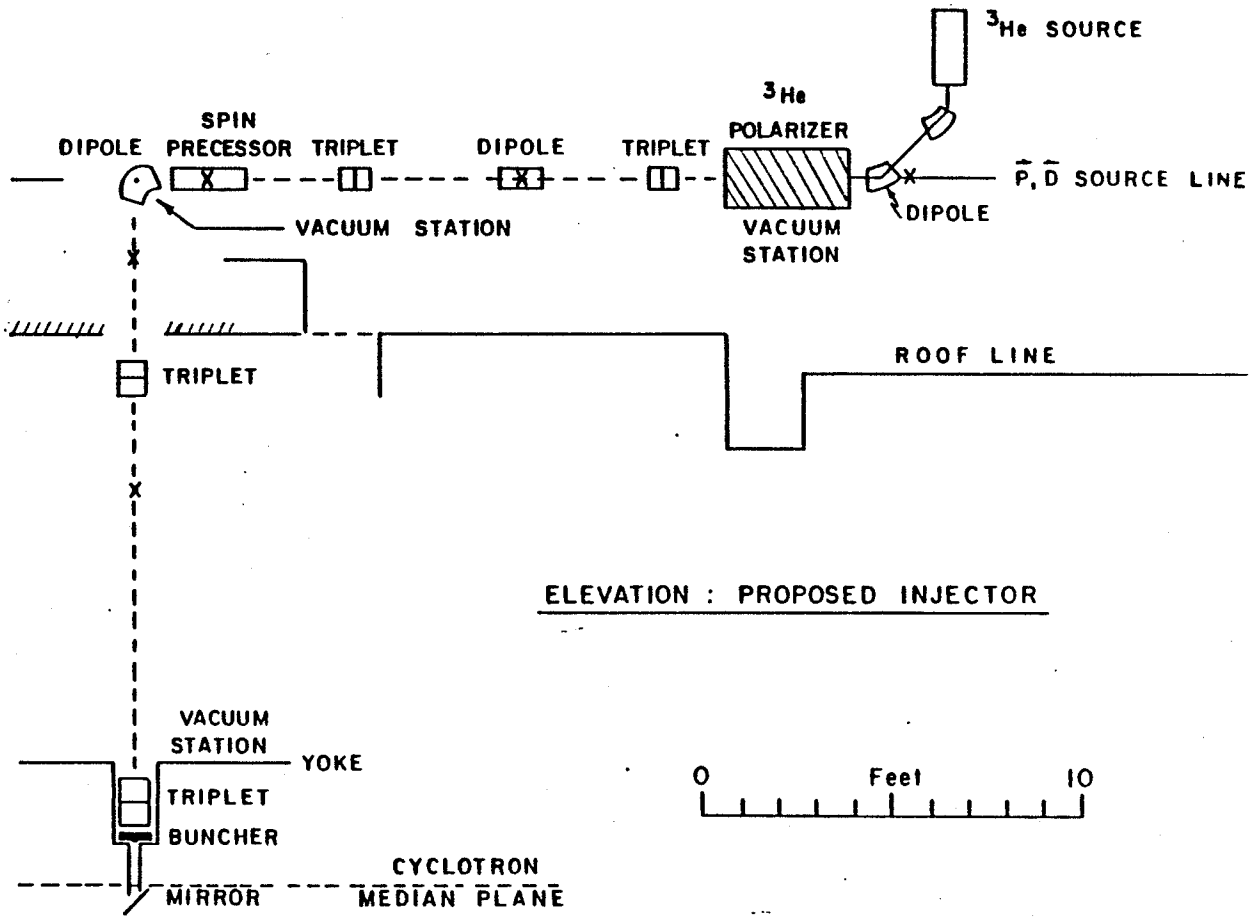

Fig. 6.3 The injector of the Princeton University cyclotron (elevation).

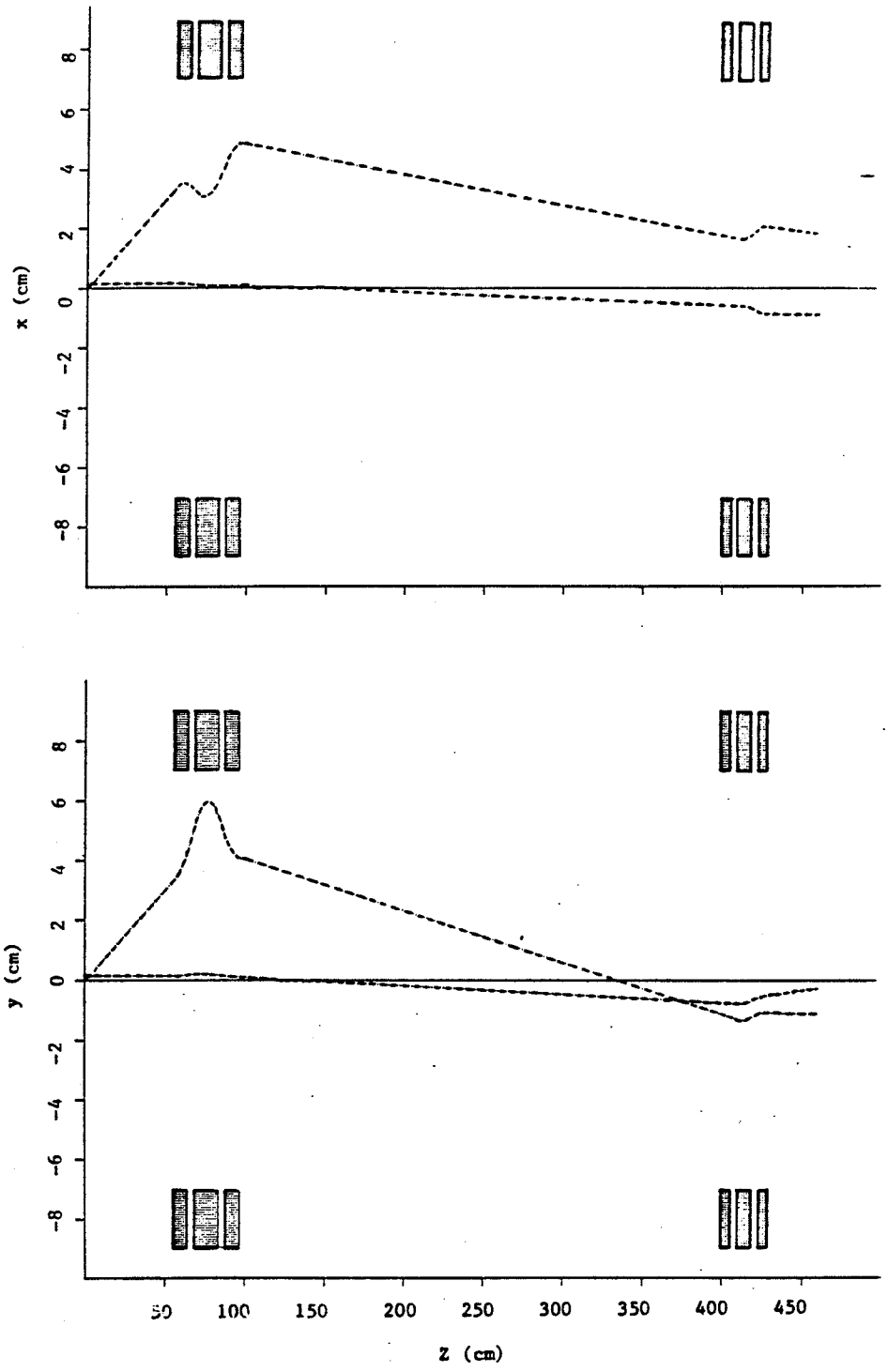

Fig. 6.4 The two computer simulated orthogonal particle trajectories through the electrostatic quadrupole triplets. The optics was chosen so that a beam of 140 mm mrad would form a uniform column of envelope whose diameter was 1.1 mm when this beam entered the cyclotron magnetic field.

6.3. It consists of a 90° bending/switching magnet at 4.63 m above the cyclotron median plane, two pairs of deflection electrodes (~0.1 radian), three electrostatic quadrupole triplets, a beam buncher (combined first- and second-harmonic) and an electrostatic mirror. Computer simulated trajectories for two mutually orthogonal paraxial rays through the electrostatic quadrupole triplets are shown in fig. 6.4. The optics are chosen so that a beam of 140 mm mrad will form a uniform column of envelope 1.1 mm in diameter when it enters the cyclotron field. In simulating the trajectories, we utilized a program SPEAM (developed at TRIUMF) which solves the beam envelope equation (or generalized Kapchinskij-Vladimirskij equation) by numerical integration. See ([KAP59], [LAP71], [EMI72], [TRI73]) for more details. A 46° mirror deflects the beam by 90° and then injects it into the cyclotron orbit. In the computer study, a model proton beam of 300 mm mrad was chosen. It was assumed to have injection energy of 15 keV with ±10 eV energy spread (this includes the contribution to the energy spread from the high voltage power supply). A beam buncher was then placed right after the last stage quadrupole triplet (z=56.5 cm). A superimposition of the fundamental and the 2^{nd} harmonic RF voltage is applied so that it compresses the portion of the beam which lies within ±45 RF phase degree to ±3 degree (see appendix 6-C). Recall that the PU cyclotron has ±3 degree RF phase acceptance for a separated turn extraction mode of acceleration. It reduces to ±1.5° when, in addition, a beam with high energy resolution is to be obtained. Placement of any strong focusing element downstream of the buncher increases the beam RF phase spread at the injection point by a large amount, and therefore the buncher has to be the last element before the mirror. This is the optimum position for a beam buncher for the assumed beam optical parameters.

Three electrostatic quadrupole triplets are employed along the axial injection system with another three triplets assigned to the beam lines leading to each ion source. A 90° bending magnet selects the beam line. All three triplets have a 5.08 cm (2″) aperture. A beam waist is formed inside the bending magnet. The first two triplets are used for beam transport whereas the last one is mainly for phase space matching.

A more complete description of the axial injection system is given below.

1) The electrostatic mirror consists of an inner electrode (at 14.3 kV for the 15 keV proton beam) and an outer electrode which is at ground potential. The latter has a surface formed by 0.127 mm (0.005″) thick parallel copper wires 1.83 mm (0.072″) apart. With this choice of wire spacing, an ion which enters the mirror through a space between wires will, on the average, be displaced by one spacing inside the mirror, and emerges through the next gap spacing thus reducing the loss of beam due to the wires. It has about an 85% transmission efficiency. The electrode surface is inclined at 46° to the median plane of the cyclotron. Both electrodes are water cooled. The gap between these electrode is 4 mm. The average electric field is 38 kV/cm but E_{max} is as high as 400 kV/cm where there can be a breakdown problem. The whole structure is shielded from the dee RF by a copper ground shield which surrounds the outer electrode. Some more descriptions can be found in appendix 6-B.

2) At the entrance to the cyclotron magnetic field (at z=11 cm), there is a large radial field component. This component depolarizes the incoming polarized beam to some extent. A depolarization study was carried out and the result

is shown in tables 6.5 to 6.8. It is shown there that up to 2% depolarization is expected for some fringe ray components. It is also expected that the average depolarization over the whole beam is 0.5 to 1% for a polarized $^3He^{++}$ beam.

3) The beam buncher is placed at z=56.7 cm, consisting of a half-wavelength cylinder, the ends of which face cylinders of identical inner and outer diameter. The outer cylinders are grounded while the inner one has an RF voltage applied in fundamental mode. The inner cylinder is actually split into two halves so that the second-harmonic RF can be applied between the two halves. Thus an ion will see a combined first- and second-harmonic RF field at the first and third gap crossing while it sees only the second-harmonic RF field at the second gap crossing. The beam is expected to have a diameter as large as 5 cm inside the buncher, and therefore the gap crossing is not an impulse but is spread over 3 cm. In order to improve the buncher action, fine copper wires will cover the cross sections of the cylinders so that the gaps are well defined by these screen surfaces. See appendix 6-C for more detail. The buncher needs V(first-harmonic) = 469 volt and V(second-harmonic) = 29 volt to compress 1/4 of the reference DC beam (of 360°) to 2.8° in RF phase. The two harmonic components have to have a 180° phase difference between them. The actual beam will have a compressed beam phase width which is much larger than the reference beam. The difference in optical path length from the buncher to the mirror between the on-axis and the marginal ray is 1.0 mm for the beam optics described in appendices 6-B and 6-C. The beam from the source is expected to have 20 eV energy spread. This corresponds to an additional 0.4 mm spread along the path. The total is equivalent to an

Table 6.5 Survival of the beam polarization through the axial magnetic field of the cyclotron as a function of the proton beam's radial position and its divergence at the entrance to the cyclotron magnetic field. This table shows that the depolarization effect is negligible.

Proton at V = 15000. eV

Mass= 1.0 Spin= 0.5 Charge= 1. Myu= 2.7928456

Starting condition; R0= 1.59074202 mm

Maximum Divergence = 60.0 m Radian Upright ellipse

% Polarization

as a function of radial position (R in mm) and dR/dz (divergence in m radian)

at the entrance to the cyclotron field

R	dR/dz (m Radian)											
mm	-60mR	-50mR	-40mR	-30mR	-20mR	-10mR	0mR	10mR	20mR	30mR	40mR	50mR	60mR
0.00	100.0	100.0	100.0	100.0	100.0	100.0	100.0	100.0	100.0	100.0	100.0	100.0	100.0
0.16	*	100.0	100.0	100.0	100.0	100.0	100.0	100.0	100.0	100.0	100.0	100.0	*
0.32	*	99.9	99.9	99.9	99.9	99.9	99.9	99.9	99.9	99.9	99.9	99.9	*
0.48	*	99.9	99.9	99.9	99.9	99.9	99.9	99.9	99.9	99.9	99.9	99.9	*
0.64	*	99.8	99.8	99.8	99.8	99.8	99.8	99.8	99.8	99.8	99.8	99.8	*
0.80	*	99.6	99.6	99.6	99.6	99.6	99.6	99.6	99.6	99.6	99.6	99.6	*
0.95	*	*	99.5	99.5	99.5	99.5	99.5	99.5	99.5	99.5	99.5	*	*
1.11	*	*	99.3	99.3	99.3	99.3	99.3	99.3	99.3	99.3	99.3	*	*
1.27	*	*	*	99.1	99.1	99.1	99.1	99.1	99.1	99.1	*	*	*
1.43	*	*	*	*	98.9	98.9	98.9	98.9	98.9	*	*	*	*
1.59	*	*	*	*	*	*	98.6	*	*	*	*	*	*

Table 6.6 Survival of the beam polarization through the axial magnetic field of the cyclotron as a function of the deuteron beam's radial position and its divergence at the entrance to the cyclotron magnetic field. This table shows that the depolarization effect is negligible for the vector component of the deuteron beam.

Deuteron at V = 15000. eV

Mass= 2.0 Spin= 1.0 Charge= 1. Myu= 0.8574376

Starting condition; R0= 1.59074202 mm

Maximum Divergence = 60.0 m Radian Upright ellipse

% Polarization (Vector component)

as a function of radial position (R in mm) and dR/dz (divergence in m radian)

at the entrance to the cyclotron field

R	dR/dz (m Radian)												
mm	-60mR	-50mR	-40mR	-30mR	-20mR	-10mR	0mR	10mR	20mR	30mR	40mR	50mR	60mR
0.00	100.0	100.0	100.0	100.0	100.0	100.0	100.0	100.0	100.0	100.0	100.0	100.0	100.0
0.16	*	100.0	100.0	100.0	100.0	100.0	100.0	100.0	100.0	100.0	100.0	100.0	*
0.32	*	100.0	100.0	100.0	100.0	100.0	100.0	100.0	100.0	100.0	100.0	100.0	*
0.48	*	100.0	100.0	100.0	100.0	100.0	100.0	100.0	100.0	100.0	100.0	100.0	*
0.64	*	99.9	99.9	99.9	99.9	99.9	99.9	99.9	99.9	99.9	99.9	99.9	*
0.80	*	99.9	99.9	99.9	99.9	99.9	99.9	99.9	99.9	99.9	99.9	99.9	*
0.95	*	*	99.8	99.8	99.8	99.8	99.8	99.8	99.8	99.8	99.8	*	*
1.11	*	*	99.7	99.7	99.7	99.7	99.7	99.7	99.7	99.7	99.7	*	*
1.27	*	*	*	99.7	99.7	99.7	99.7	99.7	99.7	99.7	*	*	*
1.43	*	*	*	*	99.6	99.6	99.6	99.6	99.6	*	*	*	*
1.59	*	*	*	*	*	*	99.5	*	*	*	*	*	*

Table 6.7 Survival of the beam polarization through the axial magnetic field of the cyclotron as a function of the deuteron beam's radial position and its divergence at the entrance to the cyclotron magnetic field. This table shows that the depolarization effect is negligible for the tensor component of the deuteron beam.

Deuteron at V = 15000. eV

Mass= 2.0 Spin= 1.0 Charge= 1. Myu= 0.8574376

Starting condition; R0= 1.59074202 mm

Maximum Divergence = 60.0 m Radian Upright ellipse

% Polarization (Tensor component)

as a function of radial position (R in mm) and dR/dz (divergence in m radian)

at the entrance to the cyclotron field

R	dR/dz (m Radian)												
mm	-60mR	-50mR	-40mR	-30mR	-20mR	-10mR	0mR	10mR	20mR	30mR	40mR	50mR	60mR
0.00	100.0	100.0	100.0	100.0	100.0	100.0	100.0	100.0	100.0	100.0	100.0	100.0	100.0
0.16	*	100.0	100.0	100.0	100.0	100.0	100.0	100.0	100.0	100.0	100.0	100.0	*
0.32	*	99.9	99.9	99.9	99.9	99.9	99.9	99.9	99.9	99.9	99.9	99.9	*
0.48	*	99.9	99.9	99.9	99.9	99.9	99.9	99.9	99.9	99.9	99.9	99.9	*
0.64	*	99.7	99.7	99.7	99.7	99.7	99.7	99.7	99.7	99.7	99.7	99.7	*
0.80	*	99.6	99.6	99.6	99.6	99.6	99.6	99.6	99.6	99.6	99.6	99.6	*
0.95	*	*	99.4	99.4	99.4	99.4	99.4	99.4	99.4	99.4	99.4	*	*
1.11	*	*	99.2	99.2	99.2	99.2	99.2	99.2	99.2	99.2	99.2	*	*
1.27	*	*	*	99.0	99.0	99.0	99.0	99.0	99.0	99.0	*	*	*
1.43	*	*	*	*	98.7	98.7	98.7	98.7	98.7	*	*	*	*
1.59	*	*	*	*	*	*	98.4	*	*	*	*	*	*

Table 6.8 Survival of the beam polarization through the axial magnetic field of the cyclotron as a function of the $^3He^{++}$ beam's radial position and its divergence at the entrance to the cyclotron magnetic field. This figure shows that the depolarization effect (about 2%) is negligible.

$^3He^{++}$ at V = 15000. eV

Mass= 3.0 Spin= 0.5 Charge= 2. Myu=-2.1276240

Starting condition; R0= 1.59074202 mm

Maximum Divergence = 60.0 m Radian Upright ellipse

% Polarization

as a function of radial position (R in mm) and dR/dz (divergence in m radian)

at the entrance to the cyclotron field

R	dR/dz (m Radian)											
mm	-60mR	-50mR	-40mR	-30mR	-20mR	-10mR	0mR	10mR	20mR	30mR	40mR	50mR	60mR
0.00	100.0	100.0	100.0	100.0	100.0	100.0	100.0	100.0	100.0	100.0	100.0	100.0	100.0
0.16	*	100.0	100.0	100.0	100.0	100.0	100.0	100.0	100.0	100.0	100.0	100.0	*
0.32	*	99.9	99.9	99.9	99.9	99.9	99.9	99.9	99.9	99.9	99.9	99.9	*
0.48	*	99.8	99.8	99.8	99.8	99.8	99.8	99.8	99.8	99.8	99.8	99.8	*
0.64	*	99.7	99.7	99.7	99.7	99.7	99.7	99.7	99.7	99.7	99.7	99.7	*
0.80	*	99.5	99.5	99.5	99.5	99.5	99.5	99.5	99.5	99.5	99.5	99.5	*
0.95	*	*	99.3	99.3	99.3	99.3	99.3	99.3	99.3	99.3	99.3	*	*
1.11	*	*	99.1	99.1	99.1	99.1	99.1	99.1	99.1	99.1	99.1	*	*
1.27	*	*	*	98.8	98.8	98.8	98.8	98.8	98.8	98.8	*	*	*
1.43	*	*	*	*	98.5	98.5	98.5	98.5	98.5	*	*	*	*
1.59	*	*	*	*	*	*	98.2	*	*	*	*	*	*

additional spread of 6°. This is much larger than the acceptance width of 3°, and therefore we expect to lose marginal rays.

4) An electrostatic quadrupole triplet at z=66 cm has a 50.8 mm (2″) aperture for beam passage. The length is 66 mm (2.6″), 101.6 mm (4″) and 66 mm (2.6″) each with a 20.3 mm (0.8″) gap between them. The radius of curvature of the pole-tip is 22.9 mm (1.15″). A non-magnetic stainless steel is used. Each of the quadrupoles is supported by a pair of 19.1 mm (0.75″) diameter ceramic insulators and mounted on a 190.5 mm (7.5″) inner diameter (203.2 mm = 8″ outer diameter) mild steel tube. Two beam trajectories are shown in fig. 6.4. The main function of this triplet is for beam emittance matching to the cyclotron acceptance. As such, this lens determines the acceptance of the axial injection system. It needs 1.1 kV maximum DC to the poles.

5) The main objective of a 9″ (228.6 mm) pneumatic gate valve at z=137 cm is to isolate the upstream portion (which includes the ion sources) from the downstream portion and the cyclotron. The large aperture of this valve helps pumping.

6) A pair of deflection magnets, one at z=198 cm and the other at z=213 cm are for providing corrections for any beam misalignment in the x and y direction. Each has a 50.8 mm (2″) gap with a 101.6 mm by 101.6 mm (4″ × 4″) area. They provide up to 100 mradian of beam steering capability.

7) The first vacuum box at z=190 cm is made of aluminum with a size of 30.48 cm by 30.48 cm by 50.8 cm (12″ × 12″ × 20″) and is attached with two 6″ (15.24 cm) cryo-pumps and turbo-molecular pumps via gate valves. This is

the main part for pumping the axial injection system to 1×10^{-7} Torr. Only one of the two pumps at a time may be needed so that the other is always on stand-by in case there is a vacuum burst *etc.*. The x and y deflection magnets are housed in it, as well as some beam diagnostic devices.

8) A second electrostatic quadrupole triplet at z=250 cm is identical in construction to the above-mentioned quadrupole. This lens is not needed for beams which enter the axial injection system at z=463 cm as can be seen in fig. 6.1. This element is, however, required for beams that enter the injection system possibly at z=370 cm.

9) The structure of the third electrostatic quadrupole triplet at z=411 cm is identical to the quadrupoles described above. Its function is to focus the beam so that the beam forms waists in the middle of the 90° bending/switching magnet directly above the triplet. The voltage requirement is rather modest (600 V DC).

10) A 90° bending/switching magnet has a 12.7 cm (5″) pole piece diameter and a 3.048 cm (1.2″) gap. Thirty six turns of 4.7625 mm (0.1875″) square copper tube windings with 200 A will provide a 0.3 T maximum field. Three beam lines branch out from here. It is envisaged that polarized sources occupy each of the horizontal beam lines while an ECR source uses the vertical beam line.

11) A second vacuum box at z=354 cm houses the third quadrupole lens and the 90° bending magnet. A minimum of two collimators and two fluorescent screens are planned to be housed inside. A minimum of three beam ports are required as was described above. The three pumps mentioned above are

planned to be attached onto this box via gate valves. A number of see-through windows as well as various feed-throughs (for the quadrupoles, the bending magnet, the cooling water, vacuum gauge, *etc.*.) are planned to be attached to it.

12) There is a varying strength of leakage magnetic field along the axial injection system arising from the cyclotron. This can do a lot of harm to the quality and stability of the beam being transported depending on the strength of its horizontal component. Provisions are made to shield the horizontal component of the leakage field throughout the axial transport line.

Appendix 6-A

An Axial Injection System of the Princeton University Cyclotron based on Axial Magnetic Lenses

The system consists of the following elements.

1) An electrostatic mirror at z=0 (median plane of the cyclotron) is identical with the one described in the main text. It operates at 14.3 kV for a 15 keV proton beam.

2) A beam buncher (combined first- and second-harmonic) at z=56.7 cm is also identical to the one contained in the main text.

3) An axial magnetic lens at z=66 cm produces up to a 0.3 T axial magnetic field with an operating magnetic field for a 15 keV proton beam of 0.1655 T. Its dimensions and parameters are as follows.

   Dimension:

   Solenoid length=10.16 cm (4.0″) winding, overall length= 14.224 cm (5.6″), inner diameter=10.16 cm (4.0″), outer diameter=18.796 cm (7.4″), 0.635 cm (0.25″) thick stainless steel inner tubing, 0.635 cm (0.25″) thick outer tube for magnetic field return path (B=0.35 T at maximum in the return path), two mild steel side walls of 1.27 cm (0.5″) thickness

   Winding:

   20 turns/layer×6 layers of 0.47625 cm (0.1875″) square copper tubing (=0.238 cm (3/32″) for water cooling). i_{max}=200 Amp. V_{max}=15 V, R=0.057 ohm 2.2 kW max.

For a 15 keV proton beam, it needs i=110 Amp., V=6.3 volt. 690 W.

Water cooling requirement:

To keep the temperature rise to ΔT=20°C at i=110 Amp., 30 cc/sec of cooling water is required (corresponds to 1.4 m/sec flow speed for parallel coupling).

4) A second (at z=250 cm) and a third (at z=397 cm) solenoidal lenses produce up to a 0.2 T axial magnetic field with an operating magnetic field for a 15 keV proton beam of around 0.12 T. The required fields for these two lenses are inter-dependent to each other and to the beam phase emittance characteristics. The second solenoid may not be required for beams that are already focused by the third lens. It is, however, possible that a polarized source (possibly the polarized $^3He^{++}$) might be placed in such a way that the beam from it enters the axial injection axis at almost floor level of the ion source compartment. The second lens is then required for focusing of the beam. The design parameters of these lenses are as follows.

Dimension:

Solenoid length (winding) = 10.16 cm (4.0″), overall length=12.954 cm (5.1″), inner diameter= 6.35 cm (2.5″), outer diameter=12.6492 cm (4.98″), 0.635 cm (0.25″) thick stainless steel inner tubing, 0.47625 cm (0.1875″) thick mild steel outer tube for magnetic return path (B= 0.2 T at maximum inside the return path), two mild steel side walls of 0.635 cm (0.25″) thickness.

Winding:

20 turn/layer×4 layers 0.47625 cm (0.1875″) square copper tubing (= 0.238 cm (3/32″) for cooling water flow). i_{max}=200 Amp., V_{max}=5 V, R=0.025 ohm 1.0 kW max.

For a 15 keV proton beam it needs i=120 Amp, V=3 volt, 350 W.

Water cooling requirement:

To keep the temperature rise to ΔT=20°C at i=200 Amp., 12 cc/sec of cooling water is required (corresponds to 0.94 m/sec of water flow speed for parallel coupling).

5) A pair of deflection magnets for steering in the x- (at z=198 cm) and y- (at z=213 cm)plane have a 10.16 cm by 10.16 cm ($4'' \times 4''$) pole face area with edge correction, a 5.08 cm ($2''$) gap, and a 0.1 radian maximum deflection.

6) A 90° bending magnet with its center at z=463.2 cm is identical to the one contained in the main chapter. The atomic beam source for polarized protons and deuterons may be mounted horizontally at this height from the median plane of the cyclotron. This bending magnet directs the beams from horizontal beam lines into the axial injection system.

Appendix 6-B

The Electrostatic Mirror

The mirror consists of a central electrode and a ground electrode which encases the former. The latter is in essence made of a thin stainless steel tube [1.708 cm (0.67″) in inner diameter and 1.8034 cm (0.71″) in outer diameter] whereas the former is made of an oxygen-free copper rod of 1.9022 cm (0.43″) diameter. Both are cut to 46° with respect to the axial injection axis to form two surfaces that define the mirror electric field. One of these surfaces (the ground) has fine thin tungsten wires (0.127 mm thick, 1.83 mm spacing) across it to form the ground electrode which is 85% transparent to the beam. The mirror voltage is 14.3 keV for a 15 kV proton beam. The gap between the two surfaces is 4.0 mm which corresponds to 5.76 mm along the vertical axis. Both electrodes are water cooled. A thin boron-nitride tube is inserted between the two electrodes to prevent electric breakdown. The ground electrode is enclosed in a thin (0.5 mm thick) oxygen-free copper tube to shield the beam and the mirror from the dee RF field.

The equations of motion of the ions are given by

$$\begin{aligned} \frac{d^2z}{dt^2} &= \frac{eE_z}{m} \\ \frac{d^2x}{dt^2} &= \frac{eE_x}{m} + \frac{eB_z}{m}\frac{dy}{dt} \\ \frac{d^2y}{dt^2} &= -\frac{eB_z}{m}\frac{dx}{dt}. \end{aligned} \qquad (6.B.1)$$

Solution of the above equations are

$$
\begin{aligned}
z &= \frac{eE_z}{2m}t^2 - \frac{dz_0}{dt}t + z_0 \\
x &= \frac{mE_x}{eB_z^2}[1 - \cos(\frac{eB_z}{m}t)] + \frac{m}{eB_z}\frac{dy_0}{dt} \\
y &= -\frac{mE_x}{eB_z^2}[\frac{eB_z}{m}t - \sin(\frac{eB_z}{m}t)] + y_0.
\end{aligned}
\qquad (6.B.2)
$$

On the other hand, the mirror ground surface is defined (in *mks* units) by

$$z = 0.00576 - x\tan 46^\circ = 0.00576 - 1.03553x. \qquad (6.B.3)$$

For the on-axis (reference) ray, dy_0/dt=0. After substituting constants and field values:

$$
\begin{aligned}
e &= 1.6021892 \times 10^{-19} \quad coulomb \\
m &= 1.6726 \times 10^{-27} \quad kg \\
B_z &= 1.335 \quad tesla \\
\frac{dz}{dt} &= 1.6952 \times 10^6 \quad m/sec \\
E &= 3.54 \times 10^6 \quad V/m \\
E_z &= E\cos 46^\circ = 2.46 \times 10^6 \quad V/m \\
E_x &= E\sin 46^\circ = 2.54 \times 10^6 \quad V/m.
\end{aligned}
\qquad (6.B.4)
$$

The equations become:

$$
\begin{aligned}
z &= 1.176954 \times 10^{14}t^2 - 1.6952 \times 10^6 t + 0.00576 \\
x &= 0.01487817[1 - \cos(1.278801 \times 10^8 t)] \\
y &= -0.01487817[1.278801 \times 10^8 t - \sin(1.278801 \times 10^8 t)].
\end{aligned}
\qquad (6.B.5)
$$

This ion emerges from the mirror surface at $t = 7.1938 \times 10^{-9}$ sec. with v_z=0. For this value of t, the other parameters are listed in table 6.9 below.

It can be seen (from "beam center shift" in the table) that the centre of curvature of the reference ion after injection is shifted by only a small amount from the corresponding center with an impulse mirror (a hard-edge mirror which has a 45° tilt angle). The mirror can therefore be regarded as an impulse mirror to first-order. One noticeable difference from an impulse mirror is the exit point of the ion from the mirror ground plane. The ion moves in the y direction by -1.83 mm. The mirror ground surface is made up of thin parallel tungsten wires. Therefore if we place them all in the $x-z$ plane direction and choose the inter spacing to be 1.83 mm then the loss of beam from these wires is minimized.

The beam on entering the mirror has about ± 300 eV spread in energy (the beam buncher that is placed upstream causes such a large energy spread). This energy spread results in the dispersion of the beam on passing through the mirror. This is also shown in table 6.9. It indicates that the effect is not significant (dx=0.23 mm, dy=0.3 mm additional vertical spread, 1.5 mrad additional beam divergence, *etc.*)

The wires that form the surface of the ground electrode distort the beam. This distortion effect has not been studied in detail.

Table 6.9 The design parameters of the electrostatic mirror for the proton beam whose injection energy is 15 keV.

The mirror design parameters

Proton beam at 15000 Volt

Cyclotron field = 1.335 tesla Mirror tilt angle = 46 degree

Mirror voltage = 14280 Volt Mirror field = 35.7 kV/cm

Mirror gap = 4.0 mm Vertical gap = 5.76 mm

x = 5.84 mm y = -1.83 mm z = -0.29 mm

v_x = 1521755 m/sec v_y = -746918 m/sec v_z = 0.0 mm

The beam center is shifted by;

x = 0.0 mm y = -0.47 mm z = -0.29 mm

Dispersion effect; (the buncher induces 300 eV in energy spread)
Proton beam at 15300 Volt

x = 5.96 mm y = -1.89 mm z = -0.41 mm

v_x = 1533190 m/sec v_y = -761856 m/sec v_z = 1298 m/sec

The beam center is shifted by;

x = 0.0 mm y = -0.62 mm z = -0.41 mm

Appendix 6-C

The Beam Buncher

In tables 6.10 to 6.14, some results of a study for the beam buncher are presented. Table 6.10 shows the degree of DC beam bunching for an on-axis beam. This beam is then subjected to an energy spread of ± 10 eV and the result is shown in table 6.11. In table 6.12, the first-harmonic component of the buncher RF voltage (V_1) is increased by 2 volt to study the sensitivity of the bunching to the fluctuation in the buncher RF voltage. A similar investigation was carried out for V_2 by reducing V_2 by 0.3 volt and is shown in table 6.13. In table 6.14, V_2 is given a two degree advancement in RF phase with respect to V_1 to investigate the effect of fluctuations in the buncher RF phase. All these show that the effect can be contained to within 0.5° in phase bunching with appropriate power supplies and controls. As was described in the main text, the major cause of phase bunching is the difference in the optical path length between the on-axis ray and the marginal rays. This difference contributes 4.4 RF degrees for rays with 60 mradian divergence. By cutting the accepted divergence down to 40 mradian, the debunching can be reduced to two RF degrees. With this reduced divergence, the phase width is approximately two degrees plus an additional one degree from space charge effects *etc.* (space charge can result in a serious phase debunching for unpolarized beams which have large beam currents).

Table 6.10 The degree of the compression of a DC beam by the beam buncher for an on-axis proton beam with the energy of 15 keV.

The beam buncher

Proton at 15000. eV

Buncher exit is at z = 0.6 cm from the 1st dee RF gap

1st harmonic buncher = 469.0 Volt

2nd harmonic buncher = -29.31 Volt

Buncher RF phase(1) vs. arrival time of ions (2 in RF degree)

1	-50	-49	-48	-47	-46	-45	-44	-43	-42	-41
2	1.3	1.3	1.3	1.3	1.3	1.3	1.3	1.3	1.3	1.2
1	-40	-39	-38	-37	-36	-35	-34	-33	-32	-31
2	1.2	1.2	1.2	1.1	1.1	1.1	1.0	1.0	1.0	0.9
1	-30	-29	-28	-27	-26	-25	-24	-23	-22	-21
2	0.9	0.8	0.8	0.8	0.7	0.7	0.6	0.6	0.6	0.5
1	-20	-19	-18	-17	-16	-15	-14	-13	-12	-11
2	0.5	0.5	0.4	0.4	0.4	0.3	0.3	0.3	0.2	0.2
1	-10	-9	-8	-7	-6	-5	-4	-3	-2	-1
2	0.2	0.2	0.1	0.1	0.1	0.1	0.1	0.0	0.0	0.0
1	0	1	2	3	4	5	6	7	8	9
2	0.0	0.0	0.0	0.0	0.0	-0.1	-0.1	-0.1	-0.1	-0.1
1	10	11	12	13	14	15	16	17	18	19
2	-0.1	-0.1	-0.1	-0.1	-0.1	-0.1	-0.1	-0.1	0.0	0.0
1	20	21	22	23	24	25	26	27	28	29
2	0.0	0.0	0.0	0.0	0.0	0.1	0.1	0.1	0.1	0.2
1	30	31	32	33	34	35	36	37	38	39
2	0.2	0.2	0.3	0.3	0.3	0.4	0.4	0.5	0.5	0.6
1	40	41	42	43	44	45	46	47	48	49
2	0.7	0.7	0.8	0.9	1.0	1.0	1.1	1.2	1.3	1.4

Table 6.11 The degree of the compression of a DC beam by the beam buncher for an on-axis proton beam with the energy of 15.01 keV.

The beam buncher (continued)

Proton at 15010. eV

The effect of beam energy spread (10 eV) upon arrival time

1st harmonic buncher = 469.0 Volt

2nd harmonic buncher = -29.31 Volt

Buncher RF phase vs. arrival time of ions (in RF degree)

1	-50	-49	-48	-47	-46	-45	-44	-43	-42	-41
2	1.3	1.3	1.3	1.3	1.3	1.3	1.3	1.3	1.2	1.2
1	-40	-39	-38	-37	-36	-35	-34	-33	-32	-31
2	1.2	1.2	1.1	1.1	1.1	1.1	1.0	1.0	1.0	0.9
1	-30	-29	-28	-27	-26	-25	-24	-23	-22	-21
2	0.9	0.8	0.8	0.8	0.7	0.7	0.7	0.6	0.6	0.5
1	-20	-19	-18	-17	-16	-15	-14	-13	-12	-11
2	0.5	0.5	0.4	0.4	0.4	0.4	0.3	0.3	0.3	0.2
1	-10	-9	-8	-7	-6	-5	-4	-3	-2	-1
2	0.2	0.2	0.2	0.1	0.1	0.1	0.1	0.1	0.1	0.0
1	0	1	2	3	4	5	6	7	8	9
2	0.0	0.0	0.0	0.0	0.0	0.0	0.0	0.0	0.0	0.0
1	10	11	12	13	14	15	16	17	18	19
2	0.0	0.0	0.0	0.0	0.0	0.0	0.0	0.0	0.0	0.0
1	20	21	22	23	24	25	26	27	28	29
2	0.0	0.0	0.1	0.1	0.1	0.1	0.1	0.2	0.2	0.2
1	30	31	32	33	34	35	36	37	38	39
2	0.2	0.3	0.3	0.4	0.4	0.4	0.5	0.5	0.6	0.7
1	40	41	42	43	44	45	46	47	48	49
2	0.7	0.8	0.9	0.9	1.0	1.1	1.2	1.3	1.4	1.5

Table 6.12 The degree of the compression of a DC beam by the beam buncher for an on-axis proton beam with the energy of 15 keV. The voltage of the first-harmonic buncher was increased by 2 V.

The beam buncher (continued)

V1 is increased by 2 Volt

Proton at 15000. eV

1st harmonic buncher = 471.0 Volt

2nd harmonic buncher = -29.31 Volt

Buncher RF phase(1) vs. arrival time of ions (2 in RF degree)

1	-50	-49	-48	-47	-46	-45	-44	-43	-42	-41
2	1.6	1.6	1.6	1.6	1.6	1.6	1.5	1.5	1.5	1.5
1	-40	-39	-38	-37	-36	-35	-34	-33	-32	-31
2	1.4	1.4	1.4	1.3	1.3	1.3	1.2	1.2	1.1	1.1
1	-30	-29	-28	-27	-26	-25	-24	-23	-22	-21
2	1.0	1.0	1.0	0.9	0.9	0.8	0.8	0.7	0.7	0.7
1	-20	-19	-18	-17	-16	-15	-14	-13	-12	-11
2	0.6	0.6	0.5	0.5	0.5	0.4	0.4	0.4	0.3	0.3
1	-10	-9	-8	-7	-6	-5	-4	-3	-2	-1
2	0.3	0.2	0.2	0.2	0.1	0.1	0.1	0.1	0.0	0.0
1	0	1	2	3	4	5	6	7	8	9
2	0.0	0.0	0.0	-0.1	-0.1	-0.1	-0.1	-0.1	-0.1	-0.1
1	10	11	12	13	14	15	16	17	18	19
2	-0.1	-0.1	-0.1	-0.1	-0.2	-0.2	-0.2	-0.2	-0.1	-0.1
1	20	21	22	23	24	25	26	27	28	29
2	-0.1	-0.1	-0.1	-0.1	-0.1	-0.1	-0.1	0.0	0.0	0.0
1	30	31	32	33	34	35	36	37	38	39
2	0.0	0.1	0.1	0.1	0.2	0.2	0.2	0.3	0.3	0.4
1	40	41	42	43	44	45	46	47	48	49
2	0.5	0.5	0.6	0.7	0.7	0.8	0.9	1.0	1.1	1.2

Table 6.13 The degree of the compression of a DC beam by the beam buncher for an on-axis proton beam with the energy of 15 keV. The voltage of the second-harmonic buncher was reduced by 0.3 V.

The beam buncher (continued)

Proton at 15000. eV

V2 is reduced by 0.3 Volt

1st harmonic buncher = 469.0 Volt

2nd harmonic buncher = -29.01 Volt

Buncher RF phase(1) vs. arrival time of ions (2 in RF degree)

1	-50	-49	-48	-47	-46	-45	-44	-43	-42	-41
2	1.4	1.4	1.4	1.4	1.4	1.4	1.4	1.4	1.4	1.3
1	-40	-39	-38	-37	-36	-35	-34	-33	-32	-31
2	1.3	1.3	1.3	1.2	1.2	1.2	1.1	1.1	1.0	1.0
1	-30	-29	-28	-27	-26	-25	-24	-23	-22	-21
2	1.0	0.9	0.9	0.8	0.8	0.8	0.7	0.7	0.6	0.6
1	-20	-19	-18	-17	-16	-15	-14	-13	-12	-11
2	0.6	0.5	0.5	0.5	0.4	0.4	0.4	0.3	0.3	0.3
1	-10	-9	-8	-7	-6	-5	-4	-3	-2	-1
2	0.2	0.2	0.2	0.1	0.1	0.1	0.1	0.1	0.0	0.0
1	0	1	2	3	4	5	6	7	8	9
2	0.0	0.0	0.0	0.0	-0.1	-0.1	-0.1	-0.1	-0.1	-0.1
1	10	11	12	13	14	15	16	17	18	19
2	-0.1	-0.1	-0.1	-0.1	-0.1	-0.1	-0.1	-0.1	-0.1	-0.1
1	20	21	22	23	24	25	26	27	28	29
2	-0.1	-0.1	-0.1	-0.1	0.0	0.0	0.0	0.0	0.0	0.1
1	30	31	32	33	34	35	36	37	38	39
2	0.1	0.1	0.2	0.2	0.3	0.3	0.3	0.4	0.4	0.5
1	40	41	42	43	44	45	46	47	48	49
2	0.6	0.6	0.7	0.8	0.9	1.0	1.0	1.1	1.2	1.4

Table 6.14 The degree of the compression of a DC beam by the beam buncher for an on-axis proton beam with the energy of 15 keV. The RF phase of the second-harmonic buncher is advanced by 1.5° with respect to that of the first-harmonic buncher.

The beam buncher (continued)

Proton at 15000. eV

The RF phase of V2 is advanced by 1.5 with respect to V1

1st harmonic buncher = 469.0 Volt

2nd harmonic buncher = -29.31 Volt

Buncher RF phase(1) vs. arrival time of ions (2 in RF degree)

1	-50	-49	-48	-47	-46	-45	-44	-43	-42	-41
2	1.3	1.3	1.3	1.3	1.3	1.3	1.3	1.3	1.3	1.3
1	-40	-39	-38	-37	-36	-35	-34	-33	-32	-31
2	1.3	1.3	1.2	1.2	1.2	1.2	1.1	1.1	1.1	1.0
1	-30	-29	-28	-27	-26	-25	-24	-23	-22	-21
2	1.0	1.0	1.0	0.9	0.9	0.9	0.8	0.8	0.8	0.7
1	-20	-19	-18	-17	-16	-15	-14	-13	-12	-11
2	0.7	0.7	0.6	0.6	0.6	0.6	0.5	0.5	0.5	0.5
1	-10	-9	-8	-7	-6	-5	-4	-3	-2	-1
2	0.4	0.4	0.4	0.4	0.4	0.3	0.3	0.3	0.3	0.3
1	0	1	2	3	4	5	6	7	8	9
2	0.3	0.2	0.2	0.2	0.2	0.2	0.2	0.2	0.2	0.2
1	10	11	12	13	14	15	16	17	18	19
2	0.2	0.2	0.1	0.1	0.1	0.1	0.1	0.1	0.2	0.2
1	20	21	22	23	24	25	26	27	28	29
2	0.2	0.2	0.2	0.2	0.2	0.2	0.2	0.2	0.3	0.3
1	30	31	32	33	34	35	36	37	38	39
2	0.3	0.3	0.4	0.4	0.4	0.5	0.5	0.6	0.6	0.7
1	40	41	42	43	44	45	46	47	48	49
2	0.7	0.8	0.8	0.9	1.0	1.1	1.1	1.2	1.3	1.4

Chapter 7

Studies of the Central Region

7.1 Introduction

An axially injected beam, when it reaches the central region of a cyclotron, has a non-zero value for its energy. This means that the trajectory of a beam from an external source in the cyclotron central region, especially for the first several turns, differs from the trajectory of a beam from an internal source in which the initial energy is near zero. It is, therefore, necessary to modify the central region of the cyclotron if an internal source is to be replaced by an external source.

During the design study of the axial injection system of the PU cyclotron, a detail of which has already been in the previous chapter, it was assumed that once the axially injected beam entered the cyclotron magnetic field, this beam would form a column with constant radius (an upright phase space ellipse whose shape was invariant until the beam reaches the mirror). This radius is given by

$$r = \sqrt{\frac{2A}{B\pi}\sqrt{\frac{2mv}{q}}}, \tag{7.1.1}$$

where A is a beam phase space area, and B, m, v, q have the usual meaning. If we assume that this is correct to first-order, then the study of the beam dynamics from the mirror onward can be carried out indenpendently.

The design study of the central region requires an accurate dee RF electric field and a magnetic field distribution throughout the central region. The beam orbit dynamics studies were carried out under the influence of these two fields in order

to determine the optimum central region geometry of the PU cyclotron. The RF electric field of the dee was obtained by employing a successive over-relaxation calculation, a method which was described in chapter 3. On the other hand, the data supplied by Michigan State University (hereafter MSU) for their K=50 cyclotron was substituted for the magnetic field. The latter was possible because both cyclotrons are regarded as having almost identical magnet structures [POL69].

In this chapter we present detailed design precedures and beam orbit dynamics investigations in the existing and in the new central region of the PU cyclotron. First, the method of magnetic field measurement on the MSU's K=50 cyclotron, which was carried out in the early 1960's, is introduced briefly. The beam orbit dynamics studies of a proton beam in the existing N=1 central region are then described. The purpose of these studies was to form a good basis for the design of a new central region in which the trajectory of an axially injected beam would lead to the same trajectory in the existing central region. Then a description of the design studies of the new N=1 central region follows. The beam orbit dynamics investigations in the existing N=2 central region as well as the design studies for the new N=2 central region are also presented. This chapter concludes with a description of the calculated total transmission efficiencies for various polarized and unpolarized ions through the axial injection system and the newly designed central region. A brief consideration to the resonant depolarization problem of the polarized ions during acceleration in the PU cyclotron is also given.

7.2 The magnetic fields

The MSU's magnetic field mapping was carried out in the early 1960's [BER66].

This mapping utilized a Hall probe to measure the magnetic field on the polar grids of points of one inch radial spacing at four degree azimuthal intervals. Data for seven different excitations of the main magnet and for four different excitations of the eight pairs of the concentric trim coil were Fourier analysed. The resulting data for the trim coil excitations and for the first three flutter components of the main magnet fields, as well as the average magnetic field, were then punched onto cards.

The SETOP program, a computer code which was developed at MSU, reads these magnetic fields to determine the precise optimum control setting parameters of the cyclotron ([BER66], [BER68]). With the particle's specification and it's maximum desired energy given as input parameters, the SETOP program interpolates (by using a double three-point Lagrangian method) the measured magnetic field in order to calculate the optimum field distribution. The field in the region where there is an axially or radially defocusing force is subsequently adjusted at the expense of abandoning isochronism so that the result always gives adequate focusing forces in both directions. The basic methods of calculating ν, ν_r and ν_z are nearly the same as those in MAPANL, an equilibrium orbit code which was described in chapter 2, and therefore we will not go into further detail here.

Unfortunately, there were no cyclotron magetic field data available at the PU AVF Cyclotron Laboratory. A brief measurement of the magnetic field for this cyclotron was carried out in the late 1960's after the cyclotron was completed. However, the result of this early measurement merely indicated that the cyclotron magnetic field was almost identical with the MSU's [PUC68], as had been expected. Therefore, for the beam orbit dynamics studies described below, the magnetic field data for the PU cyclotron has been taken from the result of the MSU measurement.

In order to obtain the magnetic field data, the program SETOP, mentioned above, was used after slight modifications to match the format of the beam orbit dynamics program NUTRACK. A contour map for a 48 MeV proton beam which was obtained in this way is depicted in fig. 7.1. The numbers shown in this figure specify the magnetic field values in tesla.

7.3 The beam orbit dynamics in the existing N=1 central region

Prior to the design of the new central region, beam orbit dynamics studies in the existing N=1 central region were carried out. The necessity of performing such studies can be seen by glancing at some features of the PU cyclotron; unlike the University of Manitoba cyclotron, whose upgrading program was treated in detail in part I of this thesis, the PU cyclotron accelerates positive ions, and the extraction of a beam is made by utilizing a precessional extraction method. There are two features that are worth noting in the precessional extraction method for a variable energy machine like the PU cyclotron: (1) the beam trajectory in the cyclotron remains constant and, (2) single-turn extraction of a beam is achievable.

Suppose the cyclotron parameters are set for the acceleration of one particular beam. If the orbit is to be constant for different particles or for the same beam with different maximum energy, the following scaling law should be satisfied [DAH73]:

$$\frac{T}{qV} = constant, \qquad \frac{Mv}{qBl} = constant, \tag{7.3.1}$$

where T : kinetic energy, q : charge, V : dee voltage, M : mass, v : velocity, B : magnetic field, l : trajectory (radius) of a beam. These equations can be combined

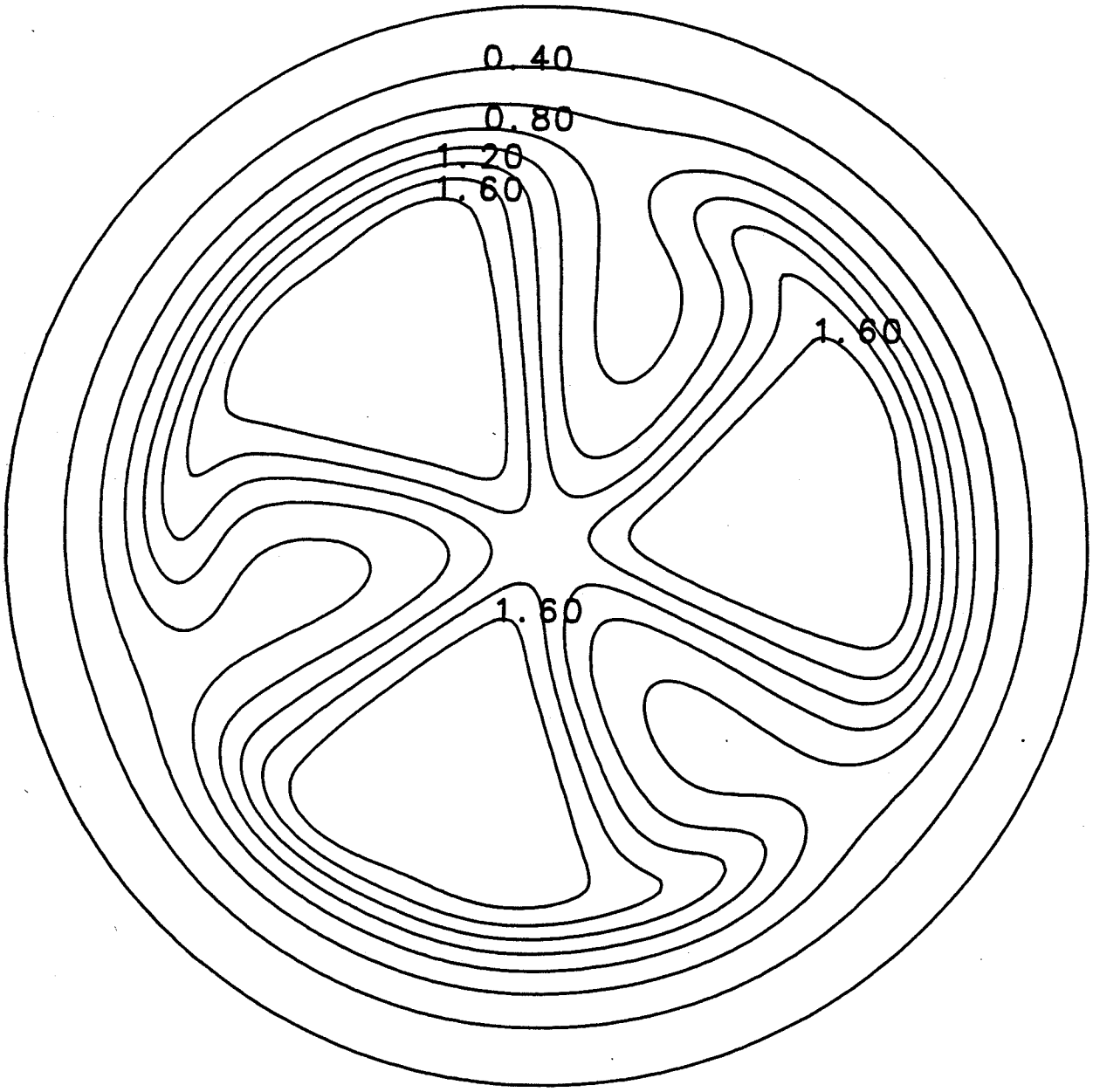

Fig. 7.1 The magnetic field contour map for a 48 MeV proton beam in the Princeton University AVF cyclotron.

to yield

$$\frac{(M/q)V}{B^2l^2} = constant, \tag{7.3.2}$$

or,

$$\frac{vBl}{V} = constant. \tag{7.3.3.}$$

These equations indicate that to form a constant orbit the ratio between (M/q) and (M_0/q_0) should be the same.

Single-turn extraction of a beam can be achieved only when the beam phase width is so narrow that the beam bunches of succeeding turns do not overlap with the preceding turns. In the case of the MSU's K=50 cyclotron, two radial slits were placed at the 18^{th} and the 28^{th} orbit turns in order to restrict the beam phase width to less than $\pm 2°$. With these slits together with the beam defining slit located at the half-turn, the MSU's machine development group was able to obtain a beam with extremely high (~0.04%) energy resolution [BLO69].

Keeping these features in mind, the beam orbit dynamics in the existing N=1 central region of the PU cyclotron were investigated. A proton beam of 48 MeV was chosen for the studies, which is the maximum obtainable proton energy for this cyclotron. The results obtained for this 48 MeV proton beam, however, should be equally applicable to other beams with different maximum energies, because of the constant orbit nature of the PU cyclotron.

Description of the beam orbit studies is divided into two segments: the radial motion and the axial motion.

7.3.1 The radial Motion

The instantaneous position of the reference particle's (N=1, 48 MeV proton set up) orbit center (the center of curvature) was traced for the first 20 turns at a constant time interval (thirty intervals per one complete orbit turn) and the result is shown in fig. 7.2. The horizontal and the vertical axes denote the directions along and perpendicular to the dee gap. The origin of this graph represents the cyclotron center. Fig 7.2 shows that the center of gravity of the overall instantaneous orbit centers converges to the cyclotron center. To obtain this figure, the cyclotron parameters were set as follows: the electric field oscillation frequency was 20.183 MHz, the dee voltage was 61.25 kV, and the intial RF phase was $-22°$, *etc.*.

Figure 7.2, however, implies that the motion of the overall beam center has a tendency to be shifted toward the positive x axis (to see this, for instance, compare the positions of the three vertices in the figure). This arises from the electric gap-crossing resonance [GOR62], one of the peculiar phenomena caused by an asymmetric configuration of the magnetic sector and the electric dee. The other effect due to this asymmetric structure is the phase oscillation of the beam.

Suppose that the dees and the sectors are asymmetrically structured in a cyclotron, *e.g.*, a three-sector and two-dee cyclotron. If δ denotes the angle between the line along the center of the dee gap and the line along the center of the hill, then straightforward analysis gives the amount of the phase oscillation due to this asymmetrical configuration as approximately [LOU71]

$$\Delta\phi = \frac{1}{12}\frac{B_3}{B_0}\sin 3\delta, \qquad (7.3.4)$$

where B_3 is the third-harmonic component of the magnetic field and B_0 is the

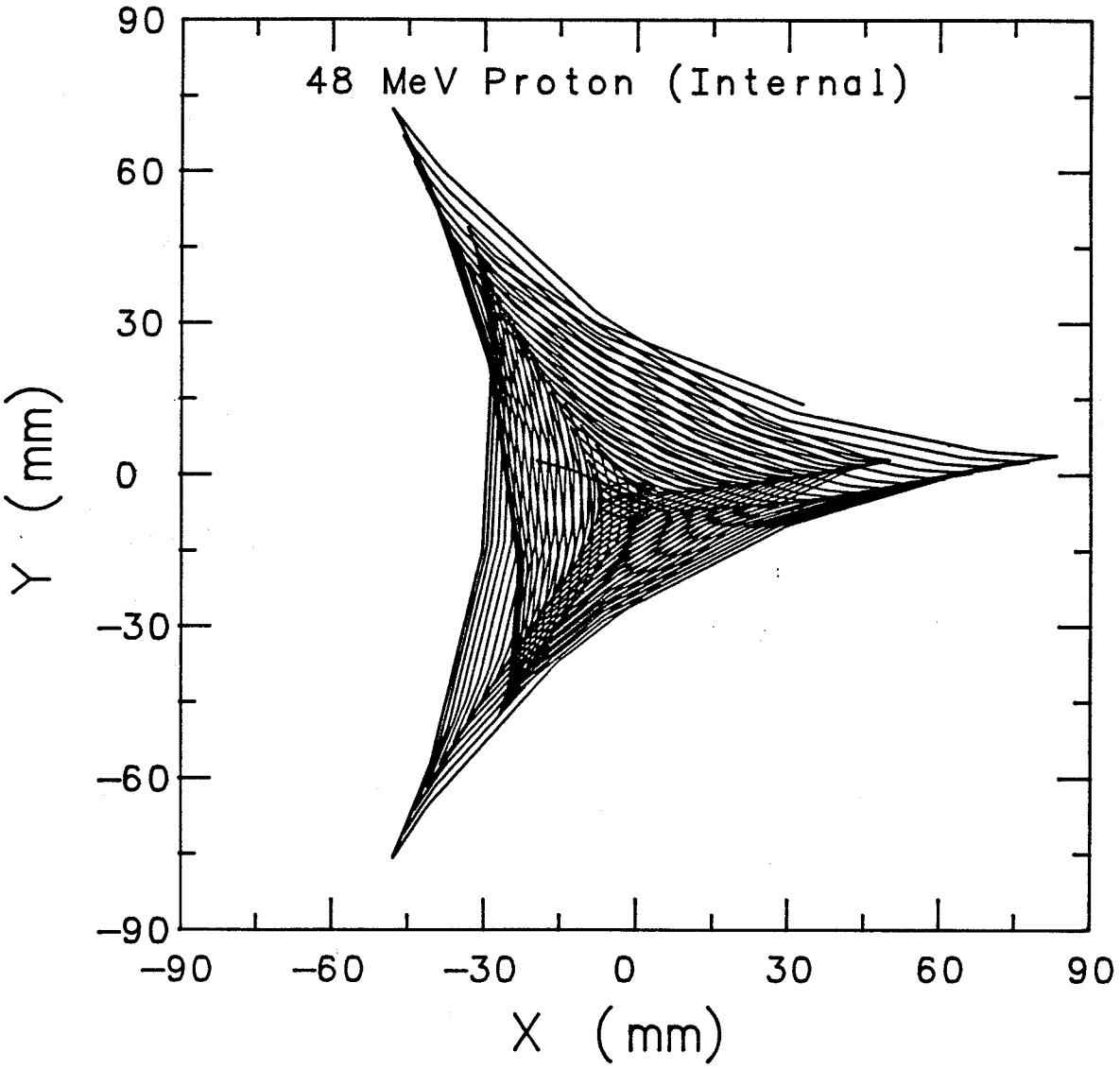

Fig. 7.2 The instantaneous position of the orbit center (center of curvature) up to 20 turns for a 48 MeV proton in the existing N=1 central region. The horizontal and vertical axes denote along and perpendicular to the the dee gap, respectively. The origin of the figure represents the cyclotron center. It is seen that the overall center converges to the origin. The electric gap-crossing resonance phenomena is also shown implicitly.

azimuthal average of the magnetic field along the radius. The above equation shows that the phase oscillation has its maximum value when δ is 30°. However, in the case of the PU cyclotron, δ is nearly zero, and therefore the phase oscillation does not lead to a problem. Even at the outer radius where the spiral angle starts increasing, the calculation based on eq. (7.3.4) revealed that $\Delta\phi$ was kept to be less than 1° per turn.

Unfortunately, minimizing phase oscillation by reducing δ maximizes another undesirable effect, the electric gap-crossing resonance phenomenon (EGCR). For a three-sector and two-dee cyclotron, the approximate change in radius of curvature of the orbit is given by [LOU71]

$$\Delta\rho = \frac{\sqrt{2m}}{q}\frac{1}{B_0}\sum_{i=1}^{k}[\frac{\Delta E_i}{2\sqrt{E_i}}[(-1)^{i+1} - \frac{B_3}{B_0}\cos 3\delta]], \qquad (7.3.5)$$

where i is the half-turn number and ΔE_i is the energy gain at the i^{th} dee gap. The first term in the above equation is due to the energy gain during the dee gap-crossing, and it oscillates, whereas the second term comes from the EGCR which has its maximum value when δ=0. This formula shows that the EGCR is dominant for low energy.

Estimation of the overall center shift due to a EGCR for 48 MeV proton beam in the PU cyclotron revealed that it is less than 1 cm. However, the PU cyclotron has three harmonic correction coils centered at r=12.7 cm (5″) in each valley. Activation of these first-harmonic coils can correct this problem.

The radial trajectory of a proton beam for up to three orbit turns in the existing N=1 central region is shown in fig. 7.3.

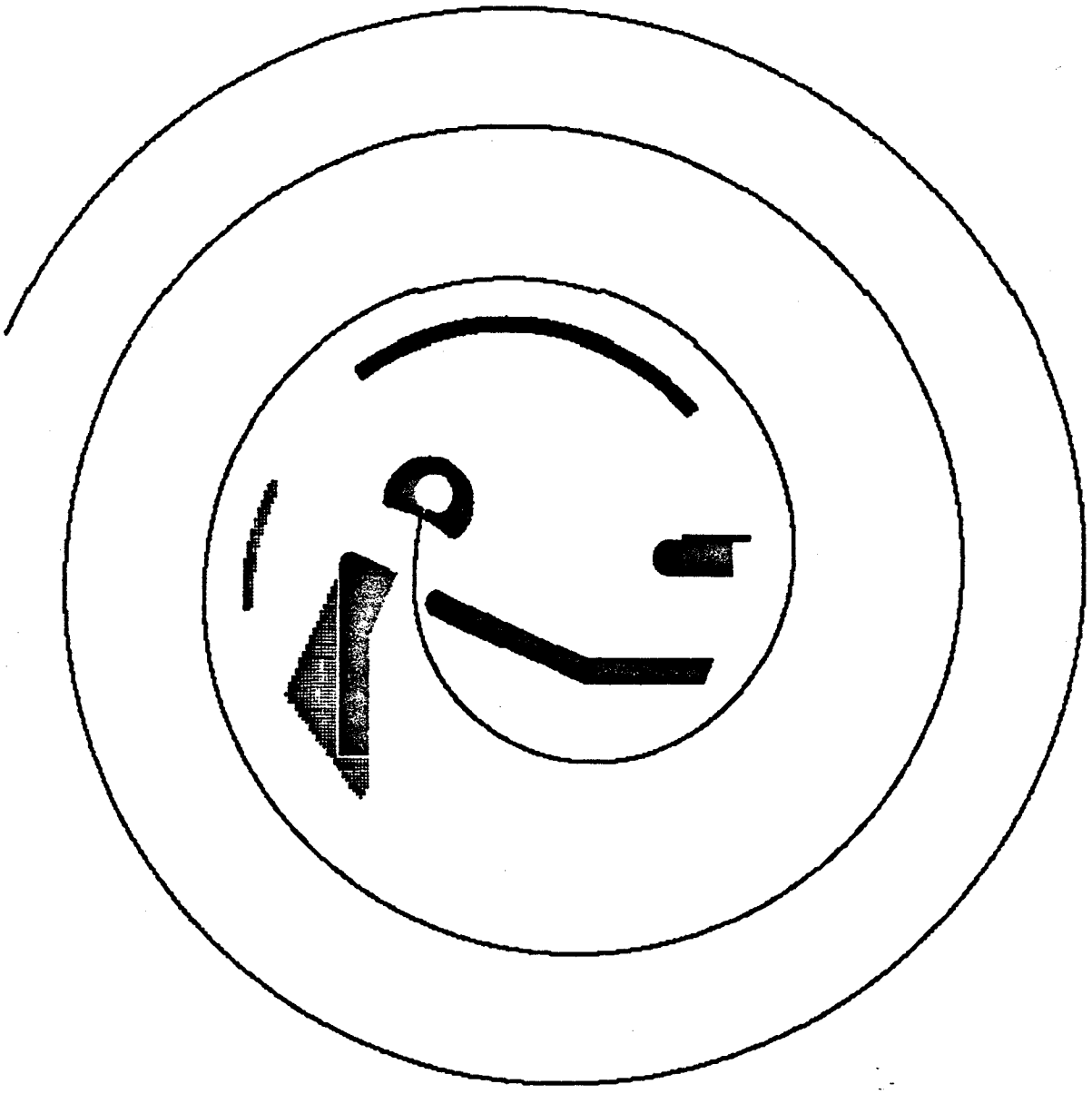

Fig. 7.3 The radial trajectory of the proton beam in the existing N=1 central region of the Princeton University cyclotron.

7.3.2 The axial motion

Fig. 7.4 shows the axial motion of a proton beam up to 20 orbit turns. In this figure, the horizontal axis represents the particle's orbit turn number and the vertical axis denotes the displacement of a particle form the median plane (z=0) of the cyclotron. The two rays shown in fig. 7.4 are orthogonal to each other, and were chosen from the two marginal rays (z_1= 0 mm, z_1'=2.16°; z_2 = 1 mm, z_2'=0°) of the phase space ellipse whose area is 120 mm mrad. Since these two particles represent the two independent solutions of the linearized second-order differential equation, the axial motion of other particles can be obtained from the superimposition of the motion of these two orthogonal particles. Fig. 7.4 indicates that the maximum amplitude of the oscillation is restricted to within ±3 mm, which shows that the beam is well-confined to the vicinity of the median plane of the cyclotron, *i.e.*, to the first-order region. This figure also clearly indicates that the oscillation amplitude of the axial motion is adiabatically damped [see eq. (2.2.5)].

7.3.3 The phase selection

Along with the beam orbit studies discussed above, the possibility of improving the existing N=1 central region of the PU cyclotron was also explored. This includes the feasibility study of restoring two phase selection slits, mentioned above, in order to achieve a beam with high energy resolution.

The phase selection mechanism utilizes the phase-dependent radial centering error. Originally this study was carried out by Blosser's group [BLO69] for MSU's K=50 cyclotron. Their results revealed that if the slits were placed at the 18^{th} and the 28^{th} turns, then the phase could be selected within ±2°.

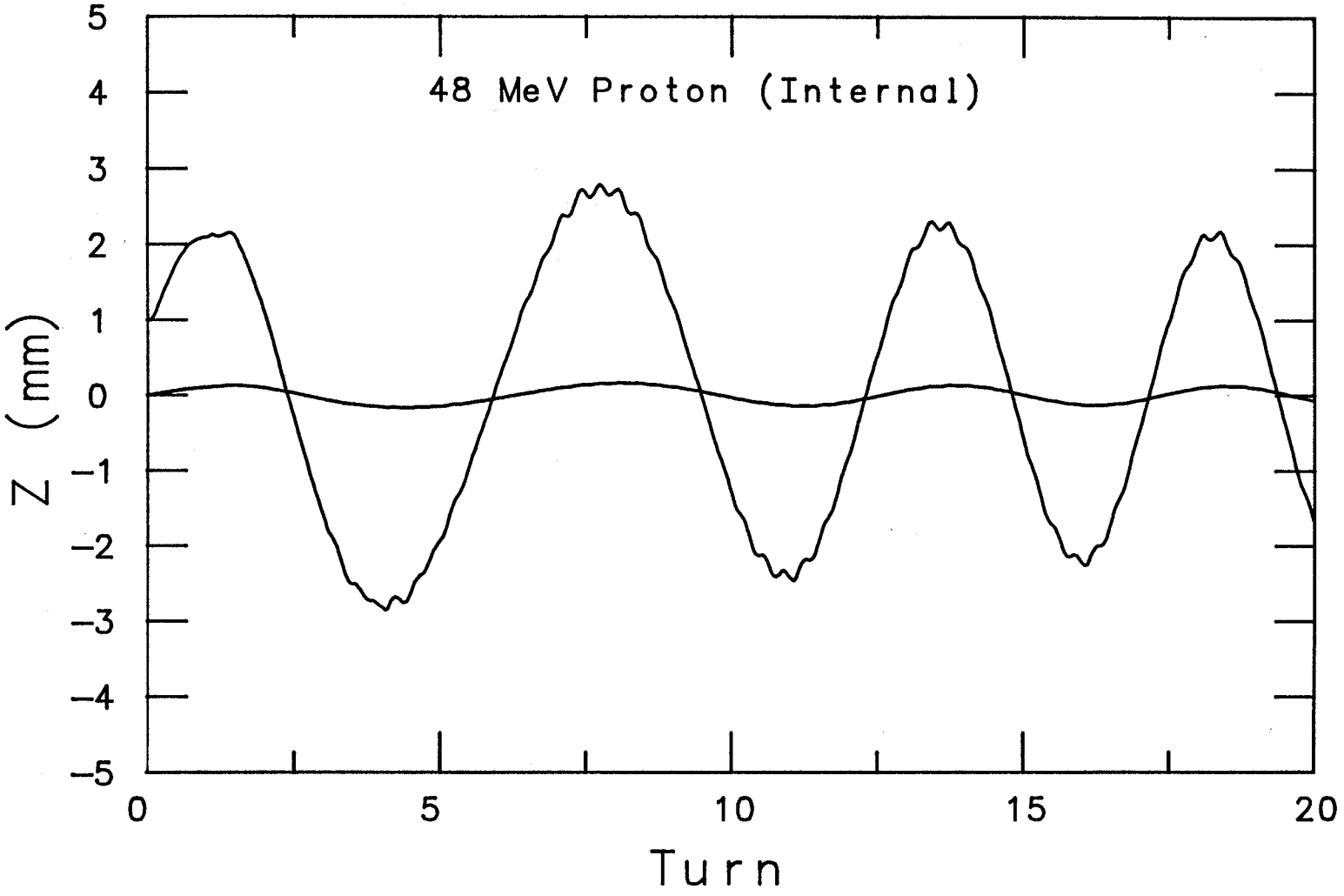

Fig. 7.4 Two particle trajectories off the median plane in the N=1 existing central region. These two particles are orthogonal to each other and were chosen from the boundary of the beam phase space whose are is 120 mm mrad. This figure shows that the motions are relatively well confined near the median plane. Adiabatic damping of the oscillation amplitude is also shown.

The study described here followed the same method used by Blosser. Thirteen representative particles were chosen to trace their trajectories up to 50 turns. Then their radial displacements from the central particle were calculated to find out the position where the maximum displacement occurs. Out of thirteen particles, seven particles were set to have initial phase spread (±6°, ±4°, ±2°, and 0°) only. The remaining six particles were set to have both divergence (±90°) and phase spread (0° and ±2°). Fig. 7.5 depicts the first seven particles radial displacements from the central ray as a function of the turn number. From this figure one can clearly see that the maximum displacement occurs at the 29^{th} turn (r=29.2 cm). The same kind of plot for the remaining six particles is shown in fig. 7.6. In this case the maximum displacement occurs at the 18^{th} turn (r=22.1 cm). Therefore these two positions are those where the half mm slits would be placed in order to achieve the beam phase width to within ±2°. To obtain these figures, the cyclotron parameters were chosen for the acceleration of a 42 MeV proton beam. However, as the scaling law indicates, once the positions of the slits are fixed, there is no need to change their position for acceleration of any particles in the same harmonic mode, because of the constant orbit nature of the PU cyclotron.

The final chapter of this thesis describes the experimental verification of these studies.

7.4 A New N=1 central region and the beam orbit dynamics

Based on the orbit studies in the existing central region described in the previous section, a new N=1 central region was designed. Fig. 7.7 represents its computer model. The ion source was replaced by an electrostatic mirror with its radial po-

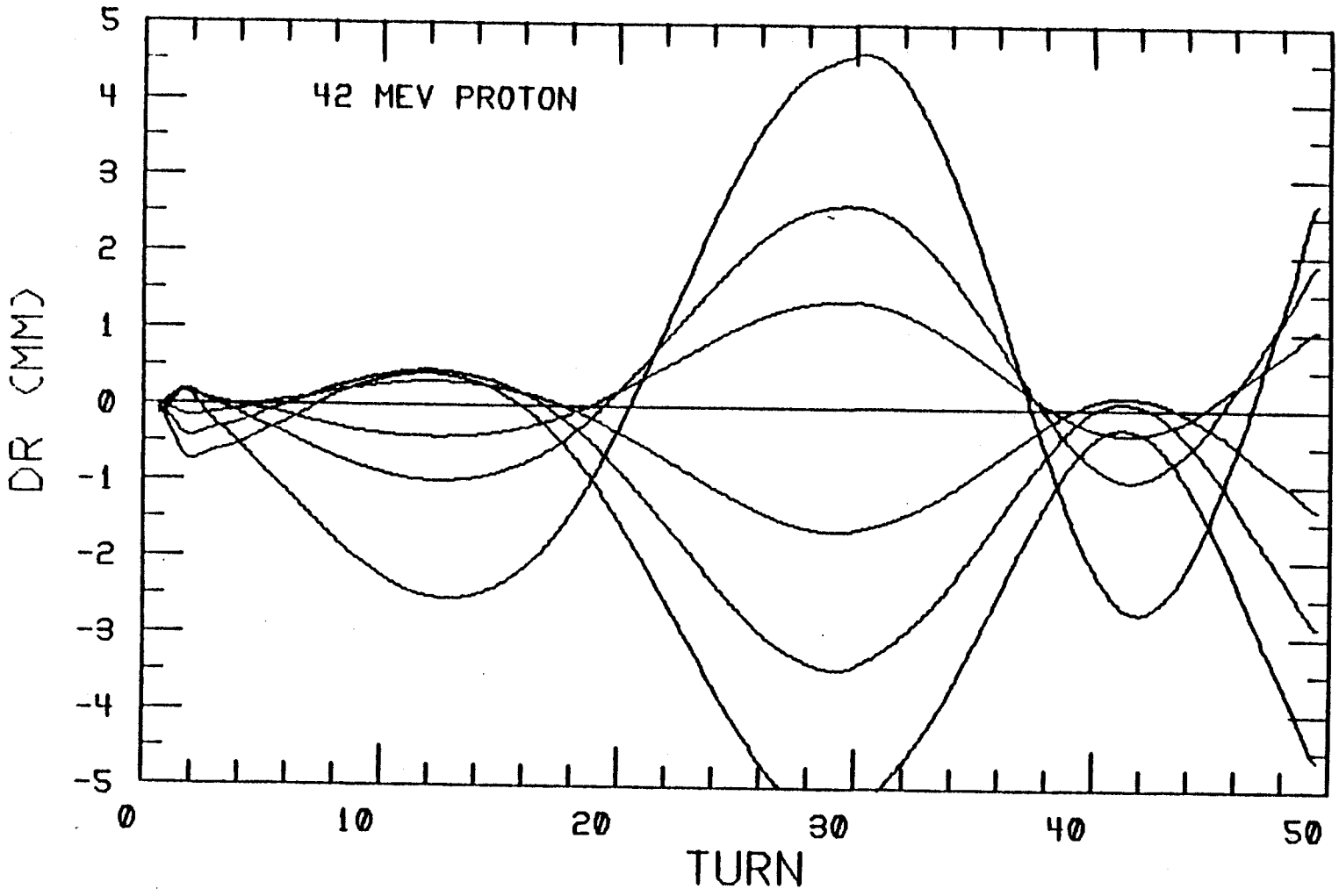

Fig. 7.5 Seven chosen particles' radial displacements as a function of the turn number in the existing N=1 central region. Each particle has initial RF phase spread ($\pm 2°, \pm 4°, \pm 6°$) centerd at the reference particle's starting RF phase. It is seen that the maximum displacement occurs at 29^{th} orbit turn.

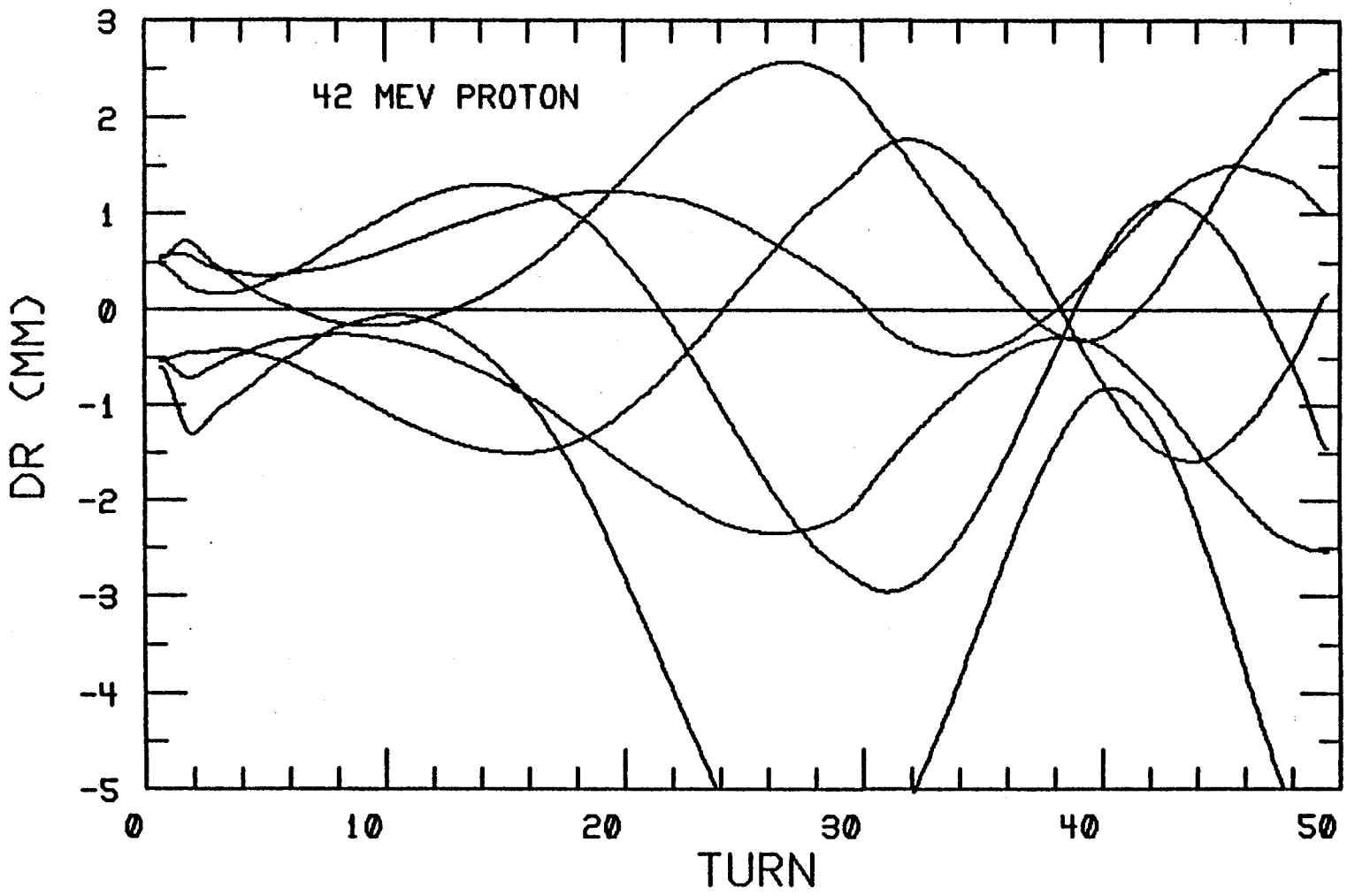

Fig. 7.6 Six particle radial displacements as a function of the turn number in the existing N=1 central region. Each particle has initial RF phase spread ($\pm 2°$) centerd at the reference particle's starting RF phase as well as the divergence ($\pm 90°$). It is seen that the maximum displacement occurs at 18^{th} orbit turn.

sition adjusted to yield the same motion of the instantaneous orbit center as the motion in the existing central region. The radial position and the shape of the puller were also optimized. The beam considered here was 48 MeV protons whose injection energy was chosen to be 15 keV.

The beam orbit studies were initiated with a search for the initial RF phase. In order to keep the rotational frequency of an ion in phase with the electric field oscillation frequency and to yield the maximum energy gain after the first gap-crossing, the initial RF phase chosen was $-65°$.

7.4.1 The radial motion

As was stated before, to optimize the center motion of a beam in the new central region, the radial position of the mirror and puller as well as the beam injection angle was carefully investigated through a successive optimization procedure. As a result, the injection angle was chosen to be $+185°$.

The instantaneous orbit center for a 48 MeV proton beam in the newly designed central region is depicted in fig. 7.8. It shows up to 20 turns. Comparing with Fig. 7.2, one can see that the motion of the center is nearly the same as the one in the exsiting N=1 central region.

7.4.2 The axial motion

The axial motion in the new central region was also optimized in such a way that the maximum oscillation amplitude of a beam would be almost the same as the one in the existing central region. This can be seen from fig. 7.9 where the displacements of two orthogonal particles from the median plane as a function of a

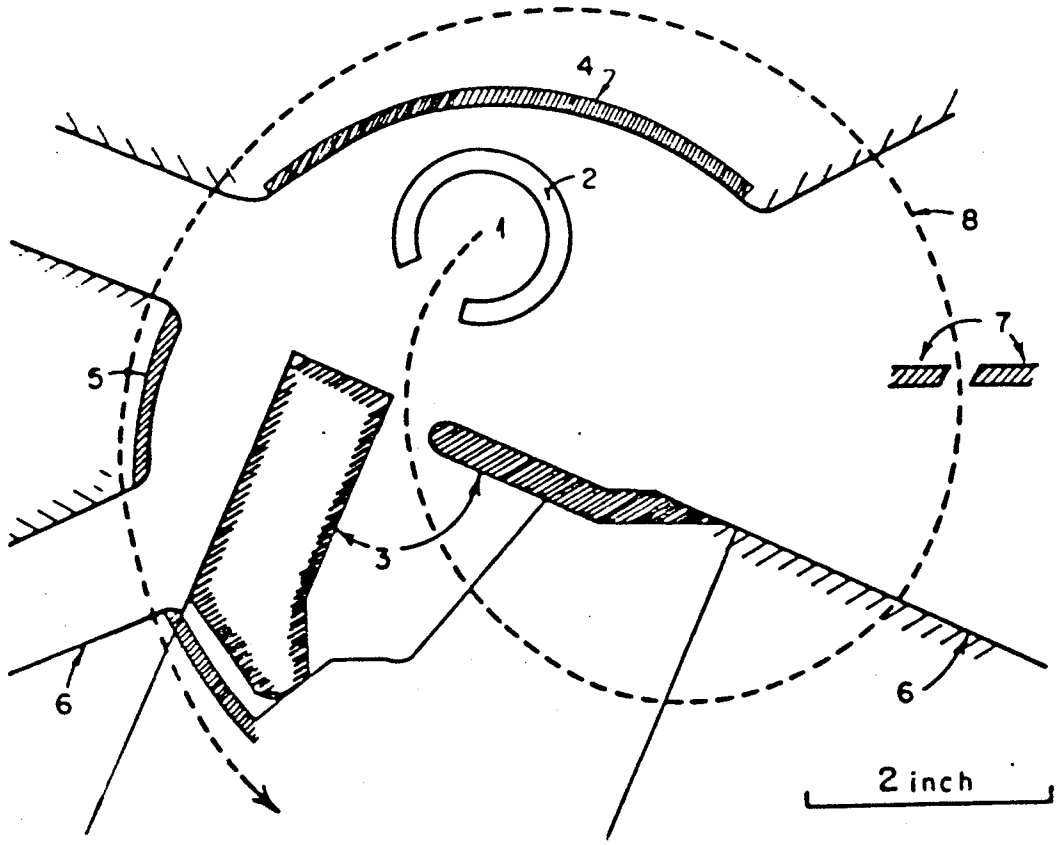

Fig. 7.7 A computer model central region geometry for the N=1 mode of acceleration. 1: electrostatic mirror, 2: RF shield, 3: puller, 4: dee, 5: dummy dee, 6: dee, 7: beam defining slit, 8: reference particle's trajectory.

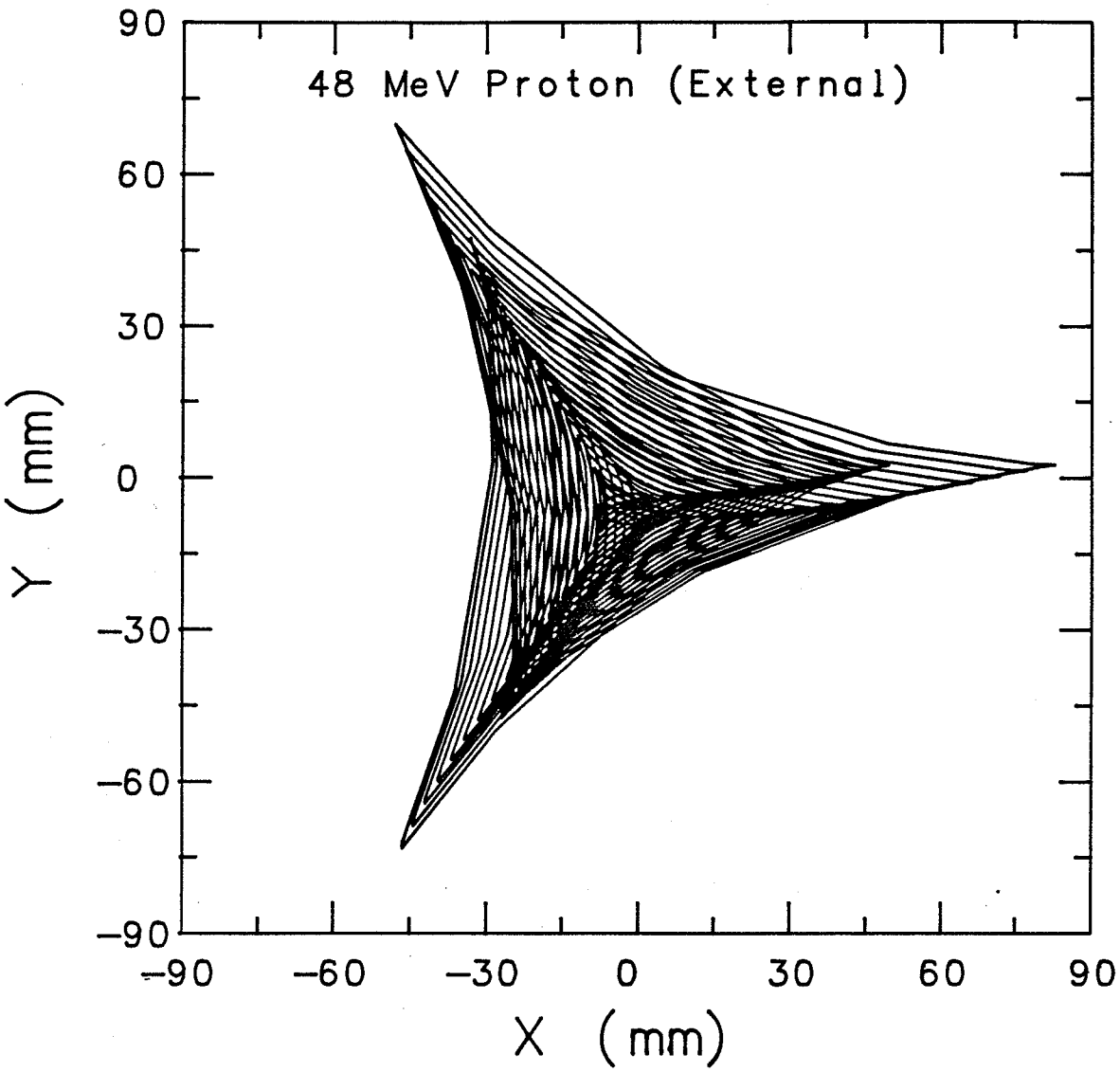

Fig. 7.8 The instantaneous position of the orbit center (center of curvature) up to 20 turns for 48 MeV proton in the new N=1 central region. The horizontal and the vertical axes denote along and perpendicular to the dee gap, respectively. The origin of the figure represents the cyclotron center. It is seen that the overall center converges to the origin. Comparing this figure with fig. 7.2, it can also be seen that the motions in the two plots are nearly identical.

turn number are depicted. The initial conditions of these particles are the same as those that were utilized to obtain fig. 7.4.

Comparing this figure with fig. 7.4, we see that in fig. 7.9 the maximum oscillation amplitude is restricted to less than 3 mm which is nearly the same as in fig. 7.4. To obtain fig. 7.9 the geometry of the mirror gap was rigorously optimized by varying the width to height ratio of the gap. For example, figs. 7.10 and 7.11 illustrate the axial motion of a beam with different width to height ratios of the mirror gap. Fig. 7.10 shows the axial motion up to the third turn when this ratio is 5 by 5 mm whereas fig. 7.11 is the case when it is 5 by 7 mm. It can be seen in fig. 7.10 that in passing the mirror gap, the beam is over-focused and this subsequently leads to the large oscillation amplitude at later turns. On the other hand, an increase in the gap height reduces such an over-focusing as can be seen in fig. 7.11. Fig. 7.8 is the extension of fig. 7.11 for up to twenty turns of orbit.

7.5 The beam orbit dynamics in the existing N=2 central region

The beam dynamics investigations in the N=2 central region was carried out with a 28 MeV deuteron beam, which is the maximum obtainable energy of a deuteron beam in the PU cyclotron. The cyclotron setting parameters predicted by the SETOP program for this beam are as follows: ν_{RF}=22.53 MHz, and V_D (dee voltage) = 49.8 kV. Based on these values, numerical orbit tracing was performed and the first one and half orbital turns together with the central region geometry is shown in fig. 7.12. When we compare this figure with fig. 7.3 where the geometry of the existing N=1 central region and the first three turns of orbit are depicted, we notice that the ion source here is much thrusted into the puller region. This

Fig. 7.9 Two particle trajectories off the median plane in the newly designed N=1 central region. These two particles are orthogonal to each other and were chosen from the boundary of the beam phase space whose are is 120 mm mrad, which is the same as those in fig. 7.4. This figure shows that the motions are relatively well confined near the median plane. The maximum oscillation amplitude is alomost identical to fig. 7.4.

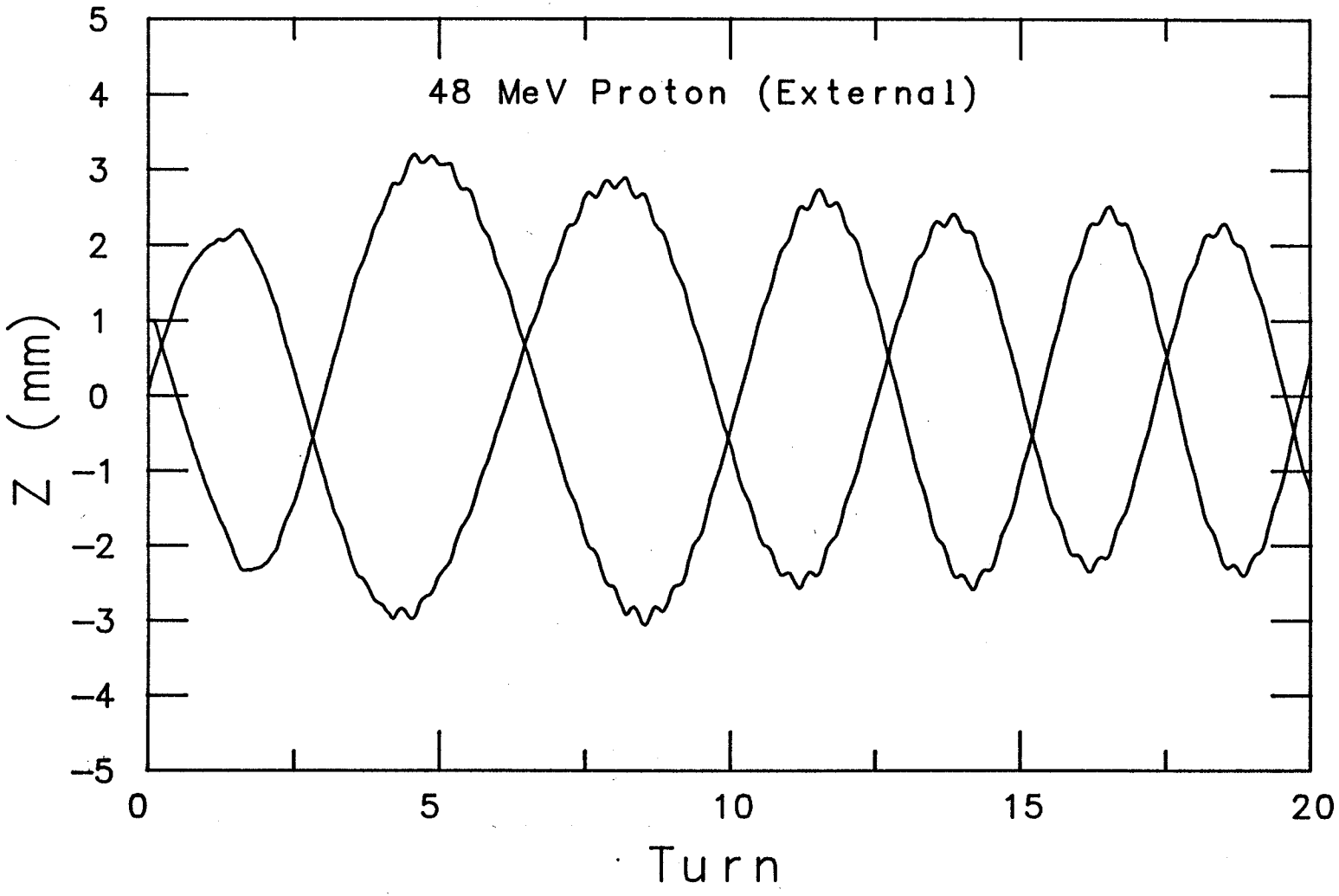
48 MeV Proton (External)
Z (mm)
5
4
3
2
1
0
−1
−2
−3
−4
−5
0
5
10
15
20
Turn

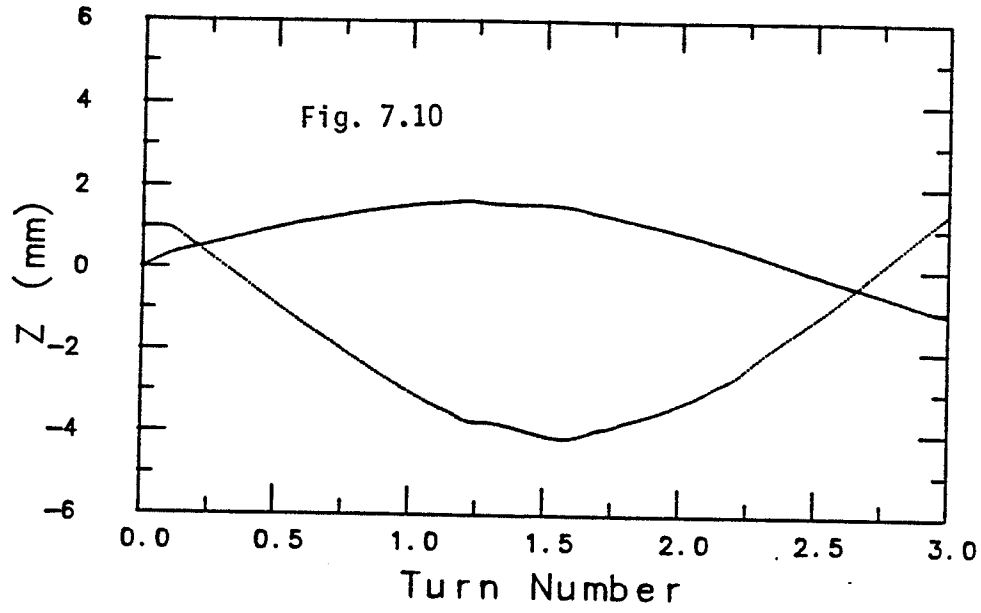

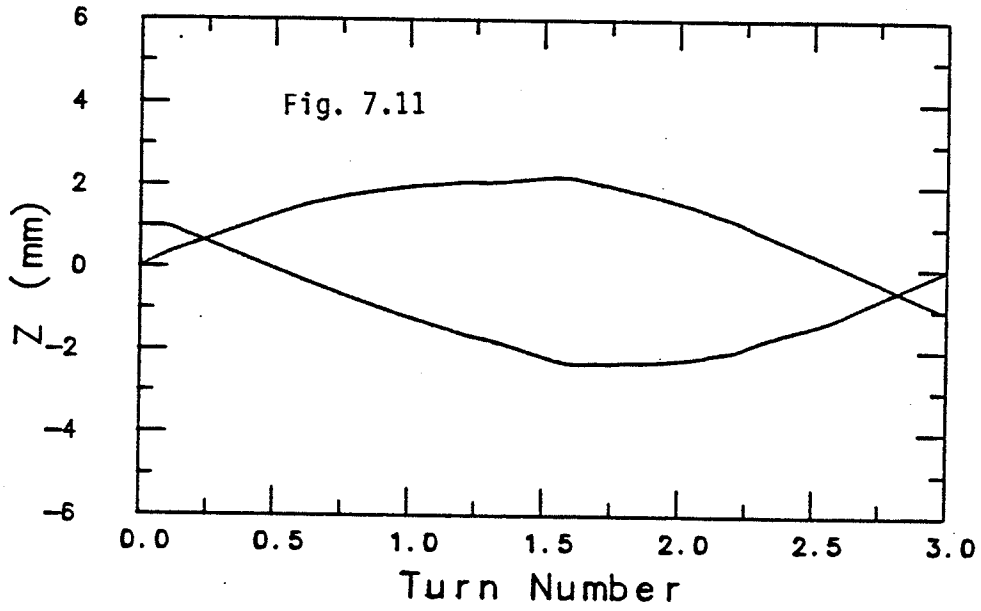

Figs. 7.10, 7.11 Comparison of the the axial motion of a beam with different width to height ratios of the mirror gap. Fig. 7.10 is the case when this ratio is 5 mm by 5 mm and fig. 7.11 is when it is 5 mm by 7 mm. The two particles' initial conditions are the same as those in fig. 7.9. These two figures show that the oscillation amplitude of the axial motion is significantly reduced when the width to height ratio of the mirror gap is optimized.

is because of the nature of the second-harmonic mode of acceleration; the electric field oscillates twice while the beam makes one complete orbital turn.

The beam orbit dynamics study that was carried out with this geometry, revealed that the starting RF phase (ϕ_0) of a 28 MeV deuteron beam was $-11°$. The instantaneous motion of the beam orbit center employing this starting RF phase is depicted in fig. 7.13. This figure shows the motion of the center up to the 20 orbital turn. From the figure, we notice that the center of gravity is not well converged into the origin of the graph, the center of the cyclotron.

Fig. 7.13 also implies that the center shift due to the electric gap-crossing resonance is much more severe than that of the beam in the N=1 central region. In order to estimate the amount of center drift for a 28 MeV deuteron beam, we demonstrate in fig. 7.14 the precessional motion of the average center (averaged over one complete turn) for this beam up to 80 orbital turns. Since $\nu_r \approx 1.02$, near the center of the cyclotron, the amount of the orbit turn number that is required for a beam orbit center to make one complete cycle is given by $N = 1/(\nu_r - 1) = 50$. Therefore, it is enough to take 80 turns to look into the center precession. Fig. 7.14 indicates that the amplitude of the center precession is approximately 8 mm.

The axial motion for this 28 MeV deuteron beam, however, appeared to be well confined to the vicinity of the median plane, as can be seen from fig. 7.15. This figure describes the displacement of two orthogonal particles from the median plane of the cyclotron as a function of the orbit turn number. The two particles' initial conditions were chosen from the phase space whose area was 120 mm mradian at the beam injection point. Fig. 7.15 indicates that the oscillation amplitude of the axial motion is restricted within ± 2 mm.

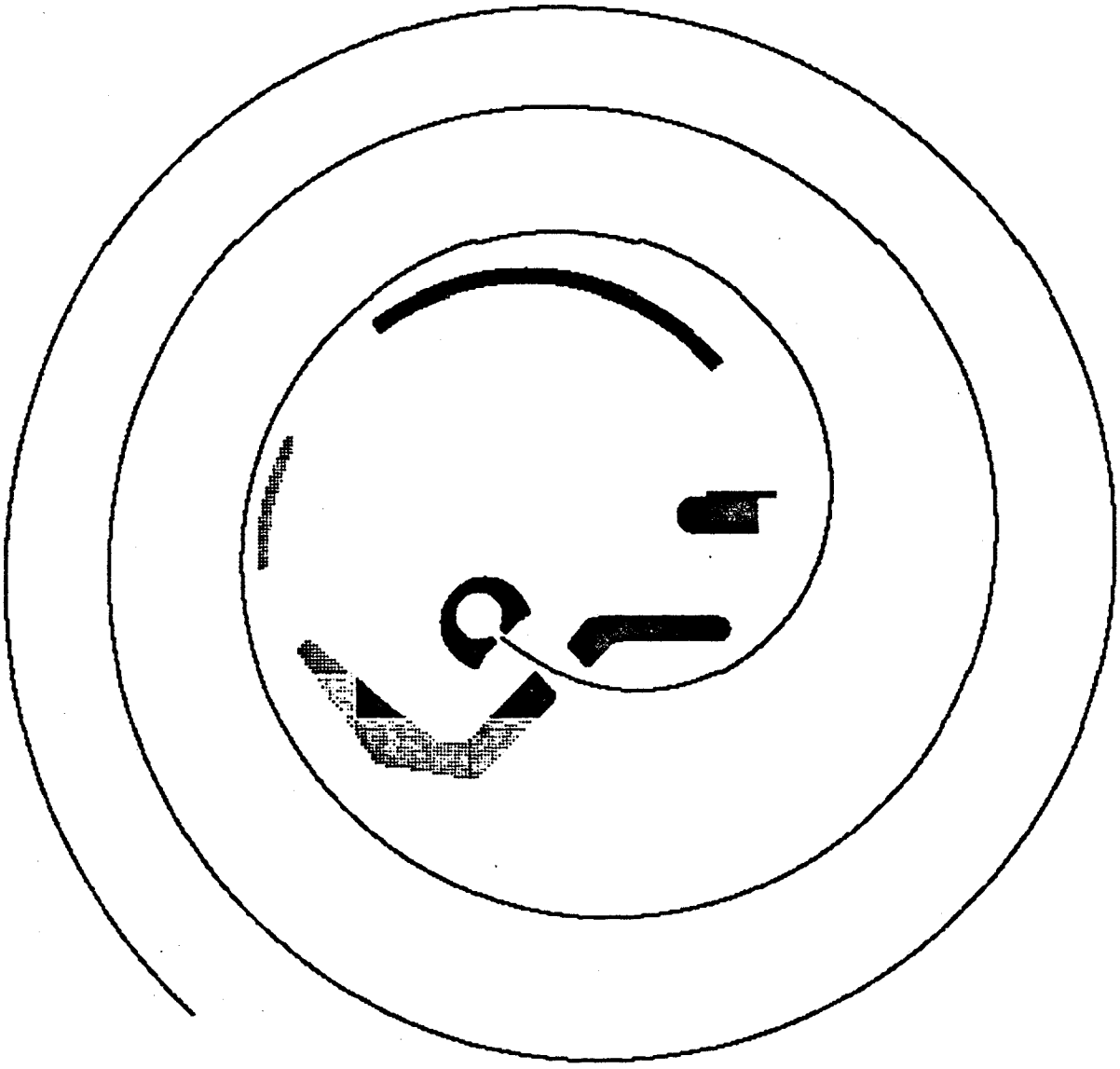

Fig. 7.12 The radial trajectory of the deuteron beam in the existing N=2 central region of the Princeton University cyclotron.

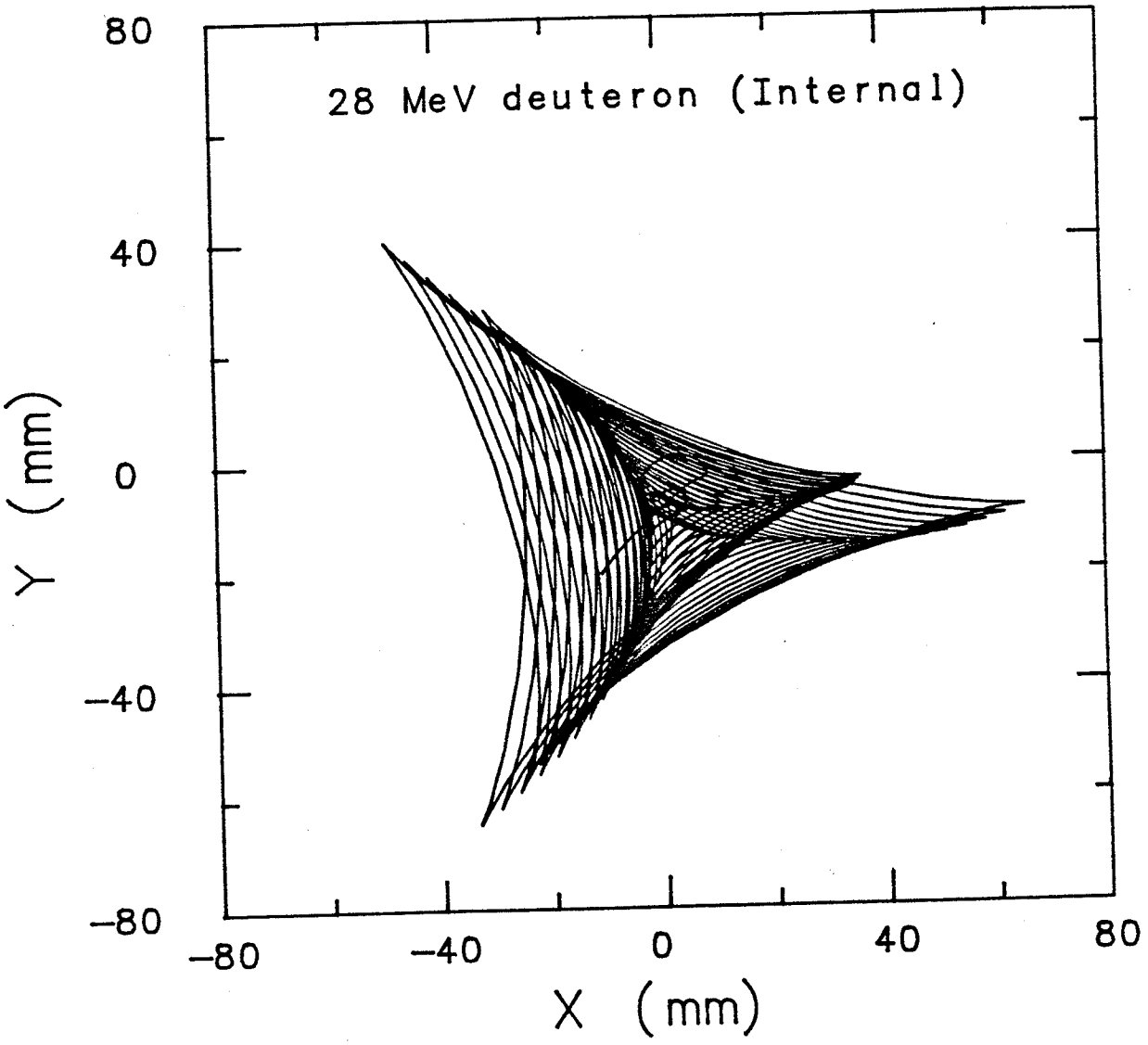

Fig. 7.13 The instantaneous position of the orbit center (center of curvature) up to 20 turns for 28 MeV deuteron in the existing N=2 central region. The horizontal and the vertical axes denote along and perpendicular to the dee gap, respectively. The origin of the figure represents the cyclotron center. It is seen that the overall center does not converge to the origin.

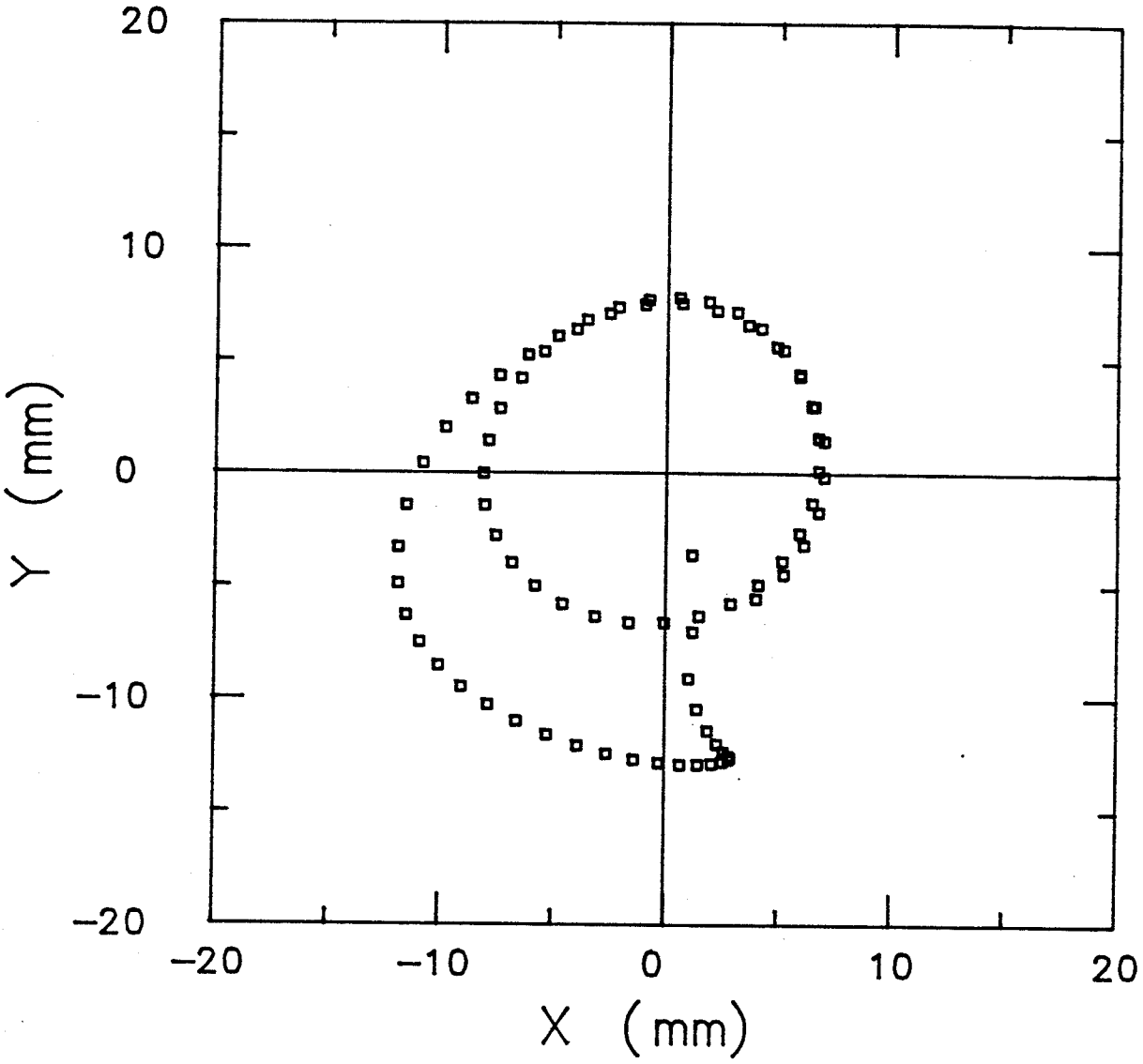

Fig. 7.14 The precessional motion of the 28 MeV deuteron beam's orbit center up to 80 orbit turns in the existing N=2 central region. Each square in this figure represents the position of the center as averaged over one complete orbit turn. This figure shows that the precessional amplitude is approximately 8 mm.

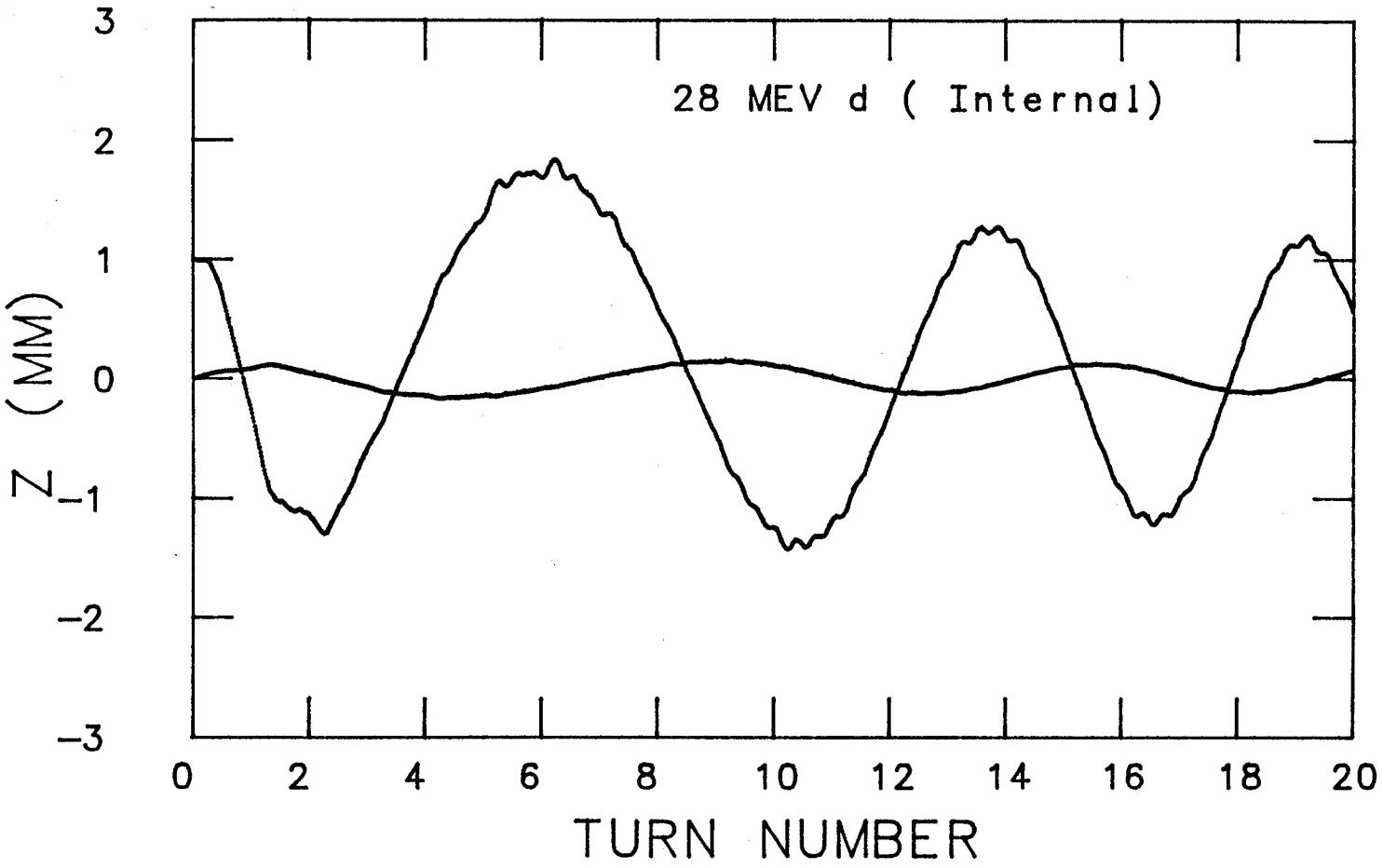

Fig. 7.15 The two deuteron particles' trajectories off the median plane in the existing N=2 central region. These two particles are orthogonal to each other and were chosen from the boundary of the beam phase space whose are is 120 mm mrad. This figure shows that the motions are relatively well confined near the median plane. The maximum oscillation amplitude is about ±2 mm.

7.6 The New N=2 Central Region and the Beam Orbit Dynamics

Based on the beam dynamics investigations that were carried out for the existing N=2 central region, a new N=2 central region was designed. Fig. 7.16 shows the geometry of the new N=2 central region and the beam trajectory for the first three orbital turns.

We first describe how to obtain the most optimum injection energy for any beam that is to be accelerated in the new N=2 central region. From the second equation of eq. (7.3.1), we have

$$\frac{M_1 v_1}{q_1 B_1 l} = \frac{M_2 v_2}{q_2 B_2 l}. \tag{7.6.1}$$

Using $v = \sqrt{2T_1/M_1}$, the above equation then leads to

$$\begin{aligned} T_2 &= \frac{1}{2} M_2 v_2^2 \\ &= \frac{M_1 T_1 q_2^2 B^2}{q_1^2 B_1^2 M_2} \qquad in \;\; keV. \end{aligned} \tag{7.6.2}$$

If we take the reference beam to be the 48 MeV proton beam, whose parameters are given by: T_1=15 keV, M_1=1.672$\times 10^{-27}$ kg, q_1= 1.602192 $\times 10^{-19}$ coulomb, B_1=1.363 T, then we can rewrite eq. (7.6.2) as

$$T_2 = 5.259 \times 10^{11} \frac{q_2^2 B_2^2}{M_2}. \tag{7.6.3}$$

Therefore by utilizing eq. (7.6.3), we can obtain a precise beam injection energy for any beam with any harmonic mode, if the magnetic field at the injection point is known. For example, the magnetic field at the injection point for the 28 MeV deuteron beam in the new N=2 central region is 1.5196 T. With this value, the beam injection energy, obtained from eq. (7.6.3), is given as 9.32449 keV.

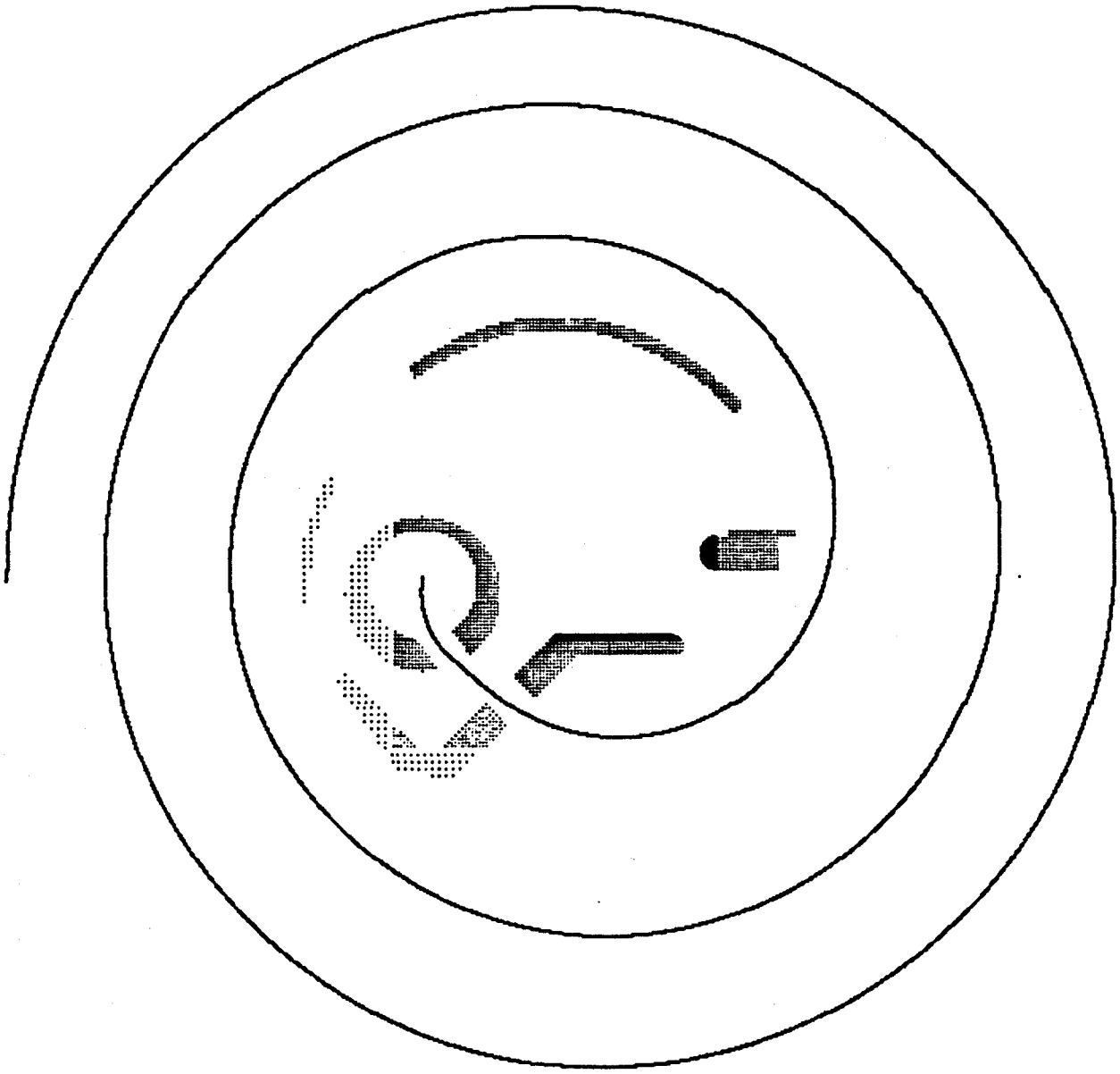

Fig. 7.16 The radial trajectory of the deuteron beam in the newly designed N=2 central region of the Princeton University cyclotron.

In fig. 7.17, we illustrates the motion of the instantaneous orbit center for the 28 MeV deuteron beam in the new N=2 central region. This figure describes the center motion up to 20 orbital turns. Fig. 7.18 also shows the motion of the center, as averaged over one orbital turn up to 80 turns. Comparing these two figures with the corresponding figures for the existing N=2 central region (fig. 7.13 and 7.14, respectively), we see that the centering of a 28 MeV deuteron beam in the new central region is much better than the beam orbit centering in the existing N=2 central region; the maximum amplitude of the center precession was reduced to 2.5 mm (see fig. 7.18).

The reference particle's initial RF phase and the injection angle in this new geometry were found to be respectively $-108°$ and $260°$. With these parameters, the axial motion of the two orthogonal particles' was investigated and the result is displayed in fig. 7.19. As in the case of the design procedure of the new N=1 central region, the gap to height ratio of the mirror as well as the puller-gap height was rigorously optimized in order to obtain fig. 7.19, which indicates that the axial motion is well confined near the median plane of the cyclotron. The maximum oscillation amplitude is resctricted to be ± 2.5 mm.

7.7 The calculation of the transmission efficiency

Obtaining a reliable estimate of the overall beam transmisssion efficiency through a designed axial injection system and the new central region was one of the central concerns of this study; a straightforward method would be to select a sufficiently large number of particles and find out the fate of each particle by tracing the trajectory from an ion source to the extraction channel of the cyclotron (or until

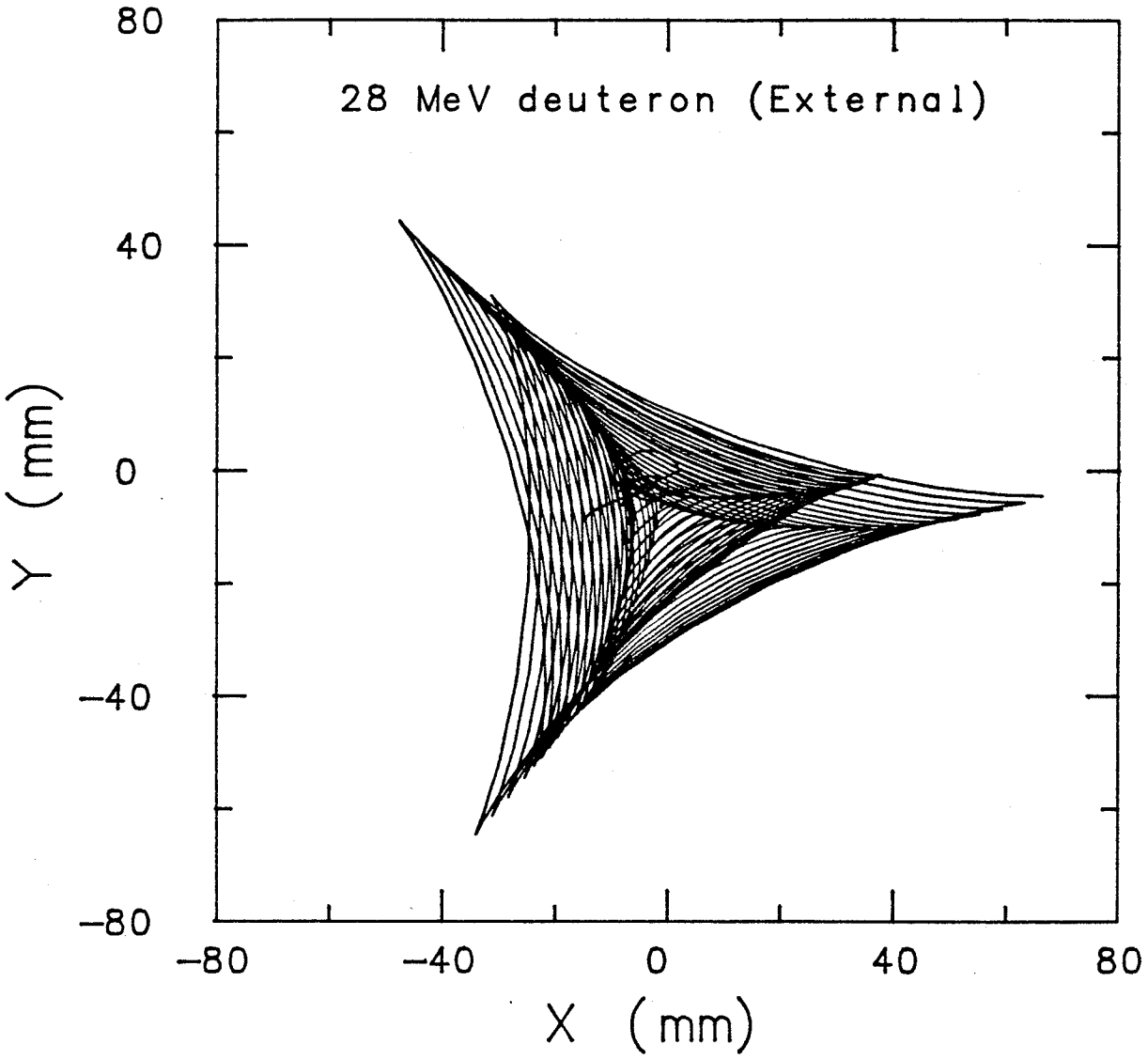

Fig. 7.17 The instantaneous position of the orbit center (center of curvature) up to 20 turns for 28 MeV deuteron in the newly designed N=2 central region. The horizontal and the vertical axes denote along and perpendicular to the dee gap, respectively. The origin of the figure represents the cyclotron center.

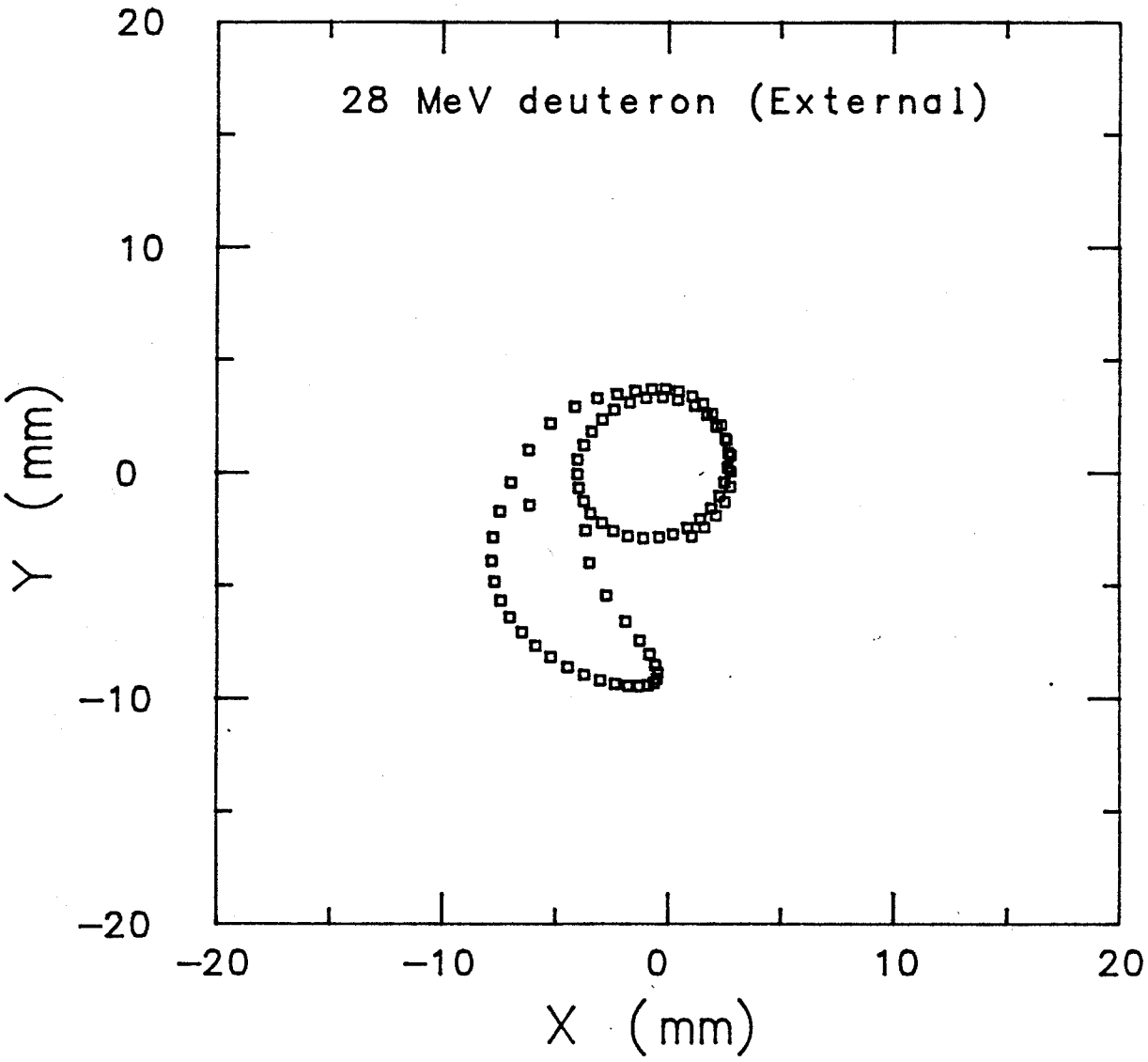

Fig. 7.18 The precessional motion of the 28 MeV deuteron beam's orbit center up to 80 orbit turns in the newly designed N=2 central region. Each square in this figure represents the position of the center as averaged over one complete orbit turn. This figure shows that the precessional amplitude is approximately 2.5 mm, much improved compared with fig. 7.14.

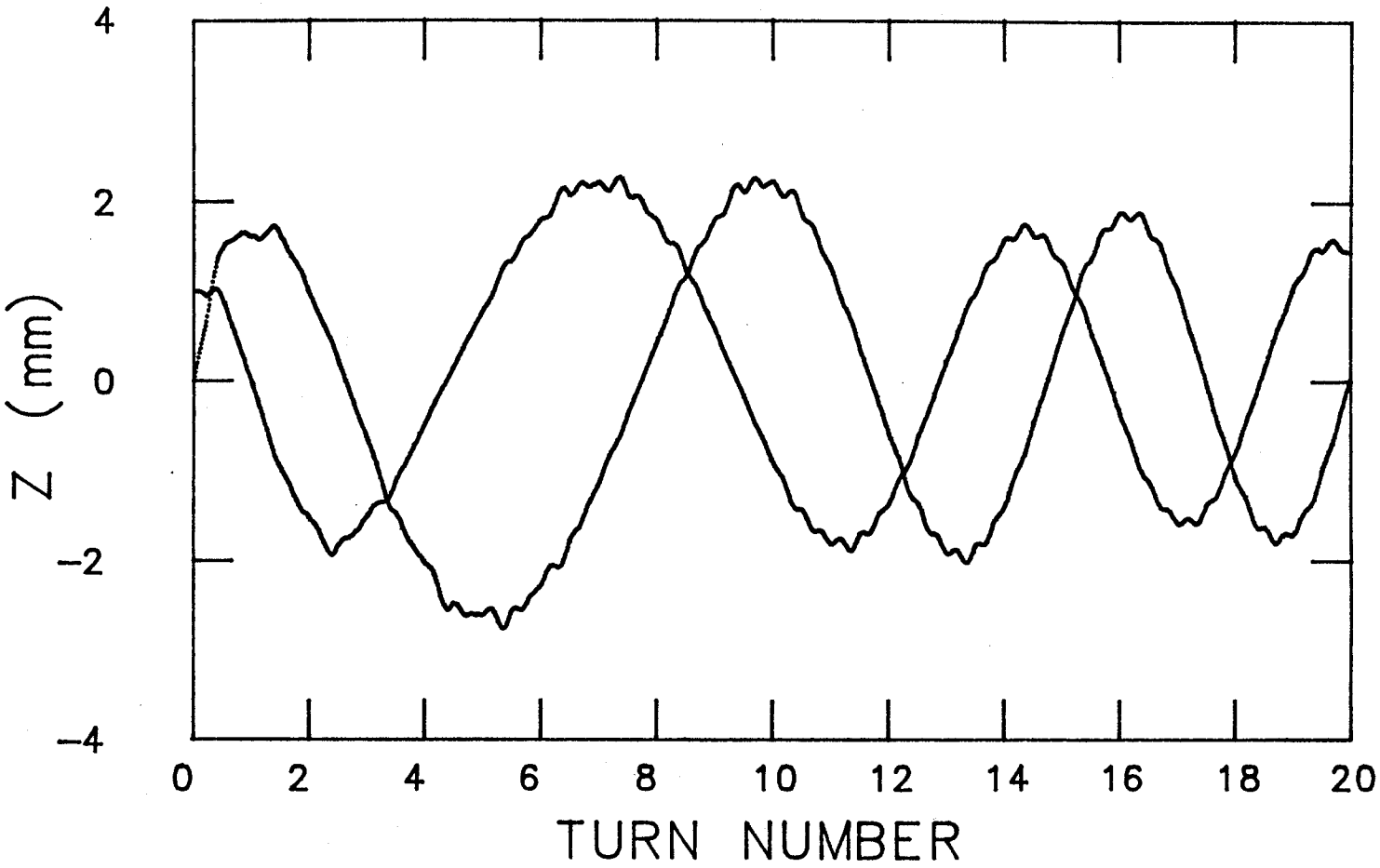

Fig. 7.19 Two deuteron particle trajectories off the median plane in the newly designed N=2 central region. These two particles are orthogonal to each other and were chosen from the boundary of the beam phase space whose are is 120 mm mrad. This figure shows that the motions are relatively well confined near the median plane. The maximum oscillation amplitude is about ±2 mm.

the particle is lost). However, this requires an unacceptably large amount of computing time. Therefore, an alternative method was devised, which yields nearly as accurate a result as the above but takes up a reasonable amount of computing time. With this method, the trajectory of each particle is traced from a beam buncher to a point after the electrostatic mirror, the last element of the axial injection system. A computer code INJECT was developed for this purpose. In this code a DC beam from an ion source, with its beam properties (the electric charge, mass, injection energy and the energy spread, the emittance and its shape specified as an initial parameter) enters the buncher and becomes a bunched beam. The buncher operates in the combined modes of the first and the second-harmonic RF (see chapter 6) and is specified by five buncher parameters: the position, the first-harmonic buncher voltage and its phase, the second-harmonic buncher voltage and phase (two more fixed parameters, the lengths of the first-harmonic and the second-harmonic buncher are variable parameters). The bunched beam then passes through a drift space and enters the cyclotron magnetic field. The field values (including the fringe field) along the injection system are other input data and have been mapped for various excitation levels of the cyclotron magnetic field. For simplicity, the field was replaced by a step function type with no fringe field (this approximately represents the field for a low excitation). The beam is then reflected 90° by an electrostatic mirror. This code then traces the trajectories further to the "starting point for acceleration" which is the effective starting point of the motion of the design particle inside the cyclotron.

The motion of the particles inside the central region of the cyclotron was traced separately from the "starting point for acceleration" to the 30^{th} turn where the

third-slit is placed. Practically all the computing time is taken by this portion of the calculation. In order to overcome the problem arising from the limitation in computing time, 63 representative particles for orbit tracing were chosen and then by interpolating between them, the acceptance phase space windows were constructed [for each of the phase selection slits:each has half mm radial aperture and is placed at the 0.5 (r=3.582 cm), the 15^{th} (r=20.141 cm) and the 30^{th} (r=29.746 cm) turns]. At the "starting point for acceleration", the "windows" represent a multi-parameter space which includes the effect of the finite phase space area, the beam energy spread and the dee RF phase effect. The computation of the beam transmission efficiency then means to count the number of particles that falls inside all three "windows" (the "combined windows") against those that falls outside of at least one of the "windows". Fig. 7.20 shows three of the "combined windows" (for zero energy spread) that correspond to +2,0,−2 RF degree respectively. It is seen from this figure that they are well separated, meaning that by restricting the size and adjusting the shape of the phase space area, a beam can be made to avoid falling onto the $+2°$ and $-2°$ "combined windows" thereby restricting the beam bunch size to less than ± 2 RF degrees. It is noted that once the beam passes through the third slit there is hardly any more loss throughout the acceleration, and the extraction efficiency is close to 100%.

The transmission efficiencies have been computed based on the above method and are shown in fig. 7.21 for a proton beam as a function of the intrinsic beam emittance (which does not include the contribution from the angular momentum portion; beams produced in a strong magnetic field can have a large contribution from this). It is seen that about 3% overall transmission efficiency is expected for a

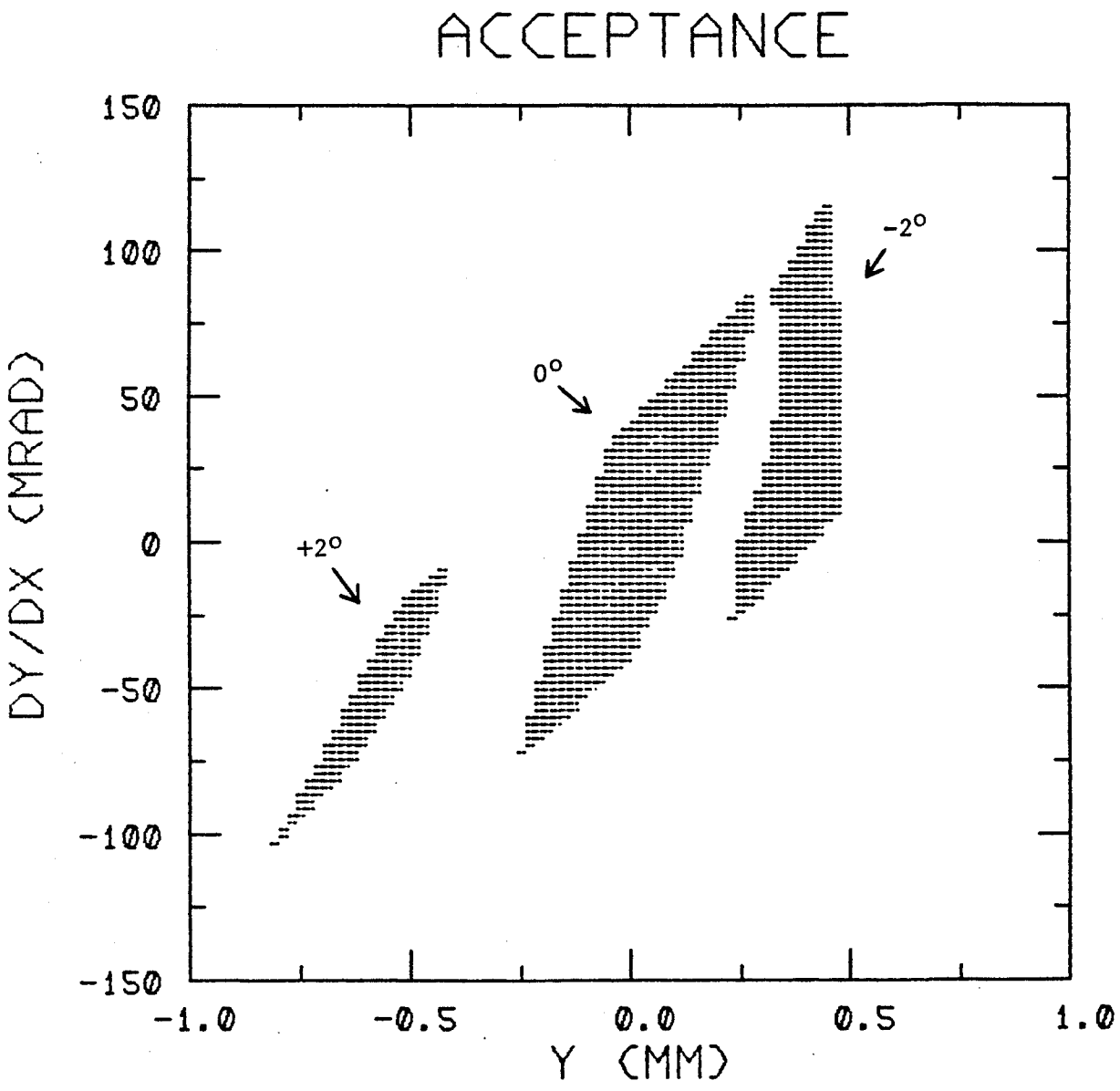

Fig. 7.20 The phase space acceptance diagram of the 48 MeV proton beam. The three separated regions represent the acceptances for the refernce phase (0°), -2° and +2° respectively, when the phase selection slits are placed. The clear separation of these three regions shows the effect of these slits. The spread in energy was not taken into account because it is small (0.2 keV) compared with the injection energy (15 keV).

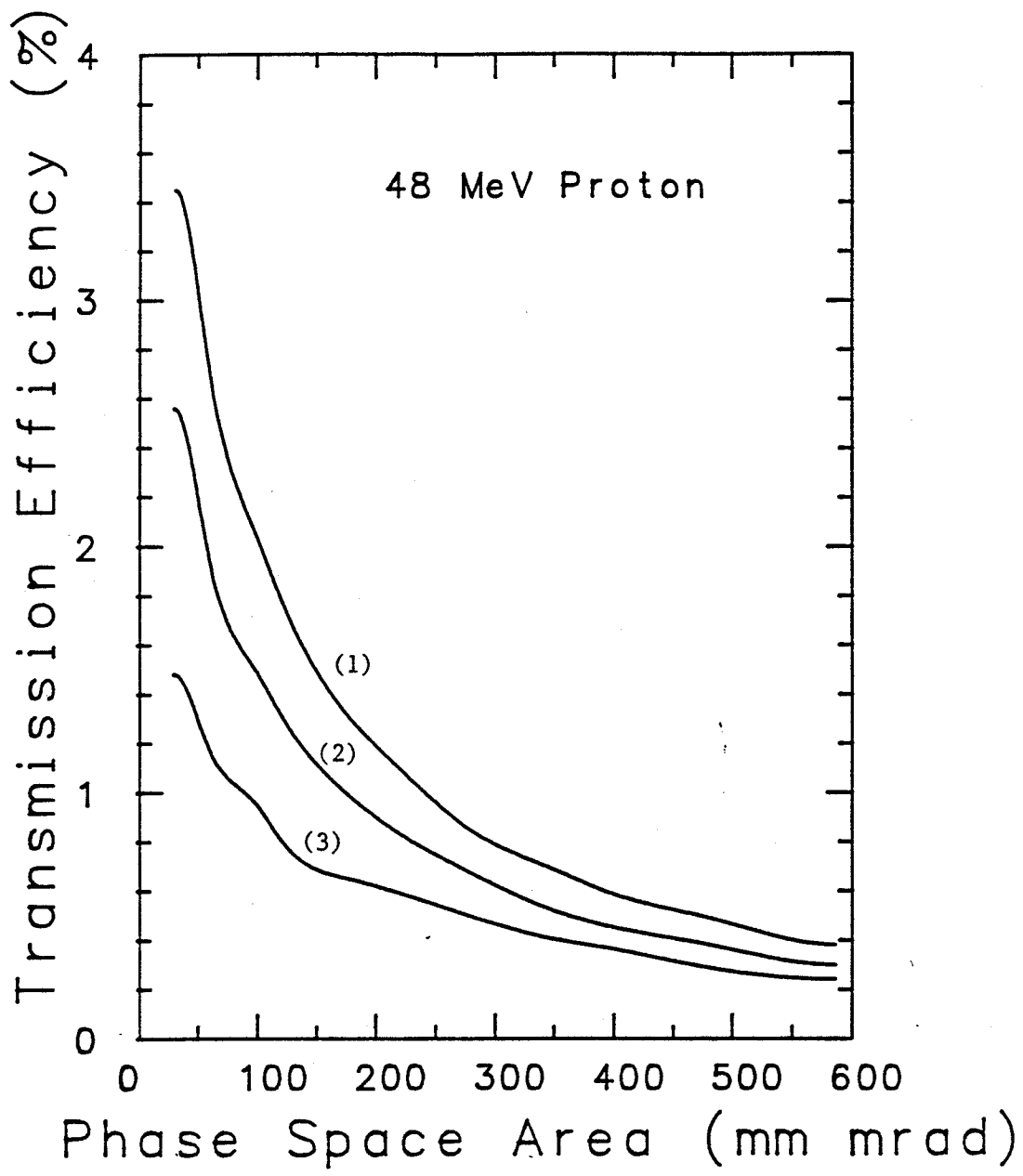

Fig. 7.21 The total transmission efficiencies of the 48 MeV proton beam along the axial injection line and the new N=1 central region. The phase selection slits which would select the beam phase within $\pm 2^\circ$ are placed in the calculation. The three curves correspond to the energy spread of 20, 60, 100 eV for (1), (2) and (3), respectively.

typical unpolarized proton beam with 16 mm mrad at 15 keV and a 20 eV energy spread. It is also seen that the efficiency drops down by 1/2 when the energy spread is increased to 100 eV. However, a number of meshes along the axial injection system will reduce the transmission efficiency. After allowing for this loss, the efficiency will be around 2% for a low intensity beam from the source. With a 2 mA beam axially injected this would give a 40 μA proton at 48 MeV. In reality, however, for a high intensity beam from the source (several milliampere) where space charge effects play a dominant role, the efficiency is expected to drop down significantly. In this case, in fact, the beam debunches rapidly as soon as it bunches after passing through the buncher. We thus expect an upper limit of the order of a 10 μA proton beam extracted at this energy. The efficiency is only 0.3% for a beam of 150 mm mrad (190 mm mrad at 10 keV) with 100 eV energy spread. This corresponds to a value from a commercially available source for polarized protons. The fact that the bulk of the emittance for this beam originates from the electromagnetic angular momentum at the ionizer can modify the above estimation slightly. In fact, the efficiency is now double-valued, depending on the sense of the angular momentum upon injection. Investigations concerning this, however, revealed that the efficiency is no worse than for the beam with the same amount of pure intrinsic emittance provided that the beam is injected with the sense of rotation of the angular momentum properly chosen. Thus, 100 μA out of the source will result in 200 nA of 48 MeV beam. Since this is a constant orbit cyclotron the result can be easily adapted for the deduction of transmission efficiencies for all the other energies in the N=1 mode by applying the appropriate scaling law, as discussed earlier in this chapter.

The efficiency was also calculated for a polarized $^3He^{++}$ beam of 26 keV with

an emittance of 24 mm mrad and 100 eV energy spread. It predicts that, with 30 particle nano ampere (pnA) from the source, 0.3 pnA is available. This is the typical parameter for the University of Birmingham source [BRO86]. However, the Birmingham source might be upgraded to produce of the order of 1 μA of polarized $^3He^{++}$ ions simply by replacing the PIG source by a custom built ECR source.

The study described above has been carried out with a provision of obtaining a beam with an extremely high energy resolution (0.04%). Achieving a beam with such a high energy resolution should be compromized with the reduction in the beam transmission efficiency. When a more intense beam is required, one can simply remove the phase selection slits to maximize the beam transmission in the cyclotron central region. With this approach, however, we have to allow a significant loss of particles during extraction. We note that single-turn extraction of a beam in the PU cyclotron requires a beam to have about 6° phase width. Therefore, instead of restricting the radial width of each phase selection slit to 0.5 mm to obtain less than $\pm 2°$ phase width, we can readjust the radial width to achieve $\pm 3°$ beam phase width, in order to increase the beam transmission while achieving a beam with reasonably high energy resolution.

Fig. 7.22 depicts the phase space acceptance of a 48 MeV beam at the injection point. This figure is the same type of diagram as fig. 7.20, except that the three separated regions in fig. 7.22 represent the cases of the phase spread of $+3$, 0, $-3°$, respectively. From fig. 7.22, we can see that the three regions are clearly separated, meaning that the phase can be selected within $\pm 3°$. The required radial width of each slit is 1 mm for the half-turn slit, 0.9 mm for the 15^{th} slit, and 0.8 mm for the 30^{th} slit. In order to maximize the beam transmission through the third (30^{th}

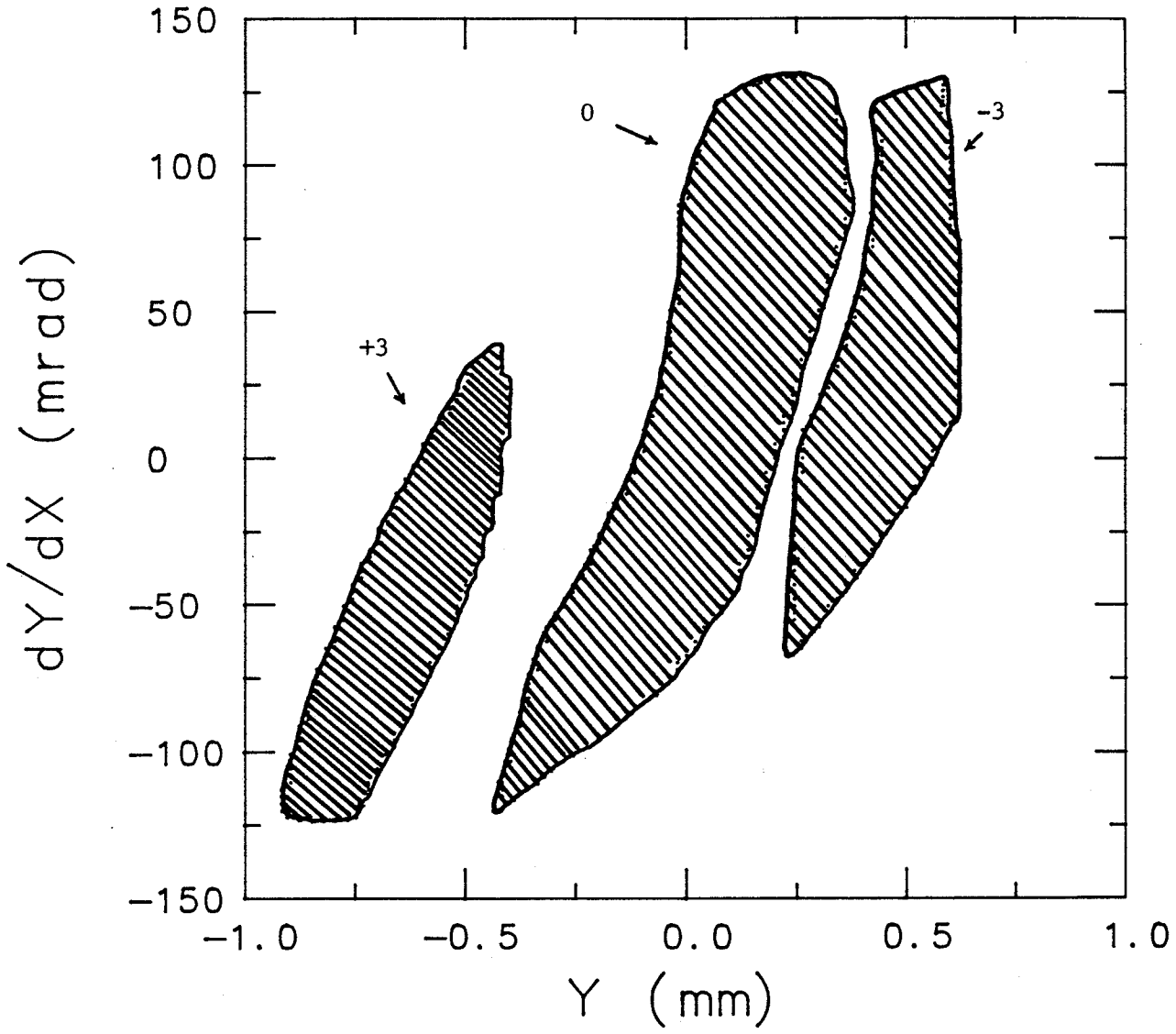

Fig. 7.22 The phase space acceptance diagram of the 48 MeV proton beam. The three separated regions represent the acceptances for the refernce phase (0°), −3° and +3° respectively, when the phase selection slits are placed. The clear separation of these three regions shows the effect of these slits. The spread in energy was not taken into account because it is small (0.2 keV) compared with the injection energy (15 keV).

turn) slit, the radial position of this slit was slightly shifted (by 0.15 mm toward the cyclotron center).

The transmission efficiency calculated by utilizing fig. 7.22 for a 48 MeV proton beam is depicted in fig. 7.23. As can be seen from this figure, there is a significant improvement in the beam transmission efficiency. There will be a further loss in the beam due to passage through meshes of the beam buncher and of the electrostatic mirror (the last element of the axial injection system). The overall transmission efficiency of a beam from an external ion source to a point just after extraction from the cyclotron is expected to be approximately 60% of the values shown in the two figures. A commercially available source can produce 100 μA of polarized proton beam. It is quoted to have 600 mm mrad in phase space area (mostly from the electromagnetic component) at 10 keV with an energy spread of 100 eV. This translates to 490 mm mrad at 15 keV, the proton beam energy chosen for axial injection for a final energy of 48 MeV. In fig. 7.23 is shown the transmission efficiency for such a beam with varing assumptions for the partition in the phase space area. In this figure, curves 1, 2 and 3 represent beams with emittance in $r - p_r$ space only with the radial dependence of its brightness;

1. proportional to r_0/r, where r_0 is the radius of the beam, r is the radial coordinate inside the beam envelope.
2. proportional to $\sqrt{1-(r_0/r)}/(r_0/r)$.
3. proportional to the two dimensional phase space area.

The radial dependence of brightness of an actual beam is thought to lie in between 1 and 3, possibly towards 3. Curves 4 and 5 represent the transmission

Fig. 7.23 The improved total transmission efficiencies of the proton beam with 100 eV energy spread, along the axial injection line and the new N=1 central region. The phase selection slits which would select the beam phase within $\pm 3°$ are placed in the calculation. The five curves represent the beams with emittance in $r - p_r$ space only with the radial dependence of its brightness;

1. proportional to r_0/r, where r_0 is the radius of the beam, r is the radial coordinates inside the beam envelope.
2. proportional to $\sqrt{1-(r_0/r)}/(r_0/r)$
3. proportional to the two dimensional phase space area

The radial dependence of brightness of an actual beam is thought to lie toward 3. Curves 4 and 5 represent the transmission efficiencies for a positive and negative angular velocity respectively with respect to the direction of the cyclotron magnetic field. The markes (a) and (b) denote the cases with a 120 mm mradian of radial phase space area superimposed on an uniform positive and negative angular velocity (converted to an equivalent angular component in phase space area).

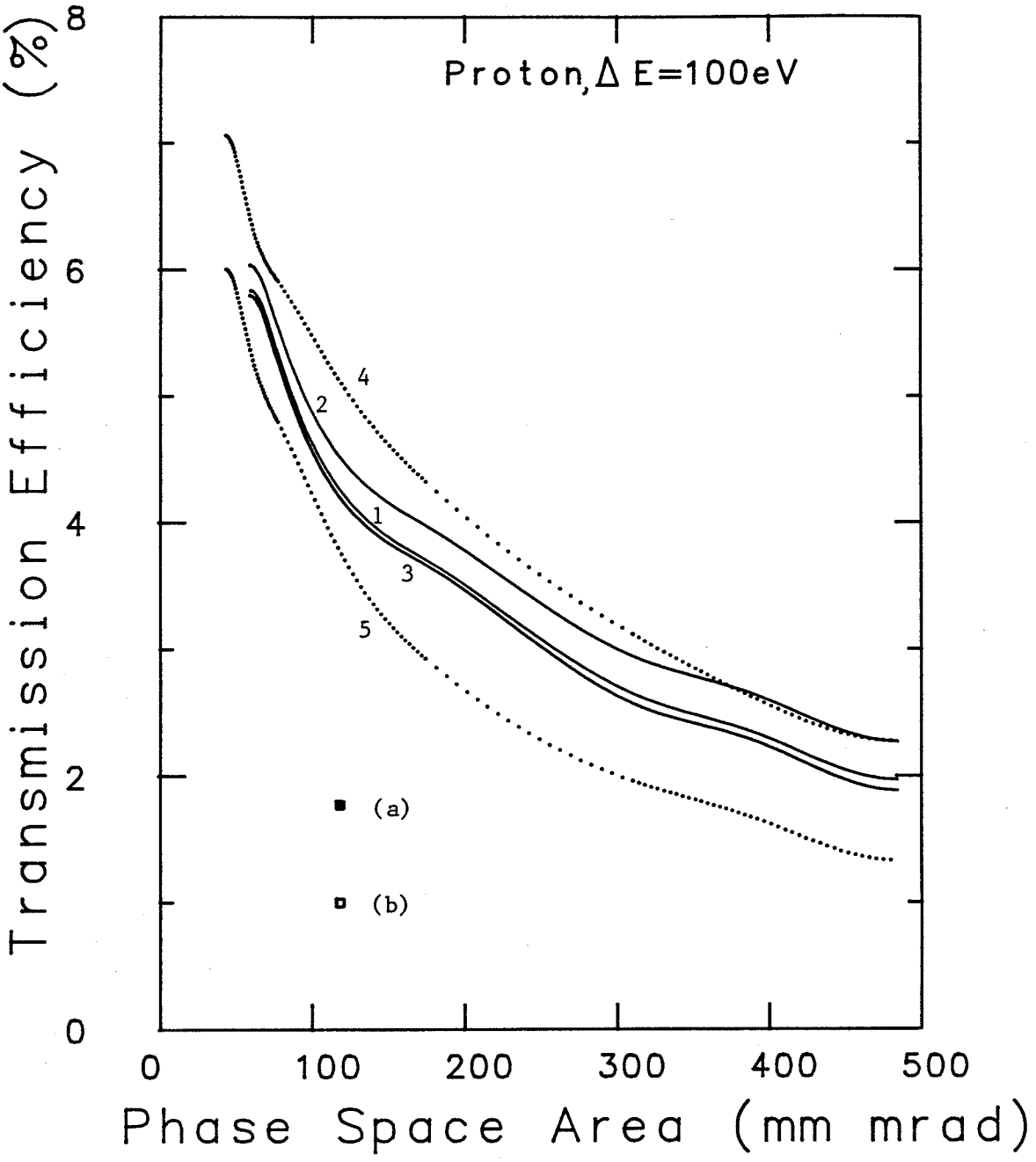
Proton, Δ E=100eV
Transmission Efficiency (%)
Phase Space Area (mm mrad)
0
2
4
6
8
0
100
200
300
400
500
1
2
3
4
5
(a)
(b)

efficiencies for a beam which has zero phase space area but has a uniform positive and negative angular velocity respectively with respect to the direction of the cyclotron magnetic field. A polarized proton beam from an atomic beam source is thought to have such an angular velocity, with, possibly, a varing degree of a radial and angular velocity spread superimposed on it. In fig. 7.23, (a) and (b) marks represent the cases with a 120 mm mrad of radial phase space area superimposed on uniform positive and negative angular velocity (converted to an equivalent angular component in phase space area). It is deduced from the figure that the transmission efficiency for the polarized proton beam quoted above is expected to be 1.8%× 0.6 = 1.8% (this translates to 1 μA), provided that the magnetic field of the ionizer of the atomic beam source is anti-parallel to the cyclotron magnetic field. The transmission efficiency for all the other final energies can be inferred from fig. 7.23 or using a simple scaling relation. A study similar to the above has been carried out for an 85 MeV polarized $^3He^{++}$ beam. Here a $^3He^{++}$ beam of 30 pnA from the existing Birmingham source is assumed to be injected at 28 keV. The beam's emittance (of $70/\pi$ mm mrad at 30 keV) arises mainly from the $r - p_r$ component. Fig. 7.24 represents the transmission efficiency for such a $^3He^{++}$ beam. In this figure, (a) and (b) represent the case for the beam having, in addition, a negative and positive angular velocity (of 39 mm mrad equivalent) respectively. It gives 30 pnA × (0.12 × 0.6) = 2 pnA for an 85 MeV $^3He^{++}$ beam. Protons and $^3He^{++}$ are the only particles that can be accelerated in the N=1 mode.

The same type of study as described above for a 28 MeV deuteron beam has also been carried out. Fig. 7.25 shows the radial displacement for an axially injected 28 MeV deuteron beam for a finite initial phase spread (±3, ±2, ±1 and 0°). This

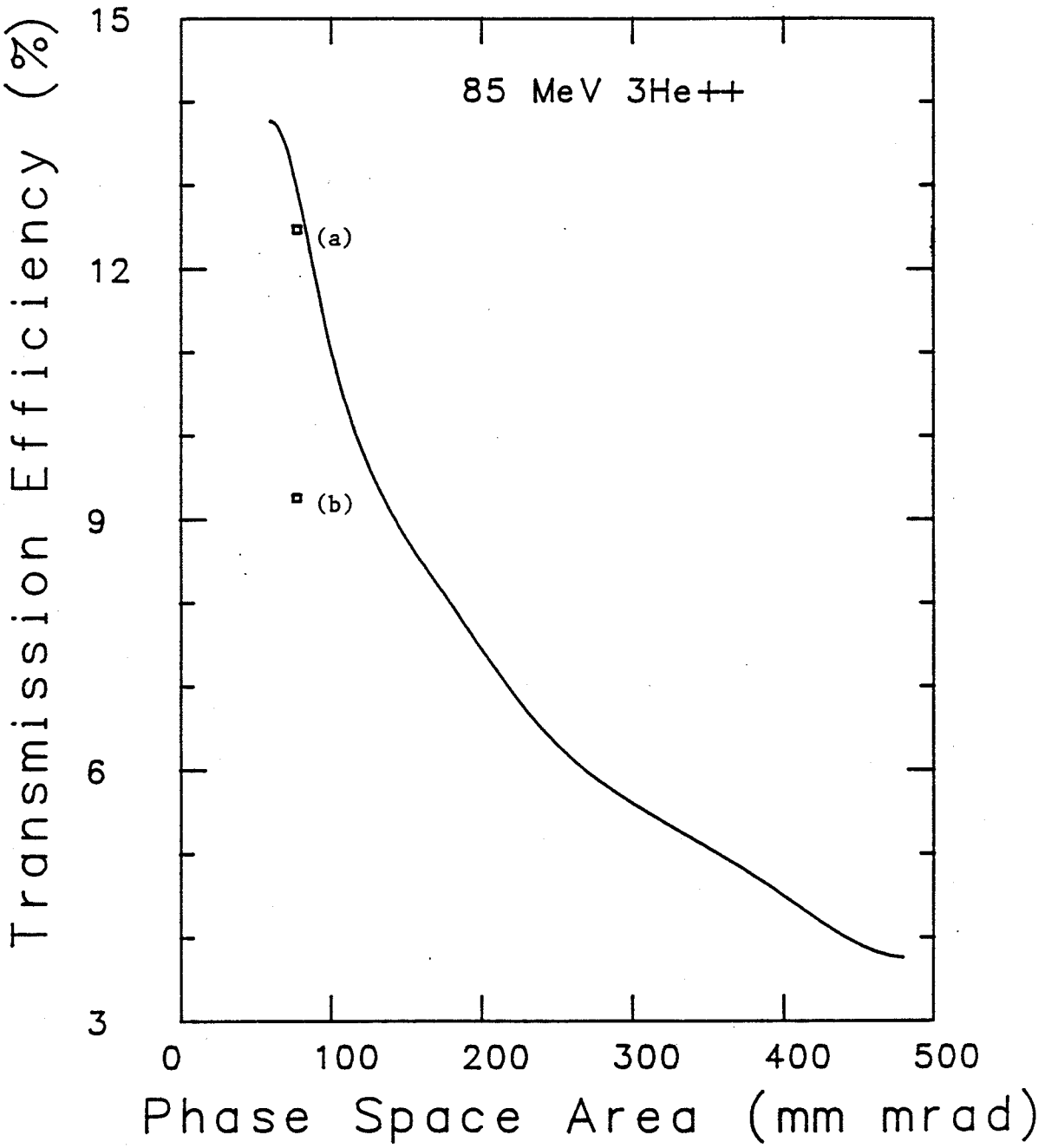

Fig. 7.24 The transmission efficiencies of the $^{3}He^{++}$ beam as a function of the beam phase space area. In theis figure, the marks (a) and (b) represent the cases the beam having a negative and positive angular velocity (of 39 mm mradian equivalent).

Fig. 7.25 Seven chosen particles' radial displacements as a function of the turn number in the newly designed N=2 central region. Each particle has initial RF phase spread ($\pm 3°$,$\pm 2°$,$\pm 1°$) centerd at the reference particle's starting RF phase. It is seen that the maximum displacement occurs at 17^{th} orbit turn. With this large dispersion, single-turn extraction is not achievable if the beam phase is to be selected within $\pm 3°$.

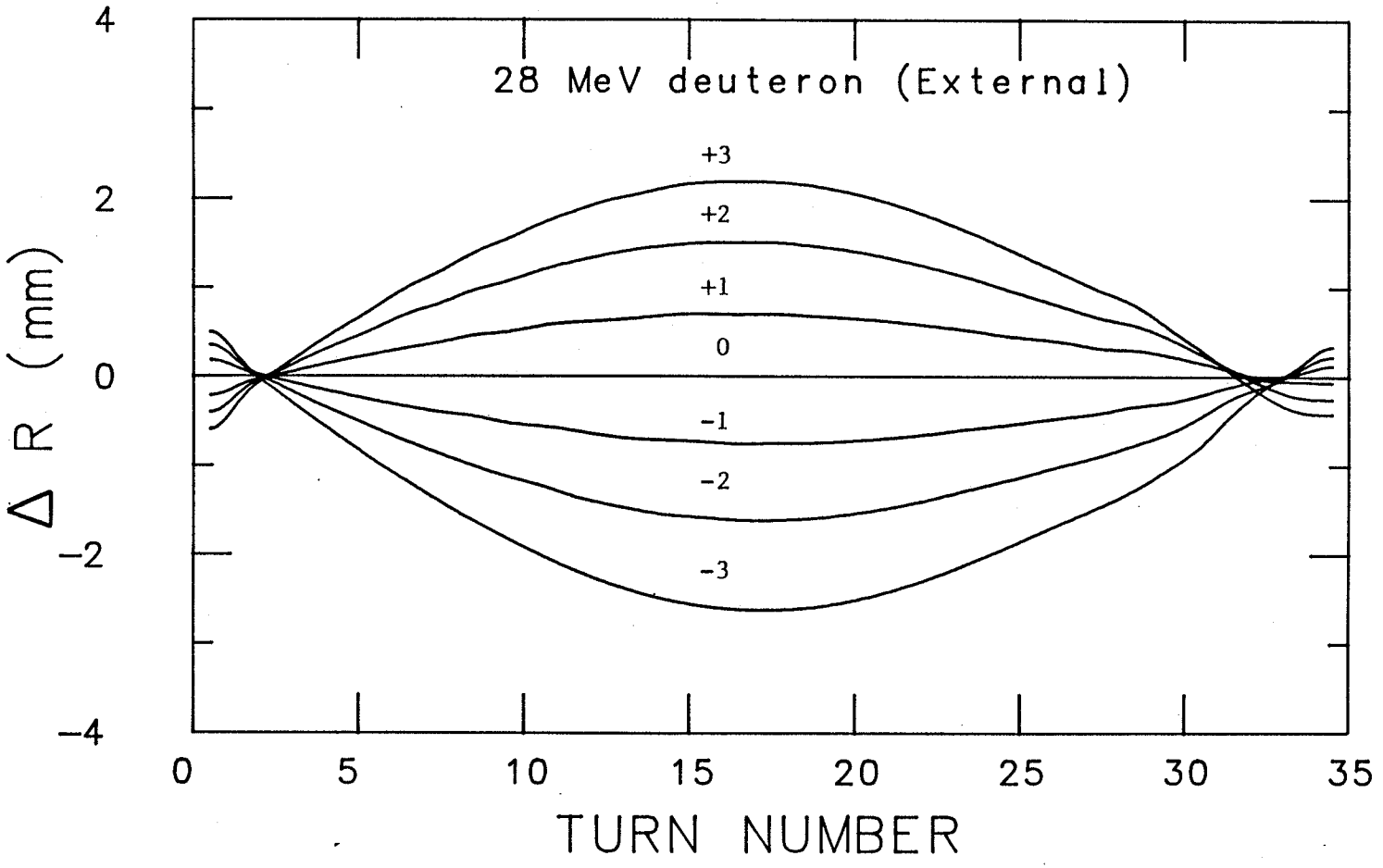
28 MeV deuteron (External)
+3
+2
+1
0
-1
-2
-3
Δ R (mm)
4
2
0
−2
−4
0
5
10
15
20
25
30
35
TURN NUMBER

figure indicated that the maximum radial displacement occurs at about the 17^{th} turn. However, figure 7.25 shows that in the case of the beam in the N=2 central region, the use of the phase selection slits reduces the beam transmission by a significant amount. Even if these slits could select the phase to within $\pm 3°$, then the extraction channel (especially the septum) would cut the beam significantly, because the required radial width of the slit is more than 3.5 mm, as can be seen from fig. 7.25. Since the turn spacing near the extraction region is of the order of 1 mm, it is necessary to restrict the radial width of the slit to less than 1 mm, otherwise the turns at the extraction region will overlap, thereby making it impossible to achieve the single-turn extraction.

Further investigation was carried out by tracing two particles, the design paricle ($\phi_0 = -108°$) and a particle with an identical starting condition but having started 3 RF degrees ahead of the design particle ($\phi_1 = -111°$), up to the 20^{th} turn. This is shown in fig. 7.26. This investigation revealed that the second particle's orbit shift builds up in the negative direction along the 0 degree line until it reaches turn 16.5, where the shift starts shrinking. The amount of the shift at its maximum is -2.55 mm. This shift turned out to consists of two components: $\Delta r = -1.44$ mm arising from the difference in the particle's energy, and $\Delta X_c = -1.11$ mm of shift in the orbit center. The first component is associated with the particle's phase excursion, and may be made to be zero by adjusting the isochronism along the radius. The second component, on the other hand, is a dispersion component that will, in a usual situation, be utilized for phase selection.

In order to see if the radial separation is also large for the case with an internal source, a separate study was carried out for the N=2 central region with an internal

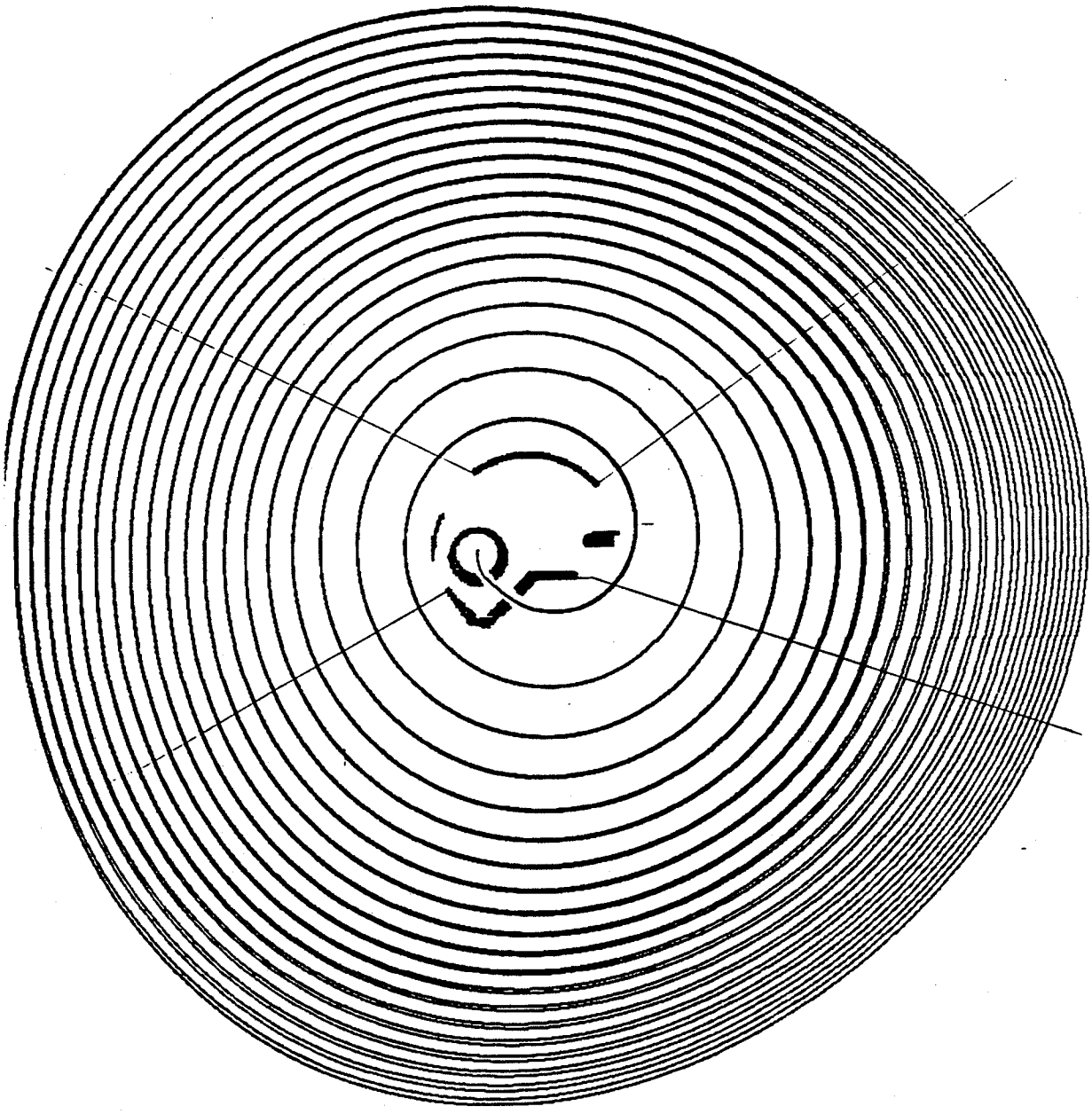

Fig. 7.26 Two particle radial trajectories up to 20 orbit turns in the newly designed N=2 central region. Out of these two particles, the first particle is a design particle (whose starting phase is -108°) and the second particle has an identical initial condition but having started 3 RF degree ahead of the design particle (−111°).

source. It indicated that the amount of radial separation is even larger (by nearly a factor of two; see fig. 7.27).

7.8 The acceleration of polarized ions

In some cyclotrons and synchrotrons ([DEJ81], [KHO75]), polarized ions suffer from a severe depolarization during acceleration in the central region. Depolarization may occur when certain conditions that hold between the betatron frequencies and the spin precessional frequency in the cyclotron magnetic field are satisfied. A thorough investigation for this requires an exact numerical integration of the spin equations of motion. In general, however, it is known that [DEJ81] there is no severe depolarization of polarized ions during acceleration in the central region of a three-sector cyclotron, like the PU cyclotron. In order to see this, we confine ourselves to the application of the analytical formula to the polarized ions that are to be accelerated in the PU cyclotron.

The resonance condition [KIM64] which leads to the depolarization of polarized ions in the central region of a cyclotron is expressed as:

$$\gamma(g/2-1) = \pm lN \pm m\nu_z \pm \epsilon_r p\nu_r \quad , \tag{7.8.1}$$

where the g-factor is defined by

$$g = \frac{2m_0C}{e}\frac{\vec{\mu}}{\vec{S}} \quad , \tag{7.8.2}$$

where $\vec{\mu}$ is the nuclear magnetic moment and $\vec{S}$ is the spin vector. Here, l and p are integers, m is an odd integer, and ϵ_r is 1 or 0 and N is an integer giving the harmonic order of the field.

Fig. 7.27 Seven chosen particle radial displacements as a function of the turn number in the existing N=2 central region. Each particle has initial RF phase spread ($\pm 3°$,$\pm 2°$,$\pm 1°$) centerd at the reference particle's starting RF phase. It is seen that the maximum displacement occurs at 17^{th} orbit turn. Comparing this figure with fig. 7.25, it is seen that the dispersion in the existing central region is a factor of two larger than that in the new central region.

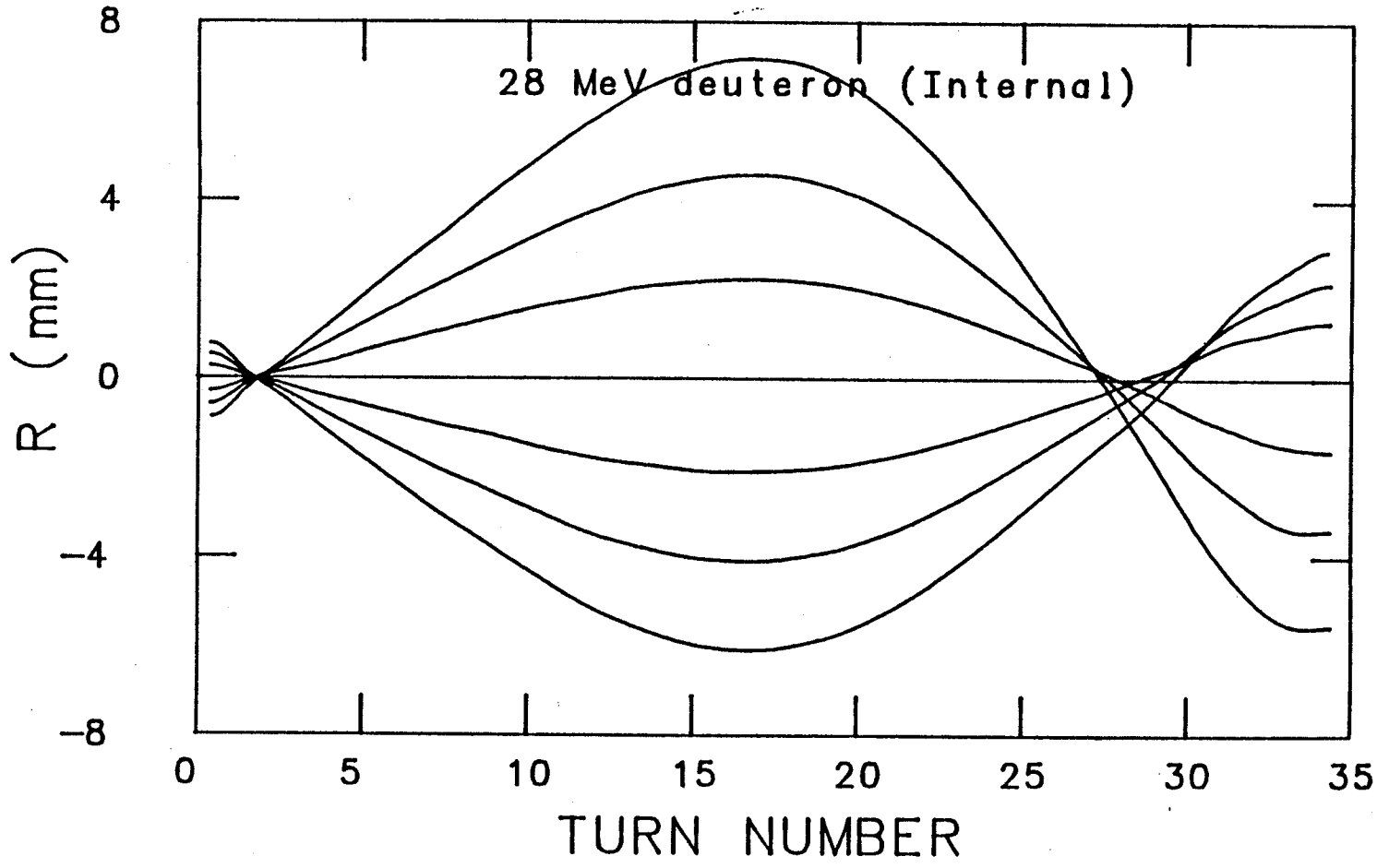
28 MeV deuteron (Internal)
8
4
0
−4
−8
R (mm)
0
5
10
15
20
25
30
35
TURN NUMBER

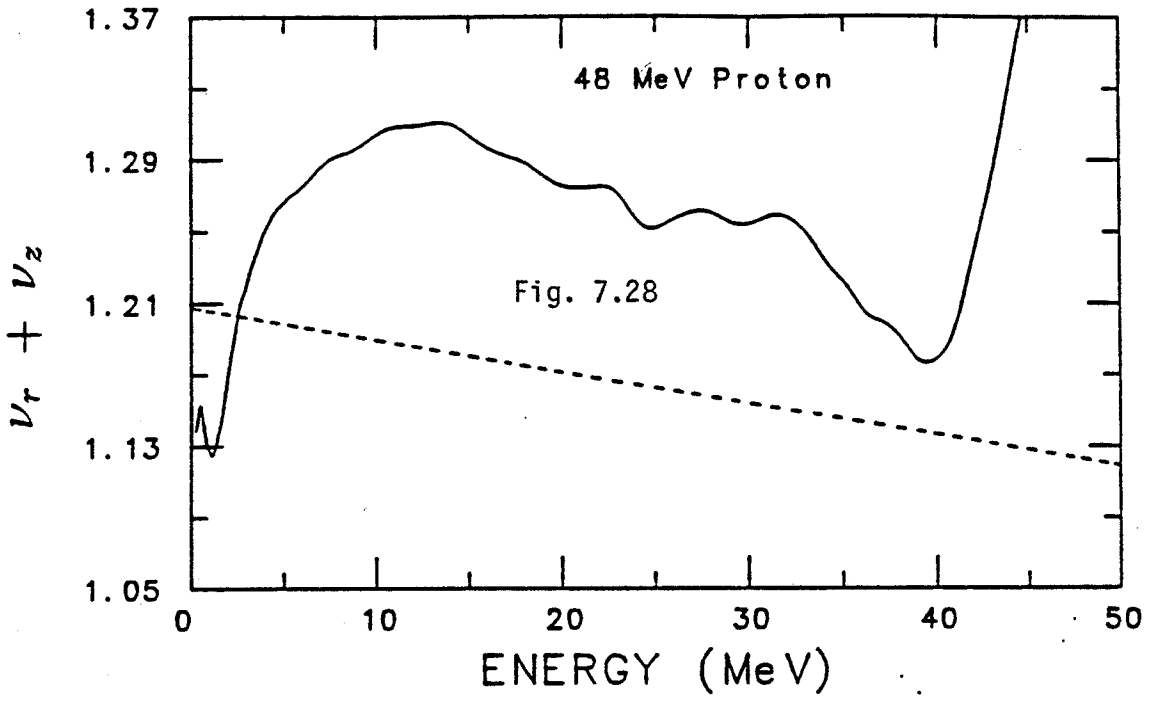

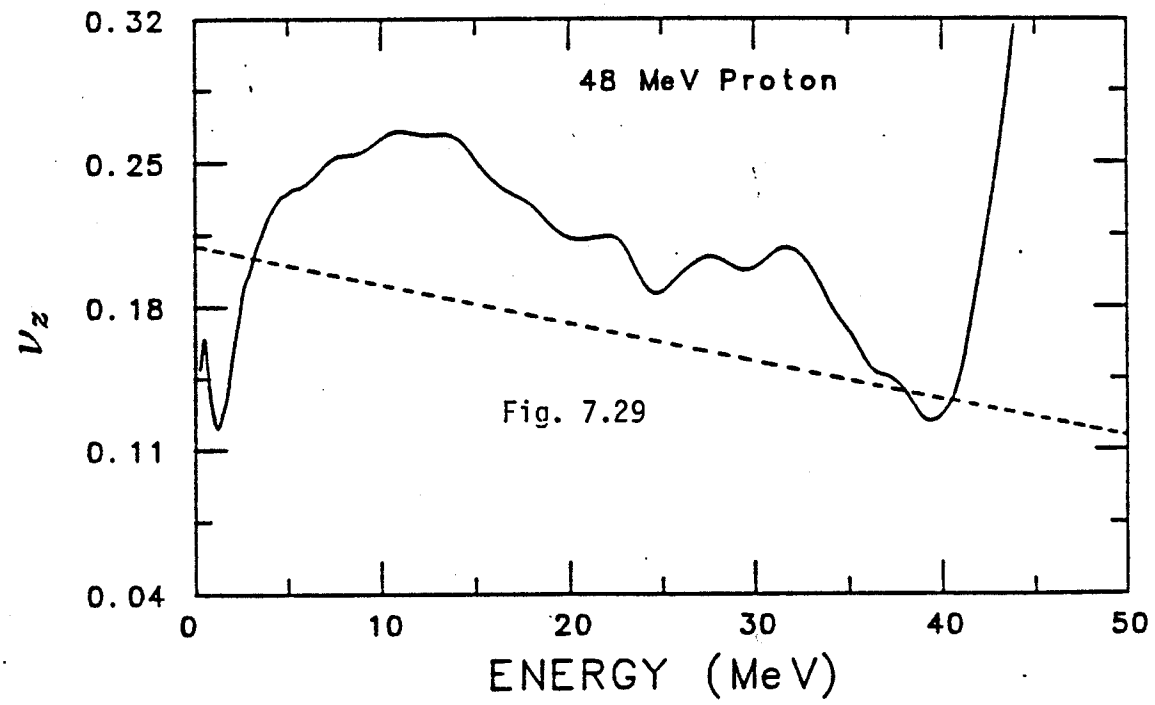

Figs. 7.28, 7.29 The depolarizing resonance crossings for a 48 MeV proton beam in the Princeton University cyclotron.
Fig. 7.28 depicts $\gamma(g/2-1) = 1.793\gamma = 3-\nu_z-\nu_r$.
Fig. 7.29 describes $1.79\gamma = 2 - \nu_z$.

Applying this formula to the PU cyclotron shows that the polarized deuteron beam is expected to be accelerated without any serious depolarization. For a polarized proton beam, it crosses one of the resonances (fig. 7.28)

$$\gamma(g/2-1) = 1.793\gamma = 3 - \nu_z - \nu_r, \tag{7.8.3}$$

and an imperfection related resonance (arising from N=2. See fig. 7.29)

$$1.793\gamma = 2 - \nu_z. \tag{7.8.4}$$

The crossing of these resonances are, however, not expected to cause any serious depolarization. In fact many existing cyclotrons around the world which satisfy these resonance conditions are known to accelerate protons without suffering any serious depolarization. As can be seen in fig. 7.28 the crossing of the former takes place at around 3 MeV where the passage through this resonance is very fast. There are all together three crossings of the latter type for a 48 MeV proton beam as can be seen in fig. 7.29. Of these only the one at around 40 MeV is of some concern (the two others are passed quickly) because the curve indicates that it remains in resonance for over 4 MeV (which corresponds to 17 turns). The N=2 (imperfection) field component is, however, not expected to be large for the PU cyclotron (which has three sector geometry) and in fact this N=2 component can be reduced if the necessity arises. In addition, the crossing at this energy is actually a double crossings which is likely to reduce the spin flip obtained from the first crossing and therefore the amount of depolarization is expected not to be large.

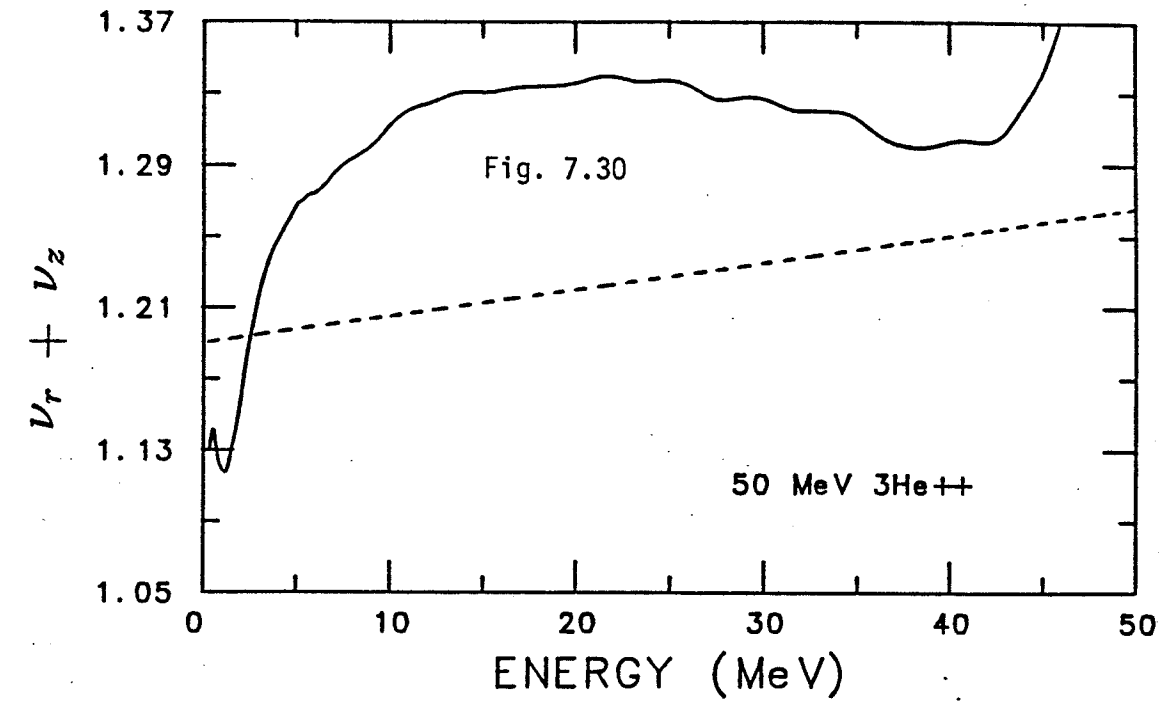

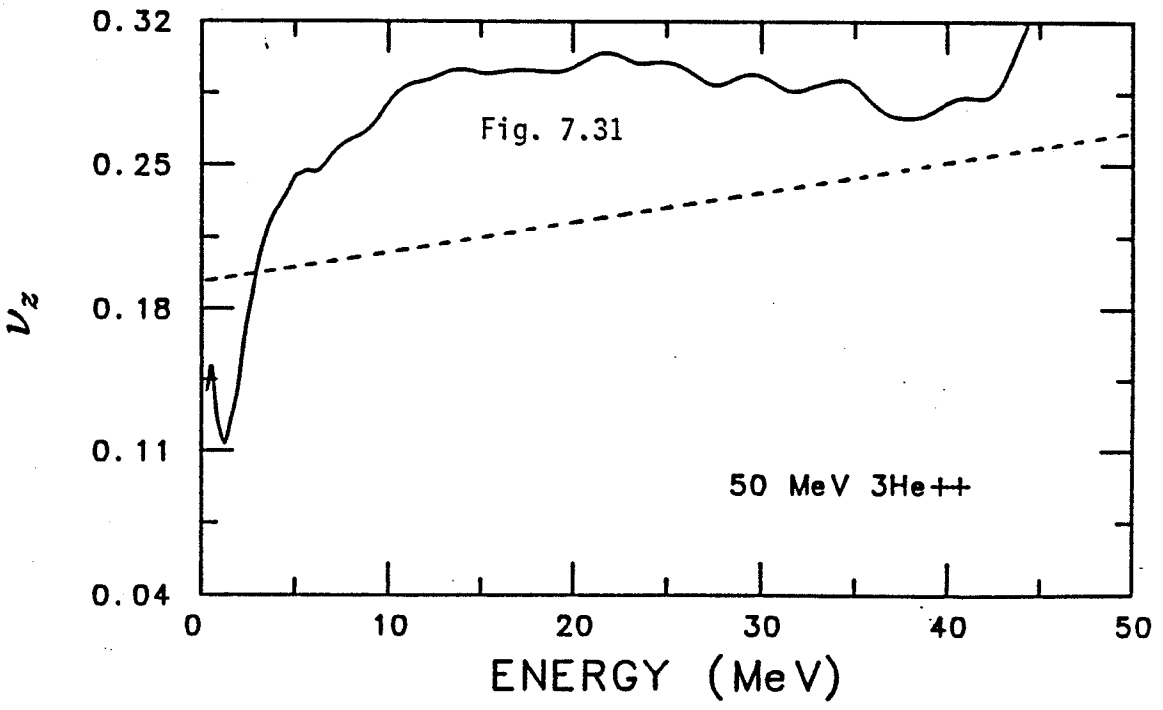

Figs. 7.30, 7.31 The depolarizing resonance crossings for 50 MeV $^3He^{++}$ in the Princeton University cyclotron.
Fig. 7.30 describes $-4.1914\gamma = -3 - \nu_z - \nu_r$.
Fig. 7.31 depicts $-4.1914\gamma = -4 - \nu_z$.

For polarized $^3He^{++}$, it crosses

$$\begin{aligned} \gamma(g/2-1) &= -4.1914\gamma \\ &= -3-\nu_z-\nu_r \end{aligned} \tag{7.8.5}$$

and

$$-4.1914\gamma = -4-\nu_z \tag{7.8.6}$$

See figs. 7.30, 7.31, 7.32 and 7.33. Fig. 7.33 indicates ($^3He^{++}$ ions remain in near resonance crossing from 7 MeV to 45 MeV) that there could be some depolarization (may be of the order of a couple of percent) for an 80 MeV $^3He^{++}$ beam. Inspection of fig. 7.32 indicates that the former crossing also requires careful attention. It is of a minor intrinsic resonance crossing in the sense that the ions need a large radial oscillation amplitude as well as vertical oscillation. We do not expect any serious depolarization from the above resonances.

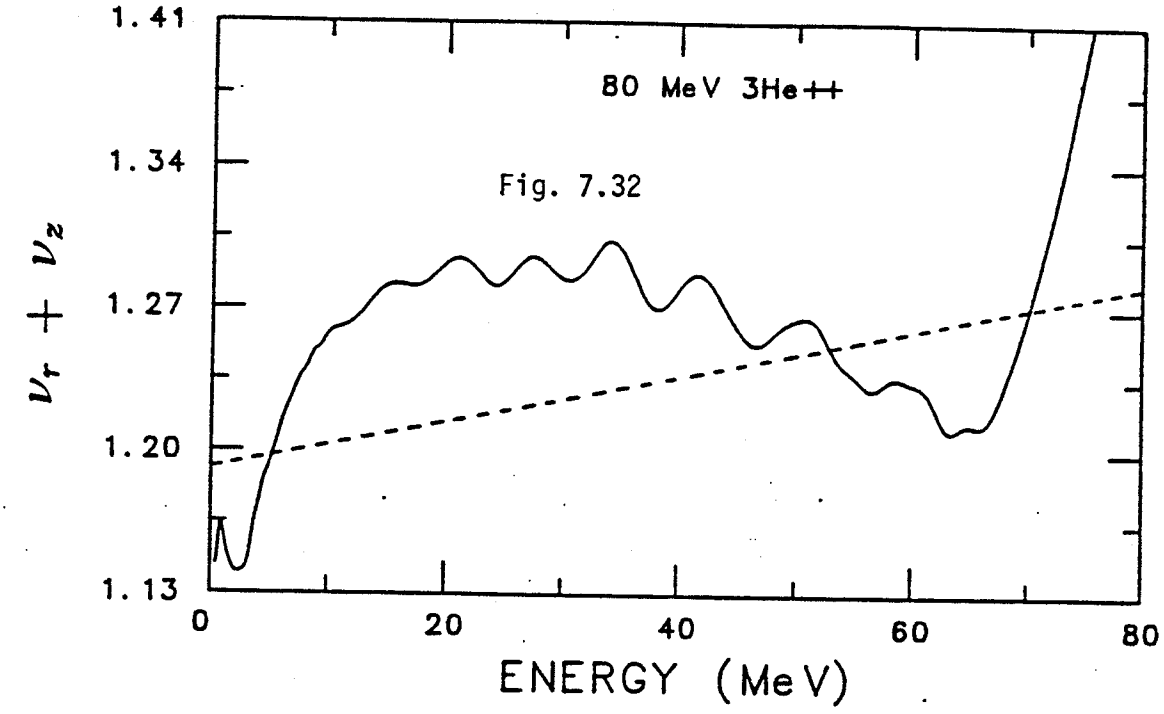

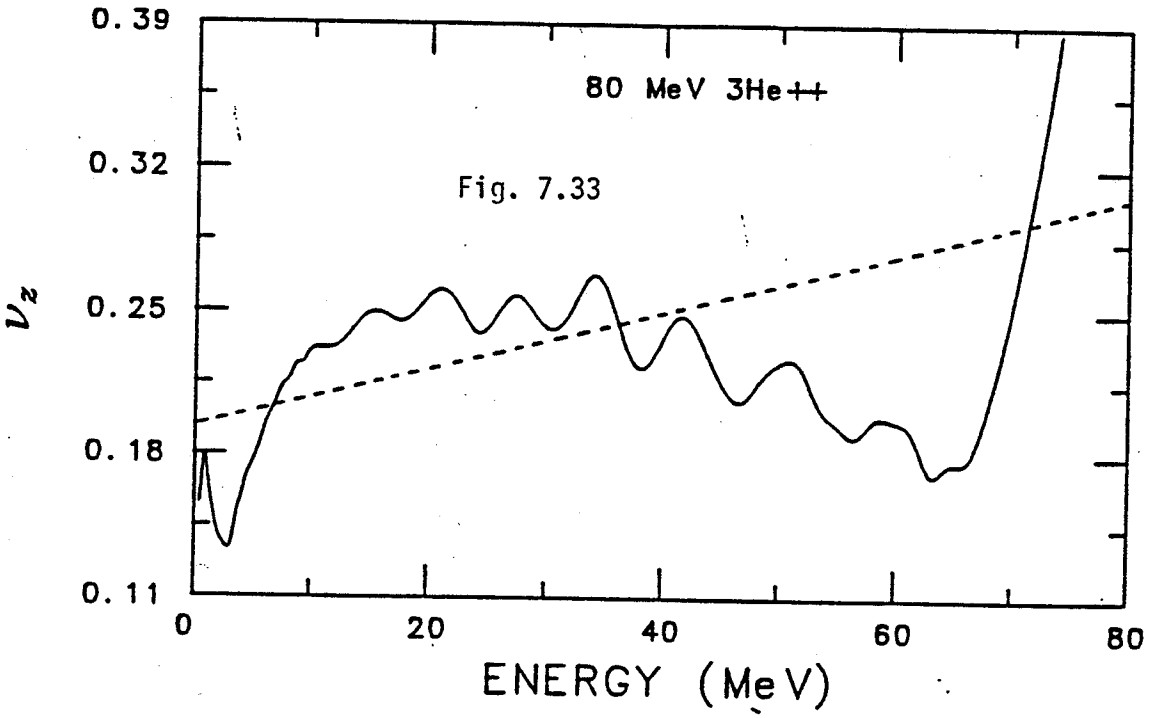

Figs. 7.32, 7.33 The depolarizing resonance crossings for 80 MeV $^3He^{++}$ in the Princeton University cyclotron.
Fig. 7.32 describes $-4.1914\gamma = -3 - \nu_z - \nu_r$.
Fig. 7.33 depicts $-4.1914\gamma = -4 - \nu_z$.

Chapter 8

Summary and Conclusion

The feasibility study for axial injection of ions into the Princeton University cyclotron has been described. The lenses along the axial injection system were carefully chosen to prevent any depolarization of polarized ions. The study revealed that the use of a magnetic lens would depolarize the polarized ions to some extent, therefore the placement of an electrostatic quadrupole lens was suggested. Then the detailed beam optics studies were carried out to match the emittance of a beam to the admittance of the cyclotron.

Simultaneously, a design study for a new central region was performed that is required in view of the axial injection system. This study started with investigating the detailed beam orbit dynamics in the existing central regions. During this procedure, the investigations for restoring the two phase selection slits were carried out to obtain a beam with extremely high energy resolution. Subsequently, it was found that the placement of the two phase selection slits at the 18^{th} and 29^{th} turns would select the RF phase of a beam within $\pm 2°$, which translates into $\pm 0.04\%$ in energy resolution.

In order to see the validity of the calculations described above, the phase of a proton beam inside the cyclotron was measured along the radius of the cyclotron. For this purpose, a gamma ray detector was placed some 70″ away from the beam probe located along the zero degree line (see fig. 7.1). The geometry of the arrangement was such that the distance from the probe head, where the impinging protons induce an emission of gamma rays from the target nuclei, is almost constant

over the entire range of the radial probe position. Prior to the measurement, the detector and its electronic system were set up by Professors R.T. Kouzes and A.B. McDonald to yield a resolution of 500 pico second. This corresponds to a 3.3 RF degree resolution at the dee RF of 18.52 MHz, the frequency at which the protons were accelerated at the time of the measurement. First, a 40 MeV proton beam was accelerated inside the cyclotron using a cyclotron setting parameters from the past. The gamma ray pulse from the probe tip was then monitored by the detector, timed against the RF, and this time of flight spectrum was recorded on a multi-channel analyzer. This gives us the time of arrival of the gamma ray pulse with respect to the dee RF voltage. Both the first and the second radial phase slits were in place throughout the measurement. Such a measurement was repeated at 1″ interval from 7″ to 30″ radius of the probe tip's position. Fig. 8.1 shows the result. The dotted curve represents the phase excursion of a proton as a function of energy of the proton predicted by a computer calculation. The solid curve represents the measured phase excursion of the accelerated beam. In the absence of an absolute phase of the curve, we can only move the measured curve vertically and judge the implication. It is, however, clear that the two curves agree very well. The cyclotron magnetic field was then changed to the profile settings predicted by the SETOP code for a 40 MeV proton beam. After optimization of the inner and outer harmonic coils by Dr. W.H. Moore for centering of the orbits, the measurement was repeated. Fig. 8.2 shows the result. The agreement is again very good.

Prior to this phase measurement, the turn pattern of the proton beam inside the cyclotron was then recorded on a chart recorder by scanning the beam probe at a constant speed along the radius of the cyclotron. This is shown in fig. 8.3. It is seen

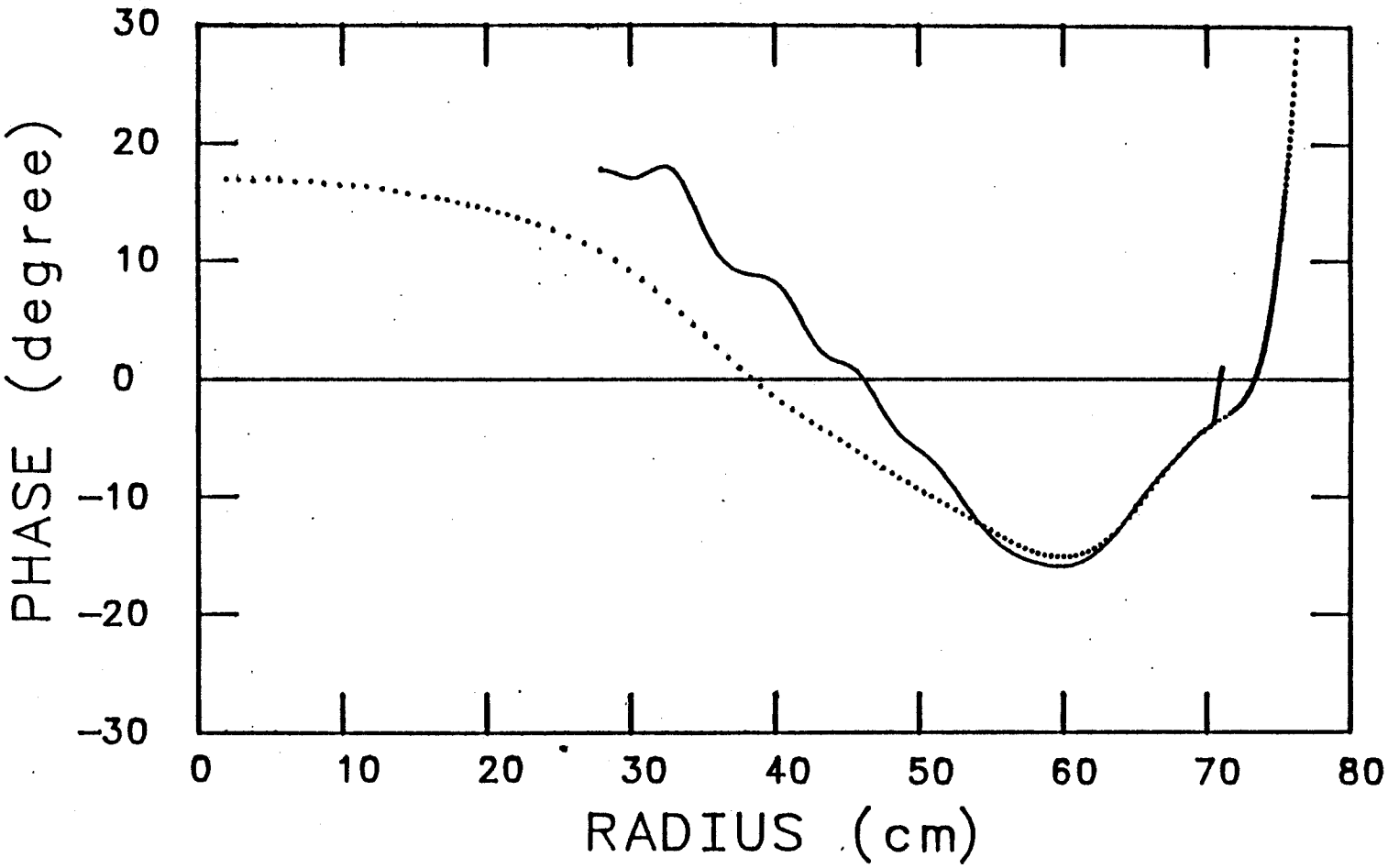

Fig. 8.1 The phase excurion of the 40 MeV proton beam as a function of the radius of a beam. The cyclotron parameters were set from the past. The solid curve represents the calculated phase excursion and the dotted curve denotes the measured phase excursion. This figure shows that the two curves agree quite well.

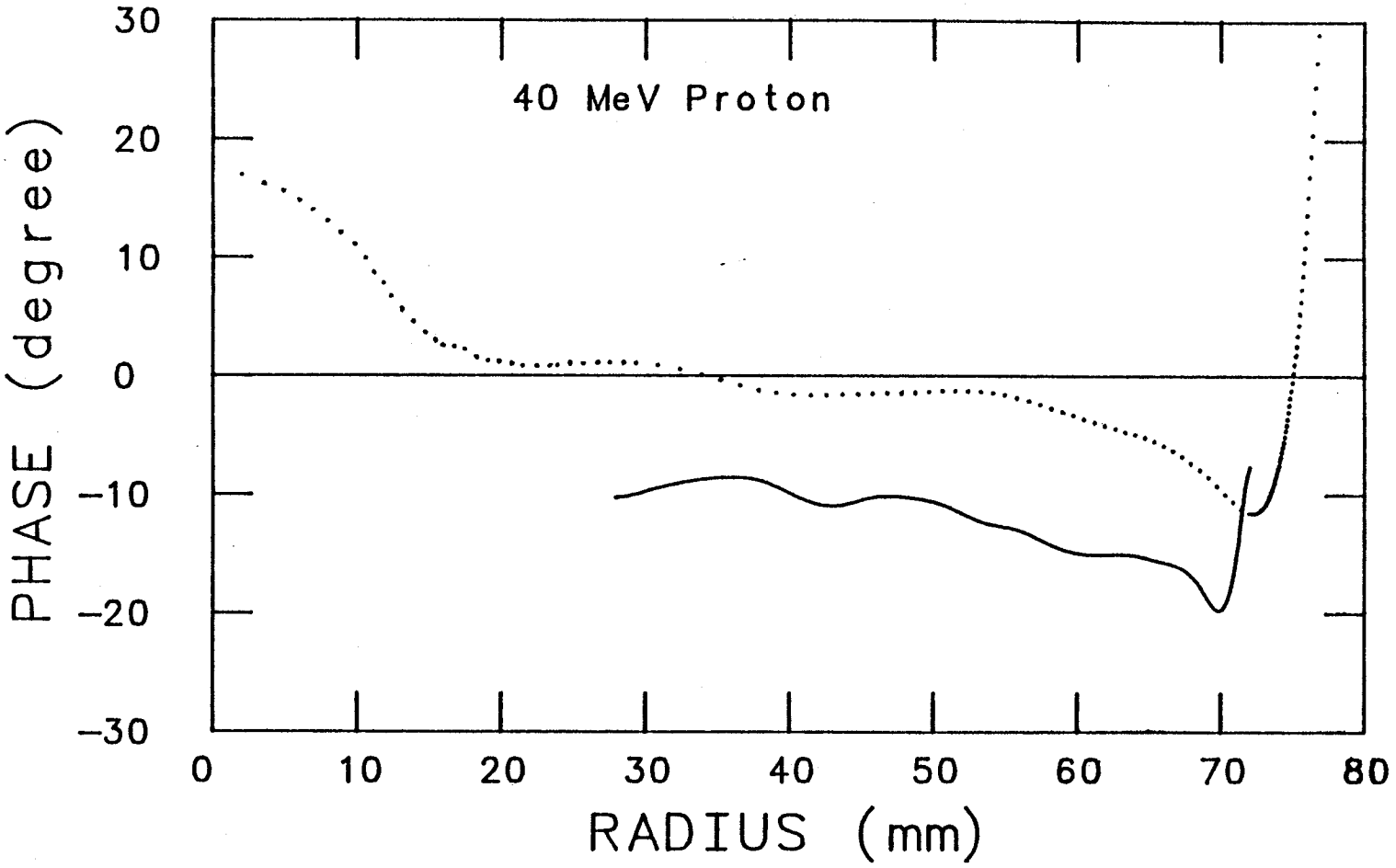

Fig. 8.2 The phase excursion of the 40 MeV proton beam as a function of the radius of a beam. The trim coil setting parameters were obtained from the program SETOP and considered as the most optimum field setting. The solid curve represents the measured phase excursion and the dotted curve denotes the calculated phase excursion. It can be seen from this figure that the two curves agree quite well.

Fig. 8.3 The turn pattern of a 40 MeV proton beam when the cyclotron magnetic fields were exactly the same as the predicted fields. This figure shows the turn pattern from the position where the first phase selection slit is in place (18^{th} turn) to the beam extraction point. It can be seen that the turns are well separated all along the radius and there is no indication of the precessional motion of the orbit center.

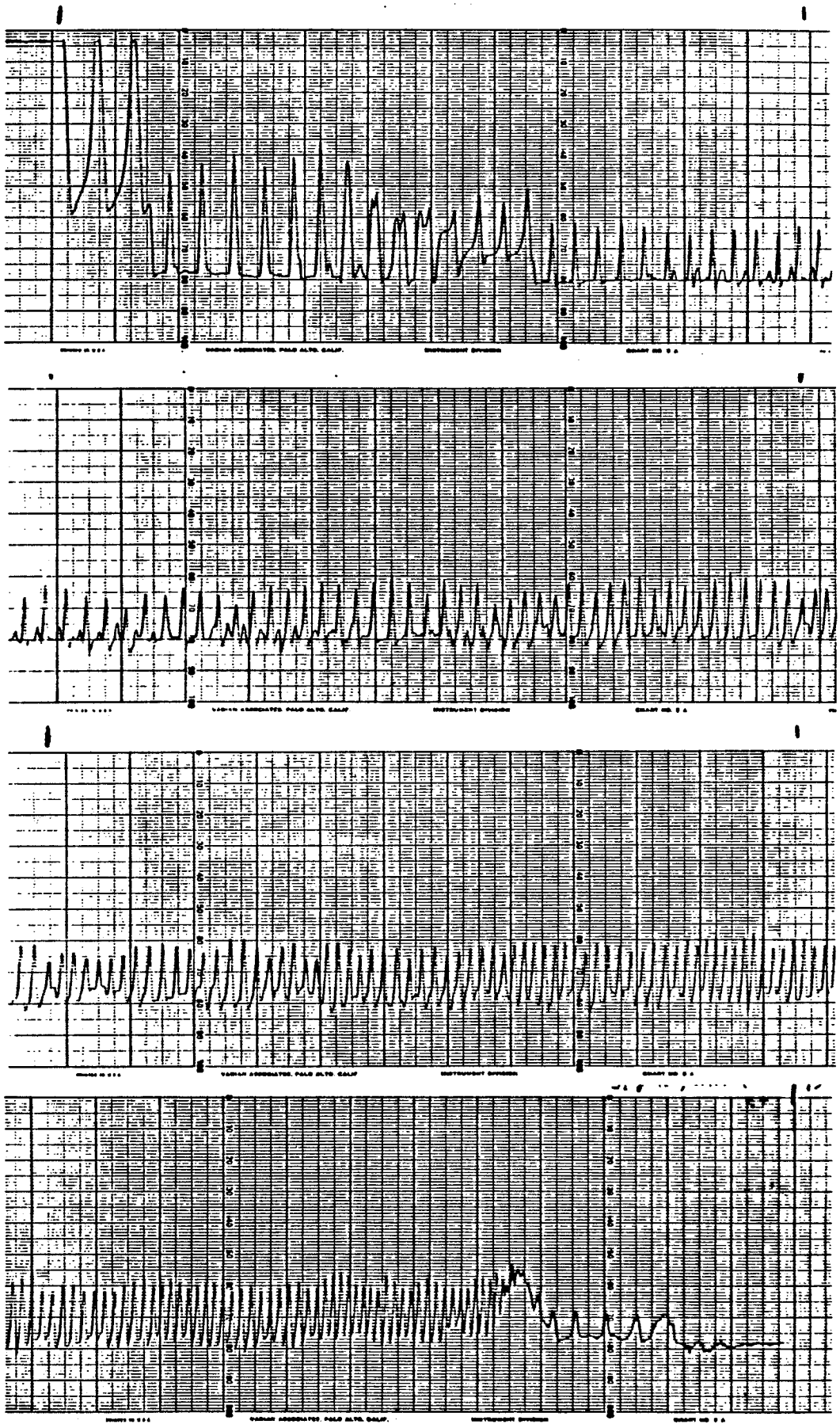

that the turns are completely separated all the way up to the last turn, and there is no indication of any precessional motion of the orbit center. Another measurement by Dr. W.H. Moore indicated that the beam had 45–50 keV energy spread; of this, 40 keV was contributed by the ripple in the dee RF voltage. An extraction efficiency of 95% was achieved. The measured gamma ray time had a FWHM of 3.5 RF degrees, which is in agreement with the prediction described above. The measurement confirms that the magnetic field of the Princeton University AVF cyclotron is, within the precision of the measurements, identical to the MSU's K=50 cyclotron.

Based on the beam orbit dynamics studies for the existing central region of the Princeton University cyclotron, a design study for a new central region was carried out. The goal of this study was to design a new central region in such a way that the motion of a beam in the new central region would yield the one in the existing central region. In this way, the existing cyclotron setting parameters can be retained without any significant modifications. The 48 MeV proton beam orbit dynamics study performed for the new central region revealed that the motion of the instantaneous orbit center had the same center motion as the existing central region. The study on the axial motion also revealed the same result.

After completing a design of the new N=1 central region, the total transmission efficiencies along the axial injection system and throughout the central region for various particles that are accelerated with N=1 mode were calculated. For this purpose, the phase space acceptance diagram at the injection point of the new central region was obtained with the two phase selection slits placed at the 15^{th} and 30^{th} turns. A computer program INJECT has been developed which has a

capability to trace the particles' trajectories along the downstream portion of the axial injection system. This region includes such vital elements as the cyclotron magnetic field, the beam buncher, and the electrostatic mirror. The result revealed that the transmission efficiency for the typical unpolarized proton beam with 15 keV energy, ±10 eV energy spread and 16 mm mrad emittance would be approximately 3%. For polarized $^3He^{++}$ of 26 keV with an emittance of 24 mm mrad and 100 eV energy spread, the result was 0.3 pnA when the source current was assumed to be 30 pnA.

In order to increase the transmission efficiency while achieving a reasonably high energy resolution with the single turn extraction capability retained, the radial width of the phase selection slits was slightly increased. In this way, the beam phase width is increased to less than ±6°. As a result, the transmission efficiency for the polarized proton beam from the commercially available source increased to 1.8% (corresponding to 1 μA). For the Birmingham polarized $^3He^{++}$ source, the result obtained was 2 pnA.

In the design of the new N=2 central region, it has turned out to be much more difficult to fulfill the three criteria: small radial motion (orbit centering), small axial motion and phase selection. The 28 MeV beam dynamics study for the existing N=2 central region revealed that the beam is widely off-centered and the gap-crossing resonance is much more severe than the N=1 case. Subsequently, the new N=2 central region was designed in such a way that the precessional amplitude of the center motion in the new N=2 central region is a factor of three smaller than that in the existing N=2 central region. The phase selection studies based on this new geometry showed that the radial dispersion is much larger than that in

the N=1 central region. Further investigation revealed that this dispersion consists of the two components: the difference in the energy and in the orbit center. Out of these two components, the first component can actually be made to be zero by improving isochronism. It is therefore suggested that the magnetic field for N=2 obtained from the SETOP program be replaced by the new field which may be drawn from another program FIELDER [GOR72], which was developed at MSU but has never been tested for the Princeton cyclotron. The second component, the radial dispersion due to the difference in the orbit center, in fact, can not be reduced unless a modification of the dee geometry is carried out.

The depolarization problem of the polarized ions during acceleration in the central region was also considered. It was, in general, known that a three sector cyclotron would not render any severe depolarization during acceleration. The analytical study applied to the Princeton University cyclotron indicated that for polarized proton, deuteron and $^3He^{++}$, no severe depolarization would be anticipated.

References

[AND79] James Anderson, Robert Batten, John Bruckshaw, Mark de Jong, Irving Gusdal, Gert Knote, Francis Konopasek, Alan McIlwain, James S.C. McKee, Saewoong Oh and Robert Pogson, "Status Report on the University of Manitoba Cyclotron", IEEE Trans. on Nucl. Sci., Vol. NS-26, No. 2, 1976-1978 (1979)

[BAN66] A.P. Banford, "Transport of Charged Particle beams", E. & F. N. Spon Limited, London, 1966

[BAT76] R.A. Batten, J. Bruckshaw, I. Gusdal, G. Knote, A. McIlwain, J.S.C. McKee and S. Oh, "Axial Injection of H^- Ions into the University of Manitoba Variable Energy Cyclotron", Nuclear Instruments and Methods 136 (1976) 15-17

[BEN69] J.R.J. Bennett, "Ion Sources for Multiply Charged Heavy Ions", Proceedings of the 5^{th} International Cyclotron Conference, 469-479, Oxford, 1969

[BER66] R.E. Berg, "Precise Methods for Pre-Calculation of Cyclotron Control Settings", MSUCP-24, 1966

[BER68] R.E. Berg, H.G. Blosser and M.M. Gordon, "Theoretical and Experimental Beam Studies for the Michigan State University Cyclotron", Nuclear Instruments and Methods 58 (1968) 327-341

[BLO69] H.G. Blosser, "Optimisation of the Cyclotron Central Region for the Nuclear Physics User", Proceedings of the 5^{th} International Cyclotron Conference, 257-273, Oxford, 1969

[BRO86] Jeremy Brown, Private Communication

[BRU83] J. Bruckshaw, V. Derenchuk, I. Gusdal, J. Lancaster, A. McIlwain, S. Oh, R. Pogson and J.S.C. McKee, "Survey Measurements of the Magnetic Field of the University of Manitoba Spiral Ridge Cyclotron", Nuclear Instruments and Methods 207 (1983) 493-495

[BUR65] J.J. Burgerjon, F. Konopasek, and K.G. Standing, "Magnetic Field Control in the University of Manitoba Cyclotron", IEEE Transactions on Nuclear Science NS-12, No. 3, 334-337 (1965)

[BUR66] J.J. Burgerjon, B. Hird, F. Konopasek, K.G. Standing, "The Manitoba Cyclotron", IEEE Transactions on Nuclear Science NS-13, No. 4, 422-425 (1966)

[CHE81] Mao-bai Chen and D.A. Lind, "The Numerical Calculation of the Three Dimensional Electric Field in the Central Region of a Cyclotron", IEEE Trans. Nucl. Sci., NS-28, No. 3, 2636-2638 (1981)

[CLA71] D.J. Clark, "Survey of External Injection Systems for Cyclotrons", Proceedings of the 5^{th} International Cyclotron Conference, 583-601, Oxford, 1969

[CLA72] D.J. Clark, "Cyclotron Injection Systems", AIP 9, 191-202 (1972)

[COH53] Bernard L. Cohen, "The Theory of the Fixed Frequency Cyclotron", The Review of Scientific Instruments 24, 8, 589-601 (1953)

[COU58] E.D. Courant and H.S. Snyder, "Theory of the Alternating-Gradient Synchrotron", Annals of Physics:3, 1-48 (1958)

[COX62] A.J. Cox, D.E. Kidd, W.B. Powell, B.L. Reece and P.J. Waterton, "Operation of a 40-inch Radial Ridge Cyclotron", Nuclear Instruments and Methods 18,19 (1962) 25-32

[DAH73] Paul Dahl, "Introduction to Electron and Ion Optics", Academic Press, 1973

[DEJ81] Mark Sybe de Jong, "The Design of an H^- and D^- polarized Ion Source and Resonant Depolarization of Polarized H^- Ions in a Cyclotron", Ph.D. Thesis, The University of Manitoba, 1981, Unpublished

[DER83] V. Derenchuk, J. Bruchshaw, I. Gusdal, J. Lancaster, A. McIlwain, S. Oh, R.Pogson and J.S.C. McKee,"Automated Cyclotron Magnetic Field Measurement at the University of Manitoba Cyclotron", Lecture Note in Physics 215, Springer-Verlag, 411-415 (Conference on Computing in Accelerator Design and Operation, W. Berlin, Sept. 20-23, 1983

[EMI72] C. Robert Emigh, "Statistical Beam Transport for High Intensity Ion Currents", Proceedings of the 1972 Proton Linear Accelerator Conference, LA-5115, 182-190 (1972)

[FOR60] G.E. Forsythe and W.R. Wasow, "Finite-Difference Methods for Partial Differential Equations", John Wiley company, 1960

[GEL79] R. Geller, "Electron Cyclotron Resonance (E.C.R.) Multiply Charged Ion Sources", IEEE Trans. Nucl. Sci. Vol. NS-26, No.2, 2120-2126, 1979

[GOR59] M.M. Gordon and T.A. Welton, "Computation Methods for AVF Cyclotron Design Studies", ORNL-2765, 1959

[GOR62] M.M. Gordon, "The Electric Gap-Crossing Resonance in a Three-sector Cyclotron", Nuclear Instruments and Methods, 18, 19 (1962) 268-280

[GOR66] M.M. Gordon, "Single Turn Extraction", IEEE Trans. Nucl. Sci., NS-13, No. 4, 48-57 (1966)

[GOR72] M.M. Gordon and D.A. Johnson, "Application of a New Field Trimming Program to the MSU Cyclotron", A.I.P. 9 (1972) 298-307

[GUS76] I. Gusdal, G. Knote, A. McIlwain, J.S.C. McKee, S. Oh and H.W. Uzat, "The Acceleration of Deuterons by the University of Manitoba Variable Energy Cyclotron", Nuclear Instruments and Methods 136 (1976) 393-394

[HAE67] W. Haeberli, "Sources of Polarized Ions", Ann. Rev. Nucl. Sci. 17, 373-426 (1967)

[HAW82] P.W. Hawkes, editor, "Magnetic Electron Lenses", 1982 Springer-Verlag

[HOP66] D.I. Hopp and J. Reginald Richardson, "Use of the $\frac{3}{2}$-radial Reaonance in Extraction from a Six-sector Isochronous Cyclotron", Nuclear Instruments and Methods, 44 (1966) 277-291

[KAP59] I.M. Kapchinskij and V.V. Vladimirskij, "Limitations of Proton Beam Current in a Strong Focusing Linear Accelerator Associated with the Beam Space

Charge", Proceedings of the International Conference on High-energy Accelerators and Instrumentation, C.E.R.N., Geneva, 274-288 (1959)

[KHO75] T. Khoe, R.L. Kustom, R.L. Martin, E.F. Parker, C.W. Potts, L.G. Ratner, R.E. Timm, A.D. Krisch, J.B. Roberts, J.R. O'Fallon, "Acceleration of Polarized Protons to 8.5 GeV/c", Particle Accelerators 1975, Vol. 6, 213-236

[KIM64] HO GIL KIM and W.E. Burcham, "Resonant Depolarization of Deuterons during Acceleration in a Sector-focused Cyclotron", Nuclear Instruments and Methods 27 (1964) 211-220

[KLE71] O. Klemperer, "Electron Optics", Camebridge University Press, 3^{rd} ed., 1971

[LAP71] P.M. Lapostolle, "Possible Emittance Increase through Filamentation due to Space Charge in Continuous Beam", IEEE Trans. Nucl. Sci. NS-18, No. 3, 1101-1104 (1971)

[LAW30] E.O. Lawrence and N.E. Edlefsen, "On the Production of High Speed Protons", Science, 72: 376-377 (1930)

[LAW32] E.O. Lawrence and M.S. Livingston, "The Production of High Speed Light Ions Without the Use of High Voltages", The Physical Review, 40: 19-35 (1932)

[LAW77] J.D. Lawson, "The Physics of Charged-particle Beams", Oxford Universty Press, 1977

[LIV61] John J. Livingood, "Cyclic Particle Accelerators", D. Van Nostrand, 1961

[LIV62] M. Stanley Livingston and John P. Blewett, "Particle Accelerators", McGraw-Hill, 1962

[LOU71] R. Louis, "The Properties of Ion Orbits in the Central Region of a Cyclotron", TRI-71-1, October 1971

[MCI75] A. McIlwain and S. Oh, "A Vertical Injection System for the University of Manitoba Cyclotron", Proc. 7^{th} Int. Conf. on Cyclotrons and their Applications (Birkhaüser, Basel, 1975), 394-396

[MUR53] R.L. Murray and L.R. Raterner, "Electric Fields within Cyclotron Dees", J. Appl. Phys., 24, 67-69, (1953)

[NEL69a] D. Nelson, H. Kim and M. Reiser, "Computer Solution for Three-dimensional Electromagnetic Field Geometries", IEEE Trans. Nucl. Sci., NS-16, No. 3, 766-767 (1969)

[NEL69b] D. Nelson, Univ. of Maryland Technical Report No. 960, 1969

[OH83] S. Oh, R. Pogson and M. Yoon, "Calculation of Three Dimensional Electric Fields by Successive Over-relaxation in the Central Region of a Cyclotron", Lecture Note in Physics 215, Springer-Verlag, 104-109 (Conference on Computing in Accelerator Design and Operation, W. Berlin, Sept. 20-23, 1983

[PIC40] A.T. Pickles and W. Sucksmith, "A Magnetic Study of the Two-phase Iron-nickel Alloys", Proc. Roy. Soc. (London) A175 (1930) 331-344

[POL69] R.E. Pollock, "Design Features of the Princeton A.V.F. Cyclotron Facility", Procedeeings of the 5^{th} International Cyclotron Conference, Oxford, 120-123, 1969

[POW65] W.B. Powell and B.L. Reece, "Injection of Ions into a Cyclotron from an External Source", Nuclear Instruments and Methods 32 (1965) 325-332

[PUC68] 1968-1969 Progress Report of the Princeton University Cyclotron Laboratory

[REI65] Martin Reiser and John Kopt, "Automatic Electrolytic Tank and Digital Computer Program for Calculation of IOn Trajectories in Crossed Electric and Magnetic Fields", Rev. Sci. Instru. Vol. 36, No. 7, 1022-1027 (1965)

[REI71] Martin Reiser, "First-Order Theory of Electrical Focusing in Cyclotron-type Two-Dimensional Lenses with Static and Time-Varying Potentials", Journal of Applied Physics, Vol. 42, 11, 4128-4138 (1971)

[RIC65] J. Reginald Richardson, "I. Sector Focusing Cyclotrons", in the Progress in Nuclear Techniques and Instrumentation, Vol. I, 1-101, North-Holland Publishing Company-Amsterdam, 1965, Ed. by F.J.M. Farley

[ROS38] M.E. Rose, "Focusing and Maximum Energy of Ions in the Cyclotron", Physical Review 53, 392-408 (1938)

[SEP67] A. Septier, "Focusing of Charged Particles", Academic Press, Vol. I,II 1967

[STA62] K.G. Standing, J.J. Burgerjon and F. Konopasek, "The University of Manitoba Cyclotron", Nuclear Instruments and Methods 18,19 (1962) 111-113

[SYM56] K.R. Symon, D.W. Kerst, L.W. Jones, L.J. Laslett, and K.M. Terwilliger, "Fixed-Field Alternating-Gradient Particle Accelerators", Physical Review 103, 6, 1837-1859 (1956)

[THO38] L.H. Thomas, "The Paths of Ions in the Cyclotron", Physical Review 54, 580-598 (1938)

[TRI73] W. Joho, C. Kost, TRIUMF Design Note, TRI-DN-73-11

[UMC77] 1976-1977 The University of Manitoba Cyclotron Laboratory Annual Report

[UMC84] 1984-1985 The University of Manitoba Cyclotron Laboratory Annual Report

[UZA85] H. Uzat, I. Gusdal, V.P. Derenchuk, J. Lancaster, F. Konopasek, "The New Implementation of a New RF System for the University of Manitoba Cyclotron", IEEE Trans. Nucl. Sci. NS-32, No. 5, 2954-2956 (1985)

[WEL59] T.A. Welton, "Computer Code for Cyclotron Orbit Calculation", Proc. of an Informal Conference on Sector-Focused Cyclotrons, Sea Island, Georgia, Feb. 2-4, 48-54 (1959)

[WOR85] Workshop on the Sixth International ECR Ion Source, Lawrence Berkeley Laboratory, PUB-5143, January 17-18, 1985

[ZIN69] T.E. Zinnerman, "Three-dimensional Electrolytic Tank Measurements and Vertical Motion Studies in the Central Region of a Cyclotron", University of Maryland, Department of Physics and Astronomy, Technical Report, No. 986 (1969)